THE ADAPTATION OF MORPHOLOGY TO FUNCTION IN LONG BONES

Md. Yusuf Haroon

THIS THESIS HAS BEEN SUBMITTED IN FULFILMENT OF THE
REQUIREMENT FOR THE DEGREE OF
DOCTOR OF PHILOSOPHY
IN THE FACULTY OF SCIENCE AT THE UNIVERSITY OF LONDON

SEPTEMBER 1996
DEPARTMENT OF ANATOMY AND DEVELOPMENTAL BIOLOGY
UNIVERSITY COLLEGE LONDON
GOWER STREET, LONDON WC1E 6BT
ENGLAND

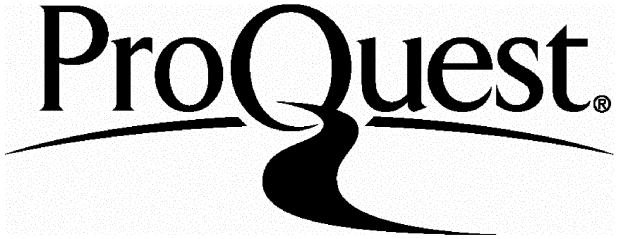

ABSTRACT

This thesis deals with the structure of equine limb bones. The initial study determined the relative proportion of fields of view occupied by more longitudinal and more oblique collagen in the cortex of the radius and has attempted to relate this information to osteonal type and type of loading. There is a higher, more oblique fraction in the compression cortex which is associated with a higher remodelling activity. The actual orientation pattern of the collagen fibres in the dark and the bright lamellae in secondary osteons in the plane of section in polarised light is determined.

Distal condylar fractures of the third metacarpal bones can be substantially explained by underlying structural features of the mineralized cartilage and bone. There is a marked preference to the orientation of the structure of the mineralized cartilage and it tends to cleave in the saggital plane. There are profound differences with age and between individuals in the density of the subchondral bone. Proximal to this, the main trabeculae are plates running in the dorso-palmar direction with small struts running in the medio-lateral direction joining them together. This structure leads to a tendency for a fracture to propagate between the saggital plates. In the skeletal tissues, fractures start either in the anisotropic trabecular bone, at the osseo-chondral junction, or at the tide-mark in the calcified cartilage at the deep surface of the articular cartilage. They may therefore spread in one or in two directions. Wherever the crack initiated, it would propagate catastrophically when it reached the zone of parallel plate structure of the cancellous bone.

The structure of the trabecular bone gives maximum strength and protection in the saggital plane in which the bone rotates, but it will yield slightly in the transverse plane and this may have a beneficial energy absorbing role. The disadvantage of this structural organisation is that it offers minimal resistance to fractures in the saggital plane.

Further to this, an anisotropic architecture in the articular cartilage of the equine McIII is described and associated with the unidirectional load that the bone undergoes.

ACKNOWLEDGEMENTS

I express my deep gratitudes to my supervisor Professor Alan Boyde whose supervision, support and guidance brought this thesis into a reality. I feel fortunate to have the chance of doing research with him. I am also very grateful to Professor Sheila J Jones who has been a continuous encouragement to me throughout the whole period, and to Dr. Christopher M Riggs whose work gave me primary inspiration. The excellent review in his PhD thesis provided me with a good foundation, and he provided me with important initial information. I have very often had the chance of sharing the knowledge and views with him.

Drs. Maria Fitzerald and Barbara Pittam made my initial stay in the Department and in London smoother. Dr. Colin Gray always extended a helping hand and without reservation. His software knowledge and suggestions made my work a lot easier. He has been very compassionate all along. Dr. Helen Liversidge was very helpful and encouraging. I also thank Dr. PGT Howell for his valuable suggestions.

I received enormous support from Maureen Aurora and Roy Radcliffe. Without their help I would not have been able to continue my research work. Thanks are also due to Sola Soetan, Christine Davis and Tim P Robson for their help. I am indebted to the Librarian, Royal Veterinary College, London for allowing me access to the library facilities.

Thanks to the World Health Organisation for granting me a fellowship for three years of the period of my study at UCL.

I very much missed my parents and in-laws. I always feel their blessings.

My son Hasin who just passed his 6th birthday keeps on asking me: "Dad, what is more important to you? Is it me or your PhD?" I find it very difficult to convince him that he is. My daughter Snigdha (10) who enjoys writing poems, can hardly consider my PhD as her subject. Perhaps, she hates it. I hope, she will like it after it is over. Both of them are missing the best period of their life.

My wife Rainy who spent more than a decade with me, is still longing for a sound life. After my fellowship ceased, she has been working hard to earn the livelihood for ourselves and our children. Without her support, I could not have finished. I will never be able to give her back these few years.

Finally, I express my loyalty to the God who created this universe, gave us knowledge to discover this, and to whom we shall return.

TABLE OF CONTENTS

LIST OF FIGURES

LIST OF TABLES

Abbreviation and common names used in the thesis

1° = primary osteon

2° = secondary osteon.

LS = longitudinal

TS = transverse

AP = antero-posterior = cranio-caudal = dorso-palmar = sagittal

ML = medio-lateral = coronal

AC = articular cartilage

CC = calcified cartilage

McIII = third metacarpal bone.

PLM = Polarised light mocroscopy

LPL = Linearly polarised light

CPL = Circularly Polarised light

AFCSLM = Autofluorescence confocal scanning light microscope

SEM = Scanning electron microscope

SE = Secondary electron emission mode

BSE = Backscattered electron emission mode

CHAPTER 1

HISTORICAL INTRODUCTION AND BACKGROUND

The biomechanical competence of bones depends upon the strength of bone tissue, which again depends on mass, density, three dimensional arrangement and the strength of the composite material. Mass denotes bone quantity while the other factors constitute bone quality.

Bone's material properties depend on the microscopic structure of the calcified matrix as well as its composition. Porosity (fraction of the material occupied by soft tissue space), degree of mineralisation, collagen fibre orientation, histological structure (primary or secondary osteonal bone) and fatigue damage are the determining factors. Changes in these variables, and also changes in microstructural and compositional status caused by remodelling cause a change in material strength (failure stress) and stiffness (elastic modulus) of bone.

Bone strength is the main determinant of the mechanical integrity of the bone itself. Certain extra-osseous factors also contribute to it. Bone structural failure depends on the force applied, and the bone's strength to resist the force. Fractional volume correlates well with bone strength. However, it is not sufficient to explain why individuals with normal values sustain fracture while those with low bone mass do not. Gardsell failed to find any difference between fracture and non-fracture groups (Gardsell et al 1989, 1990). Thus bone strength also depends upon the structural material properties and its three-dimensional architecture (Melton et al 1988), jointly referred to as bone quality. Bone quality broadly covers the architecture of bone - both cortical and trabecular, the composition and organisation of the matrix and its mineralisation profile. The loading history is an important parameter for the material properties of bone, especially in relation to the change in organisation in response to different types of strain and the extent of fatigue damage and its repair by remodelling. Bone quality is not something static. It is constantly

changing in compliance with functional history. Every change in the function of bone is followed by certain definite changes in the internal architecture and external conformation (Wolff 1892).

Bone strength and the individual's environment concomitantly contribute to the occurrence of fracture. Propensity to fall, impaired postural reflexes during falling, insufficient soft tissue over the point of impact to distribute the force of the fall, and environmental hazards are the additional factors that constitute the environment of the individual. Some point out that the force of a fall from a standing height, properly applied, is sufficient to break any adult bone (Heaney 1993).

Bone fragility depends on several factors such as trabecular connectivity, alterations in bone architecture, microfractures visible at light microscopic level, microcracks or defects at the ultrastructural level, bone quality and continuous changes in bone composition. Fatigue damage causes bone fragility, a process that involves production of histologically observable cracks. If such cracks are not repaired, their gradual development and coalescence eventually lead to bone fracture.

Mechanisms that lead to bone fragility may be different. In low turnover osteoporosis, there are larger burdens of fatigue damage causing increased bone fragility, and hence increased risk of fracture. In high turnover osteoporosis groups, faster bone loss follows increased remodelling which gives rise to larger remodelling spaces in bone structure that favour increased risk of fracture.

Various factors influence bone at both macro and micro levels throughout life. Modelling changes the overall shape of bone organs in response to physiologic and mechanical influences. Bones may widen or change in shape by the removal or addition of bone, eg., periosteal growth (addition of new layers of bone) increases the width of a long bone, while removal of bone occurs at the endosteal surface widening the lumen of the cylinder.

Remodelling is the result of coupling of formation and resorption, normally a balanced process. The cells responsible constitute the Basic Multicellular Unit (BMU: Frost 1969) or Bone Remodelling Unit (BRU: Parfitt 1983a). During the remodelling cycle,

an individual BRU gives rise to a Bone Structural Unit (BSU: Frost 1969, Eriksen 1986). The lifespan of individual osteoclast nuclei is only a few days or weeks, and that of the osteoblast is only a few months (Frost 1986). Osteocyte longevity is estimated to be about 25 years (Frost 1985).

In cortical bone, the BRU is approximately 400μm long and 200μm wide at the base. An individual BRU bores longitudinally through the cortex at a rate of 40μm per day (Jaworski and Lok 1972), known as the cutting cone, leaving new bone behind, the closing cone. During the process, new bone is laid down around a central canal containing blood vessels, along the long axis of the BRU. Thus it gives rise to a bone structural unit, a cortical osteon or Haversian system where collagen fibre lamellae are arranged in concentric layers around the central canal. Remodelling does not proceed with the same intensity on the periosteal and endosteal aspects. An imbalance in remodelling (resorption and formation) on periosteal surfaces with a net increase in bone contributes to appositional growth and fracture repair. On endosteal surfaces remodelling occurs at a higher intensity; the rate of resorption exceeds the rate of formation resulting in endocortical thinning and expansion of the cylinder in long bones.

Though BRU take a different forms in the trabecular component, yet the purpose is the same; old bone is replaced with new. Cancellous bone consists of bony trabeculae, either thin plates or spicules with a thickness range from 50μm to 400μm (Eriksen et al 1994). The trabeculae are inter-connected in a honeycomb pattern providing maximal mechanical strength. Trabecular architecture follows a pattern that ensures maximal adaptation to the prevailing stress direction.

Remodelling as a modifier of bone strength.

Remodelling brings changes in bone structure throughout life. Removal of old bone is followed by synthesis of new bone matrix and its subsequent mineralisation. Since remodelling is usually a balanced process of resorption and formation, it preserves the mechanical integrity of the skeleton. At the same time, it alters

the bone architecture and composition leading to change in its capacity to withstand varieties of strain. Moreover, if formation is not coupled with resorption, bone removal obviously leads to impaired mechanical competence.

As remodelling events proceed, older bone is replaced by new Haversian units. A net increase in porosity may result near the medullary canal due to the appearance of larger Haversian canals. This tendency is reduced on those sides of the bone where longitudinal bending stresses are habitually higher, i.e., increase in endosteal bone loss and intracortical porosity occur preferentially near the neutral axis for bending of long bones (Martin and Burr 1989), suggesting that stress inhibits remodelling as well as stimulating periosteal modelling.

In cancellous bone each remodelling event produces a small increase in porosity. If resorption continues, and is not coupled with balanced formation, the trabeculae get thinner. Further resorption leads to perforation, or thinning and disconnection of the trabeculae. Perforated trabeculae become completely unloaded, and consequently are resorbed (Parfitt 1984, 1987; Mosekilde 1990; Jayasinghe et al 1993). Whether the free ends that follow the severing of the trabeculae remain unchanged, or become coated by new bone formation, they never regain continuity (Jayasinghe et al 1993). Studies show that vertical main load bearing struts are less frequently affected than the horizontal trabeculae in vertebral bodies leading to age-related increase in cancellous bone anisotropy (Mosekilde 1989; Jayasinghe et al 1993).

SEM studies further reveal the events that the trabeculae undergo during resorption when deep vertical excavations lead to severing of the trabeculae. Trabeculae get thinner by long resorption grooves that extend along the long axes of the trabeculae from node to node. Gradually, severing of the trabeculae causes breaches in the trabecular network and connectivity. Ultimately the bone's architectural competence deteriorates with the process (Jayasinghe et al 1993; Jones and Boyde 1994).

Loading activates increased osteonal remodelling (Burr et al 1985). Remodelling affects bone strength and stiffness in several

ways; primarily in the material properties of the skeleton. According to one school of thought, during life, in normal individuals, skeletal loading produces fatigue damage or microcracks in the calcified matrix under physiological conditions (Burr et al 1985; Schaffler et al 1989, 1990). Remodelling follows to repair the fatigue damage (Frost 1963; Carter and Hayes 1977). Some studies provide evidence that fatigue cracks produced as a result of mechanical loading, lead to an increase in number of osteonal resorption cavities (Burr et al 1985; Mori and Burr 1991).

Thus fatigue related micro-damage as manifested by histologically defined cracks (Frost 1960b; Burr and Stafford 1990) does not normally accumulate with age (Frost 1960b). Several mechanisms of repairing fatigue damage have been put forward. If remodelling occurs as a reparative measure for fatigue damage, Frost hypothesised that damage causing disruption in the canalicular network triggers a cellular membrane response in osteocytes which eventually signals the appropriate cell population within the Haversian canal to begin the process of repair (Frost 1973, 1985). Others advocate a different mechanism - a breach in lamellar bonding that follows microcracks relieves the usual stress transmitted from the surrounding bone to the Haversian canal, and initiates remodelling (Martin and Burr 1982). In addition to the excitatory signals conveyed by osteocytes present adjacent to the damaged area, Lanyon proposes that the absence of continuous inhibitory signal from the osteocytes in the damaged area (osteocytes killed or damaged) to prevent osteoclast invasion eventually might work as a signal inviting repair (Lanyon 1993).

Physiologically loaded bone apparently does not sustain strain damage (Currey 1968, 1984). As Lanyon proposes (Lanyon 1987), when the strain rises above a threshold level (still unable to cause microfracture), the change that occurs in the deformed matrix such as reorientation of proteoglycans (Skerry et al 1988), are detected by the osteocytes in the vicinity. The osteocytes then signal to the appropriate cell population through their communications to initiate remodelling process. Proteoglycans are believed to be responsible providing extracellular information as they have stabilising

properties on fibrillar proteins (Meyer 1960). Pead and co-workers (1988a) showed that osteocytes receive first hand information from the deformed matrix in loading bones beyond the physiological limit. Lanyon (1987) also suggested that a few signals of short intermittent loading are enough to initiate remodelling. Obviously, these sorts of loading are not capable of producing damage in the bone matrix. Under these circumstances, the remodelling is not initiated to repair damage, but to prevent impending failure, resisting discontinuities in the bone matrix, and help to maintain the mechanical integrity of bone.

In the event of fatigue damage, although the remodelling process continually repairs the damage, it may not effectively heal all the damage the bone sustains. Thus there is always an accumulation of damage waiting for repair throughout the skeleton. This damage is thought to correspond to microcracks, which are visible histologically (Burr and Stafford 1990). Remodelling events may produce weak interfaces in the calcified matrix; cement lines may weaken the cortical bone for monotonic loading. Remodelled cortical bone is weaker and less stiff than primary bone in tension. Fatigue damage reduces the elastic modulus and material strength of bone (Carter and Hayes 1977; McElhaney et al 1970). Human secondary bone is 80% as strong and 91% as stiff in tension as primary bone (Vincentelli and Grigorov 1985).

As material strength is reduced, the bone becomes more susceptible to traumatic fracture. However, at the same time, the weak interfaces provide protection against fatigue failure. Where the failure is arrested, transverse fatigue cracks are diverted into longitudinal paths. Remodelled bone, which replaces the damaged bone following fatigue damage, is better able to resist failure by fatigue cracking.

Collagen fibre orientation

Collagen fibre orientation is a major determinant of bone strength (Vincentelli and Evans 1971; Evans 1974; Riggs et al 1993b). Remodelling at different regions subjected to different strain direction may lead to laying down of collagen fibres in different

orientation which are better capable to withstand different types of strain; this may also affect cortical bone strength (Boyde and Riggs 1990; Riggs et al 1993a).

In polarised light, cortical or cancellous bone shows a characteristic appearance, the lamellar pattern caused by alternating orientation of collagen (Gebhardt 1905, Ascenzi and Bonnuci 1964, 1967,1968; Evans and Vincentelli 1969, 1974). The concentric lamellae within the osteons contain collagen of a similar packing density. The fibres lie parallel to one another within the plane of the lamellae (Gebhardt 1905; Boyde 1972; Ascenzi and Bonnuci 1976; Reid 1986). Several other studies showed that the collagen fibres lie parallel (Jones et al 1975; Jones and Boyde 1976b) being confined in domains (Boyde and Hobdell 1969).

This pattern is absent in woven bone, where collagen fibrils are differently organised. Woven bone is formed during the formation of primary bone and in some pathological conditions like Pagets disease of bone indicating a state of high bone turnover. It also happens in bone at certain stages of fluoride treatment, when an initial high rate of bone formation is associated with inability of the bone remodelling unit to ensure proper lamellar alignment (Eriksen et al 1994). Different collagen fibril arrangement eventually affects the mechanical properties of bone.

More longitudinally oriented fibres enhance tensile strength (Martin and Ishida 1989; Boyde and Riggs 1990; Riggs et al 1993b). Higher compressive strength has been associated with bone containing many osteons of predominantly oblique/transverse collagen fibre orientation (Evans et al 1974; Boyde and Riggs 1990; Riggs et al 1993b). There is evidence that this histological feature is adjusted to optimize bones material strength to the local stress situation (Ascenzi and Bonnuci 1967, 1968; Lanyon et al 1982; Boyde et al 1984a; Portigliatti-Barbos et al 1983, 1984, 1987; Carando et al 1989, 1991; Ascenzi et al 1990; Boyde and Riggs 1990; Riggs et al 1993b). There is little information about the effects of collagen fibre orientation and its age-related changes in cancellous bone.

However, the organisation responsible for the lamellation within the osteons has been a matter of controversy for a long time.

Several workers proposed a number of models of collagen fibre orientation. Until now, the most generally accepted model (Kolliker 1889; Von Ebner 1875; Gebhardt 1905) suggested that the lamellation in polarised light is due to successive alternate lamellae of more transverse and more longitudinal fibres: lamellae lying on the plane of section appearing bright between crossed polars while the longitudinal fibres are cut in cross section and appear dark in TS. Others described differing patterns of organisation within successive lamellae (Ranvier 1889; Ziegler 1906; Ruth 1947; Rouiller 1956; Marotti and Muglia 1988; Marrotti 1990, 1993; Hasegawa 1994).

Effect of mineralisation in bone

The mechanical integrity of bone also depends on its degree of mineralisation. The stiffness and brittleness of bone depend mainly on its mineral content (Currey 1969a-b; Katz et al 1984). The degree of mineralisation depends on the rate of bone turnover. Low turnover leads to hypermineralisation and the bone becomes more brittle and stiff. Increased brittleness or stiffness reduces bone quality and favours fracture. The mineral density of lamellar bone increases with age (Jones and Boyde 1994; Boyde et al 1993; Riggs et al 1993a, 1993b; Boyde et al 1992; Reid and Boyde 1987; Grynpas 1993). However, woven bone mineralizes rapidly, and calcified cartilage is the densest phase in bone (Boyde et al 1992). With digital backscattered electron image analysis Boyde et al (1995b) found a lower rate of bone renewal in females and in osteoarthritis subjects. Difference in mineral content in old and new bone on either side of reversal or resting line offers a potential cleavage plane within the tissue (Jones and Boyde 1994). Changes may be confined to discrete regions of an individual bone, and such changes may have dramatic effects on the strength of that bone. Greater bone turnover replaces fatigue damaged bone with new bone. This also prevents hypermineralisation and consequent brittleness found in unremodelled bone (Frost 1960a).

Osteocyte death manifested as empty lacunae affects the bone quality (Schnitzer et al 1990; Wong et al 1985). Osteocytes have a life span of about 25 years (Parfitt et al 1987). Empty lacunae in the centre of trabeculae (Wong et al 1985) may be due to absence of

remodelling of the trabecular core for many years. It may also be due to inability of nutrients to reach the core osteocytes from the marrow cavity (Urist et al 1963). Following osteocyte death, the lacunae and canaliculae become calcified leading to increased hypermineralisation and brittleness, a condition termed Micropetrosis by Frost (1960a). However, unremodelled, older bone is itself more mineralised and hence more brittle, independent of the presence of osteocytes.

Bone architecture

Bone strength determines the loading capacity of any individual bone which in turn depends on cumulative representation of its mass, cortical thickness, organisation and on trabecular architecture. Trabecular bone is made up of a series of interconnected plates or rods. Cross-sectional geometry, the number, thickness, connectivity and orientation of the trabeculae are essential for the maintenance of the functional status of weight bearing bone. Irregularity of the trabecular lattice, even in the presence of maintained bone volume, weakens the trabecular bone.

Goldstein and co-workers (1993) showed that in human normal trabecular bone (metaphyseal), more than 80% of the variance in mechanical behaviour can be explained by measures of density and orientation. Mineral density, number of trabecular packets and their volume, and collagen matrix distribution also determine the mechanical integrity of trabecular bone.

Adaptation of bone to its function.

Bone architecture and its organisation needs to be able to withstand strains in various direction. This is ensured by an adaptive modelling and remodelling process. Wolff's Law states that the skeleton attempts to adapt its structure to the load it experiences. Mechanical factors stimulate modelling responses, primarily in the form of periosteal bone formation, that alter bone size and shape.

Strain in the appendicular skeleton is mainly due to bending and torsion. Periosteal growth increases the outer diameter of bone.

Necessary changes in skeletal morphology are governed by continuous feedback of mechanical information that include current loading status and existing architecture. Appreciation of strain distribution throughout the matrix is an essential phenomenon (Lanyon 1993). Although the general form of the bone is genetically determined, the components on which the mechanical integrity depends are modulated in response to the functional loading status of individual bone (Lanyon 1992b).

Bone trabeculae align themselves with the direction of pure compressive and tensile loading to avoid the high strains involved in bending. The trajectorial hypothesis of bone trabecular system was described last century where trajectories of bone trabeculae to align with the principal stress trajectories within the bone were described (Meyer 1867; Wolff 1870, 1892). Later, several other researchers also observed that peak principal stress direction aligns with trabecular trajectories (Lanyon 1974; Pauwels 1980; Hayes and Snyder 1981). So, it is usually assumed that principal stress determine the architecture of cancellous bone.

However, some workers raised objections regarding the underlying biomechanics in trajectorial explanation of the development of the characteristic trabecular pattern (Fyhrie and Carter 1986; Carter et al 1989; Turner 1992; Hert 1992, 1994). Turner (1992) hypothesised that the textural anisotropy must exactly balance the anisotropy of the peak principal stresses imposed upon cancellous bone, and hence cancellous bone architecture adapts itself to maintain a uniform and isotropic distribution of peak strain within the bone. Compressive stresses and tensile stresses affect cancellous bone adaptation similarly (Hert et al 1969, Liskova and Hert 1971; Rubin and Lanyon 1984; Lanyon 1987; Turner 1992), and the extent of deposition depends on the peak value of strain (Rubin and Lanyon 1984; Lanyon 1987). Fyhrie and Carter (1986) and Carter and co-workers (1989) have rejected the original trajectorial theory and concluded that the cancellous bone structure can be described only in terms of joint loading from different directions. Hert (1992) suggested that pressure only is responsible for the formation of the functional architecture of the metaphyseal spongiosa, since tension as maximum

principal stress is not manifested either in epiphyses or in metaphyses where cancellous bone is being formed and remodelled.

Extensive work has been accomplished on adaptive bone remodelling and collagen fibre organisation. Until now, the collagen orientation in secondary osteons is a controversial issue. It is an essential component of the strength of bone. Extended study is needed to identify the change in the micro-architecture of the cortical bone with adaptive bone remodelling, and to determine the true order of collagen in the Haversian system.

Further, several studies have been performed to understand the 3-D trabecular architecture of cancellous bone such as 3-D photography (Jayasinghe et al 1994), continuous rotation parallax of beams (Boyde et al 1989, 1990b), and Scanning electron microscopy (Jayasinghe et al 1993). Further study in the structure of bone at its macro and micro level with relation to three dimensional architecture and orientation of cancellous bone are necessary to understand the mechanism why bone fails in certain circumstances during fracture with characteristic morphology, despite absence of any apparent pathology.

Figure 1.1

The anatomy of the equine forelimb. The radius (a,b) bows in a cranio-caudal direction, while the cannon bone (a,c) is straight (after Pasquini et al 1978).

Figure 1.1

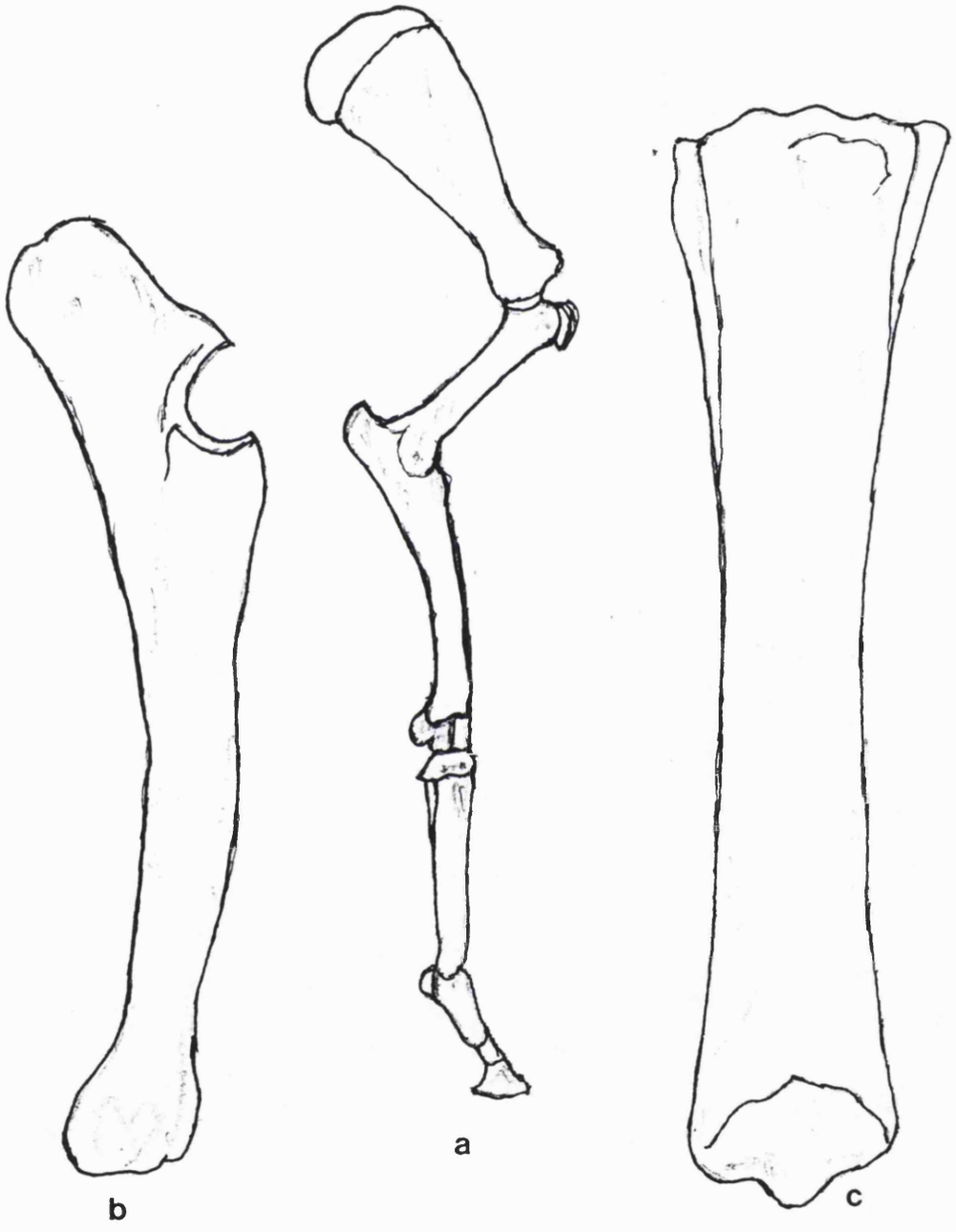

Lateral view

Anterior view

CHAPTER 2

FURTHER STUDIES INTO THE ADAPTATION OF CORTICAL BONE TO FUNCTION WITH SPECIAL REFERENCE TO THE DIFFERENT ORIENTATIONS OF COLLAGEN FIBRES IN THE TENSION AND COMPRESSION CORTICES.

2.1.1 INTRODUCTION

The biomechanical competence of bone and its maintenance depend on several factors. Of these, remodelling is a process that continues intermittently throughout life and which changes cortical bone structure to keep pace with its functional requirements. The alignment of the constituent collagen fibres is apparently modified to withstand differing loading regimes (Boyde and Riggs 1990; Ascenzi et al 1990; Riggs et al 1993a).

If primary bone exists in the first instance, remodelling replaces it with secondary osteons. These are the basic structural units (BSU) in cortical bone, each of which is delineated by a reversal line, one type of cement line. The reversal line is recognised by its scalloped appearance, discontinuity of canaliculi (Lacroix 1951), and a hypermineralised cement matrix. Some cement lines are resting lines which result when bone formation resumes after an interruption. These are recognised by their smooth surface, the continuity of canaliculi, and the contextual situation.

Osteonal bone forms approximately 2/3rds of the total compact, cortical bone in man, a proportion which falls with age (Currey 1964). Interstitial bone and circumferential lamellae constitute the rest of the cortex.

As regards the maturation stage of the mineralisation process, about 70%-75% of the final possible level of mineralisation within a new bone packet is complete within few days, while about 90% of the maximum level of mineralisation takes several months (Parfitt 1976, 1983a). This correlates well with the longer term maturation process that accounts for the observed differences in the degree of mineralisation of osteons seen in compact bone by both microradiography and BSE-SEM and the increase in the proportion of higher density bone fractions seen in the bone of older individuals

(Boyde et al 1992).

The bone forming cells lie in a continuous sheet on the bone surface where patches of cells show similar orientations (Jones 1973, 1974; Jones et al 1975). There are differing degrees of elongation and orientation - "well oriented fields of more elongated cells to areas of less elongated cells showing little or limited apparent orientation" (Jones and Boyde 1976a).

The ordering into domains of parallel cells correlates with the pattern of underlying bone collagen orientation (Jones and Boyde 1976a). The collagen fibrils secreted lie along the major axis of the producing cells (Jones et al 1975; Jones and Boyde 1976b), which determine the fibre orientation. Orientation of osteogenic cells in culture indicates that the cellular orientation does not depend on the underlying collagen fibres (Jones and Boyde 1976a). SEM evidence suggests that collagen orientation in hard tissue matrices depends on the freedom of cells to move with respect to the matrix surface (Boyde and Hobdell 1969). The amount of bone laid down depends on the number of cells which have migrated to or mitosed within the area and how active they are (Jones 1974; Jones and Boyde 1976c, 1977a, 1979).

Osteoblasts migrate and change shape in organ culture (Jones and Boyde 1977a; Taylor et al 1989). As regards the development of the collagen pattern, a rest in the cycle of activities of osteoblasts could result in an abrupt change in orientation of collagen from one lamella to another (Jones and Boyde 1977a). Varying activity rates may affect re-ordering of the cells within the monolayer, and thus possibly influence the collagen orientation (Jones and Boyde (1976a).

PTH alters osteoblast shape and alignment in vitro (PTE: Jones and Boyde 1976a, 1976c, 1977a; Jones and Ness 1977; PTH: Jones et al 1981). Osteoblasts change their shape, elongate, align, and show fewer ruffles compared to controls (Jones and Boyde 1976a, 1976c; Ali et al 1990). The cells under the influence of PTH do not cease their matrix production. Osteoblasts in longer term PTE culture still produce parallel collagen fibres (Jones and Boyde 1977a). Parathyroid hormone increases prostaglandin synthesis by bone. Osteoblasts are the major source of prostaglandins formed by bone (Nolan et al 1983; Ali et al 1990). Prostaglandins, especially PgE_2 cause bone to

resorb in organ culture (Klein and Raisz 1970; Dietrich et al 1975). Ali et al (1990) showed that the PgE_2does not change the osteoblast shape, and concluded that the cell shape change with PTH is not mediated by endogenous prostanoids, and osteoblast shape change is not essential for bone resorption stimulated by PgE_2.

However, PTH is not essential for osteoclastic activity and bone remodelling since parathyroidectomised new born rats also exhibit the resorbing phenomenon (Krukowski et al 1980).

Jones and Boyde (1977b) emphasised that the continuity of the cell sheet on the bone surface to be an important controlling factor for osteoclastic resorption. Osteoclasts can more easily insinuate themselves to come into contact with the bone when the adhesion of the lining cells is impaired after matrix production stops, or following the administration of PTH (Jones and Boyde 1977b).

Rodan and Martin (1981) based their hypothesis on this work. They suggested that the change in the shape of osteoblasts may regulate the access of osteoclasts to the bone surface. Factors that cause cell shape alteration may contribute to the resorption process. As argued, the resorbing agents such as PTH and Prostaglandins uncover the matrix by inducing cell shape change, probably via cAMP or Ca^{2+}, and thus facilitate osteoclastic invasion.
Osteocalcin released from digested matrix further enhances the process by attracting monocytic osteoclast precursors (Mundy et al 1978; Mundy and Roodman 1987).

Osteoblasts thus seem to be in control of collagen orientation in bone matrix, and to function over relatively large areas in a concerted fasion. To do this, they must be in communication. Cell processes of osteoblasts contact the cell bodies of adjacent cells. Direct intercellular communication can occur via gap junctions. Gap junctions are aggregates of transcellular membrane channels that allow direct coupling between the cytoplasm of adjacent cells (Warner 1988). Osteoblasts communicate between one another and with osteocytes through gap junctions (rat: Doty SB 1981; Jones et al 1993; man: Civitelli 1992). Human osteoblasts express at least two connexins, Connexin43 and Connexin 45. Cx43 is abundant in human osteoblast that mediate both dye coupling and electric coupling

(Civitelli 1995). Gap junctions allow the propagation of mechanically stimulated [Ca^{2+}] waves throughout osteoblastic monolayers (Xia and Ferrier (1992).

In addition to those between osteoblasts, Jones et al (1993) found (Cx43) gap junctions also between some osteoclasts and overlying mononuclear cells at sites of active resorption. This may indicate the existence of some similar functional communication system between osteoblasts and osteoclasts. Gap junction function is regulated by hormones such as parathyroid hormone and prostaglandin E_2. Schiller and co-workers (1992) showed that PTH stimulates connexin43 in cultured rat bone.

Vesely et al (1992) studied bone cell populations by "filming" for long periods in culture and demonstrated types of contact interaction that would help the osteoclast breach the osteoblastic sheet, and reach the bone surface for resorption. "Message mediated contact behaviour - MMCB" between osteoblast and osteoclast causes zeiosis of the osteoblast that leads to retraction of the cell. Subsequently, the osteoclast take the position of the osteoblast. The retraction continues, or even begins after the contact is broken. Osteoclast mass travels along the long interconnecting processes (Jones and Boyde 1977b) and nuclei can be seen to travel through them. Osteoclasts make contact by a lamelliform process, a satellite, or a tubular process. An osteoblast may return to its original position after the osteoclast moves away. Very fine microthreads that were seen to remain as connections between osteoblasts and osteoclasts after such interaction may possibly guide their return (Vesely et al 1992) for possible subsequent bone formation at the site of osteoclastic bone resorption.

The osteoclast is the sole bone resorbing cell. There is no evidence to support a direct resorptive function of cells such as osteocytes, osteoblasts, monocytes, macrophages, although some workers have found an association with resorption in vitro. Some researchers could find no resorption pits associated with monocytes (Ali et al 1984a) or macrophages (Shapiro et al 1979) lying against bone surfaces. However, Mundy et al (1977) concluded that human monocytes were able to degrade devitalised bone. Macrophages derived

from tissues in pathological conditions such as malignancy and rheumatoid arthritis could be associated with bone destruction. Human tumour-associated macrophages (TAMs) isolated from different malignant sites (primary lung carcinomas: Athanasou and Quinn 1992a; pilar tumor of scalp: Athanasou and Quinn 1992b) when incubated on bone slices were capable of bone resorption, as demonstrated by pit formation.

Inflammatory cells such as macrophages and macrophage polykaryons derived from the joint capsule of failed hip arthroplasties produced small resorption pits and surface erosion in cortical bone slices when cultured in vitro (Athanasou et al 1992). Further studies (Quinn and Athanasou 1992; Quinn et al 1994) demonstrated that the tumour-infiltrating macrophages were capable of differentiation into osteoclast-like cells which caused extensive bone resorption which could be associated with extensive osteolysis in malignancy (carcinomatous skeletal metastasis). None of the previously mentioned studies showed macrophages to cause bone resorption independently, although Chang et al (1992) concluded that macrophages derived from synovium of patients with rheumatoid arthritis, were independently able to cause extensive roughening of bone surface; a finding that suggests a possible role of the macrophages in the development of marginal erosions in rheumatoid arthritis. The resorption was not affected by local or systemic factors influencing bone resorption.

As regards the role of osteocytes in bone resorption, Scanning electron microscopic studies discredited the notion of "osteocytic osteolysis" (Jones and Boyde 1977b; Boyde 1980b; Jones et al 1985). Some workers have suggested a certain supporting role for other cells in osteoclastic bone resorption (Heersche 1978; Chambers 1981, 1985). The suggestion that the osteoblast prepares the bone surface by releasing collagenase before the osteoclast comes into action (Chambers 1981, 1985), or that the osteoclast first degrades noncollagenous bone matrix, demineralises the bone, and then leaves the site for phagocytosis of the exposed collagen fibrils by mononuclear, fibroblast-like or monocyte-derived cells (Heersche 1978) has received little support. Again several scanning electron

microscopy studies (Jones and Boyde 1977b; Boyde et al 1984b; Jones et al 1984; Ali et al 1984b) categorically nullified the above suggestions, further suggesting that the osteoclasts can resorb bone alone without the help of other cell types.

Remodelling is controlled by several local factors. It has frequently been suggested that remodelling follows micro-damage in bone as a reparative process (Frost 1963; Carter and Hayes 1977b). Fatigue microdamage is evidenced by the occlusion of the canalicular lacunar pathway due to disturbances following local fracture (Frost 1960a). However, physiologically loaded bone does not apparently exhibit strain damage (Currey 1984).

Bone adapts to the pattern of its mechanical loading. It is sensitive to changes in this normal pattern, altering mass and geometry in response to the new forces (Carter 1987; Frost 1988). Adaptive bone remodelling in response to strain distribution and its magnitudes has been demonstrated by several workers (Hert et al 1971a, 1971b; Liskova and Hert 1971; Lanyon and Baggot 1976; Lanyon et al 1979, 1982; Lanyon 1987, 1992a, 1992b; O'Connor et al 1982; Rubin and Lanyon 1982, 1984, 1985, 1987). Hert and co-workers also showed (1971b) that bone adapts to its local strain environment without any central nervous system control. It has often been surmised that strain in bone matrix is in some way read by the osteocytes (Lanyon 1987,1993) in the vicinity which then send signals via communications to osteoblasts, to initiate the remodelling process.

Increased mechanical loads stimulate modelling in cortical bone with an increase in periosteal bone formation without prior bone resorption (Pead et al 1988b; Burr et al 1989; Nunamaker and Butterweck 1989; Riggs 1990; Hagino et al 1993).

A few events of short intermittent dynamic loading are enough to produce adaptive osteonal remodelling (Rubin and Lanyon 1987, Pead and Lanyon 1989). With several experiments in vivo and in vitro, Lanyon and co-workers demonstrated a series of events that occur in bone following mechanical loading. Cellular metabolism is activated within the first few minutes of loading. Pead and Lanyon (1989) demonstrated adaptive osteogenic response in vivo (avian) following a single period of dynamic loading. Indomethacin when administered

during loading reduced the osteogenic response, suggesting that the immediate release of prostaglandins is the initial step when strain information is translated into biochemical signals.

An increase in the release of prostaglandin E (PgE) and prostacyclin (PgI2) at their maximum level within 5 minutes of a 15-minute period of cyclic mechanical loading of canine cancellous bone was demonstrated in vitro by Rawlinson et al (1991). By immunolocalisation, they showed that osteoblasts released both PgE2 and PgI2 (prostacyclin) while osteocytes released PgI2, but not PgE2. Added prostacyclin, but not PgE2, produced an increase in RNA synthesis within 6 hours as evidenced by the increase in specific activity of ^{3}H-uridine in extracted RNA. Adding prostaglandins in vitro (adult cancellous bone in culture) Rawlinson et al (1993) further showed that exogenous prostaglandin E2 increased G6PD activity in osteocytes and surface cells within 8 minutes, but had no effect on RNA synthesis at 6 hours. On the contrary, prostacyclin stimulated both G6PD activity and ^{3}H-uridine incorporation equally in osteocytes and surface cells.

Thus prostacyclin imitates the early loading related responses - an increase in G6PD activity and RNA synthesis in bone cells (Rawlinson et al 1993). Cheng et al (rat: 1994) also confirmed immediate and sustained increases in G6PD activity in response to loading (500 g, 1 Hz, 8 minutes) and prostacyclin that persisted for 18h, by which time alkaline phosphatase activity in surface osteoblasts was elevated and ^{3}H-proline incorporation into collagen increased. The sequence was similar with prostaglandin E2 but there was no change in alkaline phosphatase activity.

In vitro mechanical loading of canine cancellous bone cores (El-Haj et al 1990) also showed an increase in intracellular glucose 6-phosphate dehydrogenase (G6PD) in lining cells, and increased RNA synthesis in osteocytes 6 hours after loading. Adding Indomethacin inhibited both the responses.

An increase in the activity of the enzyme glucose 6-phosphate dehydrogenase in the periosteal cells adjacent to the bone surface immediately after a single 6 minute period of loading was also demonstrated previously in vivo (avian-cortical) by Skerry et al

(1989). The increase was proportional to the strain magnitude in the immediate vicinity of the cells. In vitro studies also documented an almost immediate increase in the activity of G6PD in osteocytes and osteoblasts which was proportional to the local strain magnitude on loading (rat ulna, 500g, 1 HZ, 8 minutes: Cheng et al 1994).

Adaptive regulation of matrix synthesis was also demonstrated in 18h organ culture of 17 day embryonic chick tibiotarsi after a single 20 minute period of intermittent loading at 0.4 Hz (Zaman et al 1992). Increased expression of the mRNA for type 1 collagen in the periosteal tissue of bones and an increase in alkaline phosphatase activity were documented.

Dallas et al (1993) also documented peak strain magnitude related responses such as a rapid increase of G6PD activity in osteoblasts and osteocytes, and increased RNA synthesis detectable after 8h (more pronounced after 24h) in organ culture following a 20 minute period of intermittent loading of chick embryonic shaft at 0.4 Hz. Both responses were blocked by indomethacin. Different sequential activities of enzymes G6PD and alkaline phosphatase in osteocytes and periosteal osteoblasts after a 5 minute period of cyclic longitudinal loading at 1 Hz of 14w rat tibia and fibula correlate well with the order of new bone formation have been confirmed in vivo by Dodds et al (1993). The G6PD activity in osteocytes and periosteal osteoblasts was immediately increased. Even after 24 hours, G6PD level in osteoblasts was higher than the controls, while in osteocytes it returned to control values. Immediately after loading, alkaline phosphatase activity in osteoblasts was unaffected, though it was increased 24 hours later. Alkaline phosphatase activity in osteocytes was not detectable in time. The response in osteocytes was transient, which suggests an early biochemical change associated with strain perception, and that in osteoblasts led to osteogenesis.

The secondary osteons which fill in the tunnels bored by osteoclasts are cylindrical structures, roughly parallel to the long axis of bone, which may extend for several millimetres with a spiral course (dog: Cohen and Harris 1958; dog, baboon and man: Tappen 1977). They are circular in cross section, 200 to 300μm in diameter. With

canal diameters of from 20 to 50μm, their wall thicknesses are up to 80μm or more (man: Johnson 1964, 1966). Lower estimates of the mean total length of human secondary osteons at 2·5mm, a diameter of 200μm, a central canal diameter of 40 μm, and a wall thickness of 75μm are given by Parfitt (1983a).

Hert and co-workers (1994) demonstrated that the osteons in long bones in man (humerus, ulna, radius, femur, tibia and fibula) are arranged in two helical systems of opposite signs, the inclination of osteon direction from the bone axis being within 5° to 15°. Similar results were found in dog and sheep. Osteon orientation in opposite oblique directions was also demonstrated previously by Lanyon and Bourne in the diaphysis of the sheep tibia (1979).

The concentric lamellae in secondary osteons are 2 to 2·5μm thick (Jaworski 1992), which is the same as the diameter of the collagen fibre bundles seen in surface views of lamellar bone matrix (Boyde 1972).

Collagen fibres in Haversian systems are, it is hypothesised, arranged in a manner best suited to perform their biomechanical function as bone adapts to its function. The proportion of longitudinal and transverse lamellae within osteons varies, so that they can be classified into groups considering their appearance in polarised light. The net lamellar orientation has been correlated with function in man and other animals (Gebhardt 1905; Ascenzi, Bonucci 1964, 1967, 1968; Evans and Vincentelli, 1969, 1974; Boyde et al 1984a).

Osteons are of three types depending on the mix of the constituent collagen fibres. Secondary osteons with a high proportion of LS collagen appear dark in a transverse section of a long bone cortex, while those with TS collagen appear bright in polarised light in a bone cross-section (Ascenzi and Bonucci 1964; Portigliatti-Barbos et al 1984; Ascenzi et al 1990). Conversely, in longitudinal bone sections the longitudinal lamellae are bright and transverse lamellae are dark (Ascenzi et al 1990). An alternate type (containing alternate longitudinal and transverse lamellae) exhibits alternation of dark and bright lamellae in both cross and longitudinal section in polarised light. Evans (1974) differentiated

osteons into predominantly dark, predominantly bright and intermediate between dark and light. Studying single isolated osteons, Ascenzi and co-workers (1990) showed that the osteons with longitudinal fibres are suited for loading in tension, and those with transverse fibres are better able to withstand loading under compression. However, osteons do not exist in isolation in bone, and the relevance of these observations is therefore not clear.

Portigliatti-Barbos et al (1983) found a characteristic distribution of osteonal types within entire cross sections of human femora. A similar characteristic collagen fibre orientation pattern - somehow or other probably correlating with regions of tension and compression - could also be demonstrated without making reference to single osteons and therefore without considering the osteonal types distinguished in Ascenzi's earlier work [eg in human long bones [femoral shaft (Boyde et al 1984a; Portigliatti-Barbos et al 1984, 1987; Ascenzi 1988); tibial and fibular shaft (Carando et al 1989); humerus, ulna and radius (Carando et al 1991); femur, tibia and fibula (Ascenzi et al 1990]. Such "mapping" relied upon measuring the brightness, in transmitted circularly polarised light, of large areas in the bone section: in fact, even entire large bone cross sections could be studied at once (Boyde and Riggs 1990; Riggs et al 1993a, 1993b).

Extensive work has been done on collagen fibre orientation. Strain character and collagen fibre arrangement have been correlated on several occasions. However, until now, no model of the collagen fibre arrangement in bone lamellae has been accepted without dispute. The most widely accepted model (Ebner 1875; Kolliker 1889; Gebhardt 1905) is that longitudinal and transverse collagen fibres alternate in successive lamellae where the fibres in each lamella lie parallel to each other. In polarised light microscopy the collagen parallel to the plane of section is birefringent, anisotropic, and hence appears bright. The cross-cut collagen is isotropic, extinguishes, and hence appears dark.

Others opined differently. The lamellar pattern, according to Ranvier (1889) and Ziegler (1906), is due to a different structure in successive lamellae, fibrous collagenous lamellae alternating with

homogenous afibrillar layers (intermediate substance). Ruth (1947), Rouiller et al 1952; Frank et al (1955), and Rouiller (1956) attributed the lamellation to the difference in amount of collagen in successive layers, collagen rich layers (compact/fibrillar lamellae) alternating with layers of diffuse lamellae (cementing lamellae) of predominantly ground substance containing a few fibres. The fibrillar lamellae (named for the dense, collagen rich layer) were supposed to contain less mineral (Rouiller et al 1952) and were believed to contain either transverse (Ruth 1947) or longitudinal fibres (Rouiller et al 1952).

Boyde and Hobdell (1969), using SEM, demonstrated that the 'lamellae' of sections appeared in surface views as "domains" within which the collagen fibre orientation is confined. Presence of "domains" of fibres within lamellae (Boyde and Hobdell 1969, Boyde 1972) has also been confirmed by several others (Frasca et al 1977; Pannarale et al 1994).

Recently some workers have disagreed with this view (Marotti and Muglia 1988; Marotti 1990, 1993; Hasegawa et al 1994). They have argued that the difference is in both the quantity of collagen in the lamellae, and in the orientation of the constituent fibres. Collagen rich and collagen poor lamellae alternate with each other. Fibres are not parallel, rather having an interwoven texture in both dense and loose layers. Collagen bundles are continuous throughout the lamellar bone. Dense lamellae are significantly thinner than loose lamellae, but they appear thicker in polarised light at the expense of the intervening loose lamellae. Marotti compared the dense and loose lamallae with transverse and longitudinal lamellae in Gebhardt's model.

It is more generally accepted that the concentric lamellae within the osteons contain collagen of a similar packing density. The fibres lie parallel to one another within the plane of the lamellae (Gebhardt 1905; Cooper et al 1966; Boyde 1972; Ascenzi and Bonnuci 1976; Reid 1986). Several other studies (Lanyon et al 1982; Portigliatti-Barbos et al 1984; Ascenzi 1988; Ascenzi et al 1990; Skerry et al 1988; Boyde and Riggs 1990; Riggs et al 1993a; Riggs et al 1993b) correlated Gebhardt's model with the strain distribution

and resulting characteristic molecular organisation of the collagen fibres within osteons.

The organisation of collagen fibres in different orientations has been associated with the types of strain. Certain weight bearing long bones provide model situations in which the effect of different types of strains on collagen orientation may be studied. The radius of the horse bows in a cranio-caudal direction with a cranial convexity. In loading, it would be expected that all such antero-posteriorly (cranio-caudally) curved, weight bearing long bones of quadrupeds would be subjected to longitudinal tension in the cranial aspect and to longitudinal compression in the caudal aspect (Rooney 1969). Strain gauge studies in vivo have confirmed these predictions in all gaits (Turner et al 1975; Rubin and Lanyon 1982; Biewener et al 1983a, 1983b). Lanyon and co-workers (1975) working with tibia also documented similar results in man. The pattern of collagen fibre orientation assessed by polarised light microscopy of whole cross sections of adult horse radii shows a strong correlation with this strain distribution. In the newborn horse radius, the collagen orientation is longitudinal in all portions of the cortex. In adults, regions of bone subjected to longitudinal compression have been shown to be composed of a high proportion of more transverse collagen (caudal cortex), whereas regions subjected to longitudinal tension are composed of mainly longitudinal collagen (Boyde and Riggs 1990; Riggs et al 1993a). Riggs and co-workers (1993b) working with equine radii also documented the different characteristic mechanical properties of cranial and caudal cortices.

Similar results were obtained in the equine third metacarpal bone, which demonstrated collagen parallel to the longitudinal axis of foal McIII, but a larger proportion of transversely oriented collagen fibres in the palmar and dorsal cortices with increasing age, a feature compatible with an adaptation to compressive strain present in this bone (Riggs 1990; Stover et al 1992).

Using CPL brightness intensity measurement (Boyde et al 1984a), Riggs and co-workers (Riggs 1990; Riggs et al 1993a) showed a greater proportion of transverse collagen and a greater degree of remodelling in the caudal cortex of equine radii.

The purpose of the present work was to examine these findings in an independent study with a different approach, to see whether the acquired difference in the caudal aspect was achieved through secondary remodelling of the primary periosteal bone that grew after birth, to provide a statistical representation of relative placement of primary and secondary osteons in two cortices, and different collagen fibre orientation within the secondary osteons; and finally to look into the prevailing controversy regarding the true arrangement of collagen fibres in Haversian systems.

2.1.2 Use of polarised light in studying bone lamellar organisation

In a polarising microscope, two polaroid filters or two nicol prisms are used. The polariser positioned between the light source and the condenser converts the transmitted light into plane polarised light. The analyser is inserted into the microscope tube.

There are certain objects through which the polarised light passes uninterruptedly. Their components have very little preferred alignment and are incapable of affecting the polarised light. Consequently when viewed between crossed polarisers, no light can pass through and the object appears dark like the background. These are non-birefringent objects, optically isotropic.

Birefringence is an optical property of well aligned submicroscopic structures. It is manifested by an object appearing bright in certain orientations between crossed polars. The vibration plane of the polarised light is altered by oriented elements having different refractive indices within the structure. These objects are birefringent (optically anisotropic, doubly refractive).

The birefringence of an object is either due to the characteristic arrangement of the molecular or atomic structure it contains (intrinsic birefringence), or may be due to ordered nonrandom structure, the regularity of which is on a scale smaller than the wavelength of light. This is due to the submicroscopic, oriented, asymmetric elements of different refractive indices within the structure (form birefringence).

Birefringent materials appear dark (isotropic) between linear crossed polars when the main structure direction is exactly parallel

with the optic axis or to the polariser or the analyser, when light passes through the object unaffected and cannot pass through the analyser, leading to extinction. An object with its structure axis perpendicular to the optic axis disappears completely every 90° during a full rotation with a change in brightness as it rotates. This is a disadvantage encountered in analysing a specimen with linearly polarised light as the brightness is not constant in all rotation positions. Hence it is necessary to examine the image at different angles of rotation.

On the contrary, circularly polarised light allows a constant image achieved using two quarter wavelength retardation plates in addition to linear polarising filters. In circularly polarised light, the signal is constant irrespective of axis of orientation in the plane of section. There is no extinction angle.

Collagen constitutes about 95% of the organic component of bone and is optically anisotropic due to the positive form birefringence generated by the parallel alignment of collagen molecules and intervening water (or embedding medium). The negative form birefringence of the apatite crystals in bone, which are mostly oriented parallel with the collagen, slightly reduces the observed total birefringence of the mixture (the birefringence of a bone section is increased by removal of the mineral component).

In polarised light, the brightness is linearly related to the section thickness. Hence plane parallel sections of uniform thickness must be used for collagen orientation analysis. The fibres parallel to the plane of section exhibit maximum brightness while those parallel to the optic axis (longitudinal) appear dark.

2.2 MATERIALS AND METHODS

Table 2.1

Principal modes of preparation and study of samples.

1. 100µm ground sections, principal planes TS (radial LS, tangential LS)
2. 40 to 50µm ground sections, including 45° to principal planes

3. Mounting in DPX.
4. Polarised light microscopy
5. PLM using Universal stage
6. Autofluorescence mode CSLM
7. Etching by chick osteoclast
8. Gold sputter coating
9. 'Conventional' SE SEM
10. SEM BSE

Seven horse radii, five of known age, 18y (2 animals), 12y, 11y, 6y, and two of unknown age were obtained. The radii were kept frozen until arrangements for preparing sections were made.

Initially, the 18y radius was cut at its midshaft plane and then at about 6 cm proximally (figure 2.1) with a band saw. From the block thus obtained, two pieces were prepared, one from the cranial and one from the caudal cortex, each about 1 cm wide and 6 cm long and containing the centres of the cranial and caudal surfaces. The pieces were marked at their extremities, distal (towards the midshaft plane) and proximal, and kept in 50% methanol. Consecutive plane parallel undecalcified sections of 100 micron thickness were cut using a Buehler Isomet water cooled diamond saw from each of the cranial and caudal pieces of a horse radius of 18 years age starting from the distal end, and then at 1cm apart proximally up to 4cm and then again two sections at 5·5 cm.

Each section was labelled with an indication as to its relative position and measured with a digital micrometer (Mitutoyo, LCD electronic calliper, resolution 0·01 mm) or a screw micrometer at several different places.

The sections were washed clean of loose soft tissue and left in 50% methanol. Afterwards they were treated with absolute alcohol for one hour and then with xylene, mounted with DPX under a large coverslip, and weighed down with pots of lead shot while drying in 37°c oven for 48 hours. Great care was taken to avoid air bubbles. Finally each section was labelled.

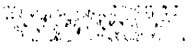

Figure 2.1

The site of the radius where the sections were taken.

Figure 2.1

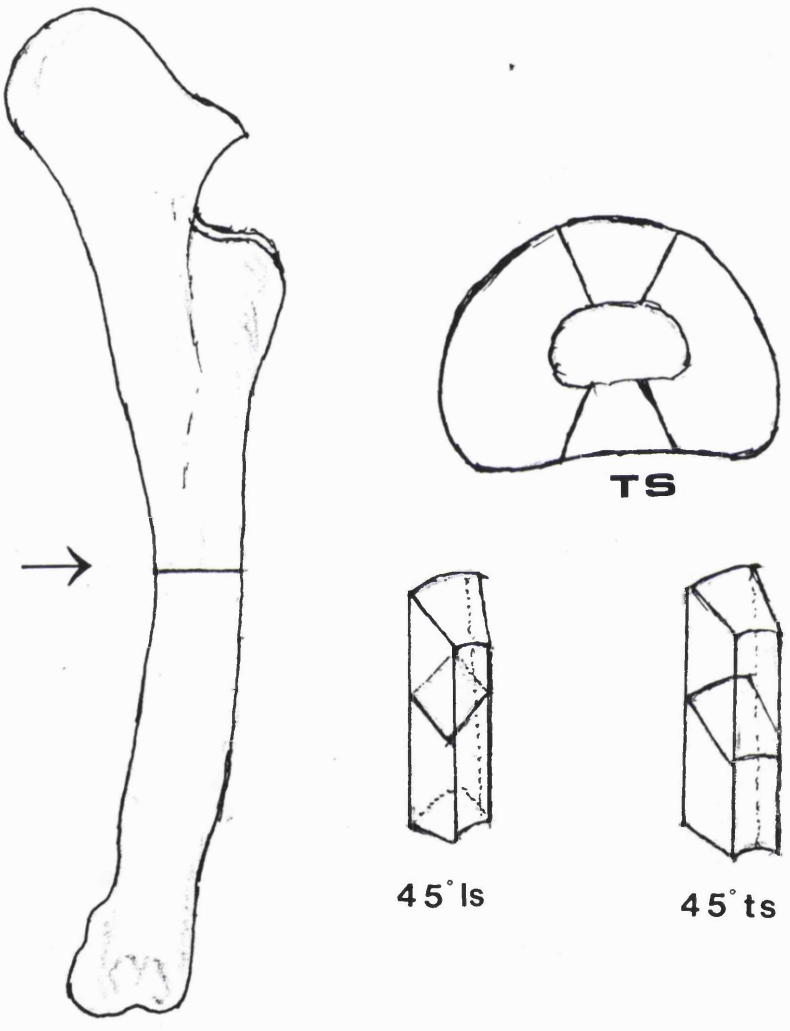

In a similar way, pairs of consecutive, plane parallel undecalcified sections of 100μm thickness were also obtained from the 11y horse radius from both the cranial and caudal cortices, at the midshaft plane and then at 1 cm intervals proximally up to 5 cm. Two pieces of cranial and caudal cortex, about 4 cm. long, containing the centres of the cranial and caudal surfaces were also obtained from a horse radius of unknown age. 30 plane parallel consecutive sections were prepared at 0·43mm intervals. Two sections of 100μm thickness from each extremity and two from the middle (distal - at the midshaft plane, 6.5 mm and 13mm proximally) were mounted in a similar way.

Similar sections from four further animals [6y, 12y, 18y(2) and one unknown age] from midshaft plane and at a plane 3cm proximal were obtained and mounted in DPX.

2.2.2 Inspection for Fatigue damage:

For basic fuchsin staining (Frost 1958, 1959) to reveal possible cracks, one section of 110μm thickness was obtained after each pair of sections taken from the caudal cortex of the 11y and 18y radii. Thus 5 sections were obtained from the caudal cortex of each of the radii of known age and three more 110μm sections from the caudal cortex of the unknown age radius were also chosen. The sections were infiltrated for 24 hours in a 1% (w/v) solution of basic fuchsin in 35% alcohol. Afterwards grinding was performed on carborundum abrasive paper keeping the sections constantly wet. The sections were thoroughly washed, air dried for 60 hours, and mounted in DPX.

2.2.3 Assay of primary and secondary osteons and collagen orientation

All the cranial and caudal sections were examined in linearly polarised light. Osteonal canals of both primary and secondary osteons were counted and the "collagen orientation", i.e bright ("transverse", TS; strictly speaking, oblique) or dark (longitudinal, LS) recorded in twenty $1mm^2$ areas using a square graticule (20

fields of the graticule, periosteal to endosteal). This was done for each pair of sections of known age, using an eyepiece magnification of X10. The magnification of the objective used was also X10. From the unknown age bone, additional twenty 1mm ^{2} areas in the sub-periosteal region were examined. Sections were about 9 mm wide on the periosteal side. 20 areas were taken from within 3mm area of the periosteum: the purpose was to look for any evidence of increased remodelling on the periosteal side.

2.2.4 Quantitative description of proportion of LS and TS collagen.

The character of the collagen orientation (LS or Oblique), in one section of the cranial and caudal cortices of radii of seven animals was observed and recorded using a Merz graticule assessing the condition at every intersection, and choosing the hits on secondary osteons. The hits were categorised as falling into the most peripheral, the midthickness or the central part of each osteons. The Merz grid contains 36 test points, covers an actual area of 1mm^2 and 20 such fields in each of the sections were examined. The number of hits in secondary osteons was thus counted categorising their positions within the osteons.

2.2.5 Examination using Circularly polarised light and Bio-Rad Lasersharp Confocal Scanning Light microscope

Further 100µm thick sections from cranial and caudal cortices of 6y, 11y, 12y, 18y (1), 18y(2) and two unknown age horse radii prepared as above and examined in Circularly Polarised Light, were again examined in the Bio-Rad MRC500 Confocal Scanning Light microscope in autofluorescence mode. The autofluorescence excited by the 488 nm line of the argon ion laser was used to identify the histological features in the sections of both cortices.

The number of the bright (more fluorescent) 2° osteons in the cranial and caudal cortex was recorded by counting in areas measuring either 3 mm AP and 6 mm ML, or 2 mm AP and 6 mm ML (where the cortex was

not broad enough) in subperiosteal, central and endocortical regions.

100 µm thick transverse sections were also prepared as above from the dorsal cortex of McIII of two horses of extreme age (2y? and 24y?) for examination in Confocal autofluorescence microscopy.

2.2.6 Tilted sections of compact bone: LPL, CPL and SEM

Cranial and caudal cortical blocks were obtained from the centre of the midshaft of the radius of an unknown age horse (aged as evidenced by histological features). Sections of varying thickness, 250µm and 100µm, were obtained in orthogonal and 45° tilted planes as follows: sagittal (AP: antero-posterior), coronal (ML: medio-lateral), transverse, 45° radial (tilted transverse), 45° tangential (tilted longitudinal) and 45°+ 45°.

The 100µm sections were cleaned, dehydrated in absolute alcohol and mounted in DPX, examined using polarised light (both linear and circular), and photographed.

The 250µm sections were used for resorption by chick osteoclasts (Boyde et al 1984b; Jones et al 1984, 1985; Reid 1986). The slices were dehydrated and defatted by chloroform:methanol extraction in a Soxhlet apparatus. The shafts of long bones from 19 day pre-hatch chicks were cleaned of periosteum and cartilage, and kept in cooled phosphate buffered saline. The bones were quickly chopped in Eagles minimum essential medium (MEM) with 10% added foetal calf serum and 2 mM L-Glutamine. Bone fragments were agitated to release cells. Drops of the cell suspension were deposited on to the slices. The slices were left for 45 minutes at 37°C and in 5% CO_2 to allow the cells to settle. Then the nonadherent cells were gently washed off with sterile medium. The slices with adherent bone cells were cultured at 37°C in 5% CO_2 in the same medium. After 48 hours, the slices were cleaned of cells, dehydrated in ethanol, air dried, mounted on an aluminium plate with double sided conductive taps and coated with gold by sputtering (Boyde and Jones 1983; Jones et al 1984) for SEM in both secondary electron emission mode (SE) and backscattered electron imaging (BSE) modes, operating at 10KV and 15 - 20 KV respectively (Boyde and Jones 1983; Jones et al 1984).

100 µm TS sections of the caudal side of the radius of an 18y

horse were similarly treated by osteoclastic resorption for 24 hours, and cleaned. These were examined using both CPL and the 3-D Edge microscope, before mounting for SEM.

Several thinner sections (40 - 50μm) were prepared from two horse radii (18y and Unknown age) cranial and caudal cortices, in the TS and 45° tangential (tilted longitudinal) planes, washed, cleaned, dehydrated and mounted in DPX before examination in a Leitz Universal Stage Polarising Microscope. Here the sample is situated in the centre of a glass sphere (actually constructed of two hemispheres) which can be tilted and rotated in 5 axis. The thickness of the object slide requires to be in between 0.9 to 1.1 mm, and the size adjusted to fit and to permit tilting. Two spherical segments, one on top of the object slide, and the other beneath the glass plate are secured with the universal stage. The various layers in the sandwich are optically united using immersion oil. The cortical slices were examined rotating the object slide on its vertical axis, from 310° to 50° (-50° to +50°) at 10° or 15° intervals. A TV CCD camera was used to transfer the images to a frame-store based image analysing computer.

2.3 RESULTS

2.3.1 Assay of osteons, interstitial lamellae and collagen orientation.

Main Features:

1. Most of the cranial, tension cortex of the radius remained unremodelled at all the ages examined. That primary bone in the tension cortex which was remodelled was replaced by osteons with mainly predominantly longitudinal collagen orientation (fig. 2.2a, 2.4ab, 2.11). A few were replaced by osteons with predominantly "transverse" (oblique) fibre orientation (fig. 2.9 and 2.11)
2. Most of the caudal compression cortex had undergone remodelling, such that the primary bone was replaced mainly by osteons with predominantly "transverse" (oblique) collagen orientation (fig. 2.2b,

2.3ab, 2.11). Some replacement, though sparse, was by osteons with predominantly longitudinal (dark) fibre orientation (fig. 2.2b, 2.11). The greater the age of the animal, or the greater the intensity of remodelling, the lesser was the number of dark (LS) osteons in the caudal cortex. Where present, they were mainly located toward the endosteal aspect.

3. In the caudal cortex, remodelling was pronounced on the periosteal side (fig. 2.3a-b, 2.7) where the sub-periosteal circumferential lamellae were substantially replaced. In the cranial cortex, remodelling was more marked towards the endosteal side (fig. 2.4a-b).

4. Almost all secondary osteons, irrespective of their character or location, exhibited bright lamellae at their peripheries.

5. In the tension cortex, the secondary osteons were of first generation, whilst, depending on age, second or third order osteons prevailed in the compression cortex.

6. Remnants of secondary osteons formed the interstitial lamellae in the heavily remodelled sites in the caudal (compression) cortex (fig. 2.3), whilst circumferential lamellae, primary plexiform and osteonal structures constituted those in the rest of the caudal cortex (fig. 2.2b), and in the cranial cortex (2.2a, 2.4).

7. The degree of remodelling did not match with (increasing) age in all the animals. Bone of similar ages from different animals did not show equal remodelling. Some younger bones exhibited a greater degree of remodelling than older ones (fig. 2.3a-b, 2.11).

8. The total count of osteons was not always greater in the caudal (compression) cortex (Table 2.2, fig. 2.5), but the number of secondary osteons in the caudal (compression) cortex was always 2 to 4 times greater than that in the cranial (tension) cortex in all ages (fig. 2.6)

Riggs (1990) described a gradual increase in the amount of remodelled tissue present in the cortices with increasing age. The present study suggests that there is substantial individual variability, such that even younger animals can be more extensively remodelled than their older counterparts (fig. 2.3), and animals at a greater age may still exhibit extensive areas of unremodelled bone in

both cortices (2.2a-b, 2.3b, 2.4b, 2.10a). This feature also is not entirely consistent with the suggestion that the collagen orientation pattern characteristic for the adult horse radius develops during the first two years of life (Riggs 1990). The continuous replacement of

Table 2.2.

Relative number of primary and secondary osteons in cranial and caudal cortices of radii of five known and two unknown age horses as percentages (Derived from the data obtained from twenty $1mm^2$ areas in each of cranial and caudal sections).

Age	Osteons	Cranial	Caudal
6y	Primary	58	0
	Secondary	42	100
11y	Primary	53	18
	Secondary	47	82
12y	Primary	55	3
	Secondary	45	97
18y	Primary	40	2
	Secondary	60	98
18y(2)	Primary	64	9
	Secondary	36	91
Unk.1	Primary	48	4
	Secondary	52	96
Unk.2	Primary	56	31
	Secondary	44	69

Figure 2.2

CPL micrographs (montage) of 100 μm thick sections of **a**) the cranial (left) and **b**) the caudal (right) cortices of a 11 year old animal. The periosteal margin of the cranial section is towards the top, whilst that of the caudal section is at the bottom.

a) Most of the bone in the cranial cortex is unremodelled: the number of 2° osteons is very low. The primary osteonal bone is dark whilst the radial woven bone struts and plexiform sheets are bright. A few bands of bright lamellae, parallel to the circumference still exist in the periosteal third of the cortex. The circumferential lamellar bands are seen to be replaced by 2° osteons in places. The 2° osteons are predominantly dark.

b) The caudal cortex is highly remodelled by 2° osteons containing predominantly bright collagen, the more so on the periosteal side. This cortex shows a few dark 2° osteons. Some part of the bone in the endocortical region of the caudal cortex is yet unremodelled and the peripheries of all 2° osteons in the both cranial and caudal cortices are bright.

fig. 2.2

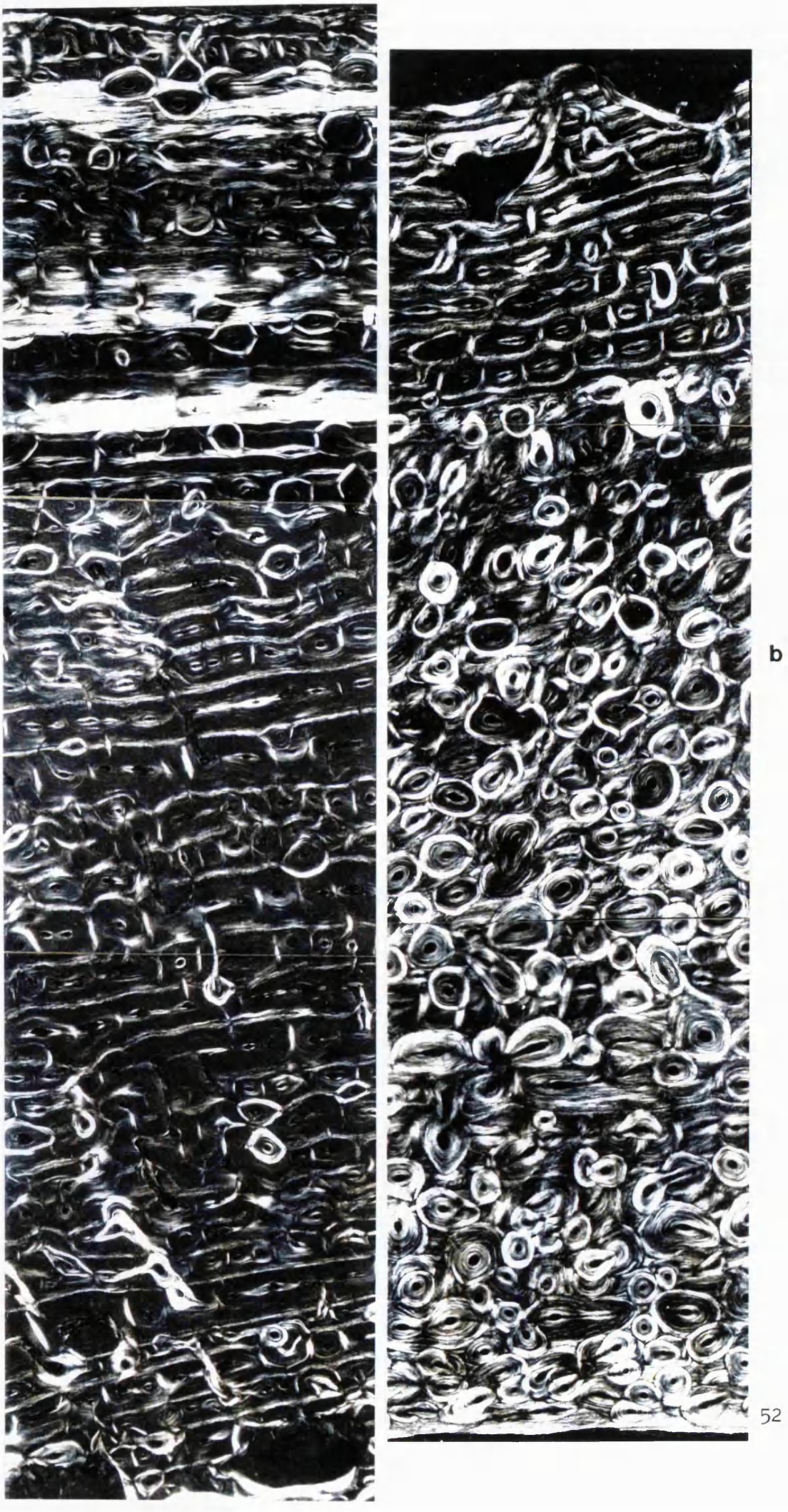

a

b

Figure 2.3

a-b) CPL micrographs (montage) of 100 µm thick sections of the caudal, compression cortex of **a)** 6 year (left) and **b)** 18 year (right) old animal. The periosteal margin is towards the bottom of each picture.

Both show extensive remodelling. The sub-periosteal circumferential lamellae are substantially replaced. Second or third order osteons are present. The cortex in the younger animal is more extensively remodelled such that the primary bone content is completely replaced. The cortex of the older one still contains a bulk of primary bone in its endocortical region. Conversion to a more cancellous structure is seen in the endocortical region of the cortex of the 6 year animal. Dark 2° osteons are very scant in the cortex of either animal.

fig. 2.3

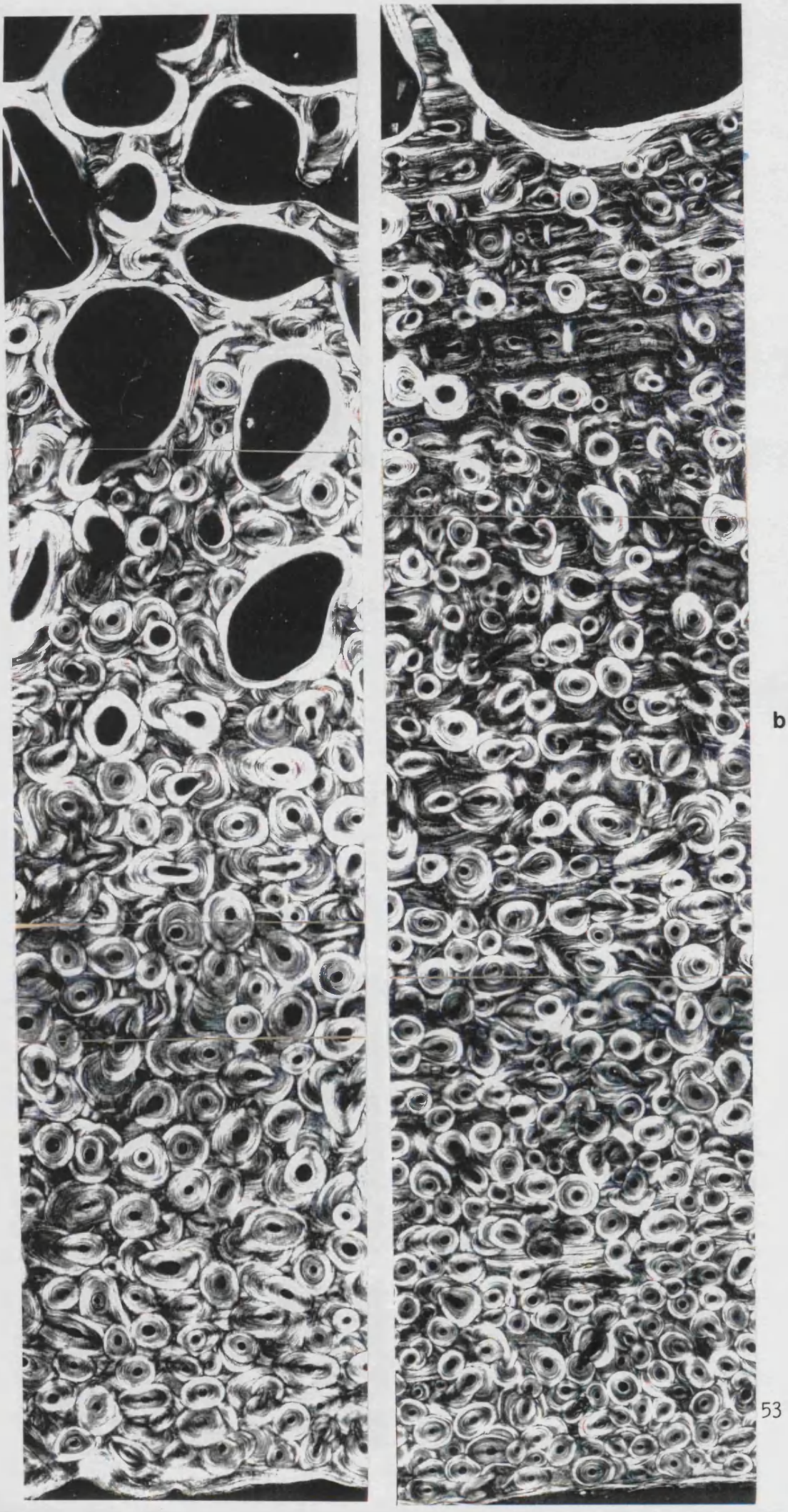

a

b

Figure 2.4

a-b) Circularly polarised light micrographs of 100 μm thick sections of the cranial, tension cortex of **a)** 6 year (left) and **b)** 18 year (right) old animal, both showing a high proportion of unremodelled bone. The periosteal margins are at the top of the picture.

The cranial cortex of the 6 year old animal is more remodelled, and shows a fair distribution of 2° osteons in its mid-cortex. The degree of remodelling is apparently greater in the endocortical (lower) region of the cortex in both the animals, very few 2° osteons contain oblique collagen fibres.

fig.2.4

a

b

primary bone, containing predominantly longitudinal collagen, by secondary osteons, containing either predominantly transverse/oblique fibres or longitudinal fibres, in both the cranial and caudal cortices eventually leads to the development of the characteristic collagen fibre orientation pattern, but this occurs over a period of time which varies in different animals.

Here is a description of the observations in more detail:

The cranial (tension) cortex: Primary plexiform and osteonal bone occupies the greater part of this cortex in all animals, and it predominates in the midcortex. These osteons appear predominantly dark in polarised light (fig. 2.a, 2.4, 2.11). In almost all cases, the plexiform framework showed brighter fibres; in some animals, some of the primary osteons were also bright (fig. 2.10b, Table 2.5-2.12).

The primary bone was partly replaced, and mostly by osteons with predominantly longitudinal fibres, within a range of 79%-96% of the total secondary osteons (Fig. 2.11). In some older animals (18y: 2 animals, 12y), the proportion of primary bone is quite high in comparison to that in younger horses (Fig. 2.4b, 2.9b). Although in the majority of animals, the number of secondary osteons was greater on the endosteal side, yet in some animals (eg 6y and 12y) the incidence was the same throughout the cortex (Fig. 2.4a, 2.9b). Exceptionally, in one animal (unknown age specimen 1, the older of the two unknowns), the periosteal aspect was greatly remodelled. In the same animal, the number of secondary osteons superceded the number of the primary osteons (Table 2.2).

In addition to the bright subperiosteal circumferential lamellae seen, a few bands of bright lamellae, parallel to the circumference were observed in the periosteal third of the cortex in all animals. These lamellar bands are separated from each other by the plexiform bone framework (Fig. 2.4b). The circumferential lamellae were partly replaced by secondary osteons with predominantly longitudinal collagen (2.2a, 2.8c).

The number of the primary osteons was greater than that of the secondary osteons (Table 2.2). The secondary osteons were mainly of

Figure 2.5

Average number of osteons in the cranial and caudal cortices of seven equine radii. Remodelling does not always increase the total number of osteons in the caudal cortex.

Figure 2.5

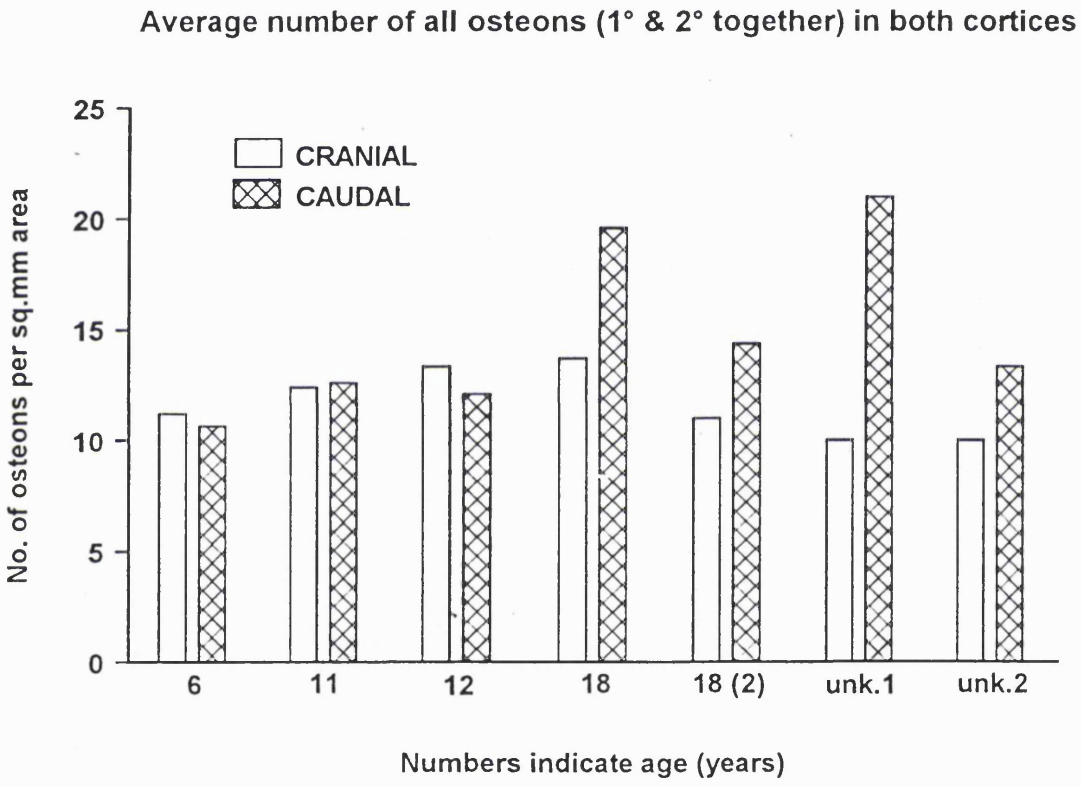
Average number of all osteons (1° & 2° together) in both cortices
No. of osteons per sq.mm area
25
20
15
10
5
0
CRANIAL
CAUDAL
6
11
12
18
18 (2)
unk.1
unk.2
Numbers indicate age (years)

Figure 2.6

Average number of secondary osteons in cranial and caudal cortices of seven equine radii per mm^2. The density increased by about three fold in the caudal cortex of some animals. The osteons were counted in an AP transect in 20 (mm^2) areas in each of the sections.

Figure 2.7

Number of secondary osteons per mm^2 in cranial and caudal cortices of radius of one animal, once in 20 areas on the periosteal side, and then again in 20 areas extending from periosteum to endosteum of each sections. The increased number on the periosteal side is quite apparent.

Figure 2.6

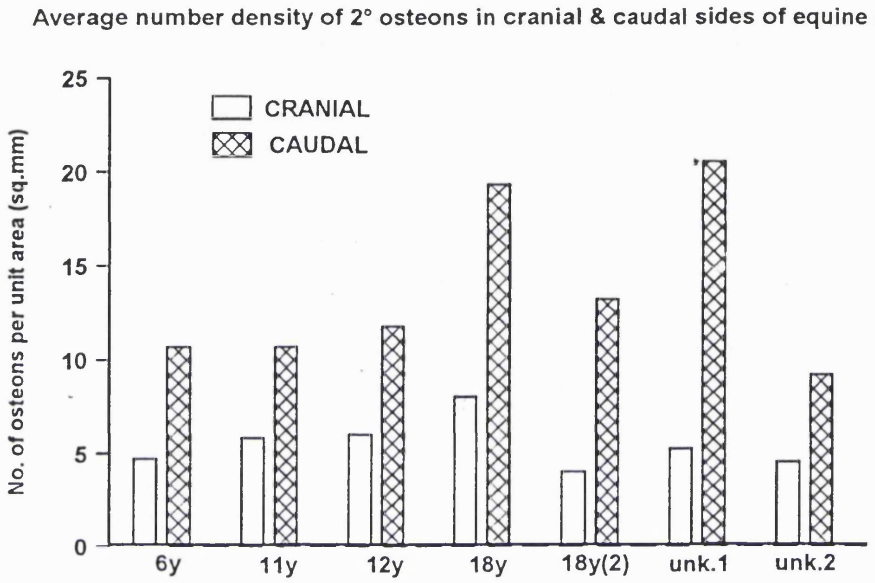

Figure 2.7

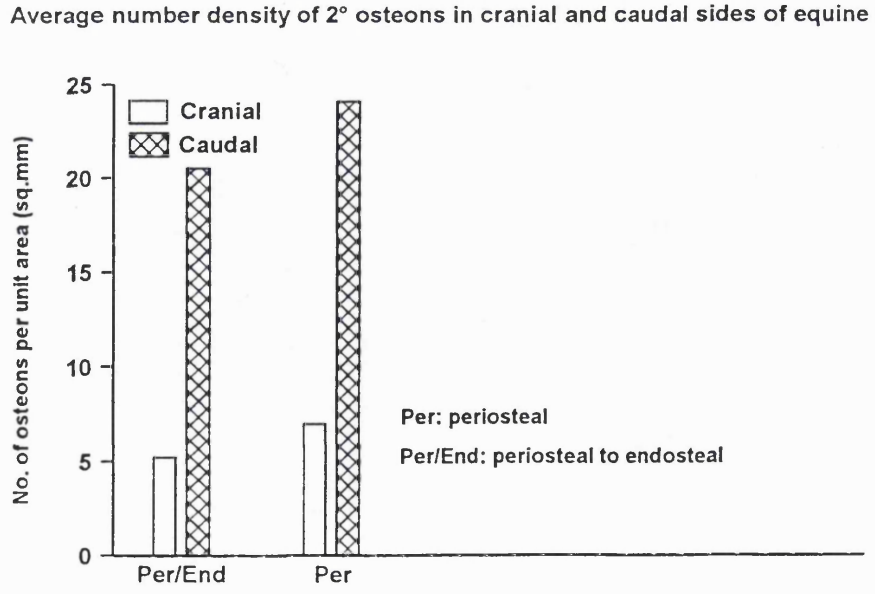

the first generation. Generally, no increase in osteonal canal size was evident, although in some animals few osteons with larger osteonal canals were observed towards the endosteum. Secondary osteons, irrespective of their location, invariably exhibited bright lamellae at their peripheries; a constant observation in all animals of all ages.

The caudal (compression) cortex: The caudal cortex in all animals was greatly remodelled and composed of secondary osteons with predominantly transverse/oblique fibres (Fig. 2.3). The number of secondary osteons was always far greater than primary osteons, which were very scant (Fig. 2.3b, Table 2.2). However, the extent of remodelling varied in different animals and without any apparent relationshiop with age. Some younger animals exhibited greater degree of remodelling than older ones; in a 6 year old, the cortex was completely remodelled (Fig. 2.3a, 2.11).

Generally, remodelling was intense on the periosteal side, where primary osteons were almost absent (Fig. 2.3, 2.7). In some animals, the periosteal lamellae were totally replaced by new osteons (Fig. 2.3). The extent of previous remodelling activity gradually reduced from mid-cortex to endosteum (Fig. 2.2b, 2.3b). Some older animals showed a greater proportion of unremodelled bone than younger animals; for example about one fourth of the volume of the cortex towards the endosteal aspect was primary (Fig. 2.2b).

Almost all animals had a very small number of secondary osteons with predominantly longitudinal fibres, within a range of 0 -15% of the total secondary osteons. In some animals these were totally absent, and more were seen in some older animals, the fraction of such osteons being more toward the endosteum and in the centre of the cortex (Fig. 2.11).

The number density of secondary osteons in the caudal cortex was usually 2 to 4 times that in the cranial cortex (2.6). The total count of the osteons in the caudal cortex was generally greater than in the cranial (fig. 2.5). Secondary osteons were generally smaller than in the cranial cortex.

Figure 2.8

a-b) LPL micrographs of the cranial cortex of an 11 year old animal showing **a)** dark 2° osteons with bright peripheries (top), **b)** 45° rotation of the specimen unmasks the bright components in the plexiform and the primary osteonal bone (middle), and **c)** CPL image of the same specimen (bottom).

Figure 2.8

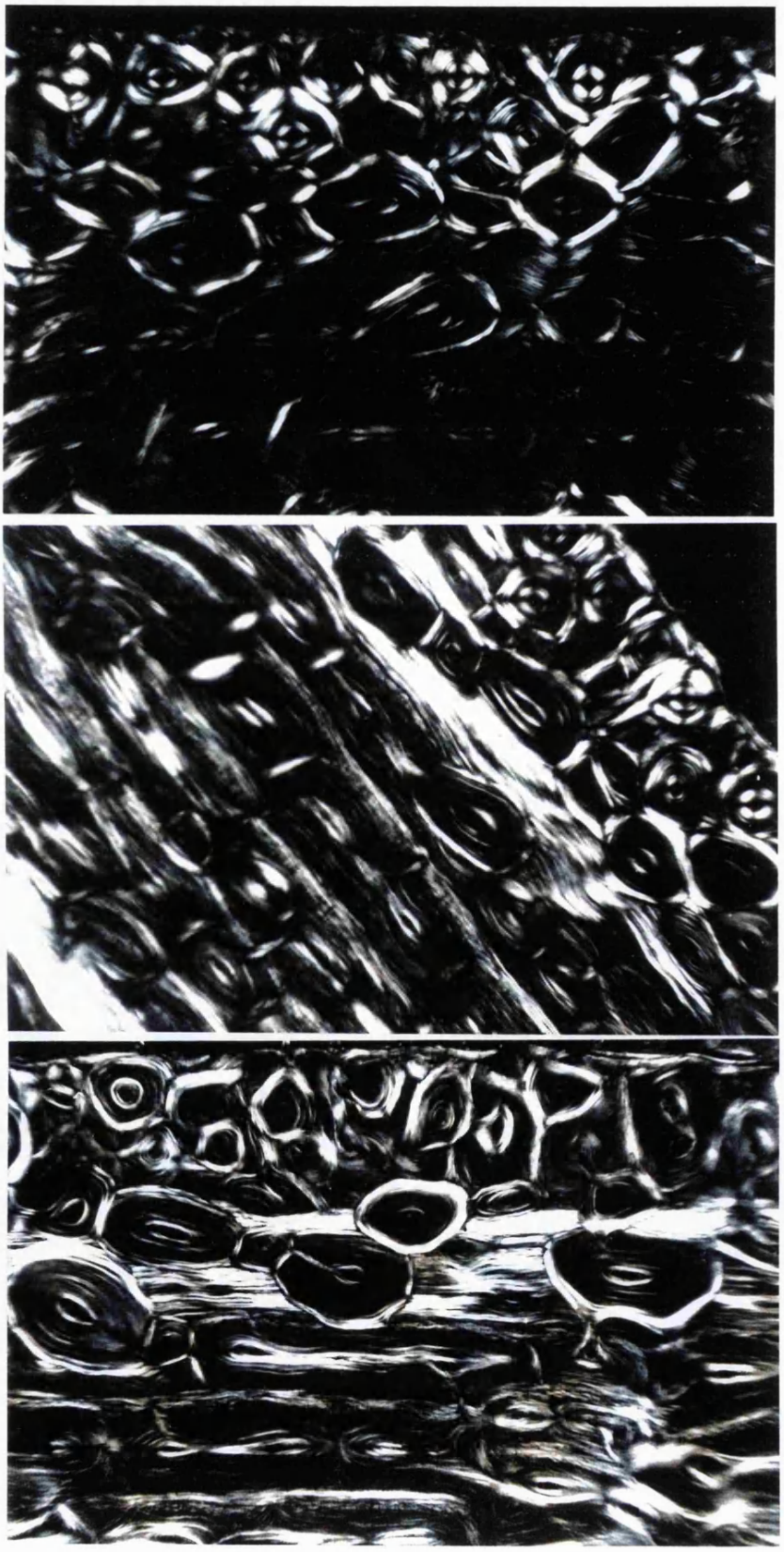

Figure 2.9

a) The cranial cortex of an 18 year (#2) old animal (top) showing a few 2° osteons containing predominantly oblique (bright) fibres.
b) The cranial cortex of a 12 year old animal (bottom) showing a fair distribution of 2° osteons in its periosteal third.

Figure 2.9

a

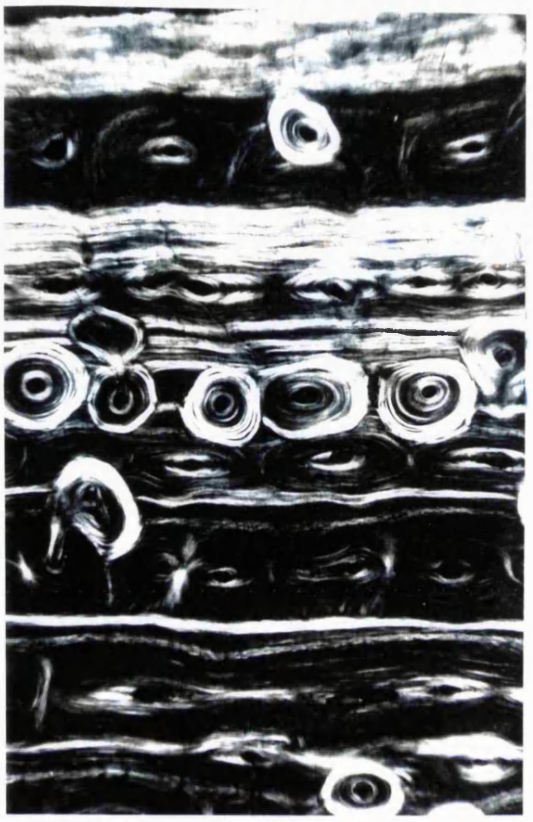

b

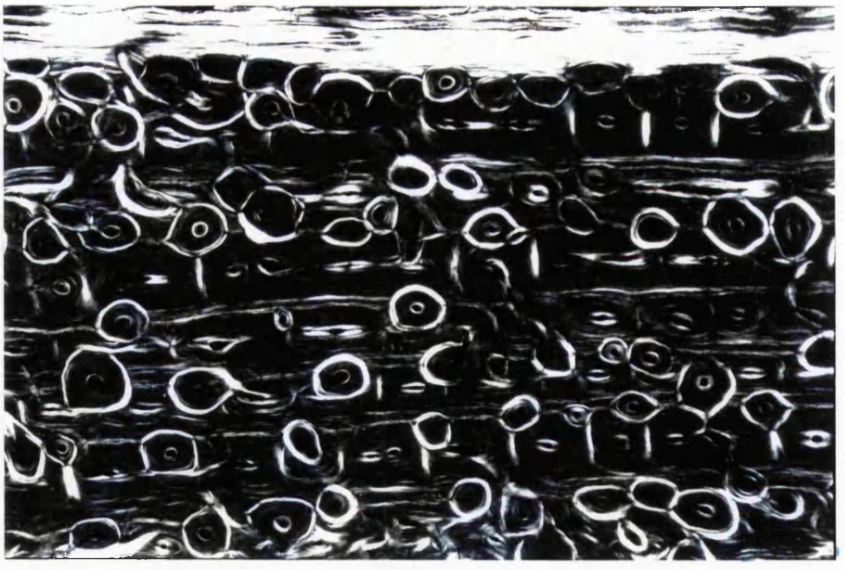

Figure 2.10

a-b) CPL image of a) the caudal cortex of an 18 year (#2) old animal showing a greater bulk of unremodelled bone towards its endocortical region. The primary bone exhibits some bright collagen in its content. Note retained Sharpey fibres.
b) The cranial cortex of a 6 year old animal showing bright collagen lamellae in its primary bone.

Figure 2.10

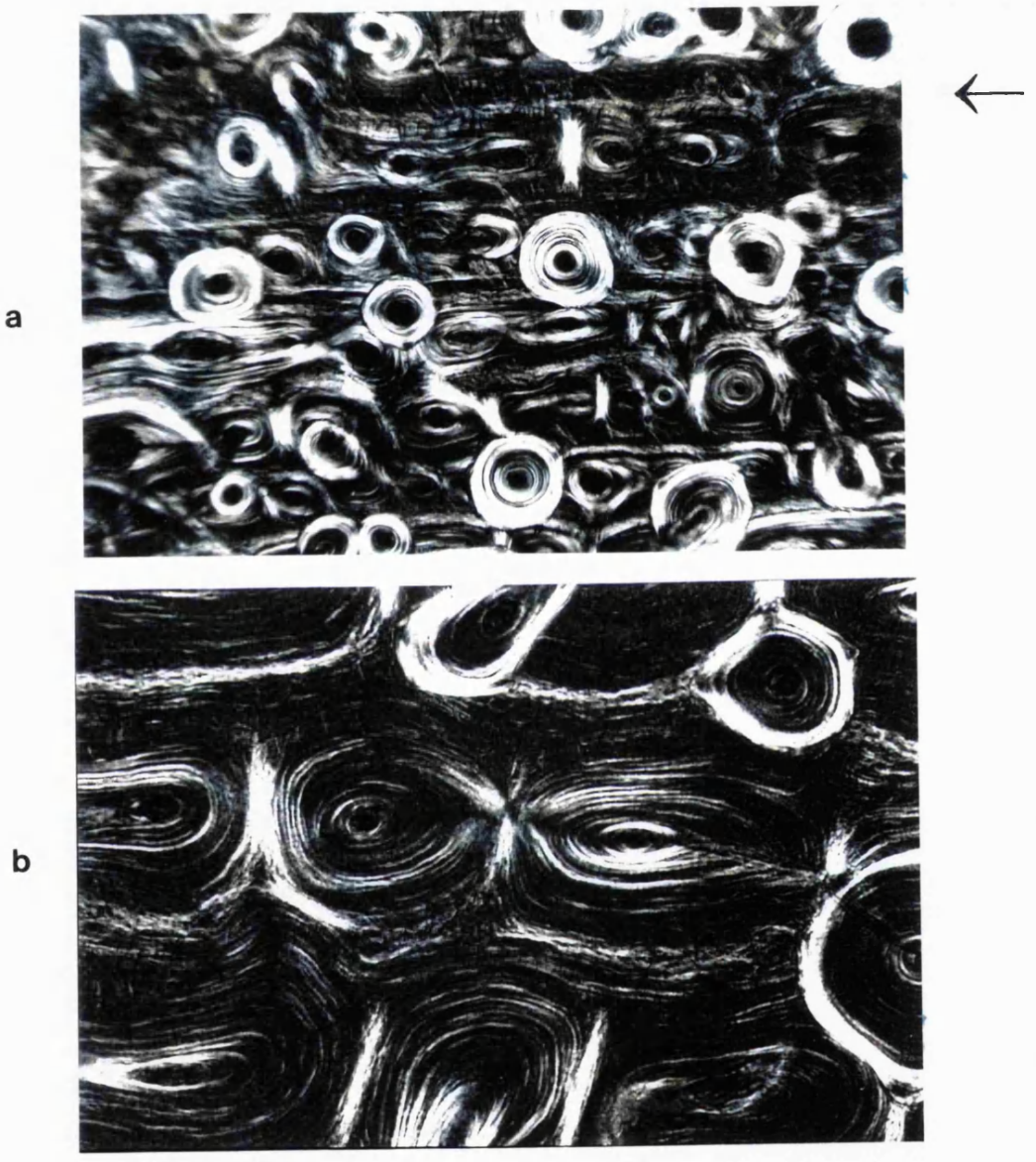

Figure 2.11

Secondary osteons with predominant longitudinal (dark) and oblique (bright) collagen orientation in the cranial and caudal cortices of seven equine radii as percentages of the total secondary osteons. The compression cortex when remodelled contained mostly secondary osteons with predominant oblique collagen orientation.

Figure 2.11

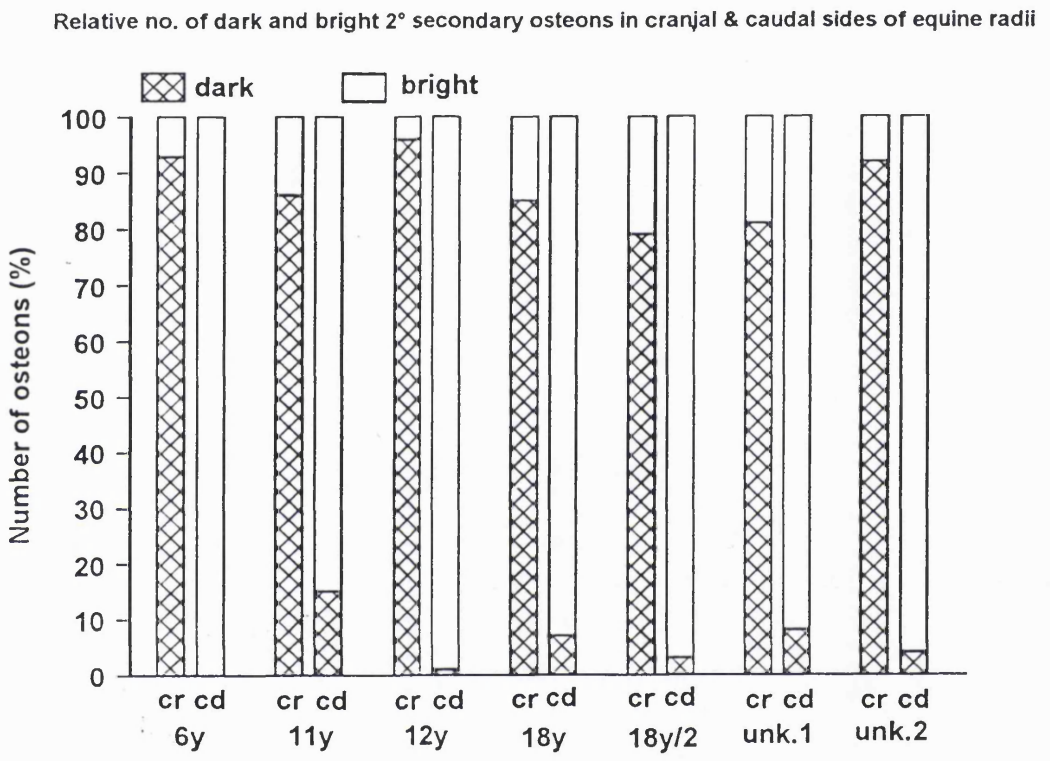
Relative no. of dark and bright 2° secondary osteons in cranial & caudal sides of equine radii
dark
bright
Number of osteons (%)
100
90
80
70
60
50
40
30
20
10
0
cr cd
6y
cr cd
11y
cr cd
12y
cr cd
18y
cr cd
18y/2
cr cd
unk.1
cr cd
unk.2

The number of osteons with a larger canal lumen gradually increased from midcortex to the endosteum, but there were exceptions, and some animals showed osteons with larger canals in the periosteal region (2.3a-b).

There were more recently resorption spaces, ie recent cutting cones, in the caudal cortex than in the cranial cortex, and their number gradually increased from midcortex to endosteum (Fig. 2.3a-b)

Secondary osteons of second or third order generations were observed in different animals (Fig. 2.3b). Interstitial lamellae were the remnants of remodelled osteons in some animals, while primary plexiform and osteonal bone structures constitute a variable amount of the cortex in cases which showed a lower degree of remodelling (Fig. 2.2b, 2.3b). The primary bone also contained bright fibres in addition to the predominantly longitudinal component (Fig. 2.10b).

2.3.2 Quantitation of collagen having different orientations in the tension and compression cortex.

The findings as described above are quite consistent with the data obtained by stereological counting of collagen lamellae, categorising them into either bright or dark, and most peripheral, centre thickness, and endosteal within the secondary osteons in cranial and caudal cortical sections. Pooling all the results for the caudal cortex for all animals and all ages, the PLM bright constituted 90% to 100% (Table 2.3, Table 2.13 - 2.19). Excluding the peripheral hits on transverse/oblique lamellae (since almost all dark secondary osteons have a bright component at their peripheries), the proportion of bright lamellae in polarised light in the secondary osteons in the cranial cortex ranged from 7% to 24% (fig. 2.12). 76% to 93% of the total oblique lamellae within the secondary osteons in cranial cortices were those present at the peripheries (fig. 2.12).

2.3.3 The question of incipient cracks.

Osteocyte lacunae and the canaliculi were well demonstrated in the basic fuchsin stained sections. There was no evidence of

Table 2.3

Proportion of oblique ('transverse'= PLM bright) and longitudinal collagen lamellae in secondary osteons in the cranial and caudal cortices of seven equine radii: expressed in terms of number of hits on either bright (oblique) or dark (longitudinal) lamellae, and also as percentages of the total hits on the lamellae in the secondary osteons in 20 areas. Merz grid contains 36 hits in 1 sq.mm area. 20 such fields in each of the sections were examined. In some animals, the compression cortex was completely remodelled with secondary osteons containing oblique fibres. The apparent bulk of oblique lamellae in cranial cortices actually represents mostly those fibres at their peripheries (see figure 2.13)

Age & site	Total hits	Oblique	Longitudinal	% (obl./Long.)
6y Cranial	188	130	58	69.15/30.85
6y Caudal	643	643	0	100/0
11y Cranial	198	129	69	65.15/34.85
11y Caudal	409	402	07	98.29/ 1.71
12y Cranial	165	106	59	64.25/35.75
12y caudal	575	575	0	100/0
18y Cranial	316	227	89	71.84/28.16
18y Caudal	662	597	65	90.18/ 9.82
18y(2) Cr.	108	76	32	70.38/29.62
18y(2) Cd.	445	445	0	100/0
Unk.1 Cr.	125	88	37	70.40/29.6
Unk.1 cd	590	543	47	92.03/ 7.97
Unk.2 Cr.	198	131	67	66.16/33.84
Unk.2 Cd.	334	319	15	95.50/ 4.5

Figure 2.12

Relative distribution of oblique lamellae within secondary osteons in the cranial (tension) cortex of seven equine radii. More than 75% of the oblique collagen present in the secondary osteons in cranial cortex lies at their (2°) peripheries.

Figure 2.12

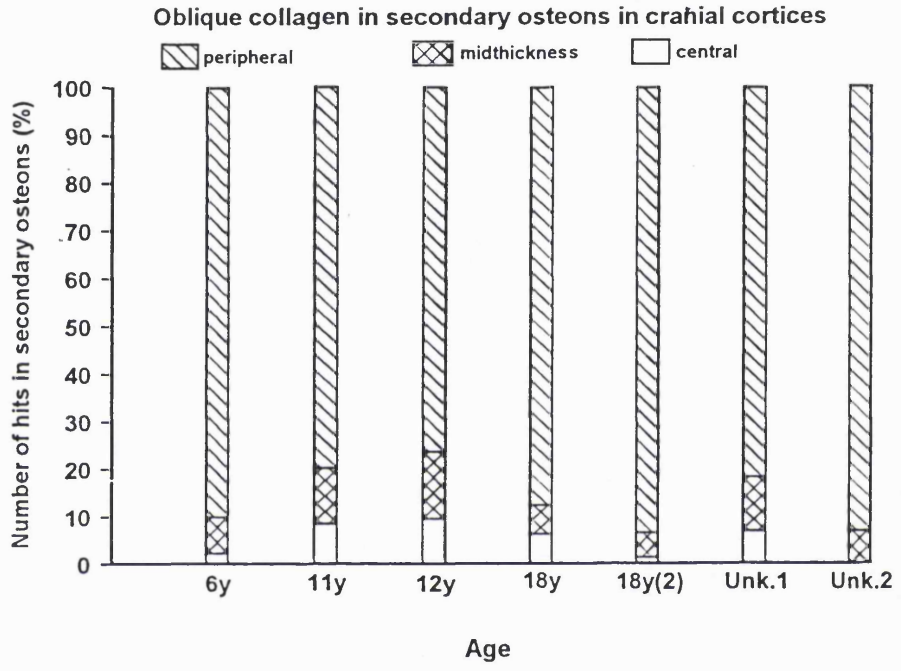
Oblique collagen in secondary osteons in cranial cortices
peripheral
midthickness
central
Number of hits in secondary osteons (%)
100
90
80
70
60
50
40
30
20
10
0
6y
11y
12y
18y
18y(2)
Unk.1
Unk.2
Age

unstained compartments (micropetrotic bone of Frost) in the sections, and there were no stained micro-cracks.

2.3.4 Observation in Confocal scanning light microscopy.

The primary bone (both plexiform and primary osteonal), whether present in the cranial or in the caudal cortex, is generally more fluorescent than the secondary bone (figures 2.13 a-b, 2.14a, 2.15a, 2.16a-b); the plexiform bone gives a higher autofluorescence signal than the primary osteonal bone (figures 2.13a-b, 2.14a, 2.16c-d). Since the cranial cortex is mostly unremodelled and contains more primary bone, its general appearance is brighter than the caudal. The greatly remodelled caudal cortex exhibits less autofluorescence (figures 2.13d, 2.15b).

The majority of secondary osteons in both cranial and caudal cortices are dark (figures 2.13c-d, 2.15b). These are the darkest components in both the cortices, and hence appear darker than surrounding bone. The caudal cortex is less bright (autofluorescent) than the cranial, as its primary bone content is greatly reduced, and contains more 2° osteons due to a greater degree of remodelling.

Some 2° osteons in both the cortices are bright with variable intensity (figures 2.13a-d, 2.14b, 2.17a-b; 2.18a-b) the number is greater in the caudal cortex (figure 2.14a, table 2.4). Some among them are even brighter than the plexiform bone structure (figures 2.13a-b, 2.14b). Again, the caudal cortex contains more of this type of 2° osteons (table 4, fig. 2.14b). In general, the caudal cortex of older animals (eg 18y-1, 18y-2) contains a greater number of both of these types (fluoresecent and more fluorescent) of osteons (Table 4). The number of bright 2° osteons is relatively less in the greatly remodelled caudal cortex of a younger animal i.e., 6y (Table 4), which eventually gives an overall lower autofluorescence signal than that of older animals.

Figure 2.13

a-b) The cranial cortex of two 18 year old horses in its periosteal aspect (top row) as seen in confocal autofluorescence mode (BioRad MRC Lasersharp 500, 488nm excitation >515nm fluorescence). The number of 2° osteons is relatively low. The primary bone gives higher autofluorescence than the new 2° osteons which appear dark. Highly autofluorescent 2° osteons in the both animals exhibit intermittent resting lines within them. FW: a & b = .76 mm

c-d) The centre of the caudal cortex (midcortex) of two 18 year old horses (bottom row) in confocal autofluorescence showing densely packed 2° osteons with different levels of autofluorescence. FW: c & d = 2.4 mm.

Figure 2.13

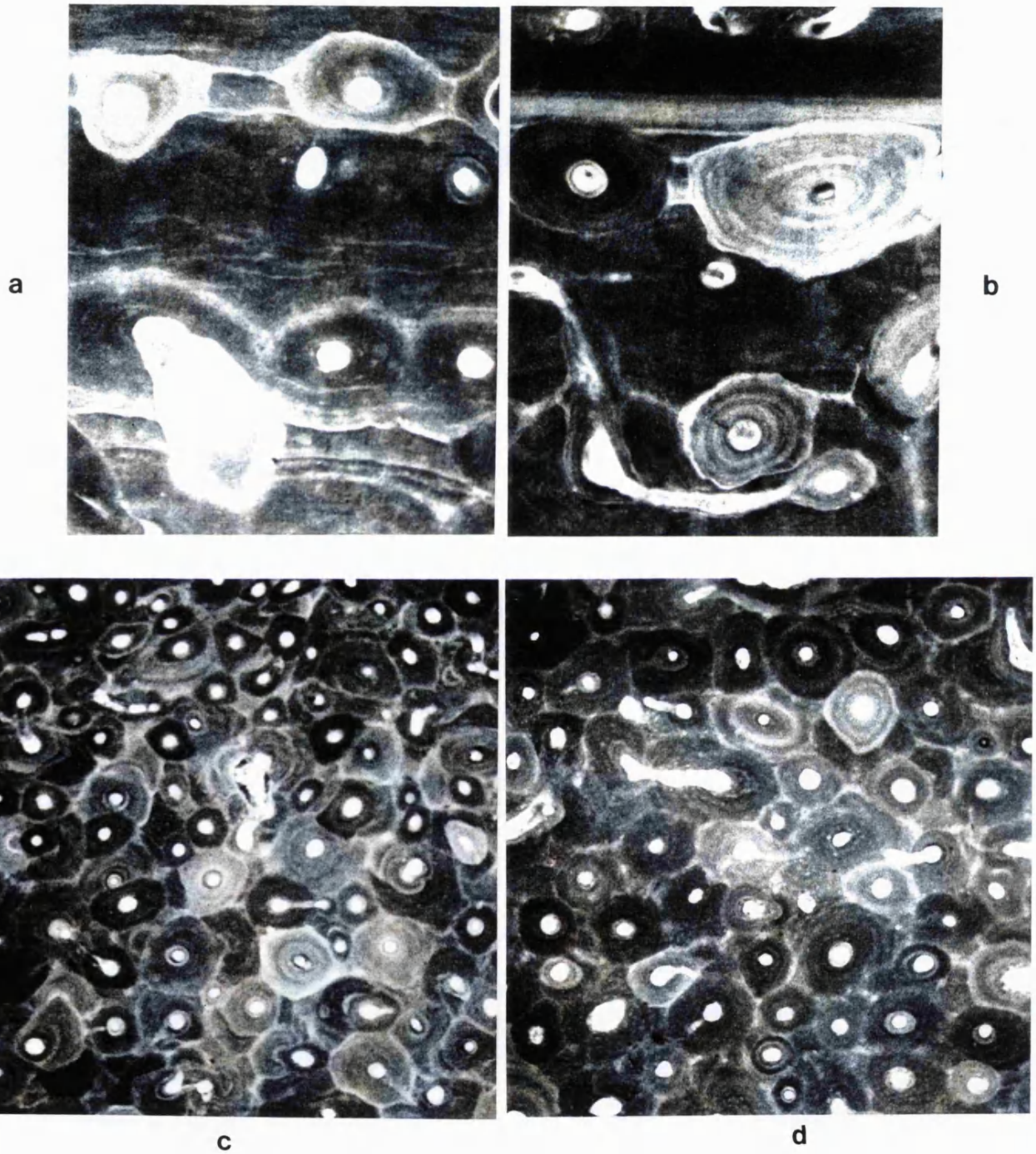

Figure 2.14

a-b) The sub-periosteal region of **a)** the cranial (top) and **b)** the caudal cortex (bottom) of a 18 year old animal as seen in the confocal autofluorescence.

a) The cranial cortex is the least remodelled, and its primary bone content is more autofluorescent than the new 2° osteons. FW = 1.35 mm.

b) Newer 2° osteons generally exhibit the least autofluorescence, but one very small 2° osteon is brighter than the darker neighbours within which it developed. Some show brighter cement lines within them. FW= 1.35 mm.

The osteons in the both cortices show different levels of autofluorescence. Different autofluorescence levels in the individual osteons indicate progressive increasing mineralisation.

Figure 2.14

a

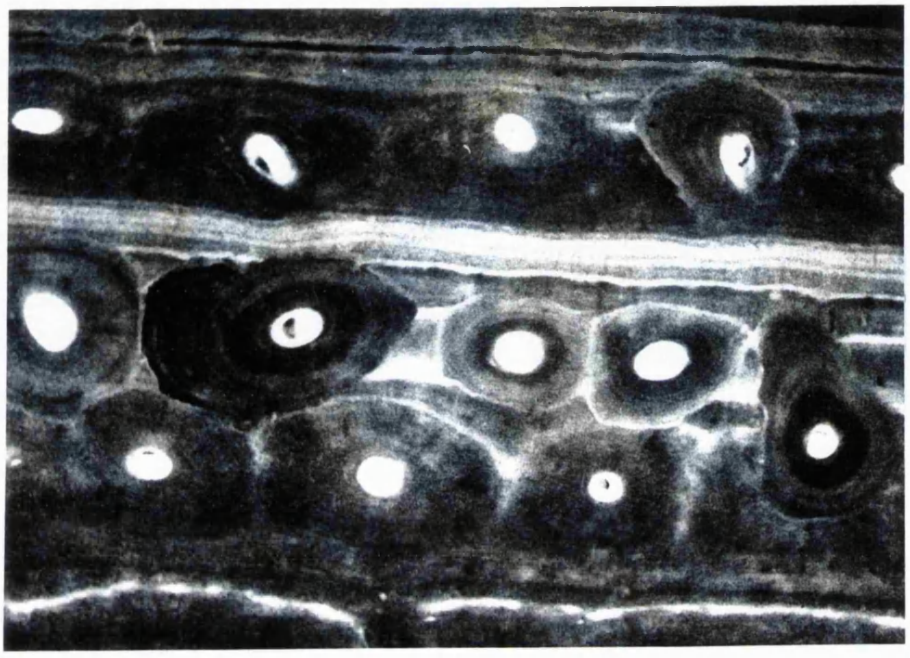

b

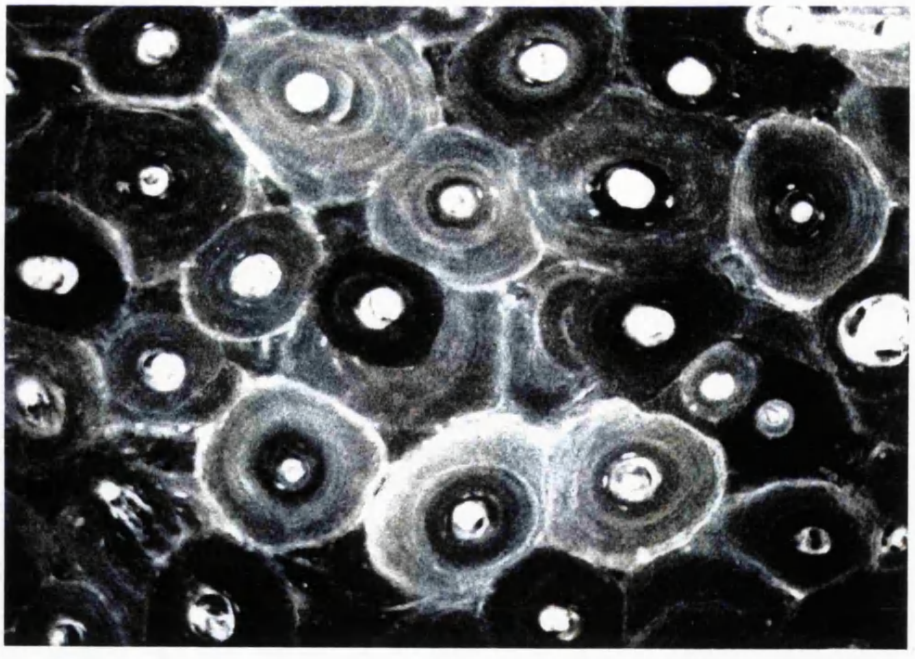

Figure 2.15

a-b) Confocal autofluorescence images of **a)** the cranial (top) and **b)** the caudal (bottom) endocortical region of two 18 year old animals. **a)** The unremodelled primary osteonal bone in the cranial cortex is more fluorescent than the 2° osteons which appear dark. FW= 1.35mm. **b)** The caudal endocortical side is remodelled, and hence exhibits less fluorescence. FW = 1.35 mm.

Figure 2.15

a

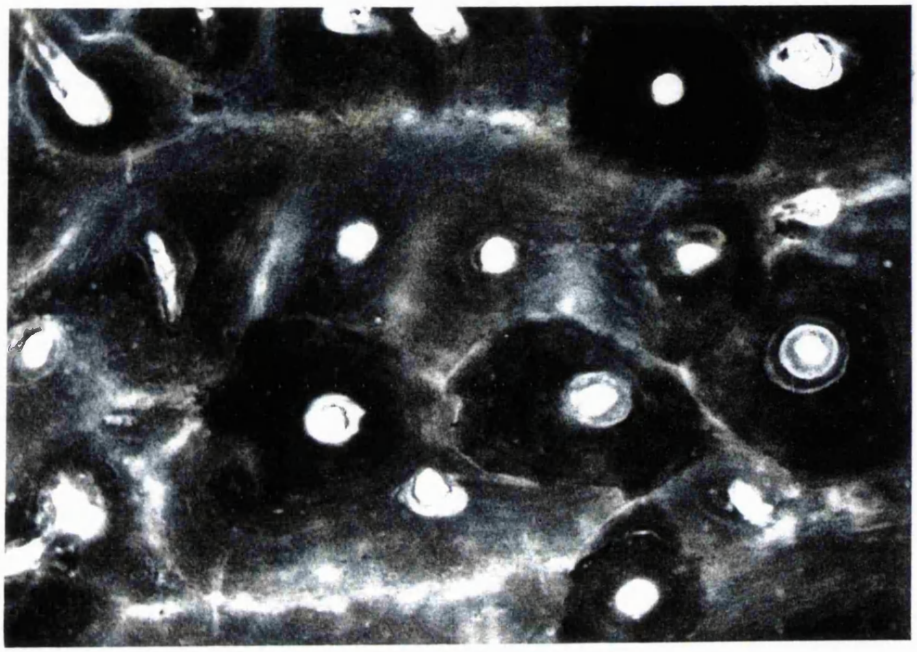

b

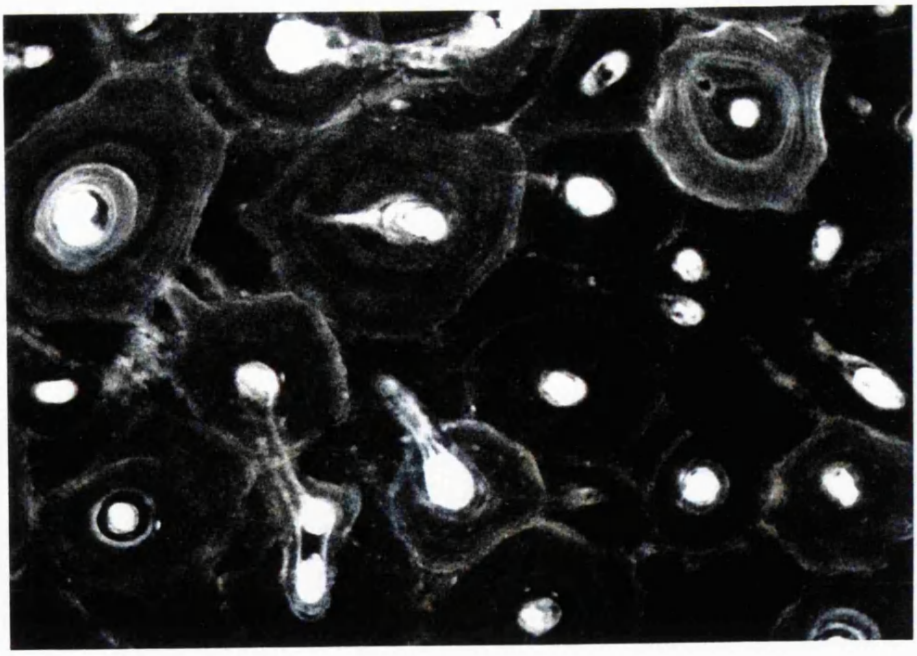

Figure 2.16

Confocal autofluorescence:

a) The primary bone in the midcortex of a 6 year horse (top left) gives higher autofluorescence signal than 2° osteons, all of which are darker. FW= 2.44 mm.

b) The primary bone in the midcortex of an 11 year horse (top right) shows more fluorescence than the 2° osteons; a brighter 2° osteon has bands with different levels of fluorescence. FW = .97mm.

c) The midcortex of a 12 year (bottom left) horse showing difference in the levels of fluorescence in the primary bone, that in the endocortical region being higher. All 2° osteons are darker irrespective of their locations. FW = 2.44 mm.

d) The endcortical region of the cortex of an 18 year (#2) animal showing more fluorescent primary bone. The woven bone content is maximally bright. This region is minimally remodelled, and the few secondary osteons exhibit much less autofluorescence. FW = 2.44 mm.

Figure 2.16

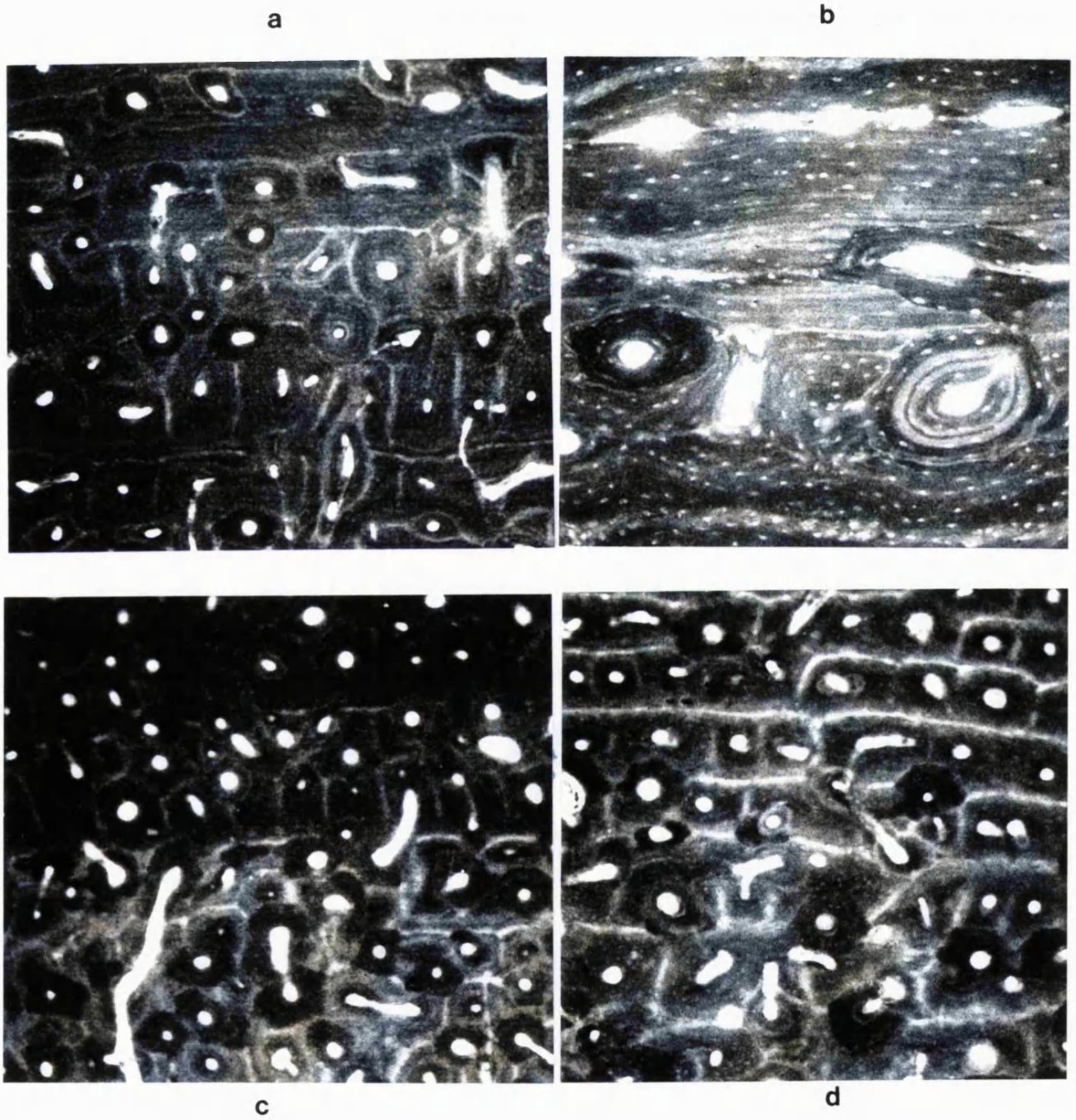

Table 2.4 Relative number of bright (more fluorescent) 2° osteons in the cranial and the caudal cortex of radii of 7 animals (in areas measuring either 3mm AP & 6mm ML, or 2 mm AP & 6mm ML) in different regions (Per = periosteal, Mid = Central, & End = endosteal).

Age/Area	Cortex	Per	Mid	End	Total
18y (1)	Cranial	18	15	85	118
(2mm x 6mm)	Caudal	70	80	168	318
18y (2)	Cranial	38	13	19	70
(3mm x 6mm)	Caudal	170	70	22	262
12y	Cranial	4	2	6	12
(3mm x 6mm)	Caudal	25	2	2	29
11y	Cranial	8	1	7	16
(3mm x 6mm)	Caudal	30	12	3	45
6y	Cranial	2	5	19	26
(2mm x 6mm)	Caudal	28	15	1	44
Unk (1)	Cranial	6	7	9	22
(2mm x 6mm)	Caudal	8	16	9	33
Unk (2)	Cranial	6	38	68	112
(2mm x 6mm)	Caudal	101	52	4	157

Resting cement lines are visible as more fluorescent bands within secondary osteons. The remnants of 2° osteons also exhibit more autofluorescence (figures 2.13 a-c).

There are fewer bright 2° osteons in the cranial cortex of some animals (eg 6y, 11y, 12y, & unk.1), whilst others (18y-1, 18y-2, unk.

2) show a greater number, indicating that the cortex of the older animal contains a higher number of dense 2° osteons (Table 4). Where present, they are seen mainly in the sub-periosteal third of the cortex and/or towards the endosteum as for example in the following animals; 18y-1, 11y, Unk.1 & Unk.2 (figures 13 a-b, 2.17a). Where the endosteal third of the cortex is greatly unremodelled, they are seen mainly towards the periosteum (eg 18y-2). The cranial cortex of some animals (eg 11y, 12y) shows no preference for the site, where they are seen in both aspects. In the centre of the cortex (figures 2.16 a-c) they are very scant, indicating that there has been the least remodelling in this area; although the cranial cortex of one animal (12y) exhibits a fair distribution of darker 2° osteons in the centre of the cortex (fig. 2.16c).

In the caudal cortex which is mostly remodelled through its whole extent, bright 2° osteons are seen more towards the endosteum than the centre of the cortex (eg 18y-1). Where the endosteal third of the caudal cortex is mostly unremodelled, the bright 2° osteons are seen more in the periosteal third than in the centre of the cortex eg. 18y-2, 12y, 11y old animals (fig. 2.14b). These are almost absent in the greatly unremodelled endosteal third of the caudal cortex (eg 11y), which appears brighter due to its primary bone content. There are exceptions as well; some animals (Unk. age 1 & 2) with largely unremodelled endosteal third of the caudal cortex show more dense (bright) 2° osteons in the centre than the periosteal third, and also exhibit few bright 2° osteons on the endosteal aspect (one of the unknown ages, unk. 1).

The transverse sections of the dorsal cortex of McIII of two animals (ie 2yF & 24yF) show similar features in confocal autofluorescence. The primary bone in the both animals gives a higher autofluorescence signal than that of the secondary bone (figures 2.19 a-b). Both the primary and the secondary bone of the older animal is more fluorescent than that of the younger one (figures 2.20 a-b, 2.20c-d). However, the plexiform bone of the older animal has the greatest fluorescence of all (figure 2.19b).

The primary bone in the whole of the dorsal cortex of the older animal apparently shows uniform autofluorescence level (fig. 2.20a);

Figure 2.17

a-b) More fluorescent 2° osteons towards the endosteum of both the cranial (top) and the caudal (bottom) cortices of an 18 year old horse. The brighter osteons show several cement lines within them. FW: a = 1.26 mm, b = 1.38 mm.

Figure 2.17

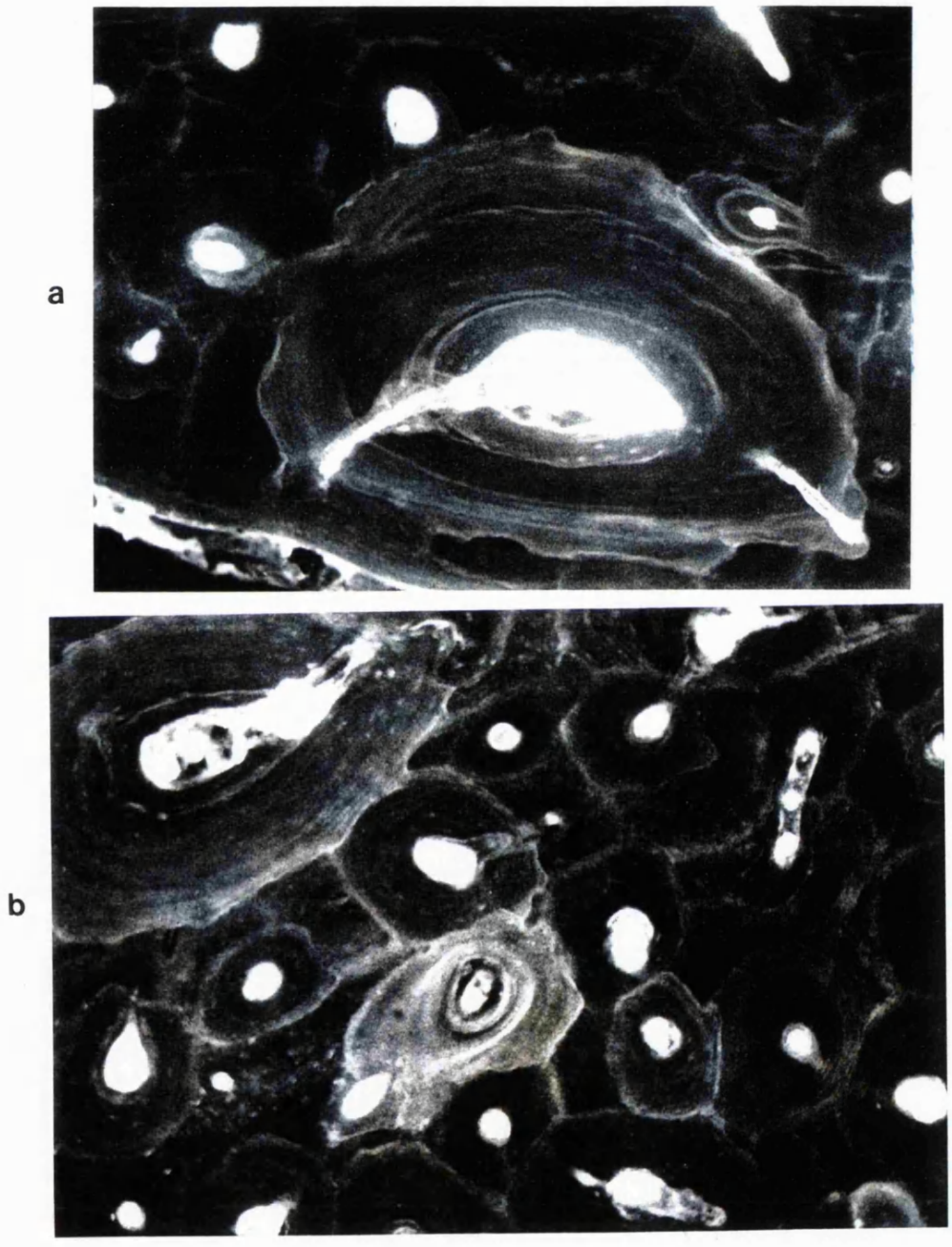

Figure 2.18

The caudal cortex of a 6 year old horse radius showing 2° osteons with contrasting autofluorescence signal in the midcortex.
FW = .63 mm.

Figure 2.18

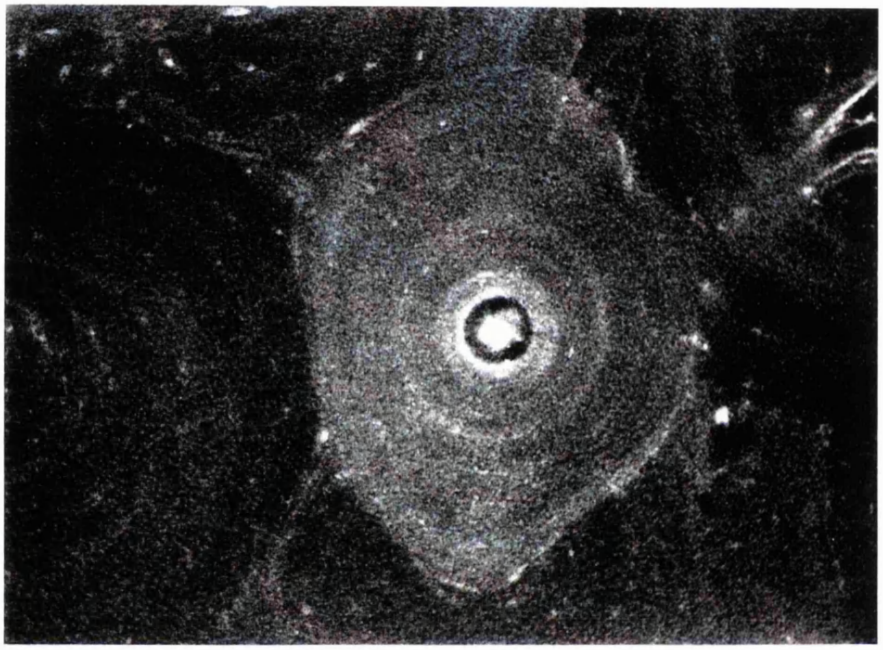

Figure 2.19

a-b) The dorsal cortex of McIII of a) 2 year (top) and b) 24 year (bottom left), showing different levels of autofluorescence. The primary bone in the periosteal region of the both animals appear brighter than the 2° osteons; the fluorescence level is apparently higher in the 24 year old animal cortex. A greater proportion of the field in the older animal is dark due to the presence of more 2° osteons.

c) An abrupt change in the fluorescence level in the cortex of the 2 year old animal (bottom left), the bone towards the endosteum appearing more fluorescent.

FW: a, b & c = 2.44 mm.

Figure 2.19

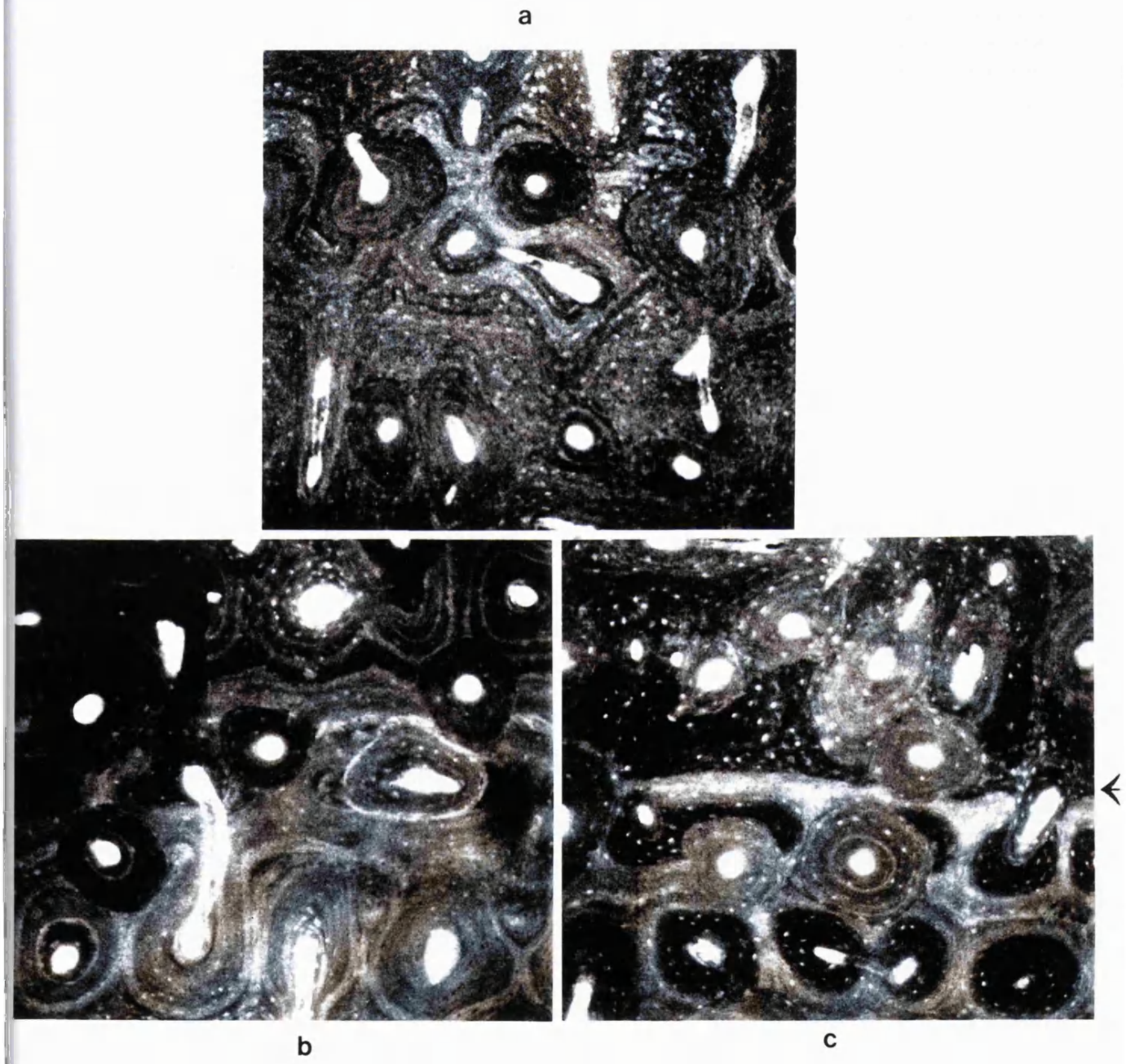

Figure 2.20

a-c) The dorsal cortex of McIII of 2 year (top) and 24 year (bottom row) horses showing different fluorescence levels.

a) The primary bone in the dorsal cortex of the 2 year animal exhibits a lower fluorescence level than the older one (b). However, the woven bone structure shows more fluorescence.
b & c) The primary bone in the dorsal cortex of McIII of the 24 year (bottom left & right) animal gives a higher fluorescence signal than the 2 year old animal.
Although the 2° osteons are darker in the both cortices, a few in the older animal (b & c) show a higher fluorescence level.
FW: a & b = 2.44 mm, c = .97mm.

Figure 2.20

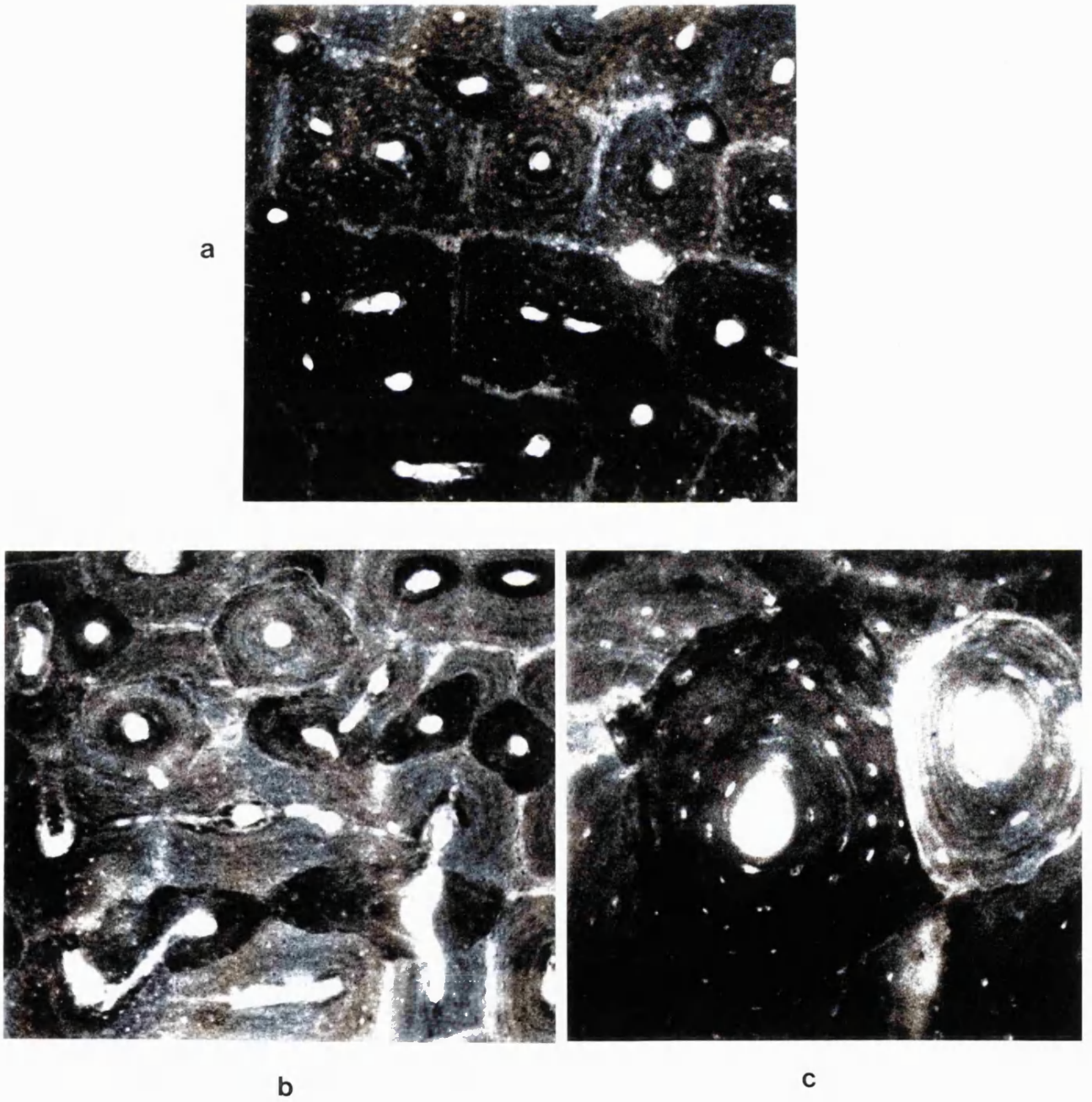

whilst that in the cortex of the younger animal show a different feature, the part in the endocortical region being brighter than the rest of the cortex (Fig. 2.19c), a feature also seen in the cranial cortex of the radius of a 12 year old horse (Fig. 2.16c). This indicates that the amount of more mineralised bone increases with age, and that the gradual increase in the degree of meneralisation density follow a gradient from endosteum to periosteum.

2.3.5 The question of collagen orientation

2.3.5a LS and Oblique sections of the cranial and caudal cortices in LPL & CPL.

Cranial cortex:

Sagittal LS - The osteons in the longitudinal sections obtained in the sagittal plane appear bright in CPL (fig. 2.21a) with their boundaries denoted by dark linear margins. The collagen fibres lie parallel to the long axis of the section.

In LPL the collagen fibres undergo extinction at 0 to 10° (2.21b), the mean being 05° and occurs at every 90° interval. The margin is dark. The osteons are maximum bright with 45°-50° rotation. Unlike the caudal sections, the intermittent dark shadow lines in between lamellae are hardly visible in most of the osteons, where visible, they are very fine. The osteons are seen to follow a straight longitudinal course.

Cranial oblique (tilted longitudinal/ 45° LS) sections - In CPL, most of the osteons are bright, with a lamellar appearance.

In LPL, the majority of osteons and interstitial tissue appears dark within 10°-20° of rotation (fig. 2.22a), when the peripheries at their whole circumference remain bright. The osteons turn bright at -35° and +55° rotation (fig. 2.22b), when the margins at the contralateral two sides turn dark.

Cranial oblique (tilted transverse/ 45° radial) sections - In CPL, osteons are bright with a lamellar appearance. Osteons

Figure 2.21

a) CPL (top) & **b)** LPL (bottom) images of a cranial sagittal longitudinal section. The fibres are dark in LPL when the section is viewed in the plane normal to the optic axis (at 0° ie the long axis of the section lying exactly parallel to the "NS"). The section is 100µm thick. FW = 700µm.

Figure 2.21

a

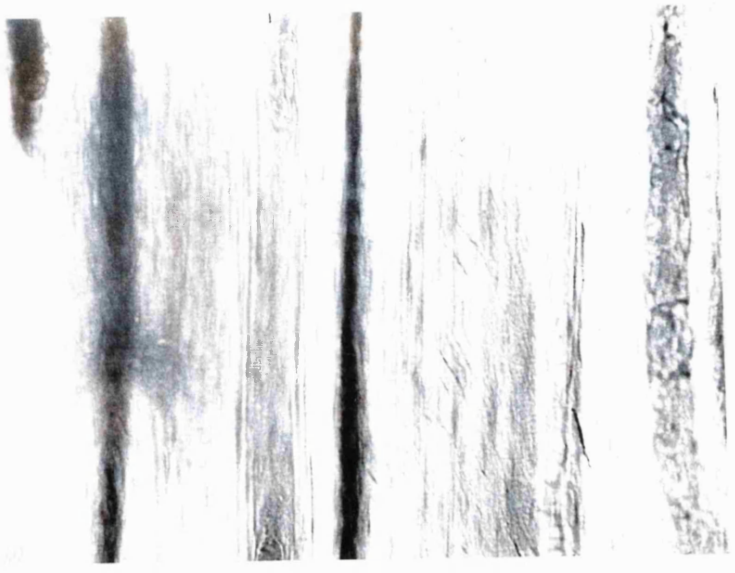

b

Figure 2.22

a-c) LPL images of cranial oblique section.

a) The maximum extinction of the cranial 45° LS section is observed with 20° rotation of the section.
b) Bright 2° osteons with dark margins are seen in 45° LS section @ 55° rotation , and in
c) 45° TS sections @ -25° (335°) of rotation.
FW: a) 1800µm, b & c) 1350µm.

Figure 2.22

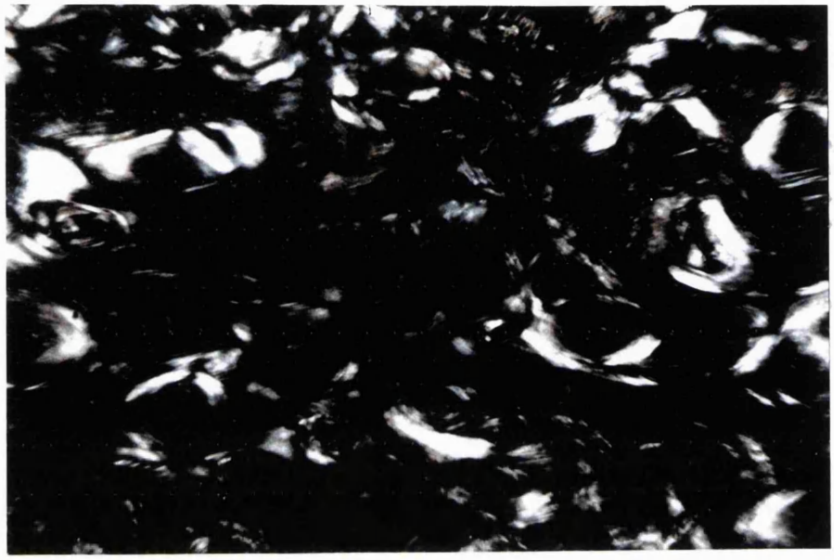

a

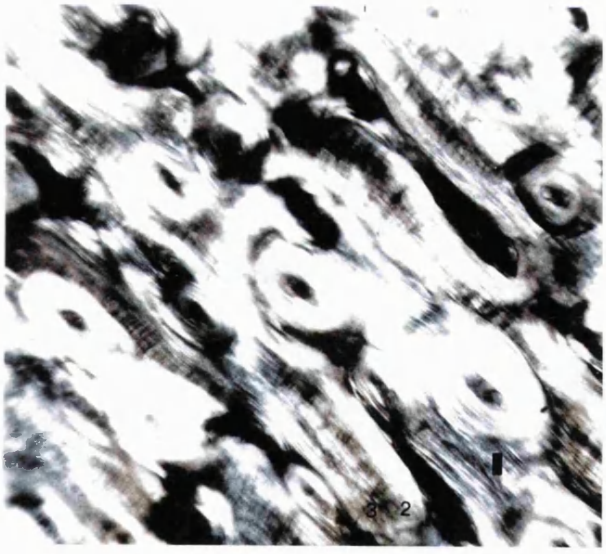

b

c

appear dark in LPL within 10°-20° of rotation; the peripheries remain bright. At around -25°, osteons turn bright; peripheries at their upper and lower circumference are dark (fig. 2.22c). The brightness of the osteons is maximal at around 60° of rotation, when the thick circumference above and below again turns dark.

Cranial tilted transverse sections (oblique/radial 45°) appear brighter than the tilted longitudinal sections (oblique/45° LS). More bright collagen in tilted transverse sections indicates that the collagen fibres are more longitudinal in the cranial cortex.

In the same sections, when the osteon proper is bright, the margin on top and below is dark; when the osteon appears dark, the margin at the same location changes from dark to bright.

In the tilted longitudinal sections (oblique/45° LS), when the osteon proper is bright, margins on the two contralateral sides are dark; when the osteon proper is dark, the margin at the same location turns bright. In longitudinal sections, the margin is dark. These observations suggest that the fibres at the peripheries are more transverse.

Caudal cortex:

Sagittal LS - In sagittal LS, all the osteons appear bright in CPL (fig. 2.23d). The straight dark margins denote the cement lines. Fibres are parallel. There are dark lamellae within the osteons. Osteons predominantly follow a longitudinal course. Some osteons are seen to take a somewhat oblique course (fig. 2.23a-b). The longitudinal sections apppear brighter than the transverse sections, indicating that the collagen is more nearly LS than TS.

In LPL, extinction occurs between 345°- 025° (fig. 2.23a-b), maximum extinction being within the range of 0-10°. Osteons are maximally bright within 45°-50° of rotation (fig. 2.23c). Dark lamellae are seen between the bright lamellae.

Caudal oblique (tilted longitudinal/45° LS) sections:

In CPL, the osteons appear bright. Alternating dark and bright lamellae are present within the osteons.

Figure 2.23

PLM images of 100 µm thick caudal sagittal longitudinal section; the longitudinal axis of the section is "NS". The osteons predominantly follow a longitudinal course.

a) Extinction occurs between -15° (345°) to 025°, the maximum being at 0-10°. The image is viewed at 0°. Osteons which take somewhat oblique course appear bright in this picture. LPL image.
b) 20° rotation of the specimen gives extinction in those osteons which appear bright at 0°. LPL image.
c) The osteons appear bright when the section is rotated to 45°. LPL image.
d) Bright osteons with straight dark margins are also seen in the CPL image (bottom right).
Corresponding features in a & b are marked with red spots.
FW: a & b) 1800µm, c) 530µm d) 1400µm.

Figure 2.23

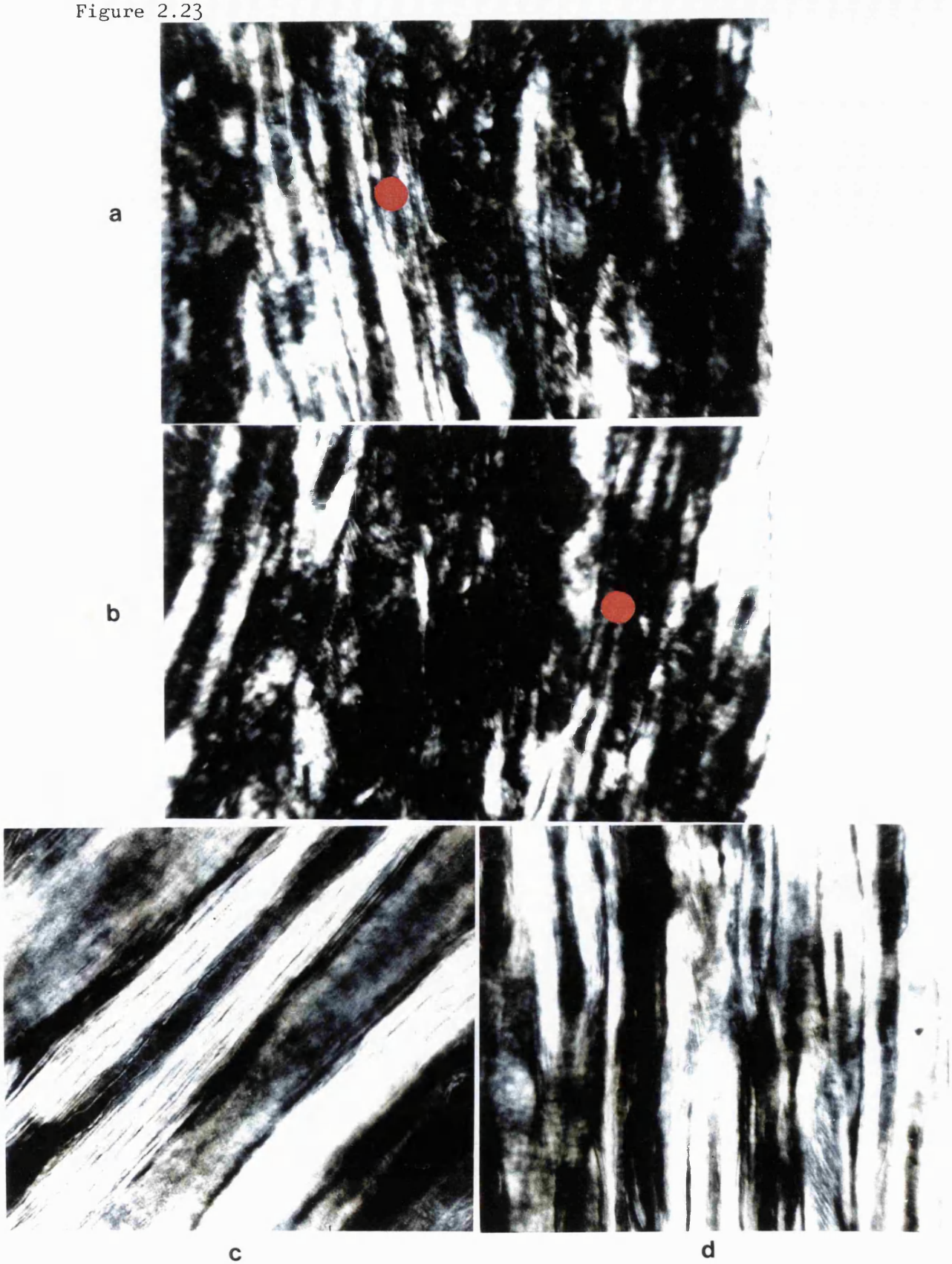

Figure 2.24

Caudal oblique sections (45° TS and 45° LS) in LPL & CPL.
a & b) 45° TS
c & d) 45° LS

a) The extinction of the osteons in 45° TS section occur at 10° of rotation, the margins are bright. LPL.
b) CPL of the same field as in a.
c) The maximum extinction occurs in 45° LS section at 20° of rotation, some remaining bright. LPL.
d) At 340° (-20°), this 45° LS section appears bright, the fibres appear parallel in this plane of the section. LPL image.
FW: a-d) 1450µm.

Figure 2.24

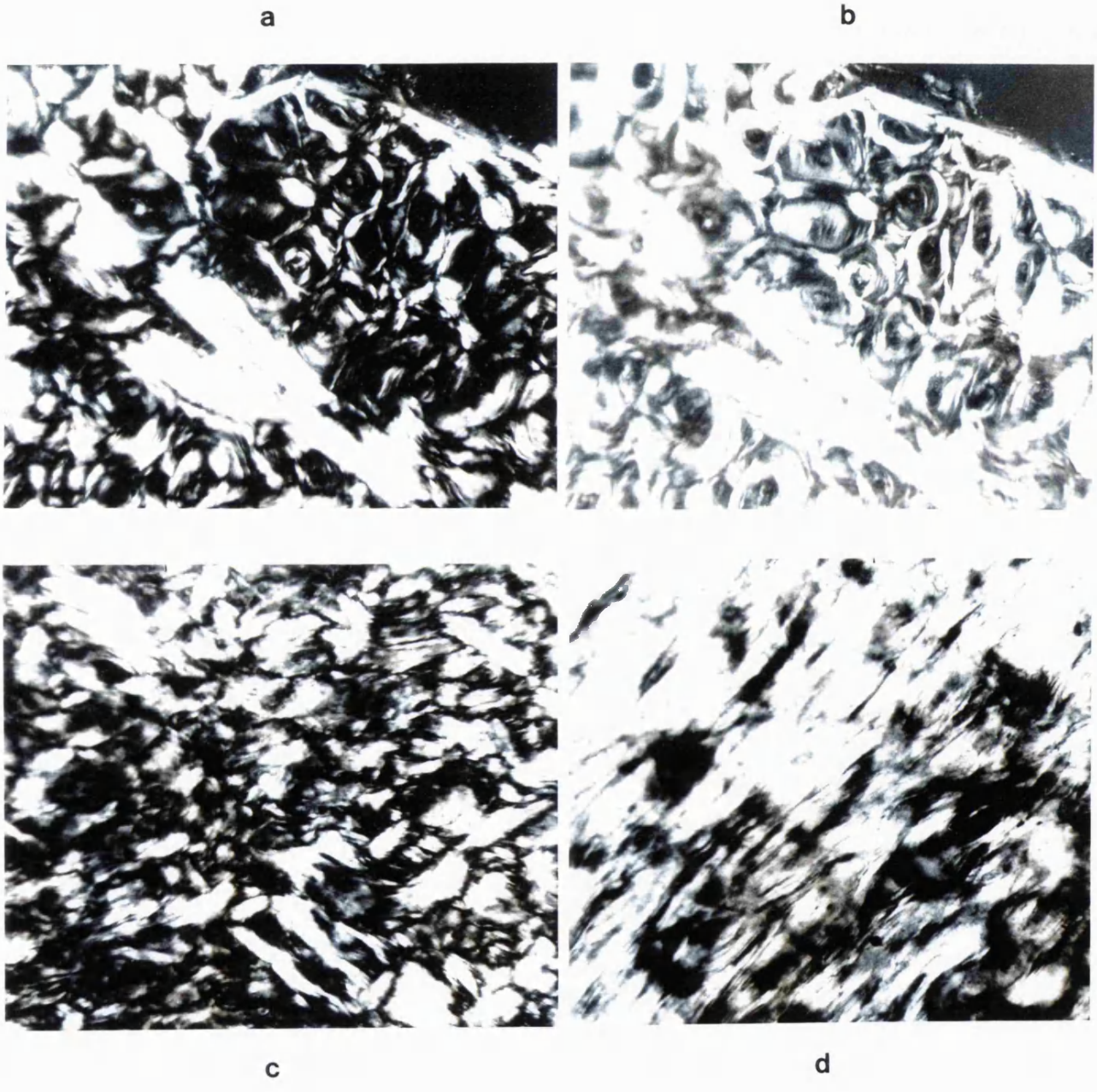

The osteons undergo extinction at different levels of rotation ie 0-40°, with the majority of fibres being dark at 20° (fig. 2.24c). Some osteons exhibit no extinction at all. The section is maximally bright at around 335° (fig.2.24d) or within 60°-65° of rotation with the whole circumference illuminated. With further rotation, the extinction again takes place between 90°-130°.

Caudal oblique (tilted transverse/radial 45°) sections:

Osteons are more circular than in tilted longitudinal sections (fig. 2.24a - CPL). Alternating bright and dark lamellae are seen.

In LPL, some osteons undergo extinction at 350°-10° (fig. 2.24b), while the majority show no extinction at any level of rotation. The previously extinguished osteons turn bright with 40° rotation, while the majority shows no change. With 85°-95° of rotation, the majority shows no change while the rest turn dark again.

Tilted longitudinal sections appear brighter than the tilted transverse sections, which indicates that the collagen fibres are more parallel to the plane of the tilted longitudinal section than that of the tilted transverse section.

2.3.5b Observations with the Leitz Universal stage polarising microscope:

50 µm thick oblique (45° LS) cranial sections

With the section oriented normal to the optic axis, here annotated 360°, secondary osteons appeared bright (fig. 2.25a). Lamellation was alternately bright and dark, but bright lamellae were dominant. Most peripheral fibres were bright. Circumferential lamellae were also bright.

With the section at + 045° tilt, (i.e. oriented to simulate a normal TS), the osteon proper appeared dark. Darkening began at +20°, and persisted between +30° to +45°: it was maximally dark at +30° (fig. 2.25b). Beyond +45° the osteons gradually became brighter. It

Figure 2. 25

LPL micrographs of 50 µm thick cranial oblique (45° LS) section (viewed in Universal stage microscope) with its periosteal margin 45° to the tilt axis showing

a) Bright osteons in the section at 360° (zero tilt, top);

b) Dark osteons with a bright margin are seen at +30° tilt (bottom left), whilst

c) At -30° (330°) the osteons turn bright with a dark margin (bottom right).

The tilt axis is vertical. Corresponding features are marked with red spots.

Figure 2. 25

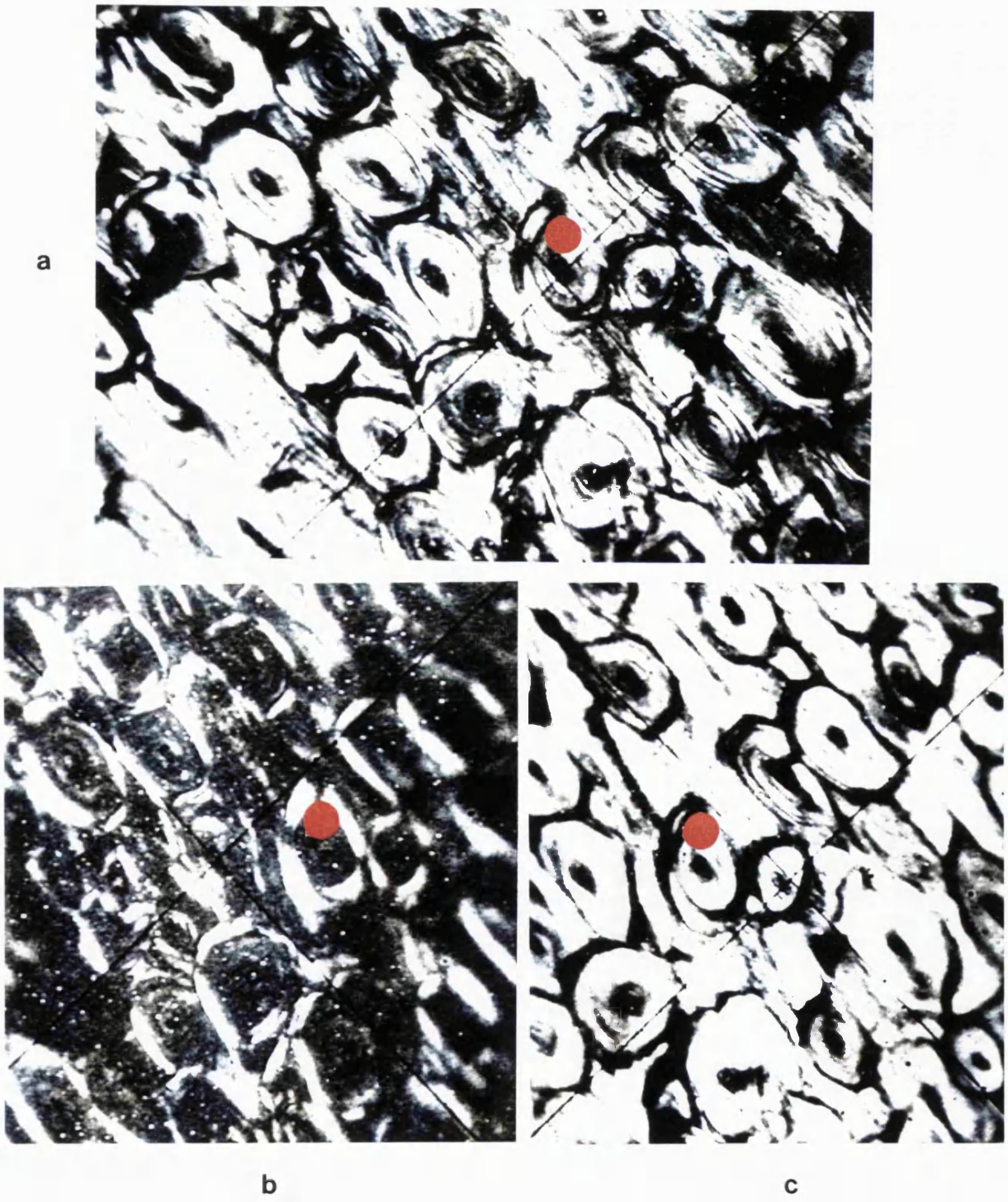

Figure 2. 26

LPL micrographs of cranial oblique (45° LS) section viewed with its periosteal margin parallel to the tilt axis in Universal stage microscope showing

a) Dark osteons with a bright margin at zero tilt (360°, top);
b & c) Towards ±45°, the osteons appear bright with a dark margin (bottom left & right).
The tilt axis is vertical. Corresponding features are marked with red spots.

Figure 2. 26

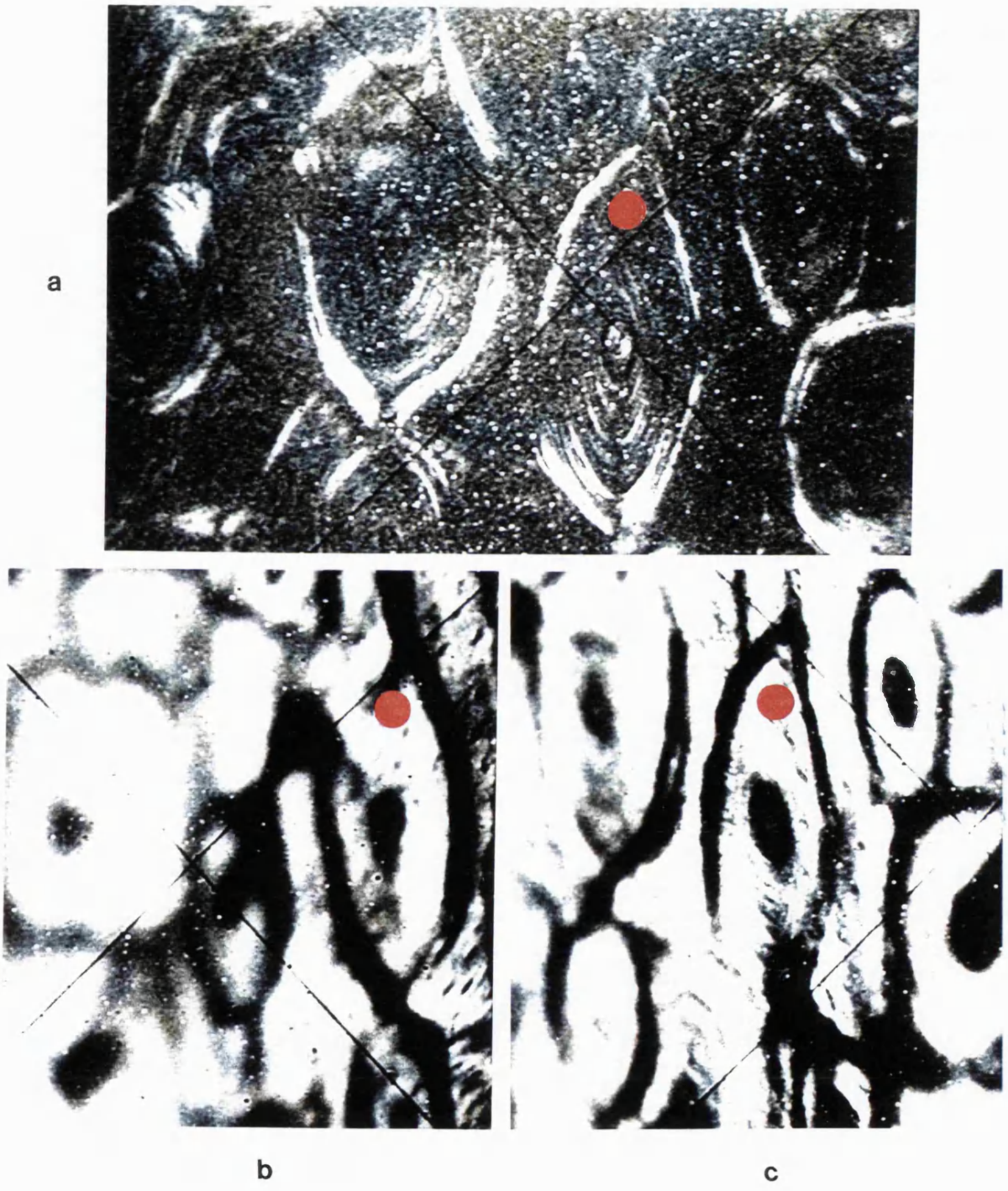

should be noted that these positions are difficult to reach because there is naturally a problem with the limitations of the depth of field of the optical system, and further that the apparent section thickness increases with tilt, which will increase the brightness of suitably oriented fields. The peripheral fibres within the osteon (at the margin) were bright all around. These fibres were maximally bright at +30° and persisted till after +45°. The circumferential lamellae were maximally dark at 35°, and then began brightening.

With a 90° tilt from the above plane, i.e., -45° (315°) osteons appeared bright and remained so beyond 315°. Brightness was homogeneous; it did not show alternate lamellation. The margin was almost dark (fig. 2.25c) with a faded bright line within. Circumferential lamellae were bright.

Furthermore, when the section was oriented such that the periosteal margin lay perpendicular to the tilt axis of the Universal stage (i.e., the longer axis of the obliquely sectioned osteon lay parallel to the tilt axis), the osteon proper appeared dark with a bright margin at all degrees of the tilt (i.e., +45° to -45°). When the longer axis of the obliquely sectioned osteon lay perpendicular to the tilt axis (i.e., the periosteal margin of the section was parallel to the tilt axis), the osteon proper was dark (fig. 2.26a) viewed normal to the section (360°), whilst the margin appeared bright. Towards ±45° (fig. 2.26 b-c), the osteon proper became bright. The brightness was homogeneous. The whole circumference of the margin was dark and distinct.

All these observations are in accord with the view that secondary osteons in the cranial cortex contain predominantly longitudinal fibres, with marginal more transverse fibres.

50 µm thick oblique (45° LS) caudal section:

Viewed normal to the section (360°) the osteons in the caudal section appeared bright, with their peripheries also bright (figure 2.27a).

Towards +045° the osteons became brighter. Maximum brightness

Figure 2.27

LPL micrographs of 50 μm thick oblique (45° LS) caudal section seen in Universal stage microscope

a) bright osteons when viewed normal to the section (at zero tilt, top);

b) the osteons turn brighter with a dark margin towards +45° tilt (bottom left); and

c) the osteons appear dark at -30° (330°) tilt.

The section is seen with its periosteal margin at 45° to the tilt axis. The tilt axis is vertical. Corresponding features are marked with red spots.

Figure 2.27

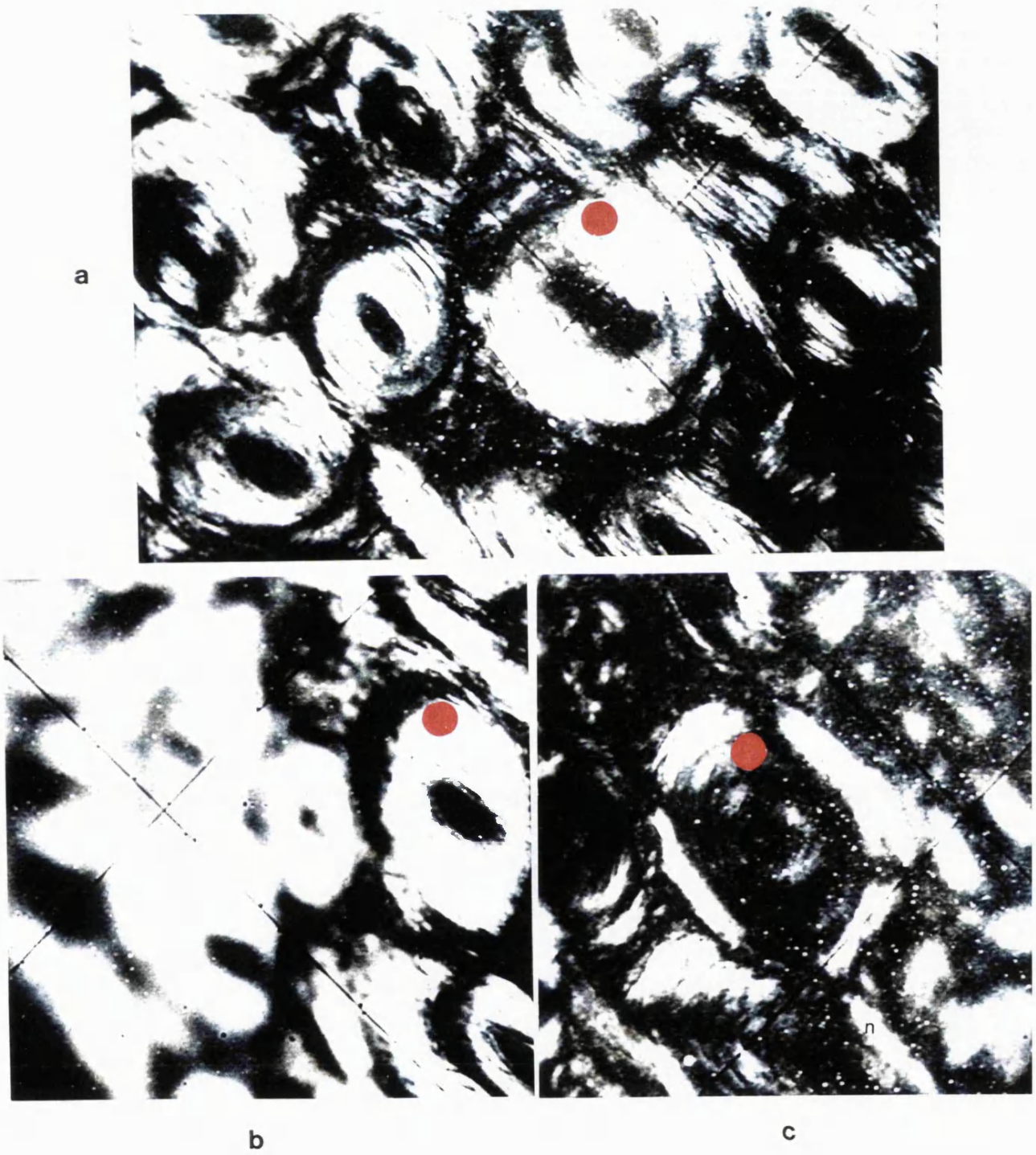

Figure 2.28

LPL micrographs of caudal oblique (45° LS) section viewed with its periosteal margin perpendicular to the tilt axis in Universal stage microscope

a) dark osteons with bright margins at zero tilt (360°, top);

b) +30°

c) -45°

The tilt axis is vertical. Corresponding features are marked with red spots.

Figure 2.28

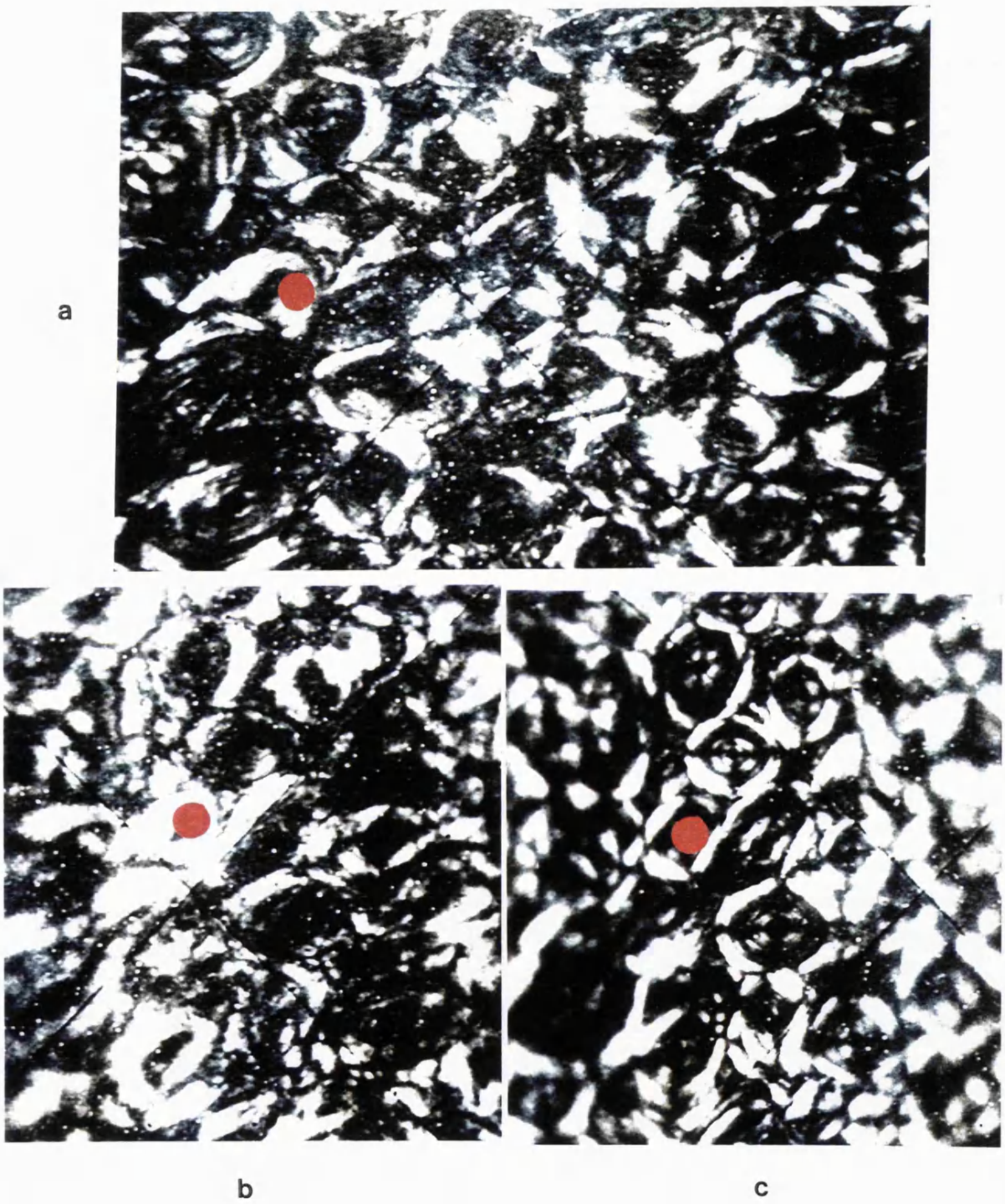

Figure 2.29

LPL micrographs of caudal oblique (45° LS) section viewed in the Universal stage Microscope with its periosteal margin parallel to the tilt axis.

a) dark osteons with bright margins at zero tilt (top);

b) +45°

The tilt axis is vertical. Corresponding features are marked with red spots.

Figure 2.29

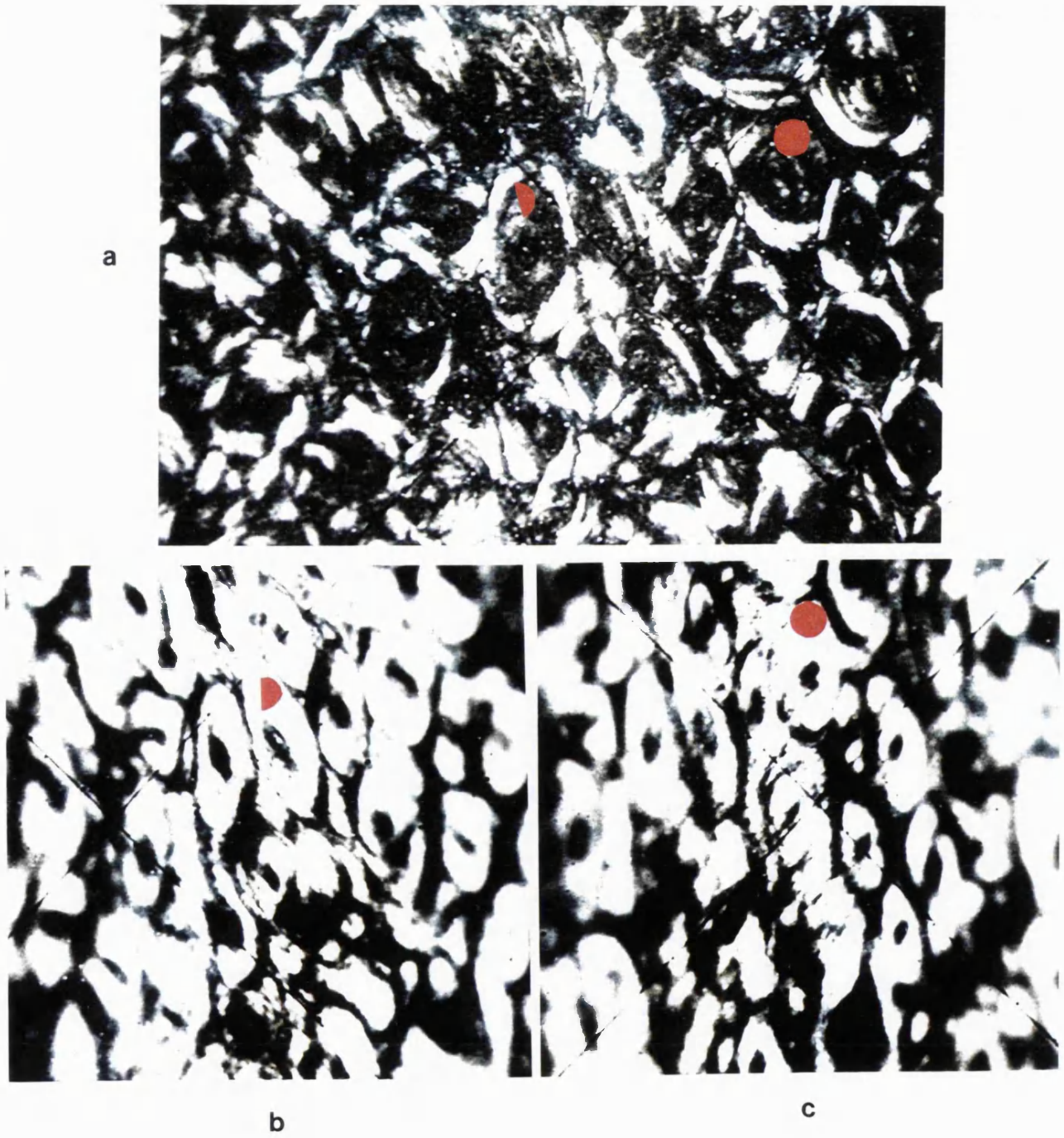

was at 50°-60°. The periphery was dark (fig. 2.27b)

Towards (fig. 2.27c) -45° (315°) the osteons appeared dark. Maximum darkness was at 325°. The extinction begins at 350°, and persists until 315° when they became faintly bright.

At -45° the osteons appeared faded bright. Beyond this tilt they gradually became brighter. The peripheral lamellae at this tilt were maximally bright. The number of lamellae was always constant.

Again, when the section was oriented such that the longer axis of the obliquely sectioned osteon lay parallel to the tilt axis of the Universal stage (i.e., the periosteal margin lying perpendicular to the tilt axis), and viewed normal to the section (360°), the osteons appeared dark with a bright margin (2.28a). The appearance was not distinct, rather meshed. Towards +45° the osteons remained dark whilst the margins changed to dark. Towards this tilt, the appearance was not distinct (fig. 2.28b). Towards -45° (315°), the osteons remained dark, and the margins bright. Here, both the osteons and the margins were distinct (fig 2.28c).

When the section was oriented such that the periosteal margin lay parallel to the tilt axis, and viewed normal to the section (360°), the osteons appeared dark with bright margin (2.29a). Towards ±45°, the osteons turned bright whilst the margins dark (2.29b-c).

These observations support the view that the secondary osteons contain oblique fibres, which are nevertheless more longitudinal than oblique. The margin contained transverse fibres.

2.3.5c **Observations with Scanning Electron Microscopy**

Although the details in the slices were somewhat distorted during the drying process, a fair idea about the organisation of the collagen fibres in successive lamellae and their orientation could be perceived.

Caudal cortical 45° radial slices:

The osteons resorbed at different locations and in different obliquities all exhibited lamellae within the base and the walls of the pits (fig. 2.30). Collagen fibre bundles (lamellae) are observed in the plane of the section around the circumference of the osteonal canals eg., immediately around the canal, within the osteon proper, and at the periphery. The lamellae in the plane of section are not visible over the whole extent of the same resorption field: at the top and the bottom extremities of the elliptical section of the osteons these are not visible (figure 2. 30d-e), whilst these are apparent on the other two sides and adjacent to the top and the bottom extremities (fig. 2.30 a-d).

These lamellae in the plane of section contain parallel fibres and traverse for some distance before they disappear within the tissue (Fig. 2.30e). Some fibres are seen to decussate and join with the adjacent layer in alternate similar lamellae. In between the alternate lamellae (which are parallel to the surface), there are wider lamellae which appear stippled (cross cut due to resorption and later distorted during air drying).

Caudal cortical 45° tangential slices:

The lamellar banding is apparent on two sides of the osteon, but is not visible at the extremities of the other two sides, which represent the top and the bottom of the elliptical section of the osteon, where no alternation is apparently distinguishable (Fig. 2.31). Lamellae lying in the plane of section are composed of parallel fibres, with wider stippled lamellae in between.

It is concluded that the lamellae in the plane of the section are oblique fibres, nevertheless more longitudinal than oblique. The wider stippled lamellae are more nearly longitudinal fibres.

Figure 2.30

BSE images of caudal cortical tilted transverse (45° radial) section, resorbed by chick osteoclasts.

The resorbed areas show a regular alternate lamellar appearance. The lamellar bands in the plane of section are composed of parallel fibres, and are not visible within the same resorption field over the whole extent. The wider stippled zones between the lamellae lying in the plane of section represents those with predominantly longitudinal fibres.

Image **b** and **c** (middle row) are the enlargements of parts of the field of view in **a**; bottom row (**d**, **e**) are separate fields.
The long axes of the oblique sections are shown horizontal.
15 kV. Au sputter-coated.
FW: a = 220µm, b = 71 µm, c = 56µm, d = 56µm, e = 113µm

Figure 2.30

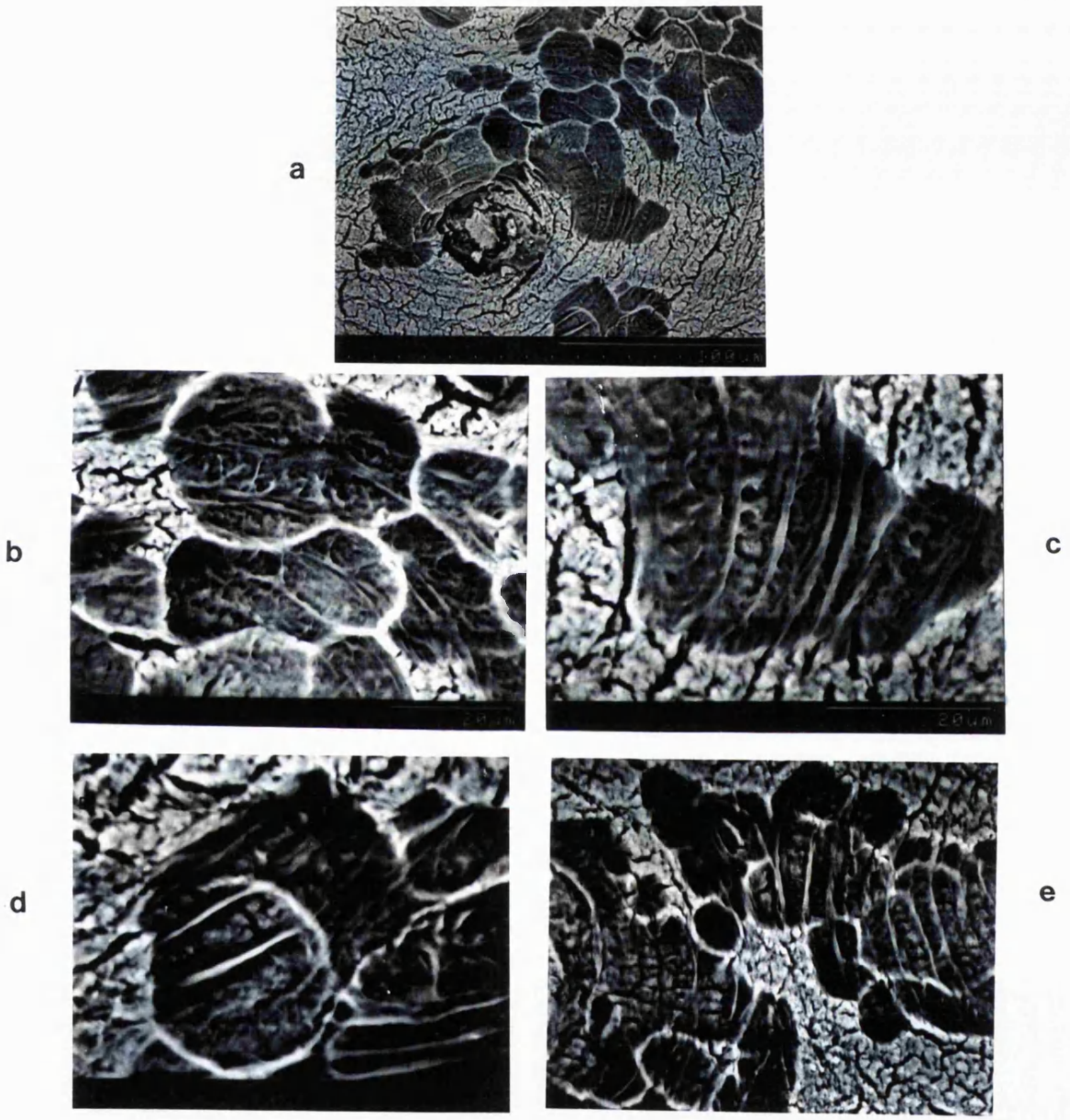

Figure 2.31

BSE images of caudal cortical tilted longitudinal (tangential 45°) section, resorbed by chick osteoclasts.

a & b) The lamellar bands are apparent on one side of osteons.

c) One corner of an osteon showing lamellar bands.

d) Lamellar bands are not apparent in one extremity of an elliptical osteon.

e) Lamellar bands at the side of another osteon.

f) Enlargement of a part of the field of view in e.

The long axes of the oblique sections are shown horizontal.

15 kV. Au sputter-coated.

FW: a = 113 µm, b = 71 µm, c = 220 µm, d = 142µm, e = 380 µm, f = 70µm.

Figure 2.31

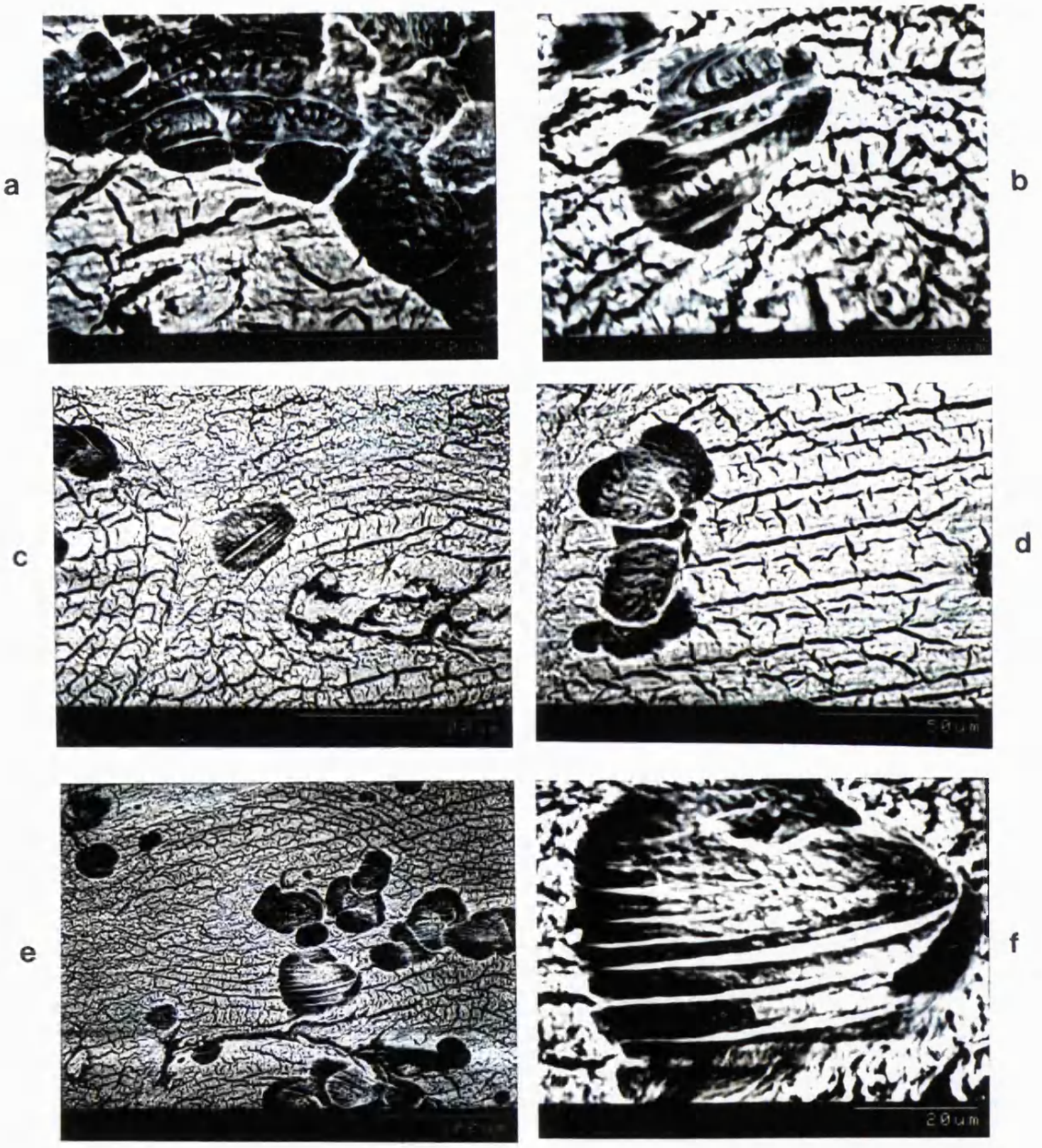

Figure 2.32

SE images of resorbed caudal cortical longitudinal (sagittal) section showing successive layers of fibres of different orientation at the base of the resorption pits:

a & b) Vertical lamellae alternate with stippled oblique lamellae (top row),

c & d) Overlapping vertical and oblique lamellar sheets of collagen (middle row), &

e) Oblique lamellar sheet with adjacent resorbed longitudinal lamellae (bottom).

LS is vertical. 10kV. Au sputter-coated.

FW: a = 38 µm, b = 22 µm, c = 38 µm, d = 22µm, e = 38 µm.

Figure 2.32

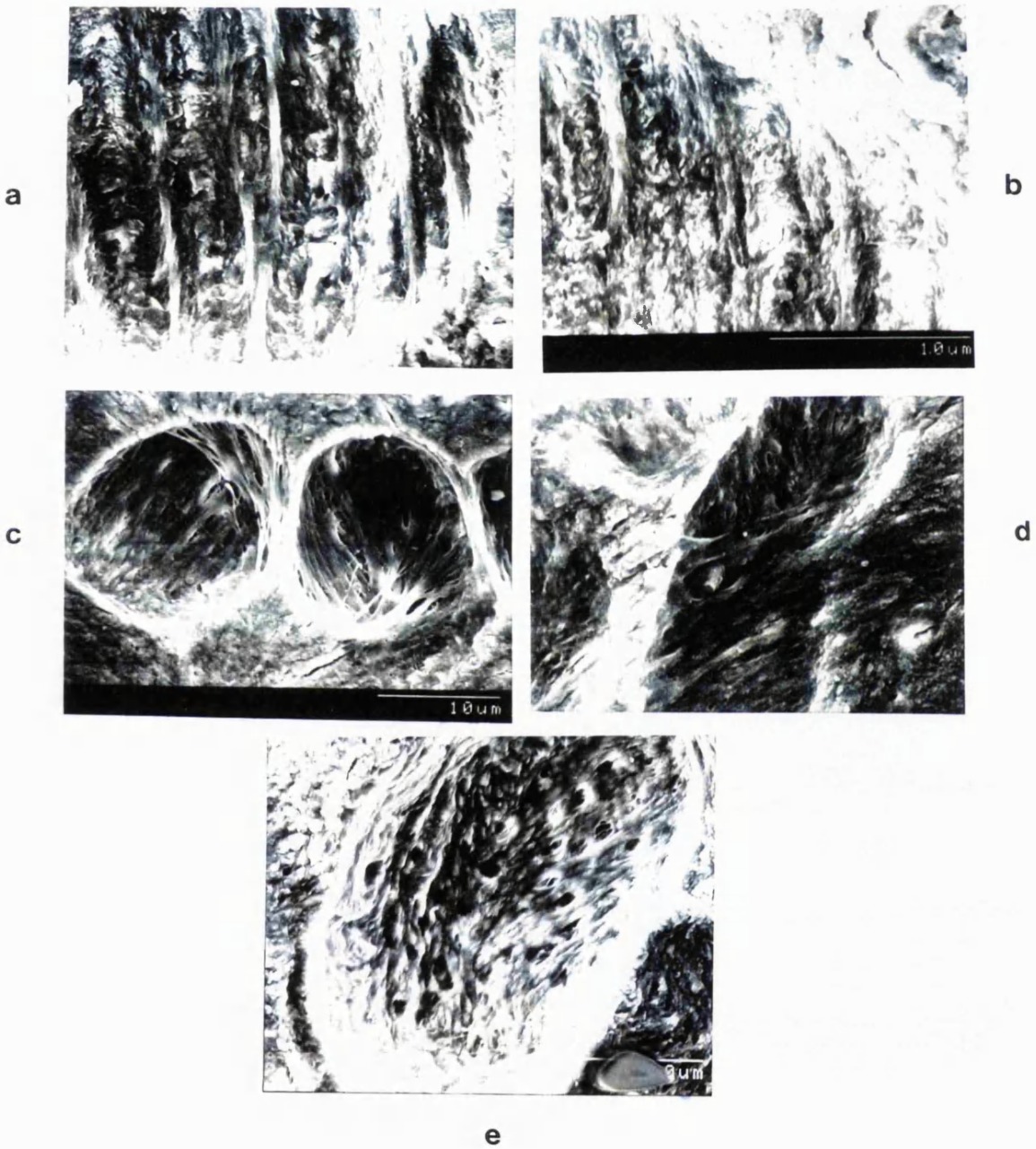

Figure 2.33

SE images of natural surface of the Haversian canal walls in caudal sagittal longitudinal section showing arrays of collagen fibre bundles forming alternate sheets in different directions.
LS is vertical. 10 kV. Au sputter-coated.
FW: a = 22 µm, b = 22 µm.

Figure 2.33

a

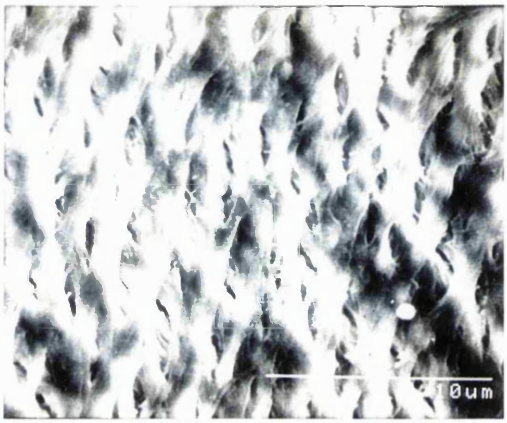

b

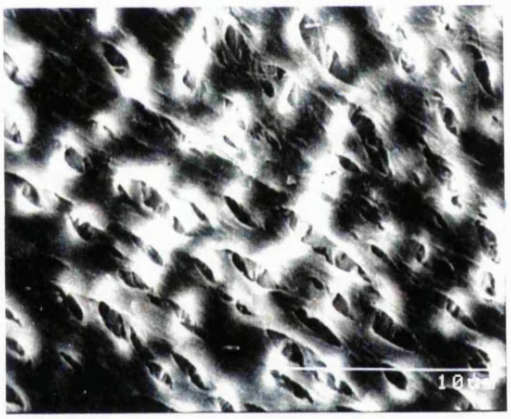

Caudal cortical sagittal longitudinal slices:

Some fibres are clamped in lamellae which are vertically oriented along the plane of the section. Between the vertically oriented lamellae, lay wider lamellae which appear stippled (fig. 2.32 a-b). Some pits exhibit collagen sheets overlapping one another in vertical and oblique orientations; in others resorbed longitudinal lamellae with intact oblique lamellar sheet are seen (Fig. 2.32d). Some resorbed fibres in the sloping edges of the pits appear stippled (Fig.2.32c-e). The natural surface of the Haversian canal walls reveals arrays of collagen fibre bundles which form alternate sheets in different directions (Fig. 2.33). In some places, sheets which are vertical lamellae overlap sheets of obliquely oriented lamellae, or the reverse. Fibres at the borders between lamellae decussate to join with adjacent lamellae. It is simple to conclude that vertical lamellae and sheets in the plane of section are indeed nearly longitudinal lamellae, whereas the obliquely oriented collagen fibre sheets and stippled zones represent oblique lamellae.

Caudal cortical medio-lateral longitudinal slices obtained in coronal plane exhibit narrow vertical lamellae with collagen fibres lying along the plane of the section, with broader stippled zones between the vertical lamellae (Fig. 2.35 a-c). Again, the vertical lamellae are composed of longitudinal fibres, and the broader stippled zones are the lamellae with oblique fibres.

45° plus 45° caudal cortical slices show fibre bundles (lamellae) lying in the plane of section, alternating with more longitudinal fibres which show a stippled appearance (2.35 d-e).

Cranial cortex

The sagittal cranial cortical slices show resorption pits with fibres nearly vertical along the plane of section. The fibres were nearly parallel to each other (Fig. 2.34 d-e).

The medio-lateral cranial cortical longitudinal slices show alternate vertical lamellae of parallel fibres in the plane of

Figure 2.34

SE images of resorbed cranial longitudinal sections showing:
a) Stippled lamellae between alternating lamellae of parallel fibres in the plane (coronal) of section (top). The lamellae of parallel fibres in the plane of section are nearly vertical.
b & c) Some pits also exhibit successive vertical and oblique lamellar sheets of collagen fibres in the longitudinal sections obtained in the same plane (middle row).
d & e) Sagittal sections showing resorbed fibres aligned nearly parallel to the vertical axis (bottom row).

LS is vertical. 10 kV. Au sputter-coated.
FW: a = 56 µm, b = 71 µm, c = 56 µm, d = 56 µm, e = 27µm.

Figure 2.34

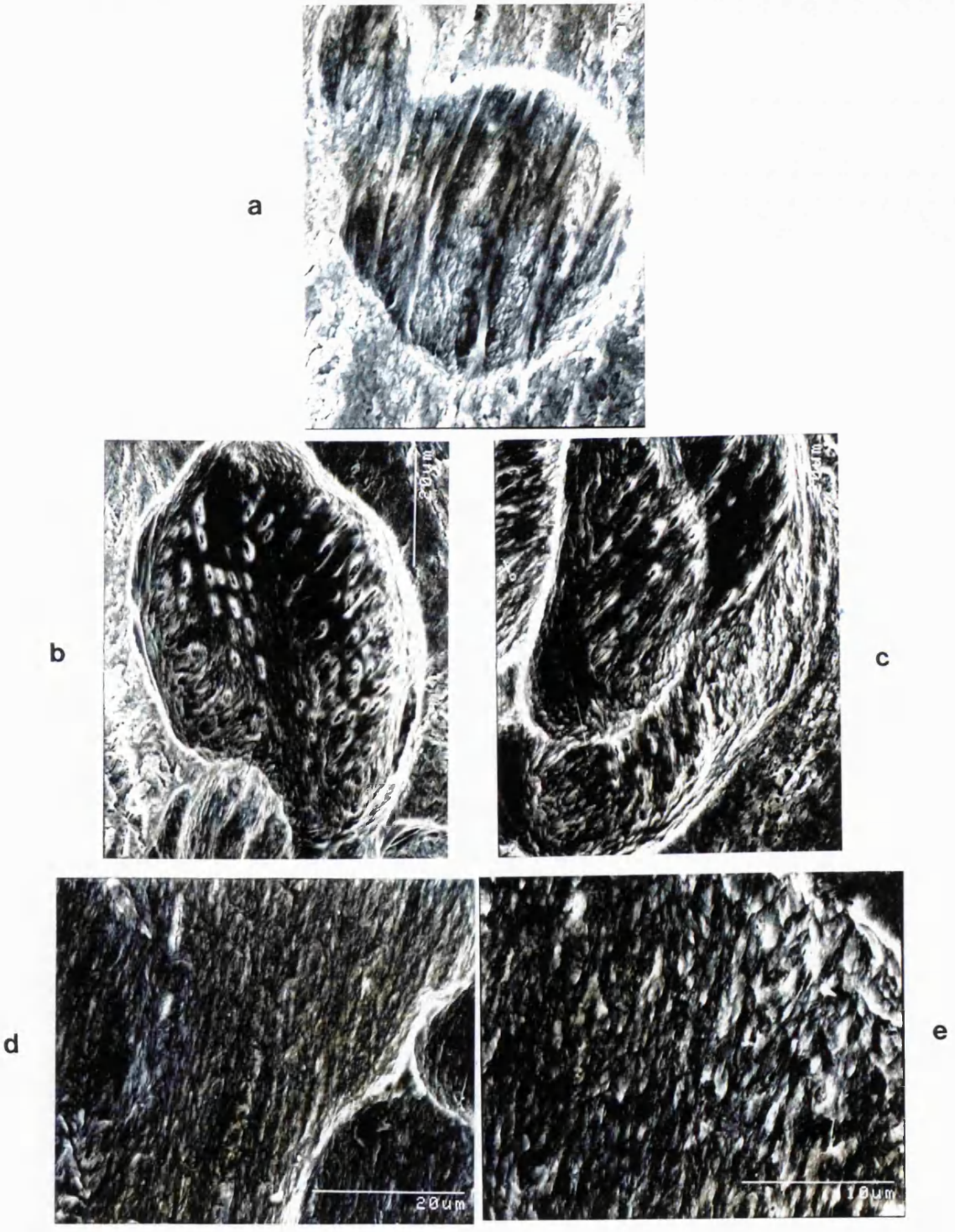

Figure 2.35

a-c) SE images of the caudal, cortical longitudinal sections in the coronal plane showing vertical lamellae of parallel fibres in the plane of the section; oblique lamellae appearing stippled.
Vertical axis is LS.
d) SE image of caudal 45°/45° section showing fibre bundles lying in the plane of section, alternating with resorbed more longitudinal fibres.

Vertical is LS. 10 kV. Au sputter coated.
FW: a = 27 µm, b = 38 µm, c = 36 µm, d = 38 µm.

Figure 2.35

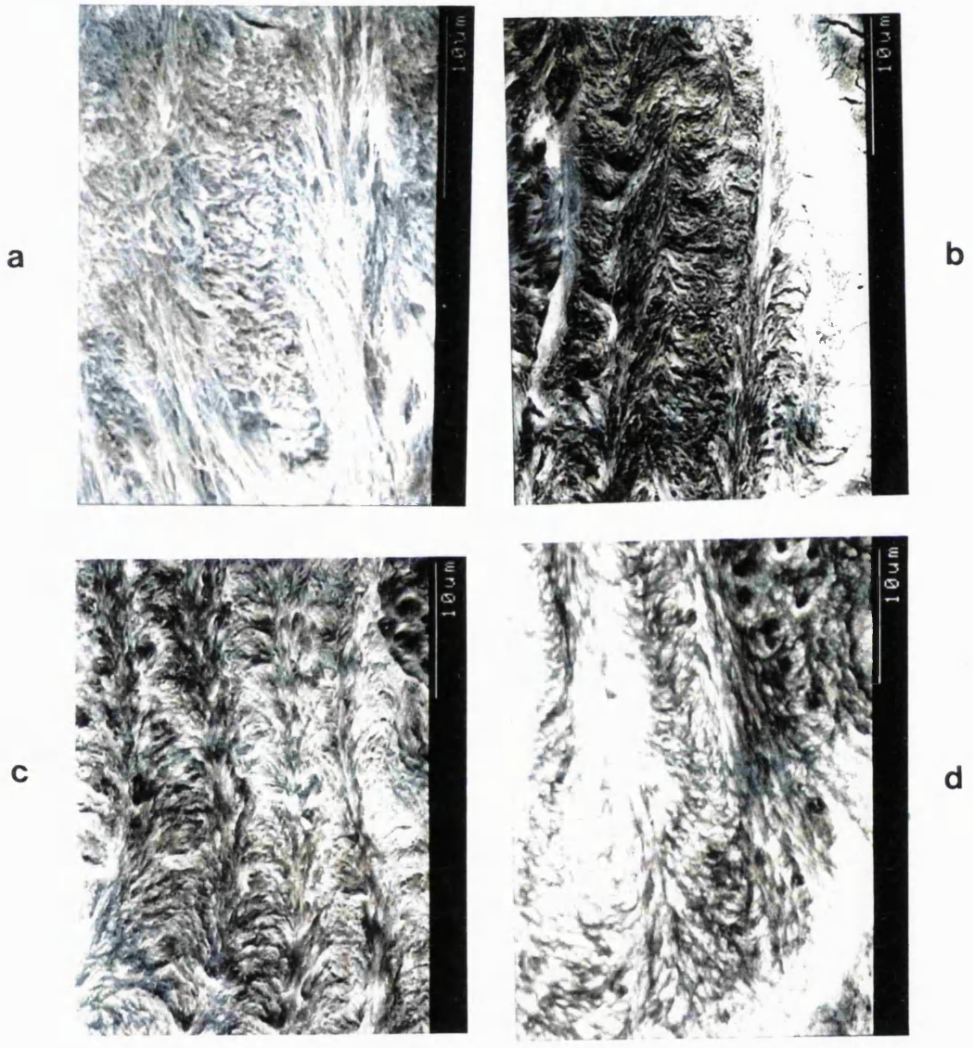

section. Between these lamellae, the lamellae appeared "stippled" (Fig. 2.34a). Some pits simultaneously exhibit alternate sheets of oblique and vertical fibres (Fig. 2.34 b-c): others have vertically aligned and parallel resorbed fibres. The resorbed stippled fibres and oblique sheets truly represent oblique fibres.

2.4 DISCUSSION

This study of cortical bone structure describes several histological features which develop in the radius as a consequence of adaptation to biomechanical funcion. The proportion of the field occupied by the dark and the bright collagen fibres, as well as the orientation of collagen fibres in the alternating bright and dark lamellae in the 2° osteons in transverse sections has been determined.

In this study, there was clear evidence of a greater level of remodelling in the caudal than the cranial cortices of equine radii of different ages. The present findings confirm the results of prior studies which showed that secondary osteons form the greater bulk of the caudal cortex (Lanyon & Baggot 1976; Lanyon et al 1982; Boyde and Riggs 1990; Riggs et al 1993a, 1993b). Increased remodelling was demonstrated in the caudal cortex of ulna-osteotomised sheep radius (Lanyon et al 1982) as a consequence of mechanically adaptive bone remodelling process. The present study and that of Riggs (1990) show that the cranial cortex also undergoes a variable degree of secondary osteonal remodelling in equine radius, even though the turnover rate is much lower than that in caudal cortex.

The present study showed that there were second or third order osteons in the caudal cortex. The interstitial lamellae were composed of remnants of older osteons. The circumferential lamellae were found to be nearly replaced by secondary osteons with more oblique collagen orientation. The volume fraction formed by remnants of older osteons in interstitial lamellae was usually greater in older animals. This is consistent with the backscattered electron imaging studies demonstrating that the cranial cortex is more

mineralized than the caudal cortex (Boyde et al 1992; Riggs et al 1993b).

However, the present study showed noticeable differences between animals. Although, for the most part the proportion of the bulk of primary bone in the caudal cortex was greater in younger bones, yet some younger caudal cortex exhibited a greater degree of remodelling than than that seen in older animals.

The proportion of dark secondary osteons in cranial and caudal cortices of younger animals was proportionately greater than that in older animals. Darker osteons are either very few or totally absent in greatly remodelled bone. This indicates that greater age is not the only contributing factor for a greater degree of remodelling and that the greater intensity of the replacement of secondary osteons containing predominantly longitudinal collagen by osteons with more oblique collagen may occur irrespective of their location in both cortices.

Although in some animals the distribution of osteons in the cranial and caudal cortex was almost uniform, in others it varied at different sites throughout the section. They were usually most numerous in the sub-periosteal region of the caudal cortex, where primary osteons were nearly absent. In the cranial cortex, evidence of osteonal remodelling was also quite apparent in the sub-periosteal bone, in places replacing periosteal lamellae near the surface.

Bone turnover in the cranial and caudal cortices cannot be strictly associated with increasing age: it is much more likely to be attributable to the 'training regime' that the animal had undergone. Osteonal remodelling is more intense in more active animals, regardless of age, body size or species (Schaffler and Burr 1984). The greater proportion of osteons containing longitudinal collagen on the caudal endosteal side perhaps associates well with the relative distribution of tension through cranial to caudal cortices.

While almost all of the whole thickness of the caudal cortex had undergone remodelling in some animals, the presence of a good amount of primary bone in the cranial cortex indicates proportionately low turnover. At an even greater age, whether all of the bone would have undergone remodelling is questionable.

Using relative CPL brightness intensity measurements (Boyde et al 1984a), Riggs and co-workers (Riggs 1990; Riggs et al 1993a) presented data suggesting a greater proportion of transverse collagen in the caudal cortex. Remodelling does not always give rise to transverse/oblique collagen. The great majority of secondary osteons in the cranial cortex contain predominantly longitudinal collagen fibres. Unremodelled primary bone structure can be found in both cranial and caudal cortices of older animals, irrespective of age. Primary bone contains predominantly longitudinal fibres in both cortices. Although few secondary osteons in the caudal cortex contain longitudinal collagen. The plexiform bone in both cortices contain transverse collagen. In some animals cranial cortex , the presence of several lamellar bands (circumferential) indicate slow growth. These lamellar bands in the peripheral third of the cranial cortex, and at the periphery of both cortices contain PLM bright collagen. The presence of the great majority of secondary osteons with predominantly oblique fibres in the caudal cortex is unquestionable. Although not many, some remodelled osteons in cranial cortex contain oblique collagen. The woven bone framework in the unremodelled bone, (in older animals and in both cortices) always shows as PLM bright.

Riggs and co-workers (Riggs 1990; Riggs et al 1993a) also described an age dependent variation in CPL brightness. After a gradual decrease until the age of 10, he showed a rise in older animals. The presence of woven bone in foetal and neonate animals explains higher CPL brightness in them.

The presence of a variable amount of unremodelled bone in older animals, independent of age, is not consistent with the suggestion that the characteristic collagen fibre orientation pattern in adult horse radius develops over the first two years of life (Riggs 1990). Continuous replacement of primary bone containing predominantly longitudinal collagen in both cranial and caudal cortex by secondary osteons containing either predominantly longitudinal fibres or oblique fibres, eventually leads to a collagen fibre orientation pattern with general characteristics special to the equine radius, but over a variable period of time and with differences between

individual animals.

The difference in the orientation of collagen fibres in newly formed osteons in the tension and the compression cortex clearly confirms that while loading initiates secondary remodelling, it is its character (tension or compression) which determines the future characteristic collagen fibre orientation at different sites, allowing the bone to withstand different types of strain. Lanyon attributed this increased remodelling to the strain environment that the bone experienced, and considered that the new bone thus formed is very unlikely to sustain fatigue damage that could have initiated remodelling (Lanyon et al 1982).

Very little evidence for resorption was observed on the periosteal side of the cortex where modelling was intense. Pead and co-workers (1988b) demonstrated that a single short period of dynamic loading caused periosteal activation for direct bone formation. An appropriate osteogenic stimulus can initiate bone formation without going through the normal resorption and formation process. They named this process as "renewed remodelling", but it is modelling, not remodelling.

Physiologically loaded bone apparently does not sustain strain damage (Currey 1968, 1984). As Lanyon proposes (1987), when the strain rises above a threshold level (still unable to cause microfracture), the changes that occur in the deformed matrix (such as reorientation of proteoglycans: Skerry et al 1988) are detected by the osteocytes in the vicinity, which then signal the appropriate cell population through their communications to initiate remodelling process (Rubin and Lanyon 1987; Lanyon 1987, 1993). Proteoglycans are believed to be responsible for providing extracellular information as they have stabilizing properties on fibrillar proteins (Meyer 1960). Pead and co-workers (1988a) showed that osteocytes receive first hand information from the deformed matrix in loading bones in excess of the physiological limit.

Rubin and Lanyon (1987) also suggested that different regions of one bone are differently "genetically programmed" to respond to a particular amount and pattern of intermittent strain. The potency of the stimulus is proportional to the magnitude of the strain. Strain

levels perceived as normal in one region induce adaptive remodelling in another. Further, a few bursts of short intermittent dynamic loading are enough to initiate remodelling. Their observations are also consistent with the studies of Liskova and Hert (1971) in that static load has little influence as an osteoregulatory stimulus in adaptive bone remodelling for the maintenance of bone. Obviously, these sorts of short intermittent loading are not capable of producing damage in the bone matrix.

No evidence of microdamage has been observed in this study in fuchsin stained sections. Riggs (1990) found only one single example of microdamage in greatly remodelled bone.

It is quite clear that the adaptive remodelling is solely dependent on the functional activity of the animals. It is almost decisive that functional strain direction and its magnitude have a definite role in determining the greater remodelling rate.

In man, with increasing age, an increase in intra-cortical porosity is secondary to an increase in the number of secondary osteons as well as in the mean diameter of the osteonal canals. The porosity is greater on the endocortical aspect (Martin et al 1980). In this study of horse bone, the degree of porosity was not associated with increasing age. Some younger bone exhibited a more extensive history of osteonal remodelling than older ones. Moreover, the porosity was more prominent near the outer cortex due to increased remodelling without an increase in Haversian canal diameter, and that in the inner cortex (endosteal) was mainly due to resorption spaces, forming osteons with larger canals, and an incomplete trabecular network.

Confocal autofluorescence somehow reflects the mineralisation profile of the primary and the secondary bone in both the cortices. Various degrees of mineralisation of osteons are seen, indicating the relative time period over which the osteons had undergone mineralisation. More highly mineralised bone generally exhibits more autofluorescence. Features observed in polarised light, such as the relative remodelling status of the bone in the tension and compression cortices, are consistent with the observations in confocal autofluorescence. The primary bone is more mineralised, and

gives a higher autofluorescence signal from the outset. The cranial cortex is greatly unremodelled, and contains a greater proportion of primary bone. Hence, the cranial cortex appears brighter than the caudal. Naturally, the primary plexiform bone is more fluorescent than the primary osteonal bone. Different remodelling intensities in different regions (ie periosteal, central and endocortical) of the cranial and the caudal cortex, and its variability in animals of different ages seen in polarised light, is quite apparent from the different levels of autofluorescence. New 2°osteons are generally the least mineralised and exhibit the least autofluorescence. The bone surrounding new osteons is always more fluorescent. Since the caudal cortex is greatly remodelled, the great majority of the 2° osteons is dark. Interestingly, the cranial cortex, which undergoes a lesser degree of remodelling and contains fewer 2° osteons, also shows a proportion of dark 2° osteons. Some 2° osteons in both of the cortices are bright; their distribution pattern in different regions of both cranial and caudal cortices, where remodelling is seen to occur with a variable intensity in different animals, suggests that these are older osteons which are more mineralised.

Occasionally, older 2° osteons in both cortices are seen to be more mineralised than the primary bone, and exhibit the highest autofluorescence. The greater number of these osteons in older animals further suggests that the secondary bone, if it is not further remodelled, can achieve a higher mineralisation density than the primary bone. Hence, an arrested or retarded remodelling process in older age will eventually lead to hypermineralisation of the existing secondary bone.

In the cranial cortex, the more autofluorescent, more mineralised osteons are distributed more in the outer and inner cortices than in the mid-cortex. Although there is variation, more highly mineralised osteons (bright in autofluorescence) in the caudal cortex are generally seen towards the periosteal side and in the mid-cortex. Very few bright (autofluorescent) 2° osteons are seen in the largely unremodelled endocortical third of the caudal cortex. This confirms the observation in PLM that the compression cortex undergoes more remodelling towards the periosteal surface, whilst the midcortex

remains mostly unremodelled in the tension cortex. The distribution of bright 2° osteons in different regions of the cranial and the caudal cortices indicates that the remodelling process does not always follow a gradient from periosteum to endosteum, although in the majority of cases an increased remodelling intensity was seen to follow a gradient from the periosteum to the endosteum.

The features of the confocal autofluorescence seen in the transverse sections of the dorsal cortex of equine McIII of two extreme age animals (ie 2yF and 24yF) are also consistent with those found in the radii. The study shows that the primary osteonal bone is more mineralised than the secondary bone, and that both the primary and secondary bone reaches a higher mineralisation level at a greater age. The mineralisation density of the cortex of both the animals (as apparent by brightness), indicates that a higher level of mineralisation is reached during first few years of life (as early as 2 year), the remaining being achieved throughout the rest. Furthermore, an abrupt change in the degree of the mineralisation of the primary bone at the junction of the midcortex and the endocortical region (as seen in the 2 year McIII and 12 year radius), suggests that the amount of more mineralised bone increases with age, and that the increase in the degree of the mineralisation has a gradient from endosteum to periosteum.

The AFCSLM findings are in agreement with the notion that increased remodelling causes a shift towards lower mineralisation densities (as in the caudal cortex) and that low turnover (as in cranial cortex) causes a shift towards higher mineralisation densities. The present study also added that, in the absence of further (continued) remodelling (as seen in the caudal cortex of older animals), the secondary bone can reach a higher mineralisation level than the primary bone. This suggests that the rate of bone turnover, as well as the continuity of the remodelling process, determine bone mineralisation density. Hypo-mineralisation follows high bone turnover while low bone turnover leads to hypermineralisation. The result of the present study is in agreement with the observation that the bone mineralisation density increases with age (Jones and Boyde 1994; Boyde et al 1993; Riggs et al 1993a,

1993b; Boyde et al 1992; Reid and Boyde 1987; Grynpas 1993). This also conforms well with the results obtained in back-scattered electron imaging (Boyde et al 1992; Riggs et al 1993b) where cranial cortex was found to be more mineralised than the caudal cortex.

Furthermore, it shows that as remodelling keeps on replacing older bone with new osteons, more and more packets of different mineralisation densities are laid down producing more interfaces within a given bone, which would obviously lead to a change in bone's material properties. Variable remodelling intensity at the sites subjected to different strain direction demonstrates that the mechanical adaptation process, where remodelling is strain-mediated, is a significant determinant of the amount, rate and location of bone formation and resorption.

It is not unjustified to argue that the characteristic difference in remodelling in cranial and caudal cortices excludes the idea of initiation of remodelling in these sites to occur following fatigue damage. If this were true, there would have been more remodelling in cranial cortex which should have sustained more fatigue damage as it was subjected to more tension than the caudal cortex. Further, till now, no evidence for fatigue damage has been found in the periosteal side where the remodelling is intense. Although one can argue that the damage cannot be seen at a given time, since it is rapidly taken out by resorption; the present study did not show any predominant sign of resorption in the subperiosteal region of the greatly remodelled caudal cortex. Damage due to strain does not apparently occur when the bone is subjected to physiological loading (Currey 1984). It is postulated that the acquired difference in the caudal cortex is the result of adaptive remodelling of the periosteal bone, primary plexiform, and osteonal structures and that differences in the perception of strain variables cause a difference in the style of deposition of collagen fibres by the osteoblasts in "closing cones".

Although several studies have established that the strain distribution affects collagen fibre orientation within secondary osteons in differing locations, yet controversy prevails regarding the organisation of collagen, and its pattern of distribution which

actually causes lamellation within the osteons.

This study of equine radii sectioned in different planes exhibits features that support the classic Gebhardt model in that the lamellation within the osteons is due to alignment of collagen fibres in different directions in successive layers. The present study shows that the fibres are actually more longitudinal than oblique. This study confirms the view that lamellation represents successive layers of bundles composed of fibres lying in different directions; more longitudinal fibres in the PLM dark zones and more oblique fibres in the PLM bright layers in transverse section. The PLM evidence is supported by SEM of the resorbed cortical bone sections, which also contradict the recently suggested alternative hypothesis that the lamellar appearance is due to alternate collagen-rich and collagen-poor layers where the fibres run in random directions (Marotti 1993). The resorbed bone exhibited successive zones of differently orientated collagen fibres within the osteons: the alternate lamellae contained collagen fibres of similar packing density.

The zones which appeared stippled between vertical lamellae in the caudal longitudinal slices were seen as alternate compact lamellae of parallel collagen fibres in the oblique slices, where the dense lamellae containing parallel fibres alternated with layers which appeared stippled, here representing the longitudinal lamellae.

If one were to accept the Marotti's view that the bright lamellae in transverse sections are composed of closely interwoven fibres running in all directions, it would be impossible for those lamellae to extinguish totally in polarised light in any orientation. However, extinction was clearly observed in tilted longitudinal caudal sections at certain degrees of tilt: the Universal stage provides an excellent opportunity to make such observations. The level of extinction observed at a certain degree of tilt, identified the lamellae to be oblique at about 35° to the long axis. This is in agreement with prior predictions that the "transverse fibres" are not transverse, but are oblique (Riggs et al 1993a), although they suggested the orientation at around 45°.

Proposals that dark (extinguished or non-birefringent) lamellae may have a different composition eg. be composed mainly of ground substance, or few fibres within the ground substance, or a composition of loosely interwoven fibres in all directions, do not appear to be true as revealed in this study. Longitudinal sagittal sections of the cranial cortex show bright collagen in PLM which are parallel to the long axis of elongated osteons. In LPL, extinction of these fibres occur when they lie parallel to either of the polars. The very fine dark shadows between bright lamellae represent the few thinner oblique lamellae. The tilted longitudinal section gave a lamellar appearance in osteons when viewed in the usual transverse plane. The linear dark boundary lines may represent the cement line which is non-birefringent, as the cement line does not contain collagen (Weinmann and Sicher 1955). The tilted longitudinal cranial section examined at a tilt +45° exhibited extinction of most of the osteons, as happens in the usual TS plane of section.

The present findings confirm that the bright peripheries of osteons in TS (almost an invariable feature), is due to the presence of more transverse fibres. It may be attributable to the pattern of the orientation of the bone forming cells during their initial recruitment at the site of "reversal of resorption", and the first few episodes of laying down of collagen when there might not have developed a definite orientation pattern of osteoblasts which associate with the future functional requirement, which depends on strain direction. As soon as the first few episodes are over, the osteoblasts adopt an orientation depending on the type of strain the bone matrix experiences. This is why these transverse components are present in both type of osteons, irrespective of their main collagen fibre orintation or of their location in either cortex. The change in osteoblast orientation that corresponds with the direction of longitudinal and nearly longitudinal (oblique) fibres in successive lamellae appears quite logical.

How it is controlled is not known, but it is clear from the above that osteoblasts are able to adapt to their function. Osteoblasts, which secrete the osteoid in an orderly manner, determine the lamellar arrangement in bone (Jones et al 1975; Jones and

Boyde 1976b). Studies have already showed that the bone forming cells respond to strain in vitro (Hasegawa et al 1985; Buckley et al 1988). The strain bone undergoes, and daily fluctuation in parathyroid and growth hormones affect re-ordering and ensure a change in rate of matrix production (Jones and Boyde 1976a, 1976c, 1977a, 1979). Buckley and co-workers (1988), inducing deformation regimen with cyclic strain, showed that the osteoblasts could undergo a reorientation of 90° within hours of an applied strain. Such a reorientation is not above dispute in vivo. However, once such a reorientation in the pattern of osteoblasts has been reached after the initial deposition of collagen fibres at the periphery, further reorientation to such an extent is not necessary for the development of the characteristic collagen orientation pattern seen in the successive lamellae in the present study; a far lesser degree of change in orientation of the osteoblasts can give rise to the typical different orientations of collagen fibres in the successive lamellae. Thus the characteristic orientation of collagen fibres in predominantly different orientations is attributable to the differing functional activity of osteoblasts in the `closing cones'

Osteons have been differentiated into three varieties depending on their appearance in polarised light - LS, TS and mixed (Ascenzi and Bonucci 1967, 1968; Evans 1974). This present study showed that the great majority of osteons present in the equine radius cranial and caudal cortices were either predominantly dark or predominantly bright, and exhibited different degrees of lamellation. Absolutely bright or dark (parallel fibred) osteons in either of the cortices could hardly be found. This may be because we rarely look exactly along the long axis of the osteon. The rare, very dark osteons still had a thick PLM bright component at their peripheries.

The present study with the >515nm Autofluorescence mode of Confocal Microscopy also confirms previous findings using backscattered electron imaging (Boyde et al 1992; Riggs et al 1993b) that the cranial cortex is more mineralised than the caudal cortex. This finding also associates with the differences in turnover rate in cranial and caudal cortices (Lanyon et al 1982; Boyde and Riggs 1990; Riggs et al 1993a). The present study suggests that the reason that

the mineralisation density is more in the cranial cortex is that the greater part of its primary bone remains unremodelled even at a greater age. This study further suggests that the secondary bone, if not further remodelled, can achieve a higher level of mineralisation density than the primary bone with increasing age. The later is better demonstrated in the caudal cortex of the radii of the greater age animals.

Marotti (1993) argues that it is only parallel fibred osteons (Marotti and Muglia 1992) that are suited to withstand tensile stress. The PLM dark lamellae are supposed to be formed by loosely interwoven fibres which reach a higher degree of mineralisation than the collagen dense lamellae, and thus better suited to withstand compression. Marotti found no correlation between the degree of matrix calcification and the ultimate tensile strength of collagen fibres. Although these features would explain the fact that the tension cortex is stronger in compression than tension, the inevitable question is, where does the tensile strength in cranial cortex come from? If it is true that the more the longitudinal fibres, the greater is the tensile strength, obviously, the answer lies within itself.

Collagen fibres provide the key element for the biomechanical strength of the osteons. Since bone adapts to function, the biological organisation of the collagen should fit well with its biomechanical need.

Background data of Chapter 2

Table 2.5a-b

Table 2.5a Number of osteons in 20 areas (from periosteum to endosteum) in pairs of undecalcified plane parallel sections of cranial cortex taken 1cm apart: the most distant sections being at 5.5cm proximal to the midshaft plane of the radius (midshaft plane, 1cm, 2cm, 3cm, 4cm and 5.5cm proximally).

18y cranial

Sections	Total no.		Bright (Obl)		Dark (LS)	
	1°	2°	1°	2°	1°	2°
Midshaft/1	103	162	4	22	99	140
Midshaft/2	113	169	3	25	110	144
1cm.prox./1	110	165	4	15	106	150
1cm.prox./2	94	169	9	25	85	144
2cm.prox./1	142	132	9	22	133	110
2cm.prox./2	126	127	11	22	115	105
3cm.prox./1	127	164	8	16	119	148
3cm.prox./2	111	165	8	27	103	138
4cm.prox./1	123	154	14	23	109	131
4cm.prox./2	137	163	20	27	117	136
5cm.prox/1	103	176	4	24	99	152
5.5cm.prox/2	80	179	10	39	70	140

Table 2.5b Number of osteons in 20 areas (from periosteum to endosteum) in pairs of undecalcified plane parallel sections of caudal cortex taken 1cm apart: the most distant sections being at 5.5cm proximal to the midshaft plane of the radius (midshaft plane, 1cm, 2cm, 3cm, 4cm and 5.5cm proximally).

18y Caudal:

Sections	Total no.		Bright (Obl)		Dark (LS)	
	1°	2°	1°	2°	1°	2°
Midshaft/1	3	425	0	405	3	20
Midshaft/2	1	486	0	477	1	9
1cm. prox./1	3	343	0	322	3	21
1cm. prox./2	0	335	0	320	0	15
2cm.prox./1	6	358	4	334	2	24
2cm.prox./2	2	349	1	339	1	10
3cm.prox./1	3	392	2	373	1	19
3cm.prox./2	1	401	0	372	1	29
4cm.prox./1	6	363	0	333	6	30
4cm.prox./2	6	400	0	373	6	27
5cm.prox/1	3	387	0	342	3	45
5.5cm.prox/2	6	411	0	356	6	55

Table 2.6a-b 11y cranial and caudal cortex:

Table 2.6a Number of osteons in 20 areas in pairs of plane parallel sections of 100µm thickness, obtained from the radius (cranial aspect) starting from midshaft plane and then at 1cm interval proximally up to 5cm (midshaft plane, 1cm, 2cm, 3cm, 4cm and 5cm proximally). Tabulated with their characteristic collagen orientation: oblique (bright) or longitudinal (dark).

Sections	Total no.		Bright (Obl)		Dark (LS)	
	1°	2°	1°	2°	1°	2°
Midshaft/1	164	107	39	23	125	84
Midshaft/2	173	99	28	26	145	73
1 cm/1	120	136	11	20	109	116
1 cm/2	132	126	16	18	116	108
2 cm./1	110	161	17	15	93	146
2 cm/2	123	140	15	8	108	132
3 cm/1	121	109	17	15	104	94
3 cm/2	118	118	12	6	106	112
4 cm/1	123	103	8	8	115	95
4 cm/2	128	104	25	12	103	92
5 cm/1	135	89	29	12	106	77
5 cm/2	131	94	11	17	120	77

Table 2.6b Number of osteons in 20 areas in pairs of plane parallel sections of 100μm thickness, obtained from the caudal cortex of 11 year old radius, from its midshaft plane and then at 1cm intervals proximally up to 5 cm, tabulated with their characteristic collagen orientation: oblique - bright, Longitudinal - Dark.

Caudal:

Sections	Total no.		Bright (Obl)		Dark (LS)	
	1°	2°	1°	2°	1°	2°
Midshaft/1	38	212	13	191	25	21
Midshaft/2	27	218	7	191	20	27
1 cm/1	43	195	13	160	30	35
1 cm/2	38	206	17	181	21	25
2 cm/1	36	215	4	176	32	39
2 cm/2	44	200	6	171	38	29
3 cm/1	42	220	1	189	41	31
3 cm/2	44	218	0	189	44	29
4 cm/1	31	226	2	181	29	45
4 cm/2	33	210	1	178	32	32
5 cm/1	39	227	2	187	37	40
5 cm/2	38	223	1	188	37	35

Table 2.7a-b Unknown age #1

Table 2.7a Total no. of osteons in a 20 areas extending from periosteal to endosteal side in each of the cranial sections of the horse radius of unknown age 1 (midshaft plane, 6.5 mm and 13 mm proximal).

Sections	Total no.		Bright (Obl)		Dark (LS)	
	1°	2°	1°	2°	1°	2°
Midshaft.	103	98	2	9	101	89
Middle (6.5mm)	90	108	23	28	67	80
Proximal (13mm)	97	107	9	24	88	83

Table 2.7b No. of osteons in 20 areas (periosteal to endosteal) in each of the caudal sections of the horse radius of unknown age 1 (midshaft, 6.5 mm and 13 mm proximal).

Sections	Total no.		Bright (Obl)		Dark (LS)	
	1°	2°	1°	2°	1°	2°
Midshaft	16	427	1	389	15	38
Middle (6.5mm)	11	399	0	365	11	34
Proximal (13mm)	18	405	0	375	18	30

Table 2.8a No. of osteons in 20 areas (on the periosteal side) in each of the cranial sections of the horse radius of unknown age 1 (midshaft, 6.5mm and 13mm proximal).

Table 2.8a-b

Cranial

Sections	Total no.		Bright (Obl)		Dark (LS)	
	1°	2°	1°	2°	1°	2°
Midshaft	104	136	49	28	55	108
Middle(6.5mm)	108	144	71	56	37	88
Prox. (13mm)	111	137	61	39	50	98

Table 2.8b. No. of osteons in 20 areas (on the periosteal side) in each of the caudal sections of the horse radius of unknown age 1 (midshaft, 6.5mm and 13mm proximal).

Caudal:

Sections	Total no.		Bright (Obl)		Dark (LS)	
	1°	2°	1°	2°	1°	2°
Midshaft	0	482	0	438	0	44
Middle (6.5mm)	1	485	0	463	1	22
Prox.(13mm)	0	477	0	425	0	52

Table 2.9a-b 6 year cranial and caudal:

Table 2.9a Number of osteons in 20 areas in 6y cranial cortex.

Sections	Total no.		Bright (Obl)		Dark (LS)	
	1°	2°	1°	2°	1°	2°
Midshaft	124	106	0	9	124	97
3 cm. prox.	135	83	0	5	135	78

Table 2.9b Number of osteons in 20 areas in 6y caudal cortex.

Sections	Total no.		Bright (Obl)		Dark (LS)	
	1°	2°	1°	2°	1°	2°
Midshaft	0	220	0	220	0	0
3 cm. prox.	0	206	0	206	0	0

Table 2.10a-b Unknown age #2 cranial and caudal:

Table 2.10a Number of osteons in 20 areas in unknown age (2) cranial cortex.

Sections	Total no.		Bright (Obl)		Dark (LS)	
	1°	2°	1°	2°	1°	2°
Midshaft	99	103	0	6	99	97
3 cm. prox.	123	75	0	8	123	67

Table 2.10b Number of osteons in 20 area in unknown age (2) caudal cortex.

Sections	Total no.		Bright (Obl)		Dark (LS)	
	1°	2°	1°	2°	1°	2°
Midshaft	66	204	66	201	0	3
3 cm. prox.	99	165	99	155	0	10

Table 2.11a-b 12 year cranial and caudal

Table 2.11a Number of osteons in 20 areas in 12y cranial sections.

Sections	Total no.		Bright (Obl)		Dark (LS)	
	1°	2°	1°	2°	1°	2°
Midshaft	168	132	8	5	160	127
3 cm. prox.	126	108	3	4	123	104

Table 2.11b Number of osteons in 20 areas in 12y caudal sections.

Sections	Total no.		Bright (Obl)		Dark (LS)	
	1°	2°	1°	2°	1°	2°
Midshaft	2	249	2	249	0	0
3 cm. prox.	11	222	8	219	3	3

Table 2.12a-b 18year #2 cranial and caudal:

Table 2.12a No. of osteons in 20 areas in 18y (2) cranial sections.

Sections	Total no.		Bright (Obl)		Dark (LS)	
	1°	2°	1°	2°	1°	2°
Midshaft	142	79	10	13	132	66
3 cm. prox.	139	81	28	21	111	60

Table 2.12b No. of osteons in 20 areas in 18y (2) caudal sections.

Sections	Total no.		Bright (Obl)		Dark (LS)	
	1°	2°	1°	2°	1°	2°
Midshaft	26	277	25	274	1	3
3 cm. prox.	23	249	17	235	6	14

Tables 2.13 - 2.19

Proportion of longitudinal and oblique collagen in undecalcified plane parallel sections of 100 µm thickness, one each from the cranial and caudal cortices of 7 animals. Hits on grid in secondary osteons were recorded, subdividing into most peripheral, midthickness and central.

B = Bright = oblique, D = Dark = Longitudinal. Total hits on grid - 36.

Table 2.13a-b 6y cranial and caudal sections:

Table 2.13a 6y cranial

1	2	3	4	5	6
Field	Hits in 2°	Periph B/D	Mid B/D	Central B/D	Total B/D
1	9	8/0	0/0	0/1	8/1
2	11	8/0	0/1	0/2	8/3
3	9	2/0	1/4	1/1	4/5
4	3	2/0	0/1	0/0	2/1
5	8	4/0	0/2	1/1	5/3
6	11	6/0	1/4	0/0	7/4
7	9	6/0	2/1	0/0	8/1
8	18	10/0	1/2	0/5	11/7
9	9	6/0	0/2	0/1	6/3
10	6	3/0	0/2	1/0	4/2
11	13	8/0	0/5	0/0	8/5
12	9	6/0	0/1	0/2	6/3
13	10	7/0	1/2	0/0	8/2
14	8	4/0	2/2	0/0	6/2
15	10	6/0	1/1	0/2	7/3
16	16	11/0	1/3	0/1	12/4
17	15	11/0	0/2	0/2	11/4
18	4	1/0	0/2	0/1	1/3
19	7	5/0	0/1	0/1	5/2
20	3	3/0	0/0	0/0	3/0

Table 2.13b 6y caudal

1 Field	2 Hits in 2°	3 Periph B/D	4 Mid B/D	5 Central B/D	6 Total B/D
1	29	15/0	10/0	4/0	29/0
2	34	17/0	13/0	4/0	34/0
3	36	15/0	16/0	5/0	36/0
4	33	16/0	14/0	3/0	33/0
5	34	18/0	10/0	6/0	34/0
6	32	14/0	10/0	8/0	32/0
7	32	19/0	8/0	11/0	32/0
8	32	17/0	7/0	8/0	32/0
9	33	18/0	9/0	6/0	33/0
10	34	12/0	12/0	10/0	34/0
11	33	20/0	9/0	4/0	33/0
12	31	17/0	7/0	7/0	31/0
13	30	19/0	8/0	3/0	30/0
14	32	17/0	12/0	3/0	32/0
15	33	10/0	18/0	5/0	33/0
16	35	15/0	16/0	4/0	35/0
17	27	15/0	10/0	2/0	27/0
18	31	14/0	14/0	3/0	31/0
19	31	11/0	10/0	10/0	31/0
20	31	20/0	6/0	5/0	31/0

Table 2.14a-b 11y cranial and caudal sections:

Table 2.14a 11y cranial

1 Field	2 Hits in 2°	3 Periph B/D	4 Mid B/D	5 Central B/D	6 Total B/D
1	13	7/0	0/4	2/0	9/4
2	11	4/1	0/4	0/2	4/7
3	12	7/1	0/3	1/0	8/4
4	1	0/0	1/0	0/0	1/0
5	7	3/0	1/3	0/0	4/3
6	12	5/1	0/6	0/0	5/7
7	4	4/0	0/0	0/0	4/0
8	15	10/0	0/4	1/0	11/4
9	18	10/1	3/3	1/0	14/4
10	14	5/0	3/5	1/0	9/5
11	19	11/1	0/6	1/0	12/7
12	6	2/0	2/0	2/0	6/0
13	5	4/0	0/1	0/0	4/1
14	4	1/0	0/3	0/0	1/3
15	7	4/1	1/1	0/0	5/2
16	6	3/0	1/1	1/0	5/1
17	8	4/0	2/1	0/1	6/2
18	14	9/0	0/3	1/1	10/4
19	9	5/0	0/3	0/1	5/4
20	13	5/0	1/7	0/0	6/7

Table 2.14b 11y caudal

1 Area	2 Hits in 2°	3 Periph B/D	4 Mid B/D	5 Central B/D	6 Total B/D
1	32	20/0	10/0	1/1	31/1
2	23	11/0	9/0	3/0	23/0
3	25	6/0	18/0	1/0	25/0
4	27	11/0	10/0	6/0	27/0
5	21	12/0	8/0	1/0	21/0
6	15	10/0	4/0	1/0	15/0
7	13	6/0	4/0	2/1	12/1
8	6	5/0	0/0	1/0	6/0
9	26	17/0	8/0	1/0	26/0
10	15	8/0	2/0	1/4	14/1
11	25	11/0	13/0	1/0	25/0
12	26	8/0	13/0	5/0	26/0
13	19	10/0	7/0	2/0	19/0
14	17	8/0	8/0	1/0	17/0
15	17	12/0	3/0	1/1	16/1
16	6	2/0	2/0	2/0	6/0
17	23	14/0	6/0	3/0	23/0
18	21	8/0	9/0	3/1	20/1
19	22	11/0	8/0	3/0	22/0
20	30	21/1	5/1	2/0	28/2

Table 2.15a-b 12y cranial and caudal sections:

Table 2.15a 12y cranial

1 Field	2 Hits in 2°	3 Periph B/D	4 Mid B/D	5 Central B/D	6 Total B/D
1	8	2/0	0/5	1/0	3/5
2	10	6/0	1/3	0/0	7/3
3	6	2/1	0/3	0/0	2/4
4	7	4/0	0/3	0/0	4/3
5	3	2/0	1/0	0/0	3/0
6	9	4/0	0/3	0/2	4/5
7	10	2/1	1/5	0/1	3/7
8	13	8/0	1/2	0/2	9/4
9	9	5/0	2/1	1/0	8/1
10	5	0/1	1/1	1/1	2/3
11	15	7/0	2/3	1/2	10/5
12	6	3/0	1/1	0/1	4/2
13	0	0/0	0/0	0/0	0/0
14	5	4/0	0/0	0/1	4/1
15	12	4/0	1/5	0/2	5/7
16	13	10/0	0/3	0/0	10/3
17	14	6/0	3/1	3/1	12/2
18	4	4/0	0/0	0/0	4/0
19	10	5/0	0/3	2/0	7/3
20	6	3/0	1/1	1/0	5/1

Table 2.15b 12y caudal

1 Field	2 Hits in 2°	3 Periph B/D	4 Mid B/D	5 Central B/D	6 Total B/D
1	34	20/0	9/0	5/0	34/0
2	35	16/0	19/0	5/0	35/0
3	34	15/0	12/0	7/0	34/0
4	35	19/0	11/0	5/0	35/0
5	30	15/0	10/0	5/0	30/0
6	31	10/0	18/0	3/0	31/0
7	32	15/0	15/0	2/0	32/0
8	28	13/0	11/0	4/0	28/0
9	25	14/0	6/0	5/0	25/0
10	18	7/0	9/0	2/0	18/0
11	33	19/0	11/0	3/0	33/0
12	30	15/0	8/0	7/0	30/0
13	31	16/0	9/0	6/0	31/0
14	27	12/0	11/0	4/0	27/0
15	28	14/0	12/0	2/0	28/0
16	30	16/0	11/0	3/0	30/0
17	34	14/0	15/0	5/0	34/0
18	28	8/0	16/0	4/0	28/0
19	17	6/0	7/0	4/0	17/0
20	15	6/0	6/0	3/0	15/0

Tables 2.16a-b 18y cranial and caudal cortex:

Table 2.16a 18y cranial

1 Field	2 Hits in 2°	3 Periph B/D	4 Mid B/D	5 Central B/D	6 Total B/D
1	18	15/0	0/2	1/0	16/2
2	15	10/0	0/4	1/0	11/4
3	16	10/1	0/3	2/0	12/4
4	15	8/1	0/4	1/1	9/6
5	14	8/3	0/3	0/0	8/6
6	17	8/1	0/6	1/1	9/8
7	15	7/2	0/6	0/0	7/8
8	22	12/1	5/4	0/0	17/5
9	21	15/0	0/4	0/2	15/6
10	16	9/0	0/5	2/0	11/5
11	15	9/0	3/2	1/0	13/2
12	16	12/0	0/4	0/0	12/4
13	15	8/0	1/4	1/1	10/5
14	16	10/0	1/4	1/0	12/4
15	14	12/0	0/1	1/0	13/1
16	17	10/0	1/6	0/0	11/6
17	15	10/0	2/2	2/0	14/2
18	10	6/0	1/3	0/0	7/3
19	11	6/0	0/4	0/1	6/5
20	17	14/0	0/1	0/2	14/3

Table 2.16b 18y caudal

1 Field	2 Hits in 2°	3 Periph B/D	4 Mid B/D	5 Central B/D	6 Total B/D
1	32	21/0	7/2	2/0	30/2
2	36	20/0	12/0	3/1	35/1
3	34	19/0	12/0	3/0	34/0
4	33	19/0	6/2	3/3	28/5
5	32	21/0	2/6	2/1	25/7
6	30	18/0	6/4	2/0	26/4
7	32	17/0	7/5	3/0	27/5
8	35	16/0	12/1	6/0	34/1
9	34	24/0	7/1	2/0	33/1
10	33	20/0	5/2	6/0	31/2
11	34	16/0	6/8	4/0	26/8
12	33	17/0	8/6	2/0	27/6
13	31	22/0	5/2	2/0	29/2
14	28	10/0	13/3	2/0	25/3
15	30	12/0	11/6	1/0	24/6
16	36	26/0	6/2	2/0	34/2
17	35	24/1	9/1	0/0	33/2
18	36	19/0	11/3	3/0	33/3
19	34	19/0	6/3	6/0	31/3
20	34	23/1	6/1	3/0	32/2

Tables 2.17a-b 18y (2) cranial and caudal cortex:

Table 2.17a 18y (2) cranial

1	2	3	4	5	6
Field	Hits in 2°	Periph B/D	Mid B/D	Central B/D	Total B/D
1	4	4/0	0/0	0/0	4/0
2	3	2/0	0/1	0/0	2/1
3	2	1/0	0/0	0/1	1/0
4	4	3/0	0/1	0/0	3/1
5	5	4/0	1/0	0/0	5/0
6	4	2/0	0/1	0/1	2/2
7	14	12/0	0/0	1/1	13/1
8	8	2/0	0/5	0/1	2/6
9	12	7/0	0/4	0/1	7/5
10	8	7/0	0/1	0/0	7/1
11	2	2/0	0/0	0/0	2/0
12	0				0/0
13	2	2/0	0/0	0/0	2/0
14	1	1/0	0/0	0/0	1/0
15	2	1/0	0/1	0/0	1/1
16	8	6/0	1/1	0/0	7/1
17	12	6/0	1/3	0/2	7/5
18	7	3/0	1/1	0/2	4/3
19	8	5/0	0/3	0/0	5/3
20	2	1/0	0/1	0/0	1/1

Table 2.17b 18y (2) caudal

1 Field	2 Hits in 2°	3 Periph B/D	4 Mid B/D	5 Central B/D	6 Total B/D
1	34	15/0	18/0	1/0	34/0
2	30	15/0	7/0	8/0	30/0
3	24	15/0	5/0	4/0	24/0
4	28	13/0	12/0	3/0	28/0
5	21	12/0	2/0	7/0	21/0
6	16	8/0	6/0	2/0	16/0
7	16	7/0	6/0	3/0	16/0
8	3	2/0	0/0	1/0	3/0
9	29	13/0	11/0	5/0	29/0
10	30	20/0	6/0	4/0	30/0
11	20	12/0	4/0	4/0	20/0
12	29	12/0	10/0	7/0	29/0
13	16	1/0	10/0	5/0	16/0
14	20	13/0	3/0	4/0	20/0
15	10	5/0	4/0	1/0	10/0
16	5	5/0	0/0	0/0	5/0
17	30	20/0	7/0	3/0	30/0
18	23	8/0	14/0	1/0	23/0
19	31	13/0	15/0	3/0	31/0
20	30	17/0	8/0	5/0	30/0

Table 2.18a-b Unknown age (1) cranial and caudal cortex:

Table 2.18a Unknown age (1) cranial

1	2	3	4	5	6
Field	Hits in 2°	Periph B/D	Mid B/D	Central B/D	Total B/D
1	13	8/3	0/1	1/0	9/4
2	2	1/0	0/0	0/1	1/1
3	4	3/0	1/0	0/0	4/0
4	9	4/3	0/1	0/1	4/5
5	4	4/0	0/0	0/0	4/0
6	2	0/0	0/1	0/1	0/2
7	5	4/0	1/0	0/0	5/0
8	15	12/0	1/0	2/0	15/0
9	10	4/1	1/3	1/0	6/4
10	9	4/0	2/3	0/0	6/3
11	5	4/0	1/0	0/0	5/0
12	6	4/0	1/0	0/1	5/1
13	5	3/0	1/0	0/1	4/1
14	4	1/0	0/0	0/3	1/3
15	6	3/0	1/0	2/0	6/0
16	7	4/1	0/2	0/0	4/3
17	4	1/0	0/2	0/1	1/3
18	6	2/0	0/2	0/2	2/4
19	5	3/1	0/1	0/0	3/2
20	4	3/0	0/0	0/1	3/1

Table 2.18b Unknown age (1) caudal

1 Field	2 Hits in 2°	3 Periph B/D	4 Mid B/D	5 Central B/D	6 Total B/D
1	34	18/0	13/0	2/1	33/1
2	36	19/0	8/0	8/1	35/1
3	34	20/0	13/0	1/0	34/0
4	30	15/0	9/0	6/0	30/0
5	29	20/0	5/1	3/0	28/1
6	26	23/0	3/0	0/0	26/0
7	24	12/0	8/1	2/1	22/2
8	18	12/0	3/2	1/0	16/2
9	16	8/0	3/5	0/0	11/5
10	31	17/0	7/3	4/0	28/3
11	34	15/0	15/1	2/1	32/2
12	35	21/1	5/4	4/0	30/5
13	32	23/0	5/2	2/0	30/2
14	33	24/1	4/2	2/0	30/3
15	29	20/1	5/3	0/0	25/4
16	25	14/2	4/2	2/1	20/5
17	23	14/2	3/1	3/0	20/3
18	34	17/0	9/2	4/0	30/4
19	33	19/0	7/1	1/6	32/1
20	34	22/1	8/2	1/0	31/3

Table 2.19 a-b Unknown age (2) cranial and caudal cortex:

Table 2.19a Unknown (2) cranial

1 Field	2 Hits in 2°	3 Periph B/D	4 Mid B/D	5 Central B/D	6 Total B/D
1	7	6/0	0/1	0/0	6/1
2	15	6/0	0/5	0/4	6/9
3	13	10/0	0/2	0/1	10/3
4	15	9/2	0/4	0/0	9/6
5	11	7/0	0/3	0/1	7/4
6	7	5/0	0/1	0/1	5/2
7	11	6/0	2/1	0/2	8/3
8	17	1/0	2/4	0/0	13/4
9	6	6/0	0/0	0/0	6/0
10	12	7/0	1/2	0/2	8/4
11	7	5/0	0/1	0/1	5/2
12	12	8/0	1/1	0/2	9/3
13	10	5/0	0/4	0/1	5/5
14	5	2/0	1/2	0/0	3/2
15	11	5/0	2/2	0/2	7/4
16	17	10/0	0/6	0/1	10/7
17	3	3/0	0/0	0/0	3/0
18	2	1/0	0/1	0/0	1/1
19	12	7/0	0/4	0/1	7/5
20	5	3/0	0/1	0/1	3/2

Table 2.19b Unknown (2) caudal

1 Field	2 Hits in 2°	3 Periph B/D	4 Mid B/D	5 Central B/D	6 Total B/D
1	32	20/0	8/0	4/0	32/0
2	27	16/0	6/2	2/1	24/3
3	26	14/0	11/0	1/0	26/0
4	10	7/0	2/0	1/0	10/0
5	5	2/0	2/0	1/0	5/0
6	5	3/0	0/0	1/1	4/1
7	30	18/0	8/0	3/1	29/1
8	23	11/0	9/0	2/1	22/1
9	18	10/0	3/0	5/0	18/0
10	8	5/0	3/0	0/0	8/0
11	4	3/0	1/0	0/0	4/0
12	3	3/0	0/0	0/0	3/0
13	29	17/0	8/0	4/0	29/0
14	27	15/0	10/2	0/0	25/2
15	20	15/0	2/3	0/0	17/3
16	10	7/0	2/0	0/1	9/1
17	4	3/0	1/0	0/0	4/0
18	23	11/0	9/0	3/0	23/0
19	20	12/0	6/0	1/1	19/1
20	10	7/0	1/2	0/0	8/2

CHAPTER 3

A STRUCTURAL PREDISPOSITION TO SPONTANEOUS FRACTURE IN EQUINE LONG BONE: AN INHERENT WEAKNESS IN ITS THREE DIMENSIONAL ARCHITECTURE.

3.1.1 INTRODUCTION

The compact bone of the radial midshaft rarely fractures: metacarpal (McIII) fractures most commonly occur in the equine forelimb long bones and this account is based on the excellent review by Riggs (1990). Condylar fractures of third metacarpal bone (cannon bone) are very frequent in young racing Thoroughbreds (Rooney 1974, Rick et al 1983). The fracture mostly involves the lateral condyle (Rick et al 1983; Meagher 1976). Sex distribution is nearly equal (Rick et al 1983). The mean age of the affected animals has been reported to be about 4 years (Meagher 1976; Rick et al 1983).

The fractures propagate through regions which are largely cancellous in nature. The striking feature is that, the fracture line almost always shows a characteristic morphology in its origin and propagation. Originating in a focal area of the subchondral region of the McIII or MT3 near the distal articular surface immediately adjacent to the sagittal ridge, the fracture line passes proximally for 3 to 4 cm before extending further axially or laterally. More lateral extension taking an exit through the cortical bone leads to complete fracture (Rick et al 1983; Riggs 1990). Complete fracture is more common than incomplete fracture. Complete condylar fractures are those which interrupt the articular surface before extending on to the periosteal surface of the metaphyseal or the diaphyseal regions proximally. Incomplete fractures do not interrupt the continuity of the proximal cortical bone (figures 3.1a-b).

It is suggested that condylar fractures of McIII are almost exclusively the result of strenuous exercise (Rooney 1974; Meagher 1976). Bio-mechanical, fatigue and osteochondritic phenomena have been associated with the occurrence of this type of fracture (Rooney 1974; Krook and Maylin 1988; Pool and Meagher 1990). Krook and

Maylin (1988) also suggested that pre-existing cartilaginous lesions in the articular surface could cause lateral condylar fractures of the cannon bone. This contradicts the finding of Pool and Meagher (1990) where degenerative joint disease was thought to be secondary to the fracture that passed through a pre-existing lesion of traumatic osteochondrosis. Further evidence (Pool and Meagher 1990) showed that, even in some fracture cases, the fracture plane passed through a different plane to the osteochondritic lesion present prior to the fracture. Riggs (1990) presented an excellent review in his thesis regarding probable pathogenesis of this type of metacarpal fractures.

Osteochondrosis occurs comparatively less frequently in the distal end of metacarpals among all other joints of the horse, and the lesion frequently seen in other locations is usually bilateral (Rooney 1975a). Moreover, where the lesion is seen associated with fracture, as in the distal end of the tibia, fracture is considered to precede osteochondrosis (Rooney 1975b). Hence, osteochondrosis can hardly be associated with the higher number of condylar fractures of McIII seen in racing horses, which in the majority of cases involve one limb (Rick et al 1983). Rick and co-workers (1983) found palmar erosive defects in the subchondral bone as revealed by radiography (pre-treatment) indicating the presence of degenerative joint disease in 6 cases among 75 animals with cannon bone fracture. This indicate some association of degenerative joint disease with fracture, but does not specifically identify the joint disease to be a major cause of distal condylar fractures.

In degenerative joint disease, excessive stress due to the lesion in the articular cartilage, may cause sclerosis of the subchondral bone leading to the structural failure. Chai et al (1991) demonstrated simillar pathology in man.

"Bucked shin", another commonly occuring pathology in the equine cannon bones is suggested to happen due to fatigue failure (Norwood 1978). But this usually occur during the first year of training in 2 year old animals. Fatigue fractures do not occur usually in horses older than 4 year (Nunamaker et all 1989). The condylar fractures of McIII usually occur in rather older animals.

Besides bone strength, strain history also contributes to the causation of fracture (Biewener and Dial 1992). Strain on the horses third metacarpal bone increases with increasing speed (Nunamaker 1986). This could perhaps be associated with the higher incidence of distal condylar fracture in the Thoroughbred.

Static loads have no effect on modelling and remodelling activity. Lower strain values corresponding to normal daily activities evoke no reaction (Frost 1986). The effects of dynamic loading is profound. Fracture resistance is largely dependent on bone mass and geometry. Trabecular architecture and bone volume fractions are related to the stress direction and magnitude.

Probing explanation is yet lacking regarding the cause of spontaneous type of fracture in the distal metacarpal condyles with the characteristic morphological fracture lines. The presence of some typical organisational features at the site of fracture may contribute to the occurance of condylar fractures with the characteristic morphology.

The aim of this study was to examine the pre-fracture micro-anatomy and pathology in largely cancellous bone regions. The questions that were addressed included (a) are there any organisational features of the bone in the regions prone to fracture which make them so; and (b) can any incipient damage be visualised at such sites prior to fracture. Clearly, the only possibility to obtain material investigating the second point was to use the contralateral limb site in fracture cases which have had to be destroyed.

In this study, 3-D micro-architecture of regions of the third metacarpal and metatarsal bones commonly involved in race track fractures were examined. The regions through which fractures usually initiate and propagate such as the immediate subchondral bone and the trabecular architecture in the distal third of the cannon bone were investigated. The microstructure and growth patterns were studied using Polarised light microscopy, the Edge 3D Microscope, fluorescence mode confocal LM (Bio-Rad Lasersharp) and SEM in both SE and BSE modes.

3.1.2 The anatomy of McIII

The McIII is the single weight bearing bone between the carpal and metacarpo-phalangeal joints. The first and fifth metacarpals are not present, while second and fourth digits are vestigial remnants, known as splint bones, which remain attached to the postero-medial and postero-lateral aspects of the third metacarpus/metatarsus proximally by syndesmosis. The distal end of the cannon bone forms a hinge joint, known as the fetlock joint, with the first phalanx (Thomason 1984).

McIII are designed to withstand large compressive loads, and can also withstand large bending loads in the medio-lateral plane. The proximal end is better adapted for greater AP bending loads than the distal end, where such bending loads cannot normally be produced. Fusion of the accessory metacarpals with McIII increases bending strength and rigidity (Piottrowski et al 1983).

From a lateral view the MCIII is relatively straight. Bone strain recording (Turner et al 1975; Biewener et al 1983a) showed that the McIII is loaded primarily in axial compression, though film/force analysis showed metacarpus to be loaded in sagittal bending, when the palmar cortex is subjected to compression and the dorsal cortex is subjected to tension. The bone also undergoes a medio-lateral bending during the swing phase of the stride. The strain pattern has also been supported later by several other studies (Rubin et al 1989; Gross et al 1990; Riggs 1990; Stover et al 1992). Demonstration of a larger proportion of transverse collagen in palmar and dorsal cortices (Riggs 1990; Stover et al 1992) as a consequence of remodelling with increasing age truly suggests the strain to be compression.

The dorsal articular surface at the distal end of McIII is convex cranially with a sagittal ridge and two smooth condylar surfaces. The subchondral bone of the dorsal surface has a very fine trabecular pattern and appears dense than the subchondral bone at the junction between the dorsal and palmar surfaces. Normally the palmar surface of the distal end of the McIII is smooth and convex. The subcondylar bone is more dense than, and lacks the definite trabecular pattern of the dorso-palmar junction. The sagittal ridge

is less dense than the condyles (O'Brien 1977). Macroscopically, the normal cartilage is smooth on the palmer surface. The width of the medial condyle is slightly greater than that of the lateral condyle.

3.1.3 Pathology of the Fetlock joint

Several studies (O'Brien 1977; Rick et al 1983; review in Riggs 1990) focused on different features observed in joint pathology. Intracapsular soft tissue swelling is only a sign of serious underlying abnormality of the cartilage and/or subchondral bone. The condylar surface and the sagittal ridge of the McIII flatten when it is associated with ulcerated lesion in the articular cartilage. Wear or score lines appear as linear grooves of varying depth of superficial irregularities to complete fissures in the articular cartilage, extending in a proximal to distal direction. Structural disorganisation and decreased radiodensity result from loss of the normal trabecular pattern in the underlying subchondral bone. Destructive subchondral lesions, less than 1 cm in diameter, are detectable. Osteophytes usually occur on either side of the sagittal ridge near the midline (O'Brien 1977). With an increase in severity, small periarticular osteophytes and osteolytic defects at the cranial distal McIII, on either side of the sagittal ridge gradually causes dishing of the periarticular region which is followed by a productive and destructive process extending down on to the cranial articular surface of the sagittal ridge and condyle (O'Brien 1977).

3.2.1 MATERIALS AND METHODS

Table 3.1

Principal modes of preparation and study of samples.

1. Boiling
2. Enzymatic cleaning using Terg-azyme, 7.5 gms in 1 litre, 5-10 days, change of solution every day, 50°C.
3. Topographical documentation (Photography)
4. 4mm square beam from McIII containing either medial or lateral notch, and AP slices with water cooled slow speed diamond saw, cleaned for SEM.

Figure 3.1

Top - Different types of the condylar fracture of the third metacarpal bone: a) Incomplete, b) Complete-nondisplaced, c) Complete-displaced (after Rick et al 1983 and Riggs 1990).
Bottom - A central 4 mm thick medio-lateral section of a third metacarpal bone from a condylar fracture case (6 year).
The photograph is taken with a 35mm camera with a 80mm macro lens. White squares = 1 cm.

Figure 3.1

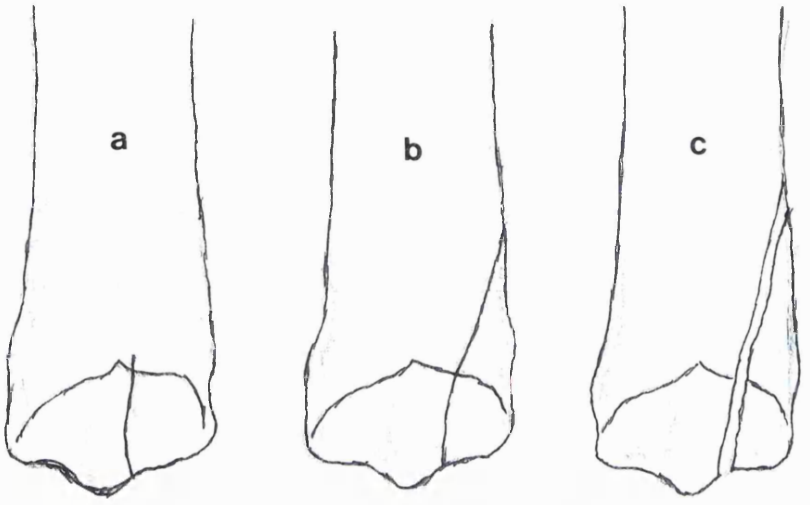

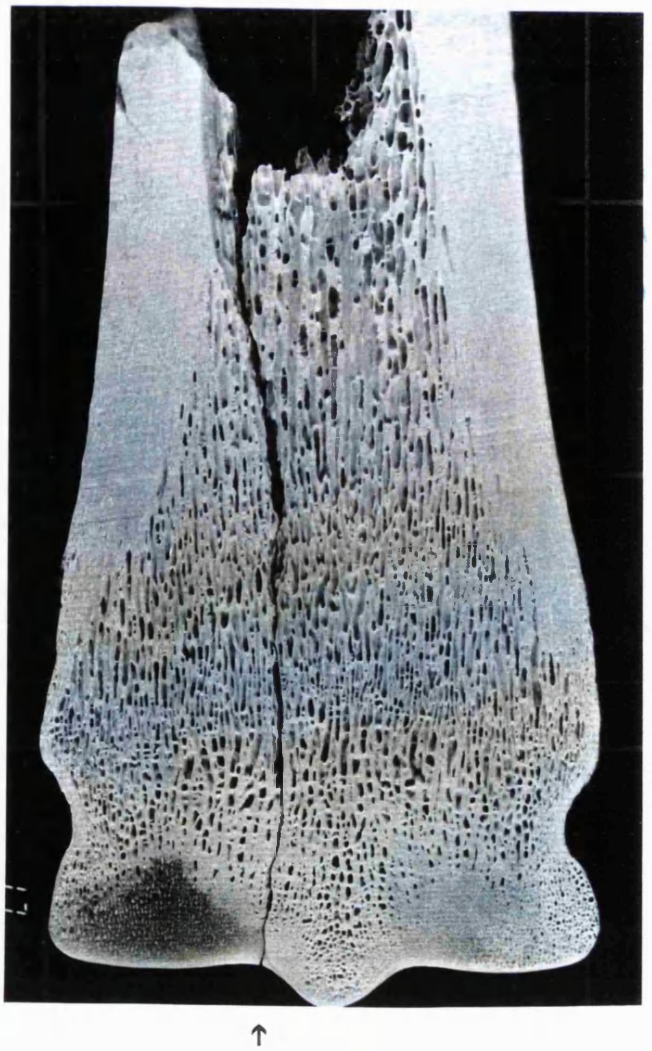

↑

5. 4mm cross-sections and intermediate slices of the beams, cleaned.
6. Mounting in DPX.
7. Polarised light microscopy
8. Autofluorescence mode CSLM
9. Subchondral (sub-articular cartilage) bone blocks, cleaned.
10. Hydrogen peroxide, 4 times diluted, 2hr / 2% 24 hrs.
11. Gold sputter coating
12. 'Conventional' SE SEM
13. Stain with Brilliant Sulphaflavine in 50% ethanol.
14. PMMA embedding and polishing.
15. Carbon coating, SEM BSE.
16. CSLM of PMMA embedded beams and blocks.

The materials studied consisted of Thoroughbred racehorse limbs within hours of euthanasia of animals destroyed because of spontaneous fractures during racing or training. Thus McIII from 16 animals, two with McIII and two with a hindlimb P1 fracture, were collected and stored with skin intact at -20°. Bones were dissected as soon as possible and sawn while deep frozen.

Each McIII was sawn medio-laterally into 3 or 4 pieces using a band saw. The thickness of the middle piece was 4mm. Experiments have been conducted to discover a satisfactory cleaning regime which will remove all soft tissue elements, including periosteal and marrow tissue, bone cells and fat. Initially some samples were boiled in a detergent solution (Nunamaker et al 1989) for approximately 15 hours. The cleaned bone, devoid of soft tissues, still contained blood and fat deep within the tissue. Other samples were treated by a commercial enzyme cleaning detergent (Boyde 1984; Riggs 1990) designed for cleaning surgical instruments (Terg-a-zyme, Aldrich chemical Co., Milwaukee, USA). However, unlike previous procedures, the bone samples had to be treated for a longer period at 50°C for 10-15 days with a solution (7.5 gm in 1 litre) change every alternate day. The later treatment, combined with mechanical debridement using a water jet, and defatting in acetone has proved to be satisfactory in generating samples with relatively unchanged bone matrix with clean surfaces available, for example, for SEM study.

Figure 3.2

Plan of sectioning of the bone at the site of the fracture.

a) The 4 mm square beams (top) contains the notch, the site of the initiation of the fracture.
b) The lower picture shows the blocks, obtained by cutting the beam at every 4 mm in the water cooled diamond saw. The images are taken with a 35mm camera with a 80mm macro lens.

Figure 3.2

a

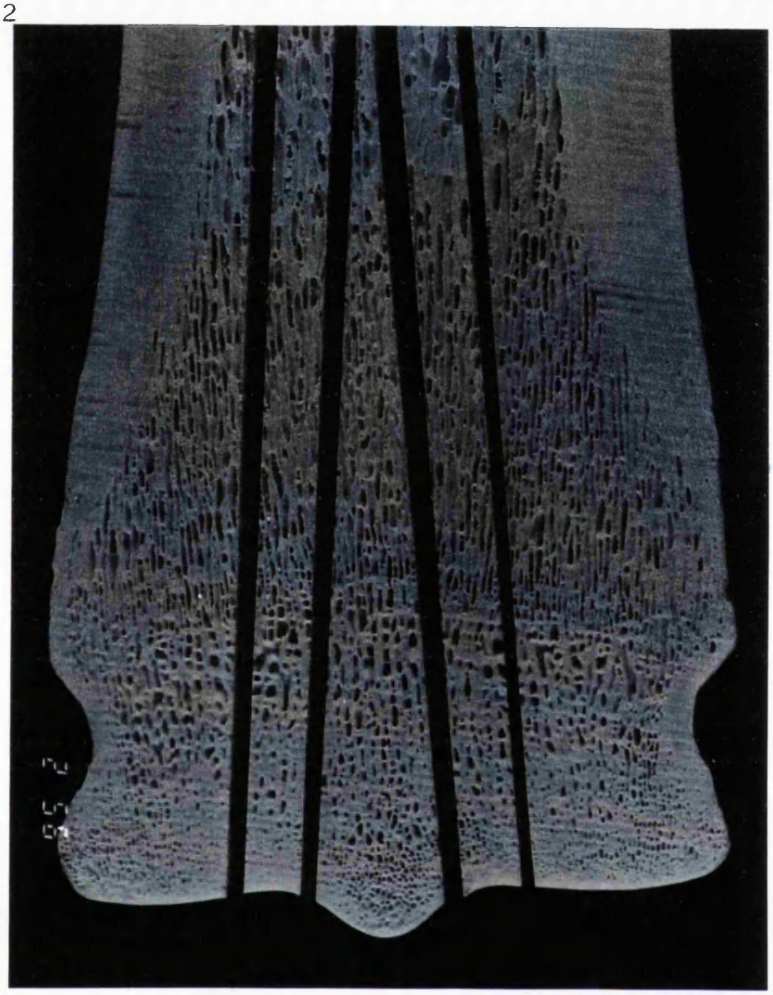

b

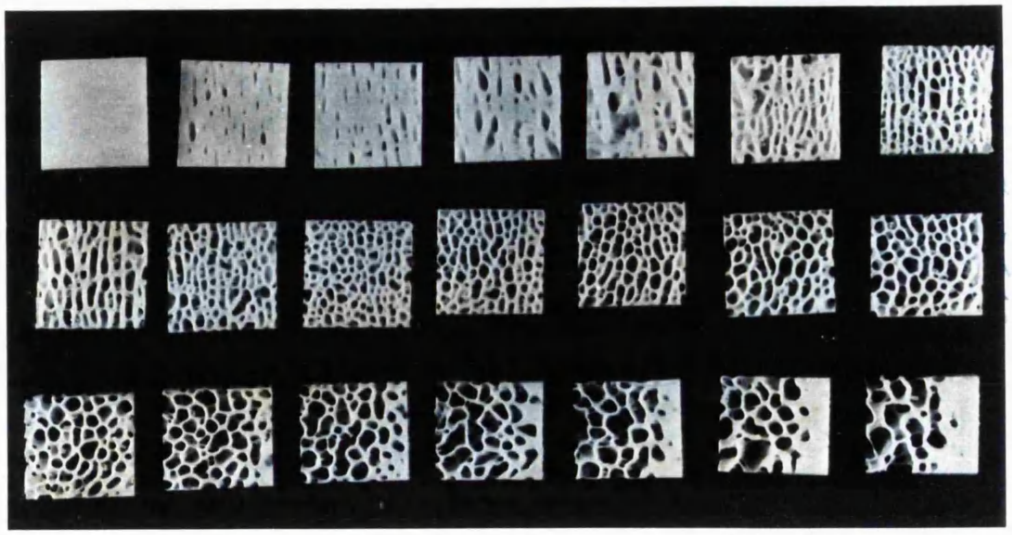

The architecture of the trabecular bone in McIII samples was studied using plane parallel 4mm slices (figures 3.2a, 3.3abc) and square section longitudinal beams (Boyde et al 1989, 1990b) cut using a slow speed, water cooled diamond saw (Buehler isomet) to minimise damage to more delicate trabecular elements. The longitudinal beams were prepared such that each contained either the medial or the lateral notch of the articular surface (fig. 3.2a). These specimens were documented by photographing all surfaces at all levels (35mm camera with 80mm macro lens). Samples were examined by SEM after gold sputter coating.

Some were stained (9 animals: 6yG, 7y, 8y, 11y, 12y-2, 18y-2, unk.) with the stable fluorescent dye brilliant sulphaflavine in 50% ethanol, dehydrated in acetone, and embedded in poly-methyl-methacrylate: PMMA (Boyde and Jones 1983; Boyde 1984; Boyde et al 1986; Reid and Boyde 1987; Boyde et al 1992). PMMA monomer has a low viscosity and penetrates well into bone. Initially vacuum embedding was tried, but discontinued because bubbles could not be avoided. However, successful embedments was achieved by serial infiltration in PMMA when 95% (by volume) distilled methyl methacrylate (BDH Chemicals,UK) was co-polymerised with 5% (by volume) styrene (BDH) at 37°C, and destabilised with 0.2% by weight 2,2-azo-bis (2 methyl propionitrile). Styrene was used to render the embedding resin more stable to electron beam bombardment (Boyde 1984; Boyde et al 1986; Boyde et al 1992) as PMMA is unstable under electron bombardment. To overcome the problem encountered in embedding the long slender beams, boiling tubes were used as disposable embedding 'capsules'. Polished surfaces are required for confocal LM and BSE SEM imaging modes. Problems were encountered in polishing all four sides of each beam, but it seems satisfactory to polish two or three mutually orthogonal surfaces (medial, lateral and anterior or posterior).

Further, one subchondral (sub-articular) bone block containing either the medial or the lateral notch of the distal condyle from each of five more animals (including younger ones) was obtained, cleaned, embedded in PMMA and polished on two faces - antero-posterior and medio-lateral for BSE. Embedded samples were trimmed, ground and polished on graded wet carborundum abrasive papers,

Figure 3.3

4 mm thick middle medio-lateral sections of the distal McIII of 3 animals of different ages:
a) 6y, **b)** 18y & **c)**11y.
The characteristic anisotropic trabecular architecture, visible with naked eyes extending from just proximal to the subchondral bone up to the site of the fusion of the growth plate cartilage (arrow marked). The trabeculae become broader with longer spaces between them towards the site of the fusion. At the site of the fusion, the anisotropic architecture is finer and thinner. Beyond this site, there is a change in the trabecular thickness and orientation.

Figure 3.3

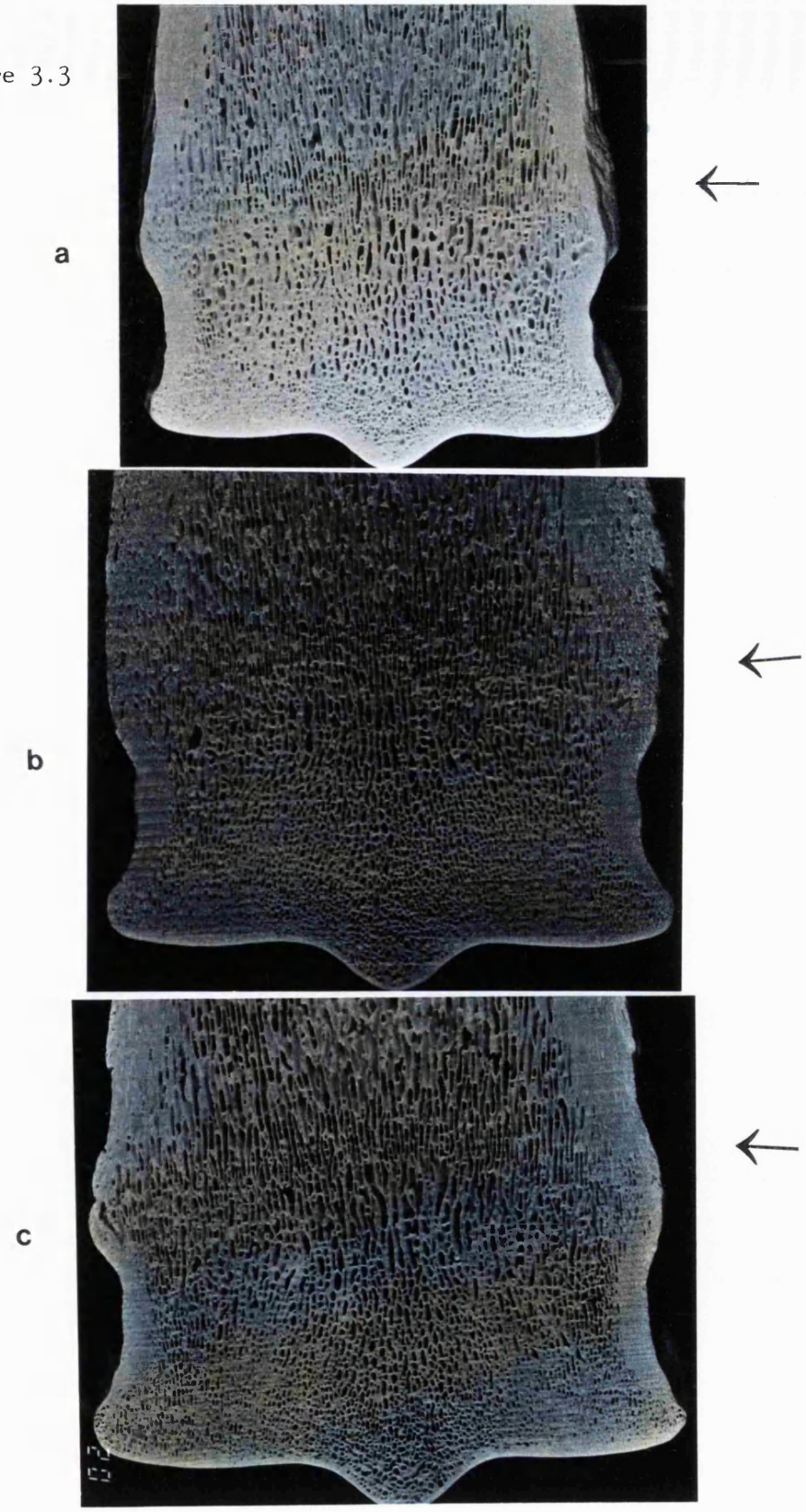

Figure 3.4 a-c:

The site of the notch besides the sagittal ridge of the distal third metacarpal bone of three animals of different ages. The fracture occurs at this site. Note extensive variation in the bone density in this region; a) 8y (top), b) 2y (middle), & c) 7y (bottom).

Figure 3.4 a-c:

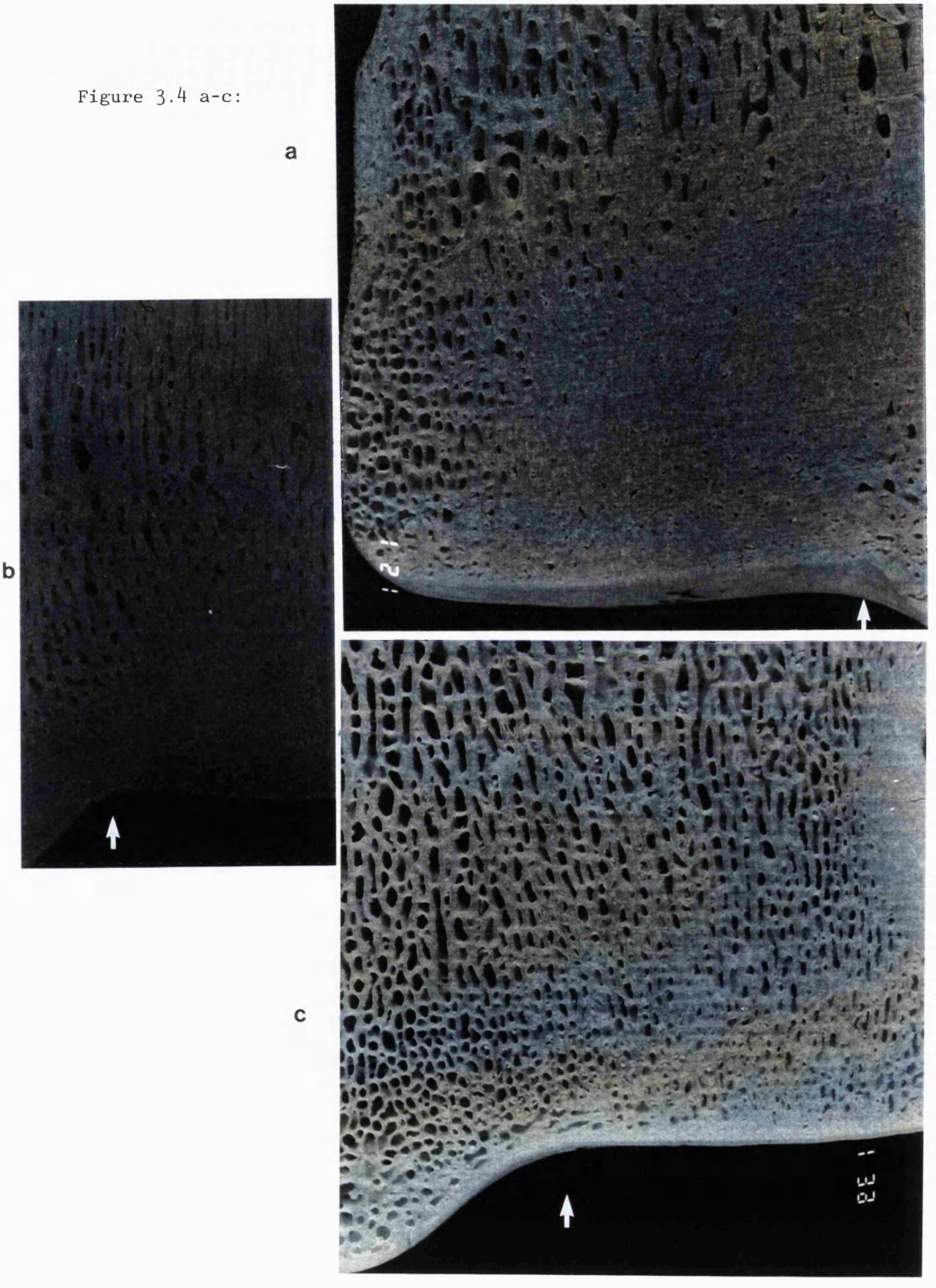

finally finishing with water dispersed diamond (on a rotary lap: Metaserv) to 0.25μm. Samples were coated with carbon to render the surface electrically conductive by flash evaporation of carbon string (Boyde et al 1992).

100μm section were also obtained at each interval while taking the 4mm cross-sections of the beams and mounted in DPX for CPL, Edge and CSLM. 4mm cross-sections from eight animals (6yG, 7y Rt. McIII; 8y Lt. McIII; 11y Rt. McIII; 18y LT. McIII; Unk. Rt. McIII; 2yF Rt. McIII; and 6wF Rt. McIII) were obtained, cleaned, dehydrated and coated with gold by sputtering for SEM (fig. 3.2b). The sex of the animals was unknown where not mentioned.

Further samples:

Further beams and antero-posterior slices were obtained from some more younger and older animals such as

1. One lateral beam and two AP slices from a 1d Lt. McIII.
2. One medial beam and two AP slices from a 6wF Rt. McIII.

Beams and one slice from each animal were cleaned and coated for SEM.

3. 6 wk Lt. McIII separated at its growth plate was cut on its transverse plane in its epiphysis, 17 mm proximal to the sagittal ridge, and in the same plane further proximally and 6 mm proximal to the growth plate.

Two sections (3mm, 280 μm) were obtained from distal diaphysis of Lt. McIII.

4. One beam and one AP slice were obtained from 9 month foetus and preserved in 70% ethanol. The surface was documented by photography.
5. From 2yF Rt. McIII a distal condylar piece were obtained from its medial aspect, cleaned and coated for SEM.
6. Two more beams and two AP slices were obtained from McIII of two more older horses (4yF and 24yF), were cleaned, dehydrated, and coated by gold sputtering.

Altogether materials from 16 animals (9m foetus, 1d, 4d foal, 6wkF, 2yF, 4yF, 6yG, 7y, 8y, 11y, 12y #2, 18y #2, 24y, Unknown age) were examined.

3.2.2 Examination

Polarised Light Microscope (CPL & LPL), High resolution Stereo microscope (Edge), Bio-rad Lasersharp Confocal Scanning Light Microscope (CSLM) and SEM in both SE and BSE mode were employed during the study of the material.

a. Topographic documentation of McIII samples by photographing the surfaces (fig 3.2 - 3.4).
b. 100µm water cooled diamond saw sections in polarised light microscopy, Edge, and Confocal scanning laser microscopy (CSLM: Bio-rad lasersharp Confocal Scanning Microscope, MRC 500 and Noran Odessey) using autofluorescence mode imaging (using >515 nm autofluorescence excited by the 488nm line of the argon ion laser)
c. Intervening cross sections of 3·5 to 4mm thickness, and beams coated with gold by sputtering, Zeiss DSM962 SEM using low kV SE and BSE modes. Stereoscopic images both SEM and CSLM.
d. PMMA embedded, polished and carbon coated beams and blocks -
(i) SEM BSE images.
(ii) SEM BSE montages to reconstruct images in 3D.
e. PMMA embedded beams and blocks in CSLM.
f. Intermediate cross-sections in CPL, Edge and CSLM.

3.3 RESULTS

In some animals, distally, the subchondral bone exhibits a very fine trabecular pattern, while in others it appears to be composed of dense cortical bone of variable density (fig. 3.4), where the trabecular pattern is lost. Density of trabeculae also varies in different animals, however, these are constant features in both dorsal and palmer aspect of the distal metacarpus.

Extensive variation between the bones of individuals has been observed even at macroscopic level; the variation being both in the cortical shell as well as in the subchondral bone and trabeculae. The thickness of the cortical shell varies irrespective of the ages

Figure 3.5

A montage of a beam of the third metacarpal bone of a 7 year old animal for about 3.5 cm from the distal end. Both orthogonal surfaces antero-posterior and medio-lateral can be seen at 45° tilt. Note the characteristic difference in the trabecular architecture on the both surfaces. a) medio-lateral & b) antero-posterior surface. Embedded in PMMA. BSE. 20 kV. Carbon coated.

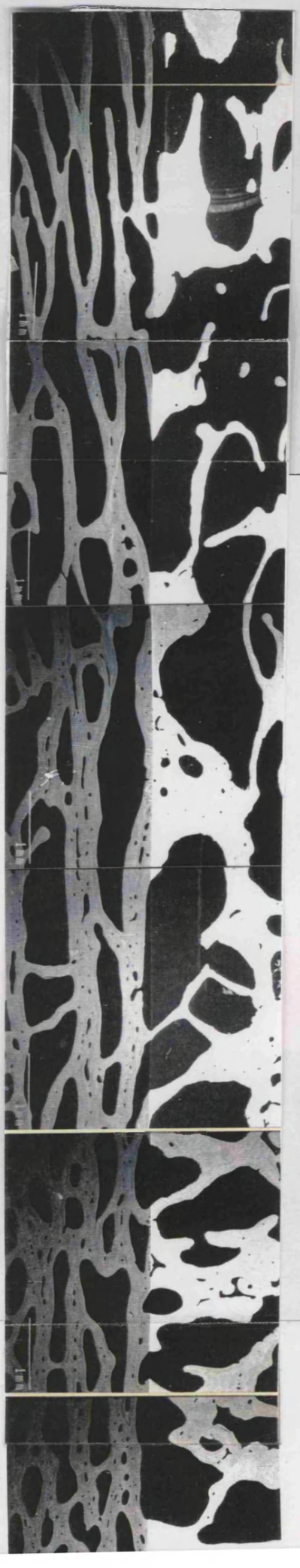

Figure 3.5

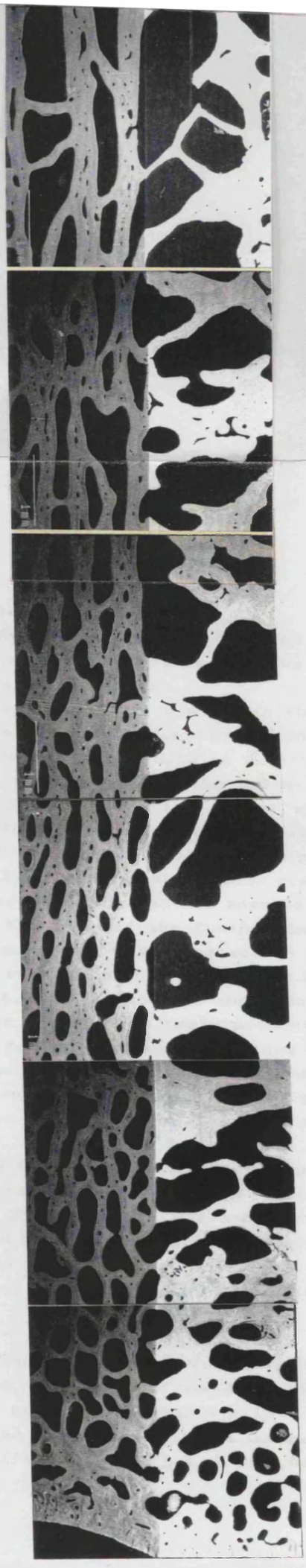

Figure 3.5

a

b

of the individuals. In some animals, the subchondral bone is very dense, so dense that it appeared to be solid compact bone for up to 15mm deep to the articular surfaces (figures 3.4). Again this does not associate with increasing age.

There is a very interesting motif in the structural anisotropy of the bone. Deep to the subchondral bone the trabeculae are predominantly parallel plates with an antero-posterior orientation joined by less extensive bone in the medio-lateral plane (figures 3.3, 3.6 a-b, 3.7a-g). It is the latter which shears in common fractures. This feature is constant proximally for about 30 - 45 mm, up to the site of the fusion of the growth plate (fig. 3.3 - arrow marked). Proximally, the trabecular plates gradually become stout and thicker with wider trabecular spaces near to the site of the fusion (Fig. 3.3). At the site of the fusion, an abrupt change in the architecture is observed, where trabeculae are fine, thinner, and more anisotropic vertical plates (figures 3.2, 3.3 - arrow marked). Beyond this point, the anisotropic appearance is lost, the dorso-palmar trabecular plates lose their predominant antero-posterior orientation and follow a somewhat oblique direction. From here proximally in the diaphysis, associated medio-lateral trabecular components are seen to emerge, which are obliquely oriented, and join with those in the AP plane resulting in the honeycomb trabecular architecture (Fig. 3.6 c-d, 3.7 h-p). Hence, vertical, dorso-palmar trabecular spaces are obliterated. The anisotropic architecture in the distal metacarpus is seen to develop right down from the subchondral bone (Fig. 3.9a-c). The architecture of the bone on the medio-lateral and the antero-posterior surfaces appears different (Figures 3.9 a-c); that on the medio-lateral (fig. 3.9a) surface is not too different from the anisotropic structure seen further proximally.

Here is a brief description of the features observed:

a) Preferred orientation of the trabeculae is seen just deep to the subchondral bone in the dorso-palmar plane with much less connectivity in the medio-lateral plane for a distance about 30 mm to 45 mm proximally (fifures 3.2b, 3.3, 3.5, 3.6a-b, 3.7a-g). The

Figure 3.6 (page 149-150)

a-d) BSE SEM image of 4 blocks from one beam of a 7y old horse.
a & b) Note the sagittal, antero-posterior trabeculae with medio-lateral cross bridges in blocks 6 (top) and 9 (bottom). The spaces are also antero-posterior and vertical. The trabeculae on the surface (AP) form almost a compact wall.
c & d) In blocks 10 (top) & 11 (bottom), the trabeculae are similarly oriented in the antero-posterior and the medio-lateral plane giving a honeycomb like appearance (following page).

Figure 3.6 (page 149-150)

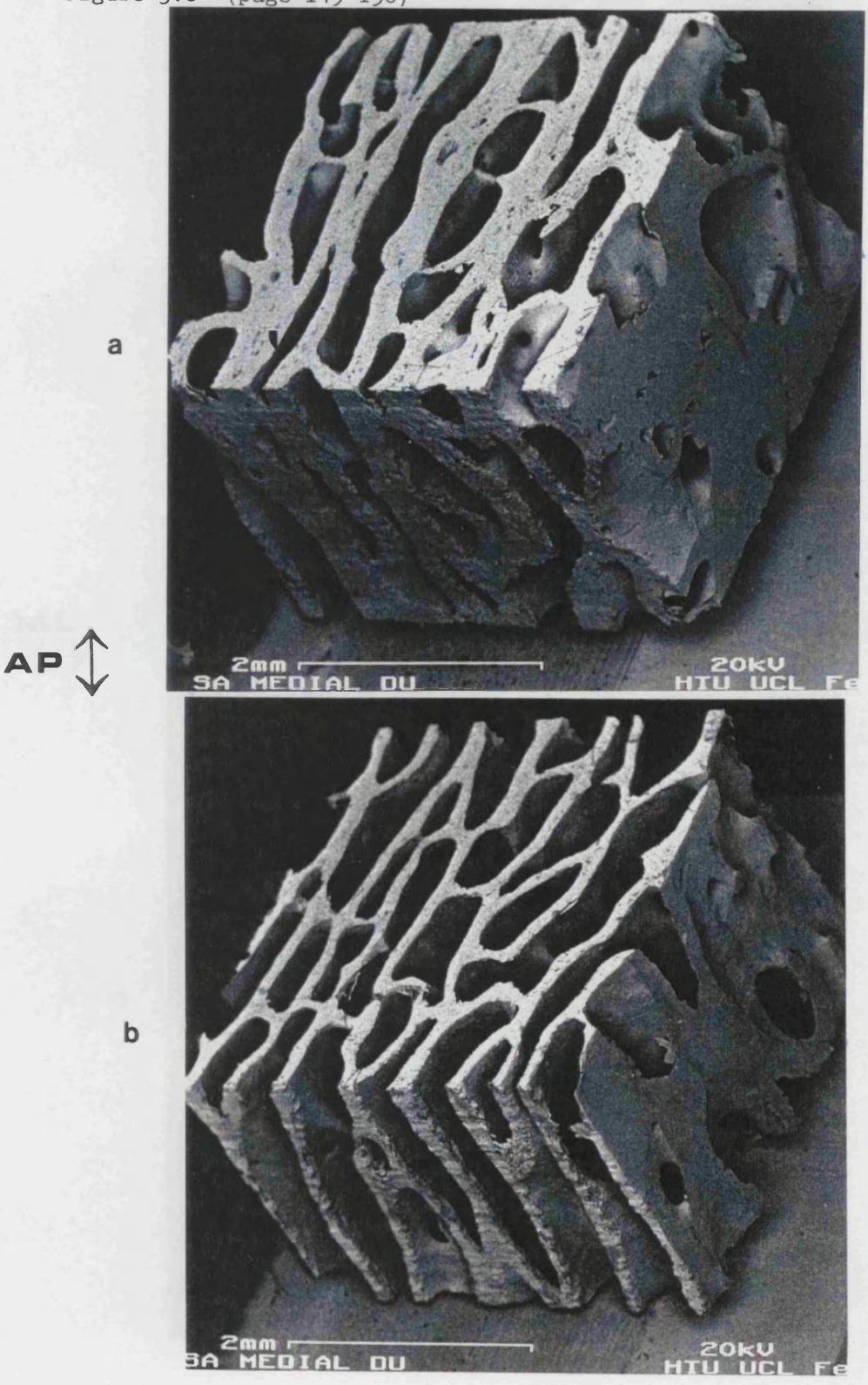

3.6

c

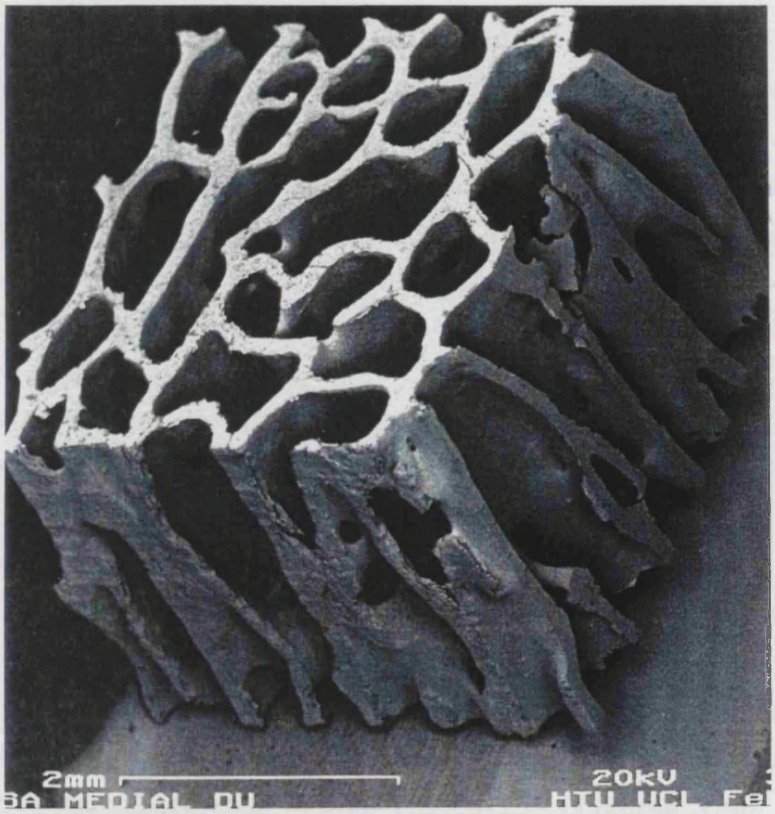

ML ↔

d

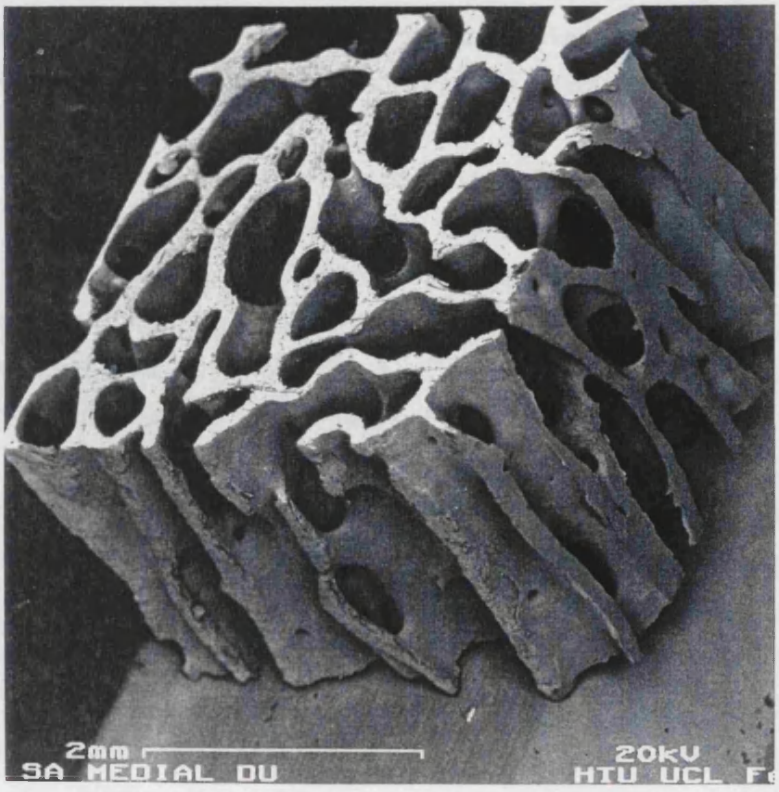

trabecular spaces are elongated parallel to the long axes of the vertical trabeculae. This structural anisotropy is seen up to the site of the fusion of the growth plate (Figures 3.3a-c). The architecture at the site of the fusion of the growth plate, although anisotropic, exhibits a totally different appearance. Here the architecture is made up of finer, thinner and more vertical columns.

b) The anisotropy is seen to develop below the subchondral bone (figure 3.9a).

c) Deep to the mineralising front, the articular cartilage and as seen in the medio-lateral plane, shows a clear tendency to cleave antero-posteriorly, which indicates an underlying anisotropy in collagen orientation (figures 3.10a-c).

d) Differences in the density of the subchondral bone between individuals are observed (figures 3.4a-c).

e) The calcified cartilage is more densely mineralised than the adjacent bone matrix (figures 3.10c, 4.9a). Large cell spaces in the calcified cartilage show active resorption (figures 3.9b, 3.14)

f) There is no evidence of incipient failure, any repair process, any callus formation or any excessive remodelling at the site prone to fracture.

g) Evidence of active remodelling with different mineralisation profile is observed (figures 3.11, 3.13, 3.14, 3.15).

h) Resorption leading to thinning of trabeculae (fig 3.16a-b) and perforation (fig. 3.15a-b, 3.17a-b, 3.18a-b) of trabeculae is evident, predominantly in the horizontal components distally in the younger individuals (ie 1 day & 6 week); the bones in the coronal plane i.e., on the medio-lateral surface exhibit extensive resorption, and especially near to the distal end (Fig. 3.13b). Burrowing of trabecular bone during resorption on an antero-posterior axis will eventually end up with the formation of trabecular plates and packets on the same axis (Fig. 3.13a).

i) Osteonal remodelling and vascular channels at the junction of the vertical and medio-lateral crossbridges, perforations at the junctions of the trabeculae, and the generation of cement lines from the remodelling process (Figure 3.11a-b, 3.12a-c) eventually weakens the structure in the sagittal plane.

Figure 3.7 (page 152: a-f; 153: g-k; 154: l-r)

LPL images of 16 transverse sections obtained from the beam of a 2 year old third metacarpal. The fibres are predominantly bright in all sections. AP axis is horizontal.

a-g) Show predominant antero-posterior trabeculae in all of the first 7 sections (distal), after which (from the section **h**) the architecture appears more like a honeycomb.

In proximal sections the trabeculae become thinner. Eventually, the remodelling events at the junction of the antero-posterior and the medio-lateral components weaken the structure in the antero-posterior plane. Note some free ends of trabeculae in the proximal (ie. m, n) sections.

The last two images (**q-r**) show the 3rd and the 5th sections viewed at 45° rotation.

FW = 2.8 mm

Figure 3.7 (p152: a-f; 153: g-k; 154:l-r)

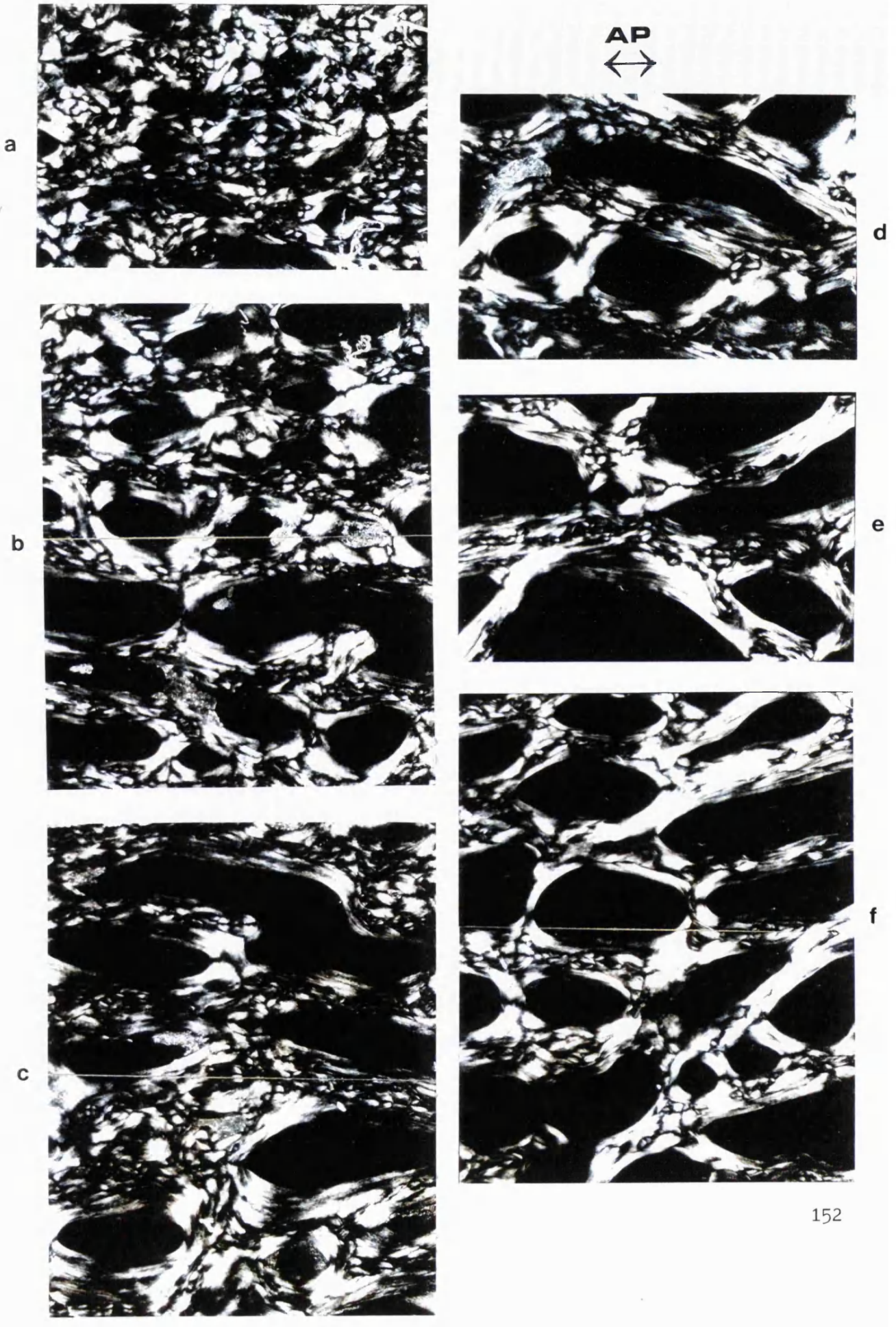

3.7

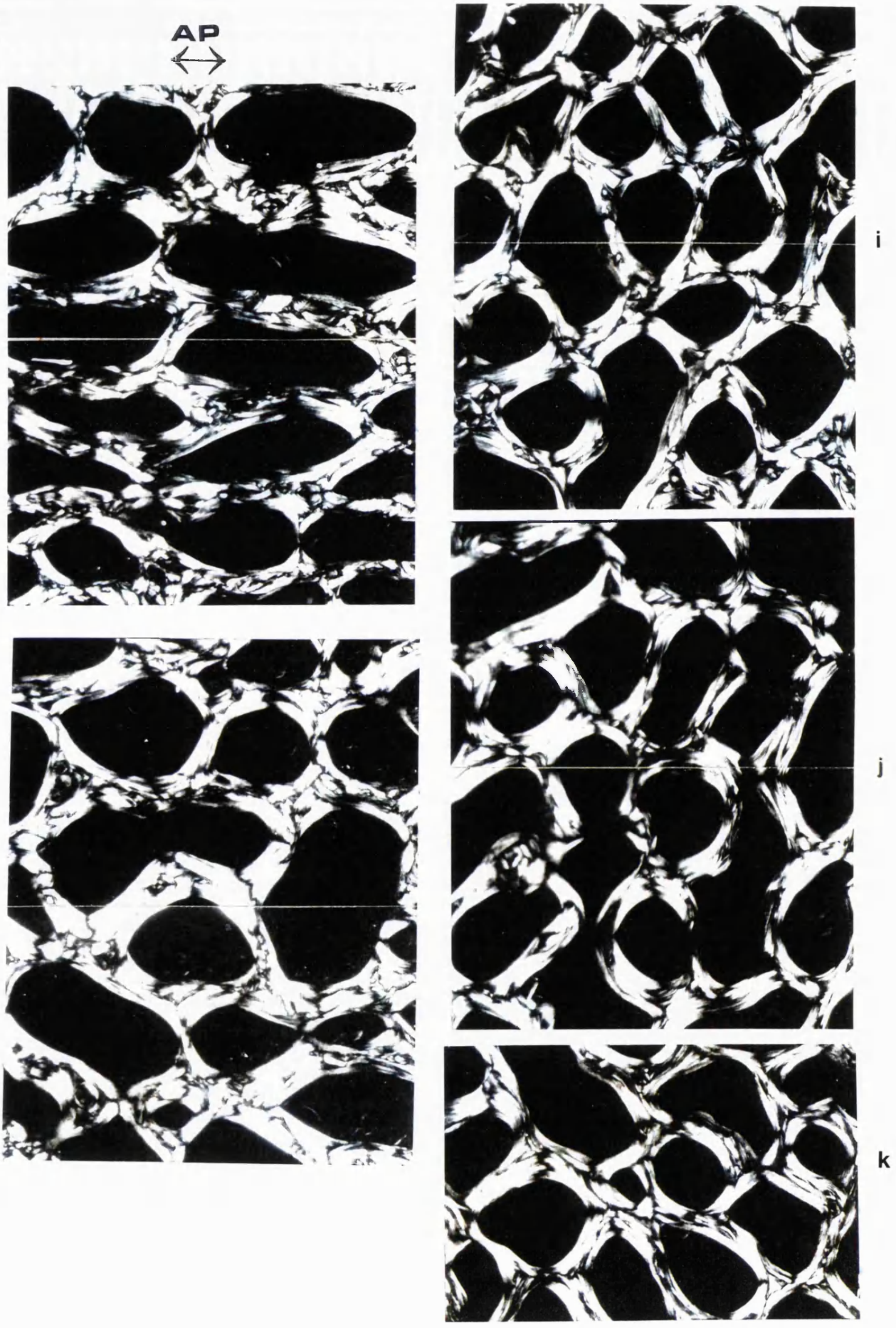

3.7

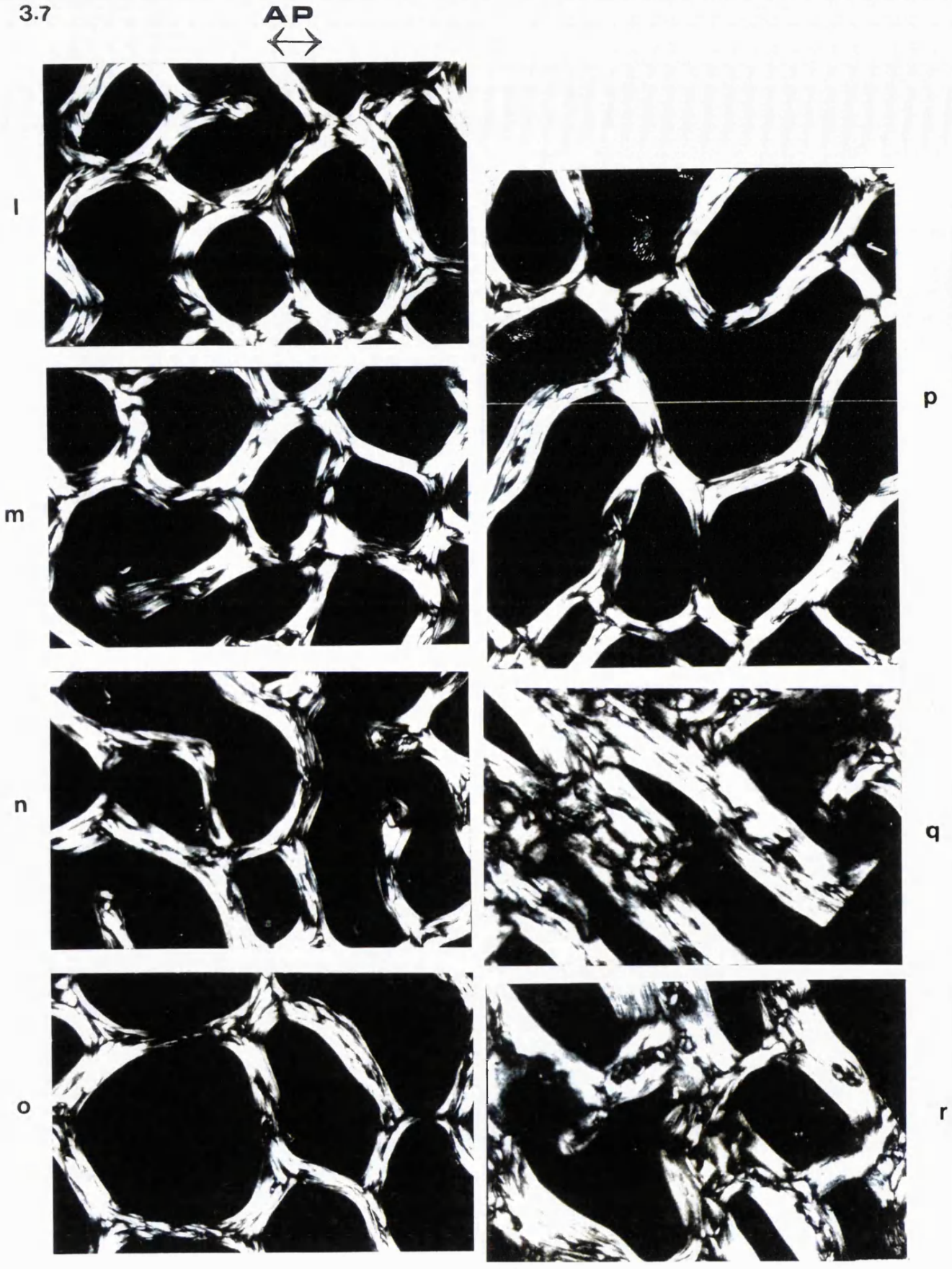

Figure 3.8 (page 155-156)

Confocal scanning light microscopic image of PMMA embedded sub-articular cartilage bone blocks.
a & b) AP (top) and ML (middle) view of a sample of the 6 week animal bone. The ML surface shows a developing anisotropic pattern.
c) The ML surface of the one day animal bone (following page) shows no obvious anisotropy.
FW: a = 2.44 mm, b = 3.17 mm, c = 3.21 mm

Figure 3.8 (page 155-156)

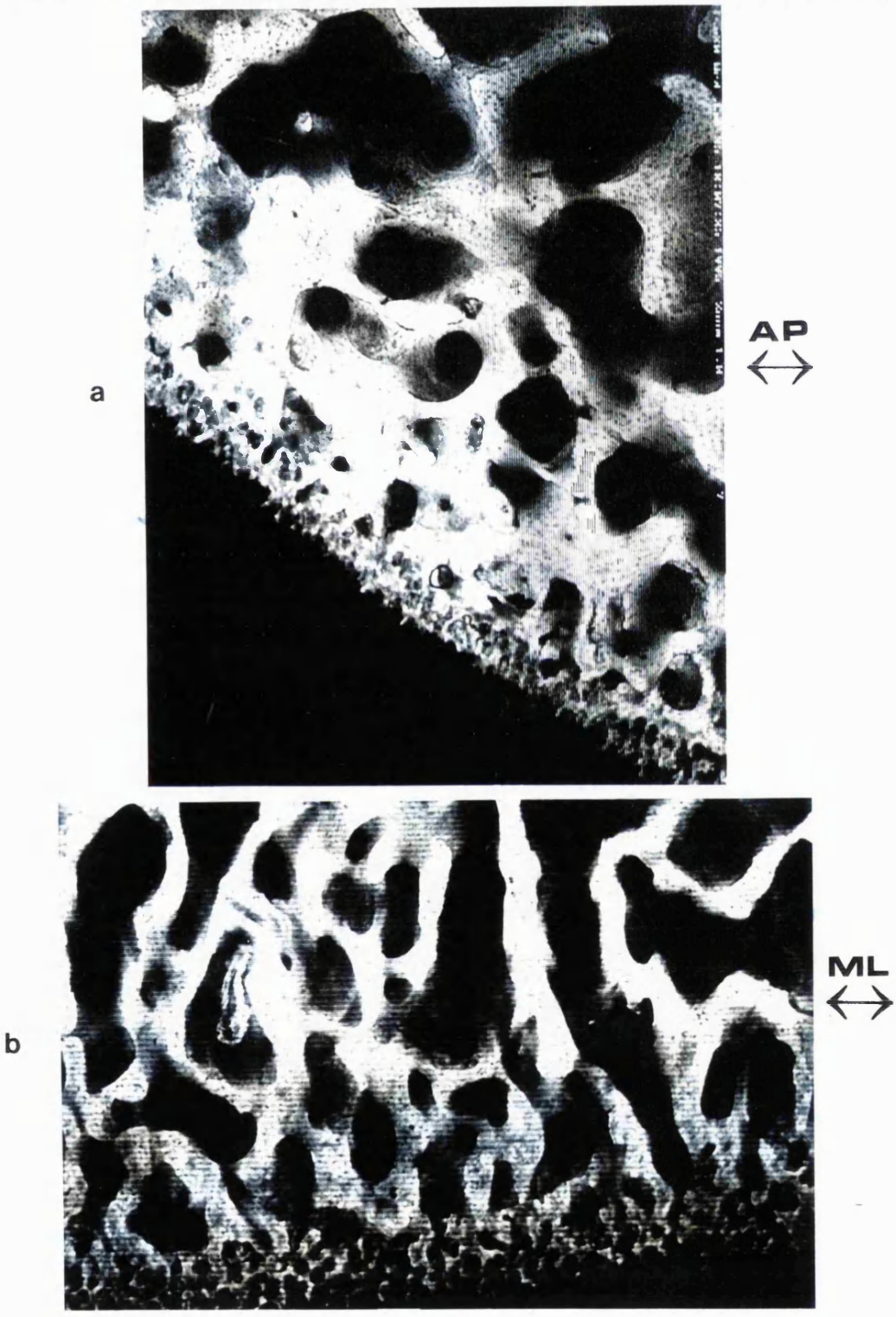

3.8

ML

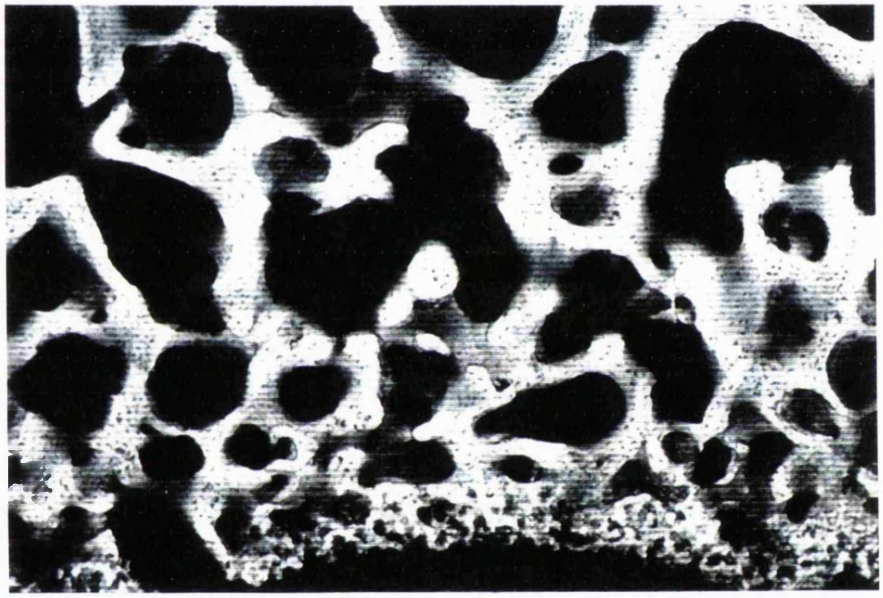

C

Examination of the longitudinal sections of the articular cartilage (containing subchondral bone proximally) in polarised light reveals extension of prior resorption spaces into the calcified cartilage (figures 3.9b1-b2, 3.14). Their extremities are found delineated by osteonal or trabecular bone which separate them from the calcified cartilage (Brooke 1971; Redler et al 1975; Clark 1990b). In some places, no lamellar bone intervenes between large resorption spaces and the calcified cartilage (fig. 3.14). The appearance of large spaces in the calcified cartilage signifies gradual replacement of the calcified cartilage zone by newly formed bone.

The different characteristic trabecular patterns in the both antero-posterior and medio-lateral planes is seen to develop at this level, ie subchondral bone (fig. 3.9). The resorption spaces are seen to dig into the calcified cartilage (fig. 3.14). As seen on the medio-lateral surface, distally near to the calcified cartilage, the trabeculae take a regular shape. The trabecular spaces are nearly round, which further proximally, turn into regular, elongated spaces between the slender and vertical trabeculae (fig. 3.9a); the later have short medio-lateral connections. On the contrary, the antero-posterior surface shows wider dorso-palmar trabecular plates in this region, with random and irregular shaped trabecular spaces between them (fig. 3.9b-c).

In neonatal bones (1 day & 6 Week) trabecular plates show similar arrangement in the both medio-lateral and antero-posterior planes. The trabecular spaces show no preference in their orientation, either antero-posterior or vertical, although the 6 week bone shows some vertical antero-posterior trabecular plates, viewed on the medio-lateral surface (fig. 8a-c). Distally, the trabeculae are dense. Lots of perforating holes (fig. 3.15ab) are seen along the trabecular plates indicating active resorption. Bone packets of different mineralisation density are observed along the trabeculae. Features of active remodelling are present (fig. 3.15, 3.17a-b, 18a-b).

The anorganic bone samples of the neonates are characterised by extensive resorption, as seen on the mineral front preparations which

Figure 3.9

LPL image of 50 μm thick decalcified vertical sections of subchondral bone & calcified cartilage from the distal condyle of the McIII.
a) 4y ML,
b) 4y AP, and
c) 24y AP.

a) 4y ML - the trabecular spaces are round and regular immediately adjacent to the calcified cartilage, and gradually take a longitudinal shape between the vertical trabeculae.
b & c) 4y & 24y AP - Wide AP trabecular plates with random irregular shaped trabecular spaces are contained within the antero-posterior sections.
Field width a = 1800 μm, b = 3 mm, c = 3.1 mm.

Figure 3.9

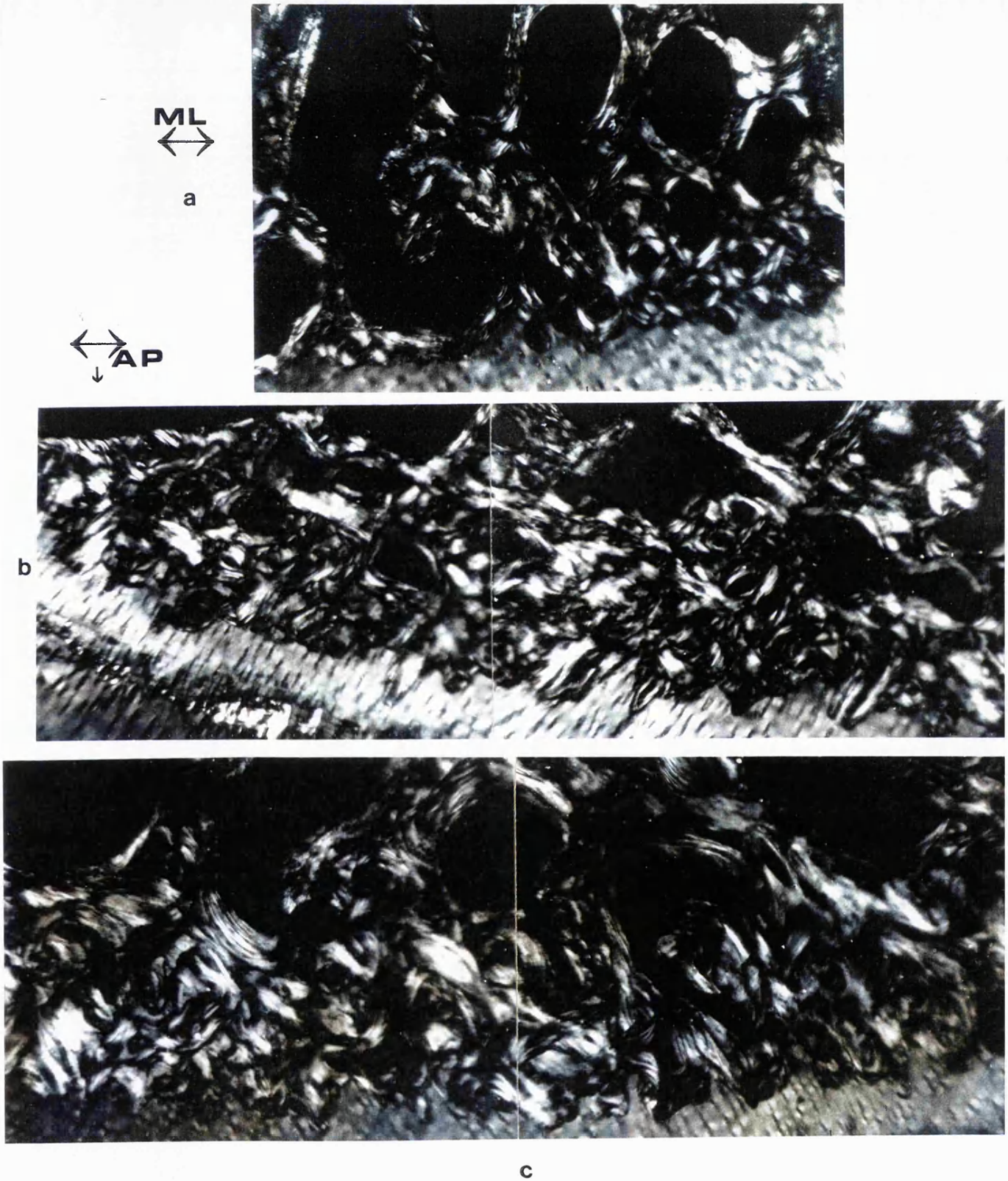

Figure 3.10

SEM and CSLM micrographs antero-posteriorly showing how the calcified cartilage has a tendency to cleave:

a) BSE image shows split lines on the distal surface (mineralised articular cartilage surface) of a distal (articular) block of a beam cut from an 11 year old metacarpus; and

b) CSLM image of ML surface of PMMA embedded bone. FW = .96 mm.

c) BSE image of ML surface of PMMA embedded bone.

a = Au-sputter coated, whilst the polished PMMA embedded block (c) is carbon coated.

Figure 3.10

a

b

c

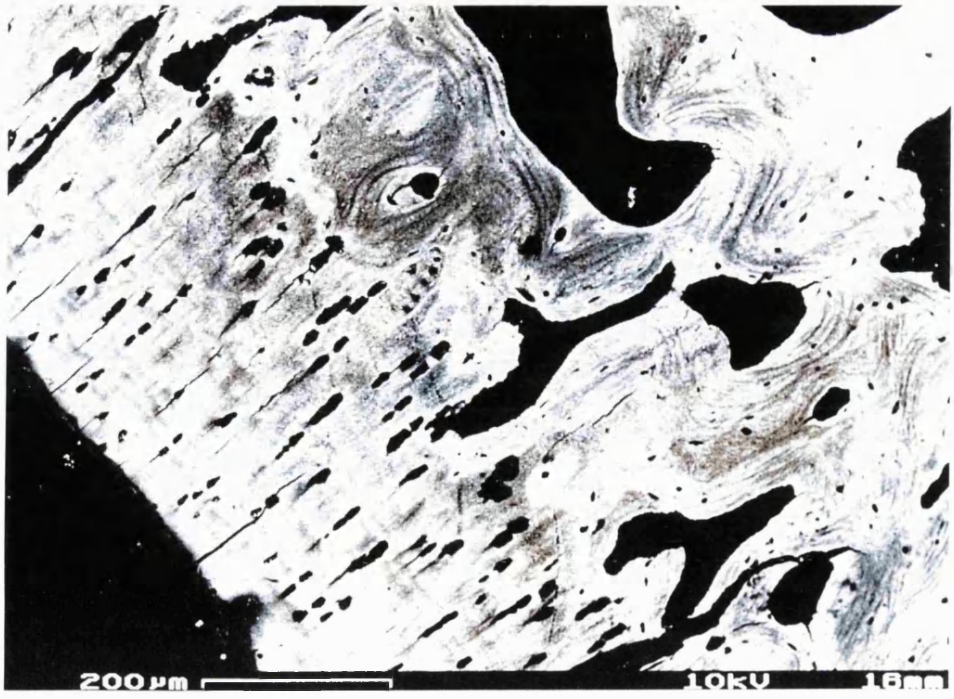

appeared rough with scalloped edges. Vascular canals seen in this surface exhibit signs of intense remodelling along their walls. Unlike resorption fields, exposed forming surfaces viewed on the mineralising front surface have a tendency of shifting toward antero-posterior orientation giving rise to antero-posterior vertical trabeculae.

The bone samples exhibited extensive resorption in trabeculae near the calcified cartilage end viewed on anterior surface i.e., medio-lateral surface (fig. 313b). The resorption fields were seen burrowing the bony tissue on the dorso-palmar axis (fig. 3.13a). In older animals, the calcified cartilage zone was also seen to be resorbed.

In other animals examined (2 years and older), the trabeculae are found oriented in a dorso-palmar plane up to the metaphyseal region for a distance of about 30 mm to 45 mm proximally. These are almost vertical plates in the antero-posterior plane and are joined by narrow medio-lateral crossbridges. This anisotropic structure is present in the ex-epiphyseal region up to the site of the fusion of the growth plate (figures 3.3, 3.5, 3.6b, 3.7a-g) Different mineralisation levels indicate active renewal; however, the intensity is less than that in the neonates where it is evidenced by the greater number of resorption fields. From the metaphyseal region proximally, no such predominance in dorso-palmar orientation of trabecular plates is observed (figures 3.3, 3.6c-d, 3.7h). The medio-lateral connections or crossbridges are replaced by trabecular plates. Somewhat obliquely oriented trabecular plates from both the planes give rise to honeycomb like trabecular architecture (3.6cd, 3.7h-p).

The 100μm thick intermediate cross-sections of the McIII beams when examined with the Edge 3D Microscope exhibited no sign of microfracture, crazing lines or cracks. Particular emphasis was placed on those sites where remodelling was present in the vertical (antero-posterior) trabeculae and at the junction of the transverse with the vertical components. The inter-trabecular spaces appear elongated antero-posteriorly. This pattern is gradually replaced more distally where the trabecular orientation in both the antero-

Figure 3.11

a) Confocal scanning light microscopic image showing osteons in an antero-posteriorly oriented plate (2yF McIII). Brilliant sulphaflavine stained. FW = 1.17 mm.

b) BSE SEM image of the trabeculae in McIII of an 11 year old animal showing porosity within the trabecular structure. Au-sputter coated.

Figure 3.11

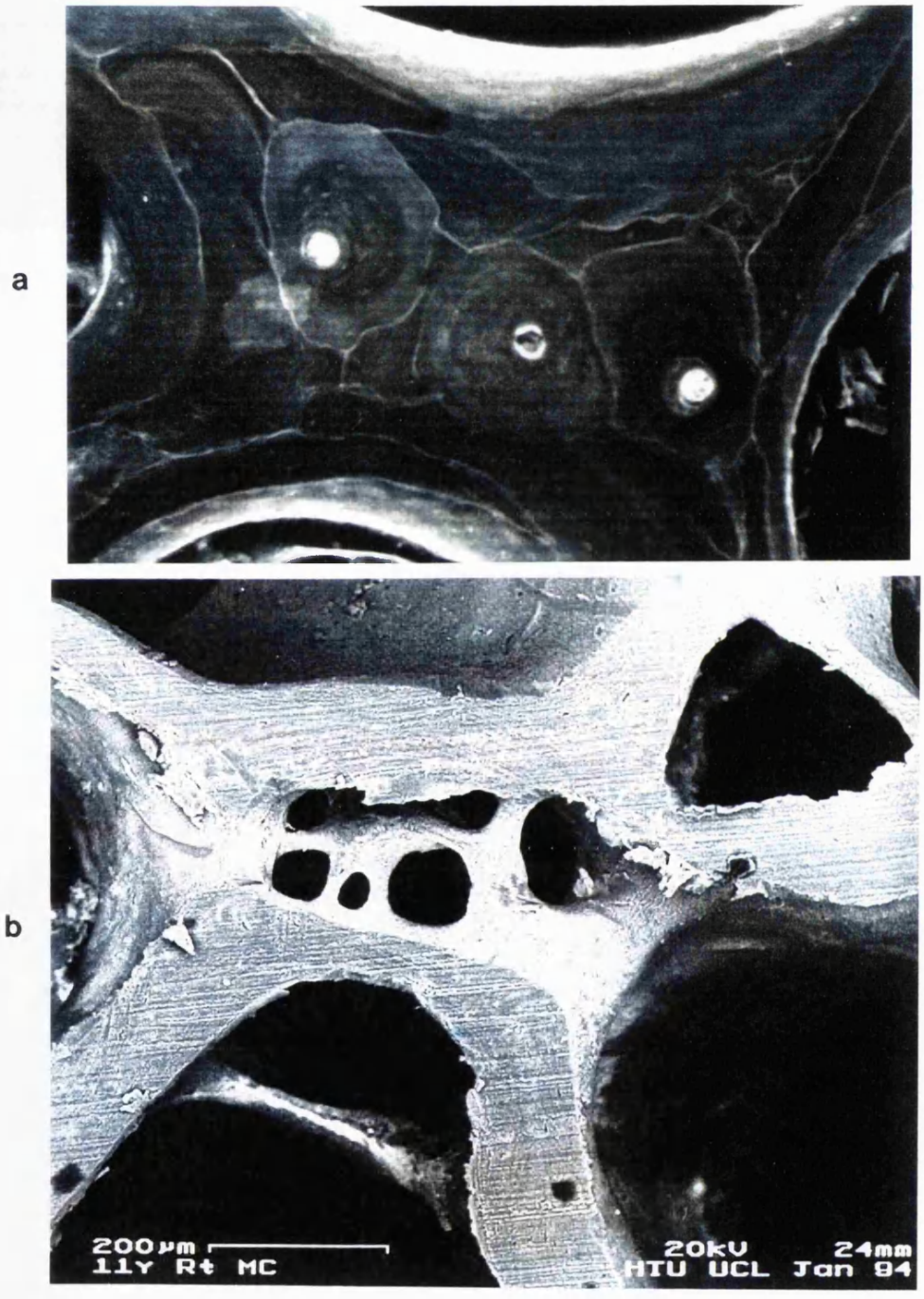

Figure 3.12

a-c) Fluorescence confocal scanning light microscopic images of the intervening transverse sections of the beams of McIII of a 7 year old animal.

a-b) Passage of vascular channels seen through the trabecular junctions in the antero-posterior plane.

c) Several cement lines indicating poor remodelling history.

FW: a = 2.25 mm, b = .94 mm, c = 1.11mm.

Figure 3.12

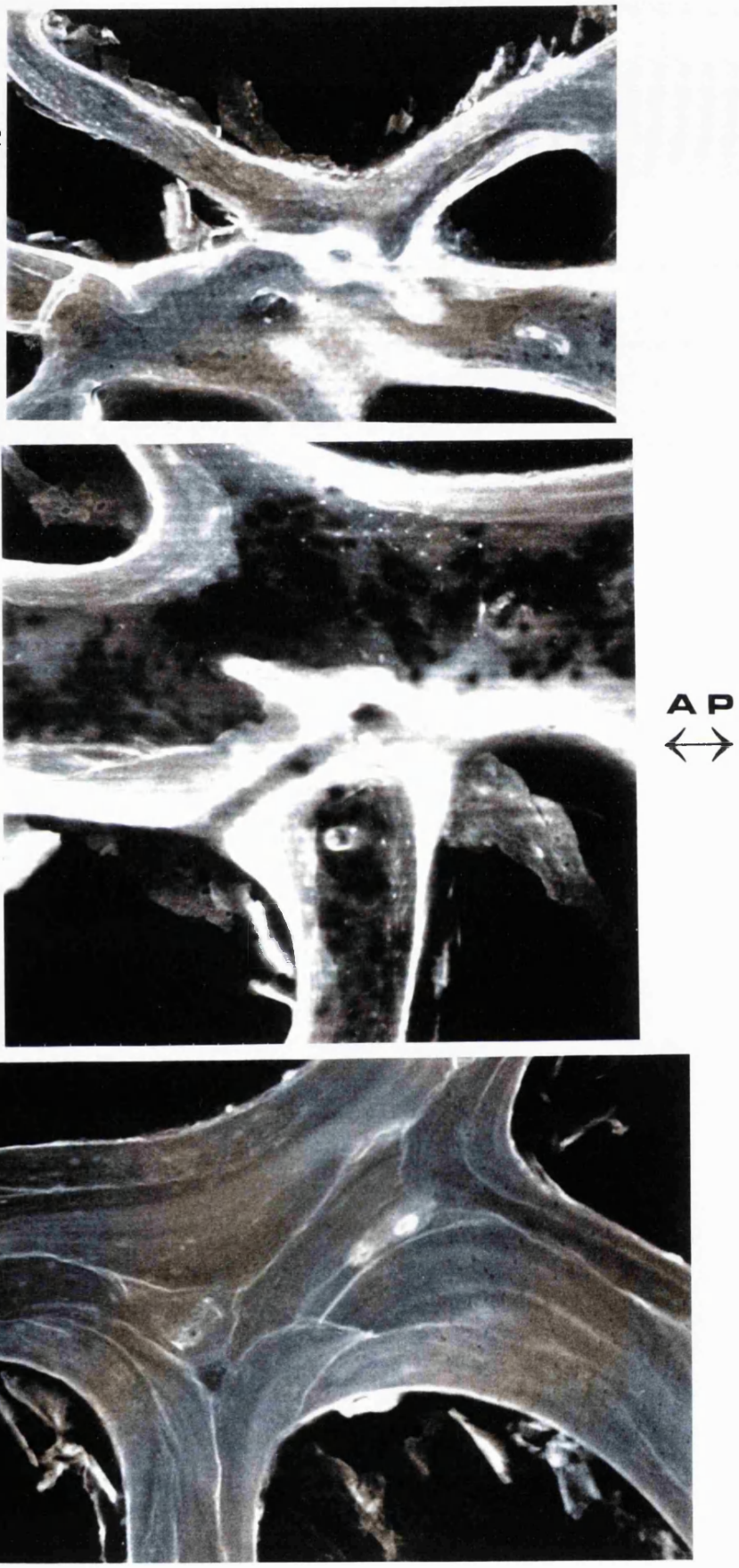

Figure 3.13

a) Anorganic (hypochlorite treated) bone samples viewed in a medio-lateral section surface from the distal MCIII of a 6 week old animal. Note a resorption space in the antero-posterior axis.
SE (1.5kV). Au-sputter coated.
b) Same sample viewed on its medio-lateral section surface, showing extensive resorption. The calcified cartilage is on the right.
SE (10kV). Au-sputter coated.

Figure 3.13

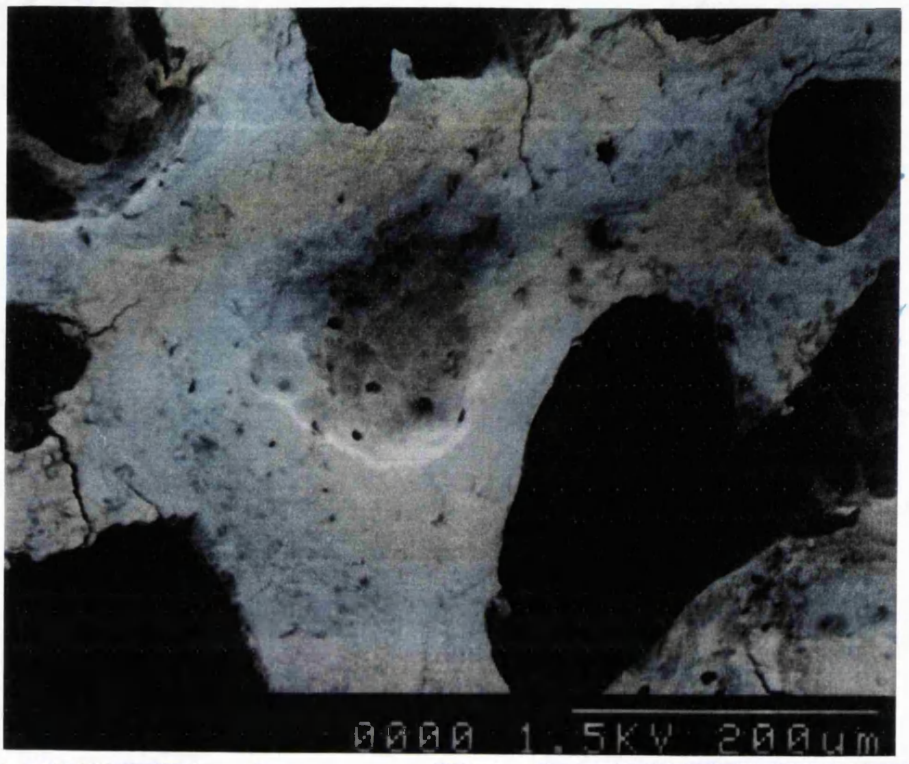

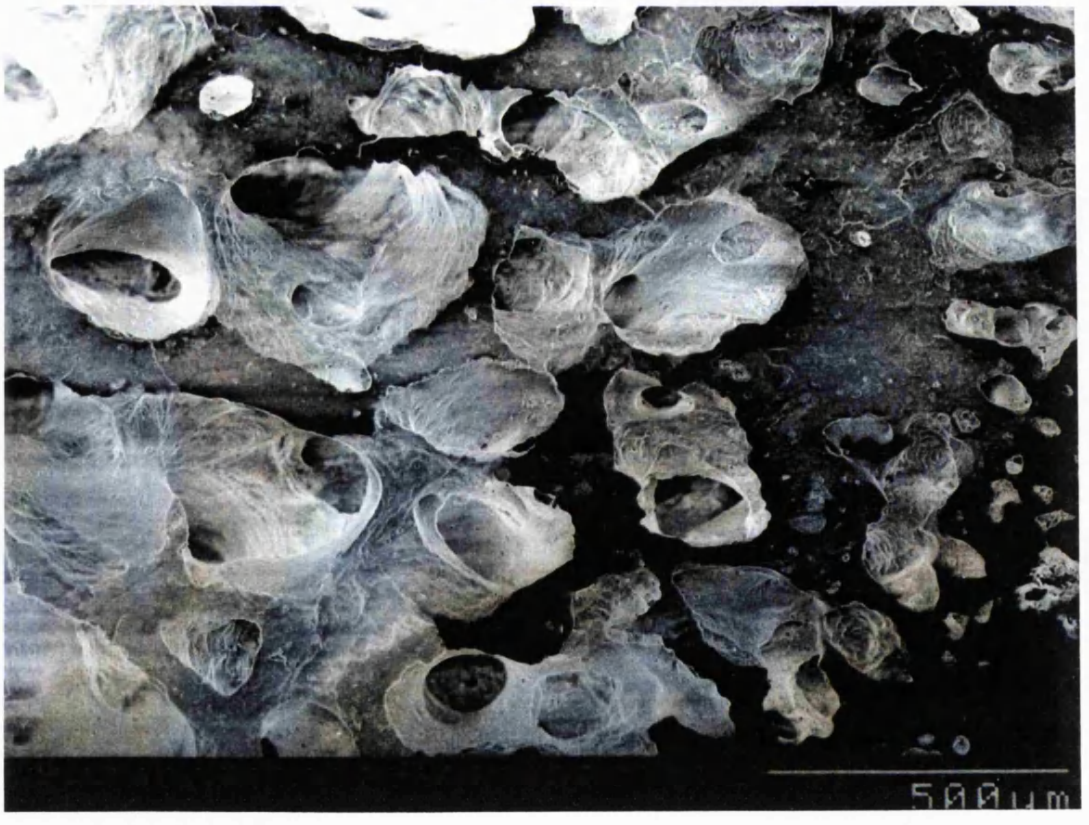

Figure 3.14

Decalcified 50 μm thick vertical section in the antero-posterior plane showing the calcified cartilage zone of the distal condyle of the third metacarpus of a 4 year old animal. The irregular tidemark zone is seen at the bottom, beyond which a little of the uncalcified radial fibre zone is visible. The top of the picture shows bone. The vertical chondrocyte columns lie parallel to the principal collagen axis. CPL image.

Figure 3.14

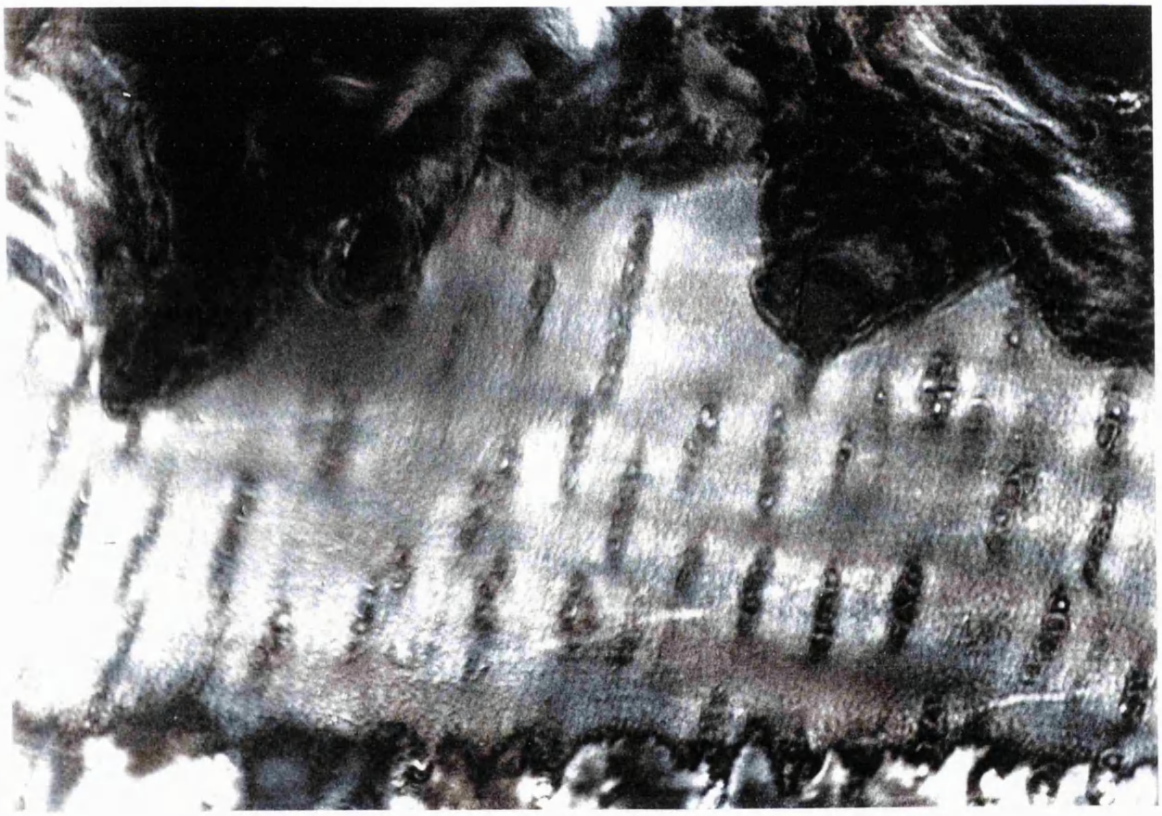

posterior and the medio-lateral planes appeared similar. Vascular channels are noted within the trabeculae mainly along their long axes (antero-posterior). In distal cross-sections the trabeculae are dense, and exhibit more osteonal remodelling than those in proximal areas, where the trabeculae become gradually thinner with less trabecular network.

PLM

The intermediate cross sections of the beam exhibit similar trabecular architecture in PLM (fig 3.7). The predominant antero-posterior orientation of the trabeculae and the trabecular spaces are apparent upto the 7th section (3.7g), after which the structure is a honeycomb. The trabeculae appear predominantly bright in the both LPL & CPL. The collagen fibres are parallel with the long axes of the antero-posterior trabeculae, and also in the cross bridges. Resorption spaces and forming osteons indicate active osteonal remodelling within the trabecular component. The trabeculae contained many bright 2° osteons in the plane of section. They are mostly elliptical in the antero-posterior axes of the trabeculae. In LPL, the trabeculae are predominantly bright when the section is viewed normal to the optic axis, and also with 45° rotation of the sections (fig 3.7q-r). Reversal lines characterise almost all the trabeculae. The younger the animal, the higher the turnover. The higher the osteonal remodelling, the higher the cement line interfaces within the trabeculae. Trabeculae in more distal sections exhibit more osteonal remodelling; a greater rate is seen at the junctions of the antero-posterior and the medio-lateral components (fig 3.7e-f, q-r). Vascular channels are observed within antero-posterior trabecular plates. Proximally, the trabecular spaces gradually become enlarged, the trabeculae become thinner, and the turnover rate is slower. The older the animal, the less the extension of the trabecular network towards the midshaft, confirming the gradual loss of trabeculae within the central shaft with increasing age.

Figure 3.15

a) 6 week metaphysis, BSE

b) partially anorganic 1 day epiphysis, SE.

Both viewed on the medio-lateral surfaces showing extensive resorption.

a = BSE (20kV), b = SE (10 kV). Au-sputter coated.

Figure 3.15

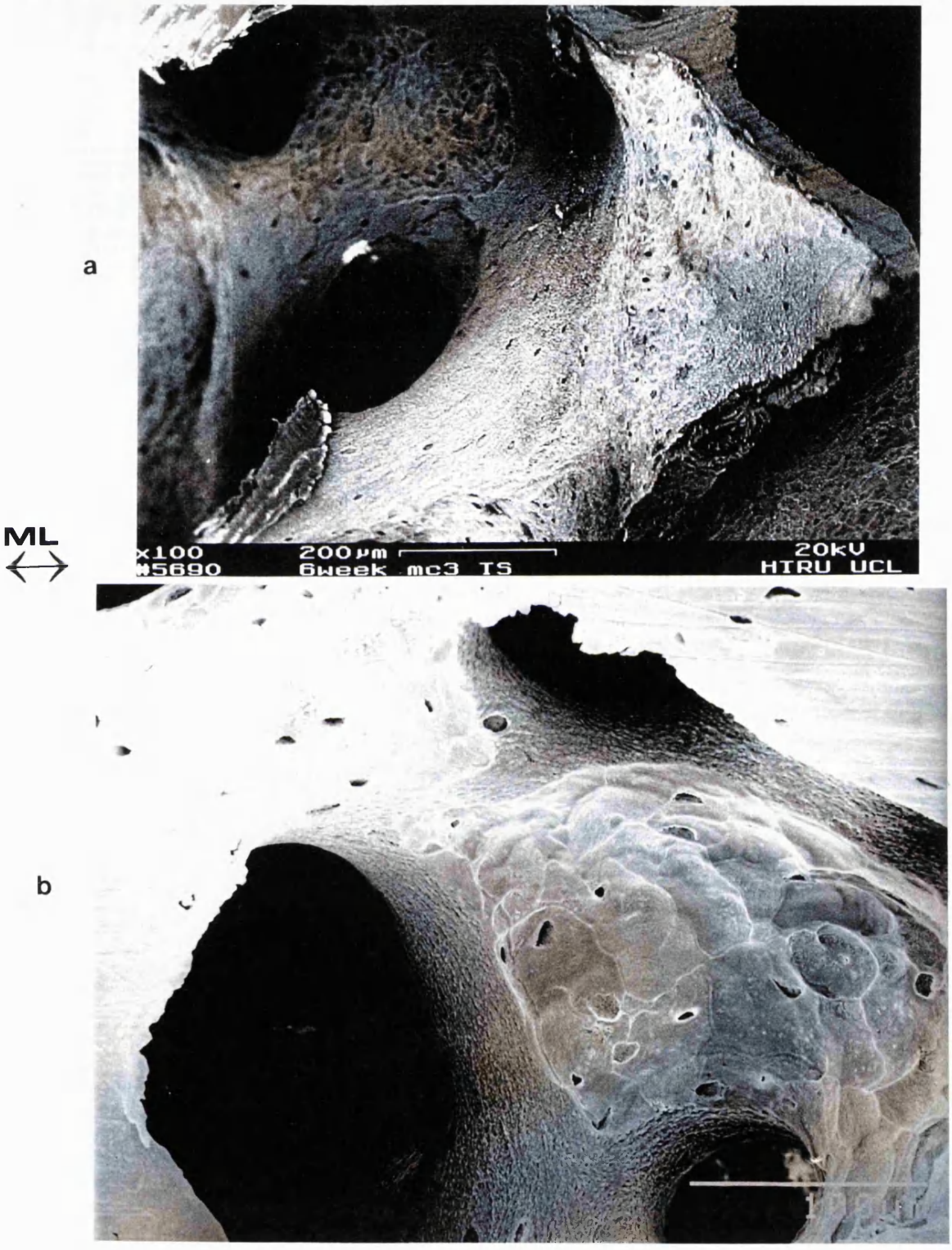

Figure 3.16

BSE images of 6 week McIII trabecular surfaces
a) extensive resorption at the base and along the surface of a trabeculum, and
b) free end of a trabeculum as a consequence of its resorption. Au-sputter coated.

Figure 3.16

a

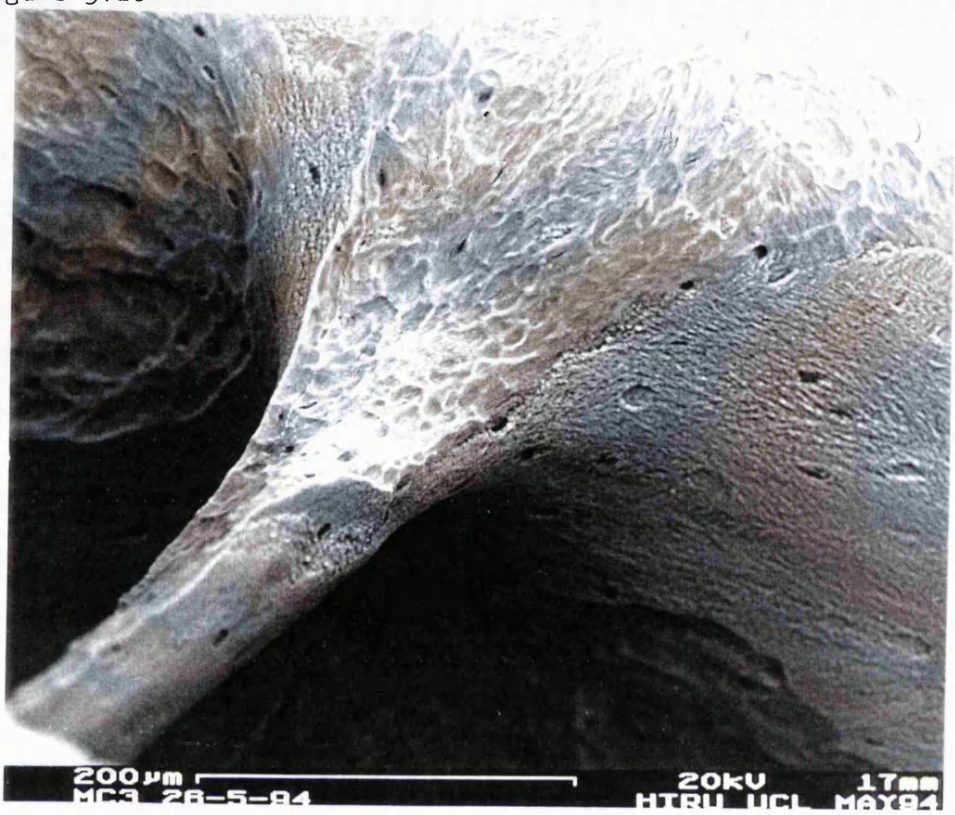

b

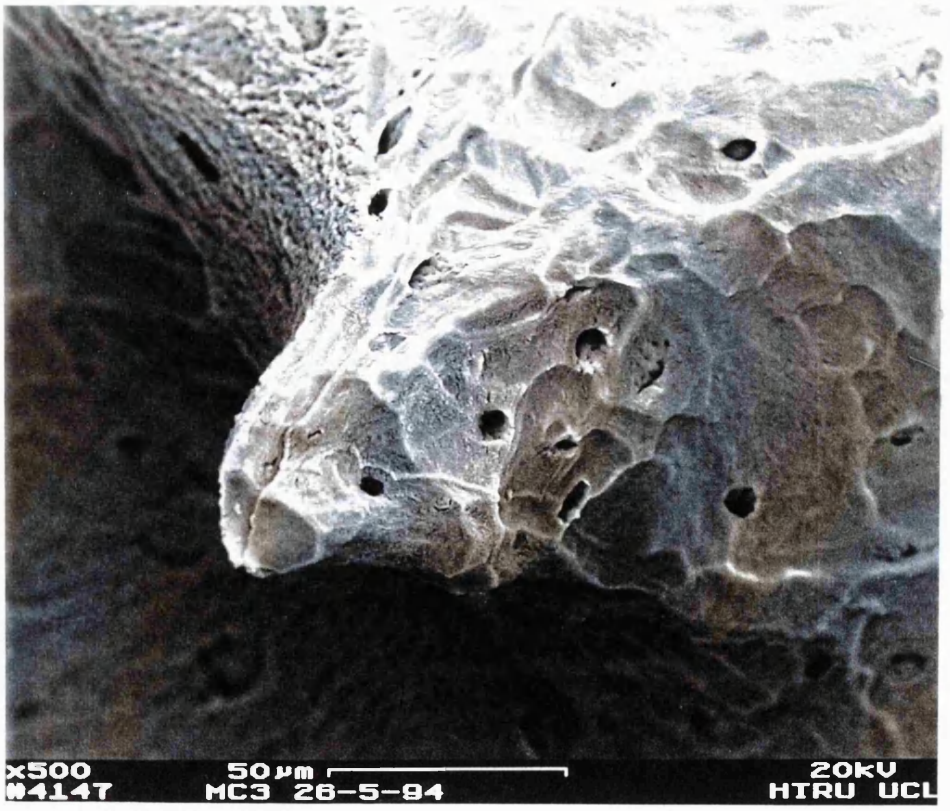

Figure 3.17

SE images of trabeculae in 1 day McIII showing extensive resorption and formation. **a)** hypochlorite treated, **b)** Hydrogen peroxide treated. AP = side to side. SE (10kV). Au-sputter coated.

Figure 3.17

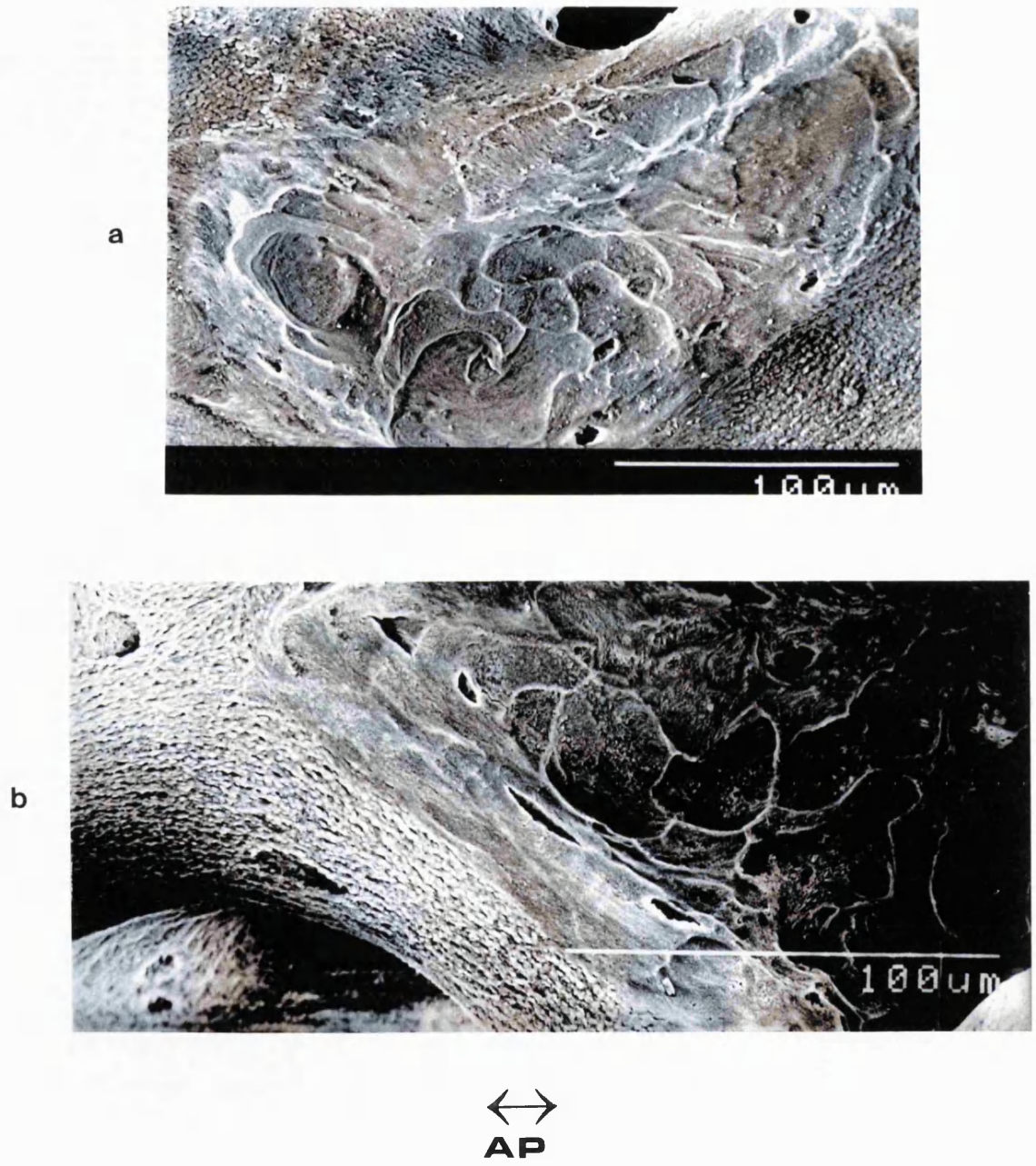

Figure 3.18

SE image of hypochlorite treated one day McIII showing resorption and formation side by side on the surface of the trabeculae.
10 kV. Au-sputter coated.

Figure 3.18

a

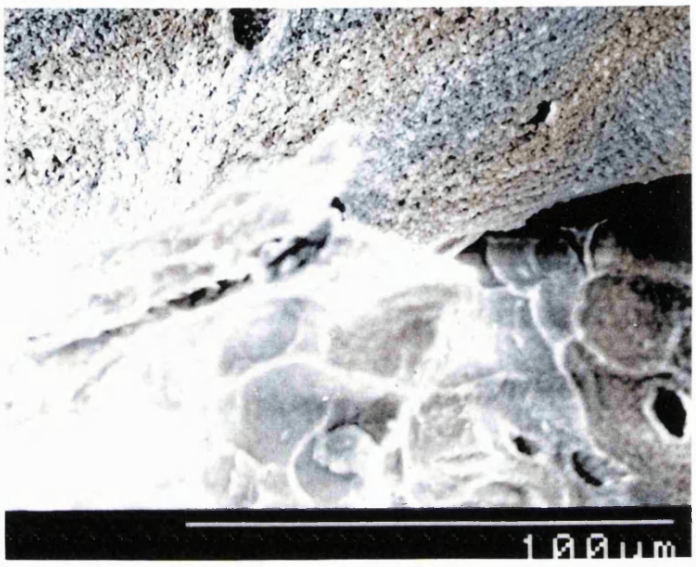

b

3.4 DISCUSSION

This study was carried out to ascertain the organisational features and, any probable pathology, which may favour the commonly occurring fracture in the distal condylar region of the equine metacarpus.

As revealed in this study, the trabeculae in the most distal region of the McIII were oriented antero-posteriorly as vertical plates. These sagittal platelike trabeculae were found to be supported with medio-lateral cross bridging and were constant in all animals with the exception of the neonates (1d & 6w). The anisotropy is finer at the site of the fusion of the growth plate.

The changing features obtained in this study with age (during post-natal period) are in agreement with the adaptation of trabeculae to strain distribution (Wolff 1870). In man, functional cancellous bone develops from primary cancellous bone which fills in the whole metaphysis in the fetal and early post natal period (Liskova 1961; Osborne et al 1980). It forms a three dimensional mesh with pronounced preference for longitudinal trabeculae. The direction of the trabeculae follows the orientation of cellular columns of the growth plate. Only in the course of the first post-natal year and under the influence of increased mechanical loading does the primary cancellous bone remodel into the secondary functional cancellous bone. The finding is also in agreement with the notion that the equine third metacarpal bone is primarily axially loaded (Turner et al 1975; Biewener et al 1983a). This means that, main strength of the cancellous bone should lie in vertical trabeculae.

It is very clear that in the distal condyle of equine metacarpal bone, the characteristic fracture line must pass through the region of transverse trabecular components where the trabecular spaces are predominantly vertical with a dorso-palmar orientation.

CSLM and BSE SEM studies revealed a clear tendency to cleave in antero-posterior plane in the cartilage deep to the mineralising front of the articular cartilage. This observation indicates an anisotropy also in underlying collagen fibre orientation, which was later confirmed by examining the articular cartilage sections in

polarised light, and looking at the mineralising front preparations in SEM (chap. 4).

No evidence documenting the presence of microcracks or microfractures in trabecular bone could be seen in this study.

In this study, although a very limited number of McIII was examined, no organisational differences were observed between right and left limbs. This is consistent with the study of Nunamaker and co-workers (1989), who found no difference for any of the section properties of McIII at any age between the left and right limbs. This fracture commonly occurs in older animals. Several studies (Meagher 1976; Rick et al 1983; Richardson 1984) of condylar fractures in Thoroughbreds favour this notion: (Rick:69 animals, 2 to 8 years old with a mean of 3.7 years); Meagher: 42 animals, 2 to 9 years old with a mean of 3.6 years). One study (Rick et al 1983) found a greater incidence of distal condylar fracture in left metacarpals in contrast the results of Meagher (1976) and Rooney (1974). It is quite unlikely that there is any preferential organisational difference between two limbs. The difference is in their biomechanical aspects. Nunamaker and co-workers (1989) also showed greater strain magnitudes at the endsections in the left limb. It seems clear that the greater incidence of fracture in the lateral condyle of the McIII is attributable to the greater load the limb sustains during racing or training in a counterclockwise direction, when the inside limb has to withstand more strain. This explanation supports the suggestion (Rooney 1974; Meagher 1976) that condylar fractures of McIII are almost exclusively the result of strenuous exercise.

The articular surface at the distal end of McIII is convex with a sagittal ridge and two smooth condylar surfaces. In some animals, the subchondral bone exhibited a very fine trabecular pattern, while in others it appeared to be composed of more compact bone of variable density but with a loss of trabecular pattern. The density of trabeculae also varied in different animals. These were constant in both dorsal and palmar aspects of the distal metacarpus. These findings are not in agreement with certain descriptions of distal subcondylar bone architecture (O'Brien 1977). However, the bone in the sagittal ridge was less dense than in the condyles, and the

cartilage was smooth on condylar surfaces. In man, the presence of more dense subchondral bone tissue with loss of trabecular pattern which showed compact bone like appearance has been associated with degenerative lesions of articular cartilage (human: Chai et al 1991).

In the present study, antero-posterior fissures were seen in the condylar grooves in the fracture cases, which indicate the presence of some pre-existing pathological process which might have contributed to the initiation of the fracture. In articular cartilage damage, the subchondral bone loses its well-defined trabecular pattern. Usually, if there is any defect in the articular cartilage or in the subchondral bone, increasing involvement in magnitude, gradually causes productive and destructive process which extends distally on to the articular surface beside the sagittal ridge in the condyle (O'Brien 1977).

Depending on extension, the fracture is either complete or incomplete. Previous studies showed that complete fracture is more common than incomplete fracture (53/77: Rick et al 1983). The fracture is thought (Meagher 1976; Rick et al 1983) to begin usually in a focal area in the subchondral region of the McIII, extends proximally for 3 to 4 cm before extending further axially or laterally, thus constituting complete condylar fracture, and less often incomplete fracture.

The present study suggests the cause of spontaneous failure of the distal condyle with characteristic morphological fracture line, and contributes to the understanding of the biomechanics of its initiation and propagation. When fracture once originates, the characteristic three-dimensional architecture of trabeculae (the trabeculae are oriented as antero-posterior plates with narrower medio-lateral cross-bridges) for a certain distance, as well as the anisotropic organisation of the subchondral component in the distal condyle leads the fracture line proximally from the articular surface through sagittal and vertical trabecular spaces to take an exit finally through the periosteal surface of the metaphyseal or diaphyseal regions. The predominant anisotropy in the pattern of sagittal trabecular plates is lost, as these plates extend further proximally in the diaphyseal region, where elongated dorso-palmar

trabecular spaces lose their distinct orientation due to the change in the form of medio-lateral trabecular components. This explains the arrest of further axial extension of the fracture line after a certain distance, and its exit laterally in commonly occurring complete distal condylar fractures.

The mineral content of the calcified cartilage is the highest in "bone". Excessive mineralisation would cause "bone" to be more brittle (Currey 1969; Katz et al 1984), a feature that could be associated with failure of the bone leading to fracture due to repeated excessive loading. This also associates with the finding (Chap. 2) that tissues in older animals are more mineralised. Lower renewal rate in the older animals leads to hypermineralisation of both the primary and the secondary bones.

The present study also showed that the density of the subchondral bone varied to a large extent in different individuals, as there was also variation in apparent trabecular bone density. In some older animals, the subchondral bone was found to be very dense. Various factors contribute to all these variations. There is no doubt regarding the effect of exercise on bone (Wolff 1892; Lanyon 1974; Lanyon and Rubin 1984; Rubin and Lanyon 1985). The influence of exercise on bone mass depends on the type and intensity and its duration (Jacobson et al 1984; Lanyon 1992a) and the age at which it is practised (Steinberg and Truetta 1981). Exercise influences both trabecular and cortical bone (Pocock et al 1986). Significant differences in bone mass between the dominant and nondominant limbs exists. More bone mass in the dominant arm than in the contralateral arm has been observed (Jones et al 1977h). Several other reports (Woo et al 1981; Rico et al 1994) also showed that prolonged exercise leads to an increase in cortical bone mass. However, Rico and co-workers (1994) found greater bone mineral density in the cortical bone, but not in the trabecular bone in the dominant arm. This was due to greater sustained physical activity that influences the cortical component of the bone, but not the trabecular bone mass. It is probable that the extensive, dense subchondral bone in some individuals in this study is due to a higher magnitude of exercise. Increased stiffness due to the dense bony tissue underneath the

articular cartilage in some individuals would reduce the shock absorbing capacity causing improper load distribution.

The present study also demonstrated remodelling events which generate cement lines in the trabeculae as revealed by Confocal microscopy and BSE imaging. These interfaces would obviously weaken the bone fracture resistance.

It is concluded from the present study that the higher incidence of distal condylar fracture in young racing Thoroughbreds is due to an association of gradual deterioration of bone quality with higher magnitude of exercise. The typical initiation, propagation and fate of the fracture line is attributable to the morphology (form and structure) of the constituent tissue components in the distal third of the MCIII.

The present findings favour the notion that the trabecular systems in the distal condyle of the metacarpus are compression systems (Hert 1992, 1994). The trabeculae in metacarpal cross sections throughout the length predominantly were bright in polarised light in both the dorso-palmar and medio-lateral trabecular components. The nature and character of the mineral and collagenous matrix, as well as the mineral-matrix association is important for the strength of bone. The strength, support and other mechanical properties of the calcified tissue are dependent partially upon the molecular structure and arrangement of its constituent mineral crystals within their organic matrix (Landis 1995). Hydroxyapatite and collagen combine together to form a composite material. Stiffness is rendered by the mineral phase while flexibility is due to the matrix (Burstein et al 1977). The crystals align closely parallel to one another and to the long axis of the fibrils with which they associate. The collagen fibre arrangement in cortical bone itself indicates the type of strain that the bone undergoes while adapting to its biomechanical function (Boyde and Riggs 1990; Ascenzi et al 1990; Riggs et al 1993a; also see Chap. 2). Birefringence in polarised light in the plane of section is a typical feature at the site of compression in cortical bone (Boyde and Riggs 1990; Riggs et al 1993a; also see Chap. 2).

The characteristic collagen deposition unveiled in the region

of compression in trabecular bone is in agreement with the finding (Turner et al 1975; Biewener et al 1983a) that the equine McIII is axially loaded in compression. Compressive strain led to the deposition of predominantly non-longitudinal collagen (bright in polarised light in the plane of section of the cancellous bone), a result consistent with that found in the cortex of equine radii (Chapter 2), as a consequence of mechanical adaptation of bone to stress stimuli. Adaptation of cortical bone to compression, giving rise to more transverse collagen fibres was also demonstrated in the palmar and dorsal cortices of the equine McIII with increasing age by Riggs (1990) and Stover et al (1992).

A bone changes its shape and architecture in response to the direction of strain (Wolff 1870; Lanyon 1974, 1992). It is equally responsive to tensile and compressive stresses (Hert et al 1969; Turner 1992). Fracture resistance is almost entirely related to bone mass and geometry. The effects of dynamic loading on modelling and remodelling activity is profound, while static loads have no such effect (Frost 1986). Rubin and Lanyon (1984) suggested that the osteogenic effect of loading is greatest when the strains and strain rates are high and the strain distribution is unusual. Bone trabeculae align themselves with the direction of pure compressive and tensile loading to avoid the high strains involved in bending.

Longitudinal bone growth is determined by the activity of growth plate cartilage (Brighton 1978), which is located between the epiphysis and metaphysis. The growth plate is a highly anisotropic structure, although the anisotropy varies: it is more distinct in rat and cow than in man (Hunziker 1994). Its cellular organisation is very characteristic. The chondrocytes which act as functional units of longitudinal bone growth, are arranged in vertical columns (Kember 1983). Like the cellular arrangement, the matrix of growth plate cartilage exhibits a well defined structural organisation (Eggli et al 1985). Elongation of the diaphysis of the equine McIII goes on with continuous dislocation of the growth plate away from the bone centre until the growth plate in equine distal McIII becomes mineralised, and closes at around 260 days during the post-natal period. The remodelling process simultaneously shapes and modifies

the structure in the distal McIII as needed for the adaptation to the prevailing biomechanical conditions. This could be associated with the observation that the trabecular architecture undergoes an abrupt change from beyond the site of the fusion of the growth plate. Furthermore, the most anisotropic area in the metaphyseal region is the site of the fusion of the growth plate. This indicates that the growth plate cartilage of the equine distal McIII is a highly anisotropic structure, the anisotropy is retained even when it becomes mineralised and that the architecture is characteristic to all age animals.

The development of the anisotropic architecture involving bone trabeculae and trabecular spaces also takes place in the subchondral bone components, as it has been revealed by examining longitudinal sections of subchondral bone in both the antero-posterior and medio-lateral planes.

Younger animals (eg 1 day, 6 wk) exhibited extensive resorption near the cartilage end viewed on either the anterior or the posterior surface in medio-lateral sections. Resorption fields in the antero-posterior axis would eventually contribute to the development of the dorso-palmar plates and spaces. The subchondral bone surface was seen to undergo extensive resorption. Invariably, all vascular channels seen in the mineralising front preparations exhibited signs of extensive remodelling. This could be associated with a feature obtained in the sagittal plane on the antero-posterior surface, where numerous vascular channels were seen to open up into large spaces in the calcified cartilage. Older animals, on some occasions, also showed similar feature which could be associated with the penetration of calcified cartilage by subchondral bone capillaries (Brooke 1971; human: Redler et al 1975; human, rabbit and canine: Clark 1990b) carrying resorbing cells with them (Clark 1990b).

Trajectories of bone trabeculae align with the stress trajectories within the bone (Meyer 1867; Wolff 1870). More recently, several other studies have shown that peak stress directions align with trabecular trajectories (Lanyon 1974; Hayes and Snyder 1981). It is usually assumed that principal stress in some way determines the architecture of cancellous bone. Certain

controversies exist regarding the trajectorial explanation of the development of the characteristic trabecular pattern (Fyhrie and Carter 1986; Carter et al 1989; Turner 1992; Fiala and Hert 1993; Hert 1992, 1994). In the trajectorial hypothesis of trabecular arrangement, one set of trabeculae is thought to be loaded in normal loading directly in tension, and another set in compression. The result of the present study appears at first sight to be in contrast to this specific mechanism of development.

However, the distal third of the McIII undergoes rotatory compression, during which the axis of loading rotates in motion, so that it develops the typical anisotropic dorso-palmar trabecular pattern as a bio-mechanical adaptation (Thomason 1985). The distal most part would be less well equipped to withstand the strain of lateral bending. The only force that could be effective in this region is rotatory axial compression. Hence, when the McIII starts taking load after birth, the strain related biomechanical responses gradually align the trabeculae vertically in a dorso-palmar orientation to exploit their maximum potential. Simultaneously, relative disuse may lead to the loss of the medio-lateral trabecular components which exist merely as horizontal struts which act as transverse crossbridges between the parallel dorso-palmar trabeculae. The development of this vertical architecture is consistent with the explanation of Pauwels (1965) describing the mechanism of modelling of oblique trabeculae into vertical load bearing columns, where bone apposition occurs in acute angles at the site of greater strain, while regions in obtuse angles undergo resorption in disuse. It is clear that in the presence of unidirectional loading in the fetlock joint, the bone grid in the distal condyle is gradually remodelled to a system of parallel trabeculae, oriented precisely in the direction of the load.

The features obtained in this study suggest the mechanism of obliteration of the transverse component and development of the textural anisotropy in the distal third of the equine MCIII. Uncoupled remodelling (net excess resorption) causes perforation and thinning of the trabeculae before complete obliteration. Perforated trabeculae become completely unloaded, and consequently are resorbed

(Parfitt 1984, 1987; Mosekilde 1990; Jayasinghe et al 1993).

Vertical trabeculae carry the direct loading and the horizontal trabeculae prevent them from buckling under large vertical loads. This means that horizontal trabeculae are not likely to be loaded during low loads. These trabeculae need to be loaded for their continuing presence. Lateral bending is very unusual in the distal condyle. Consequently, disuse gradually leads to considerable obliteration of the medio-lateral component giving rise to a trabecular pattern with an anisotropy of the vertical dorso-palmar plates and spaces, rendering the bone more prone to fracture during excessive load. In human lumbar vertebrae, it has been shown that main vertical load bearing struts were less frequently affected than the horizontal trabeculae in vertebral bodies leading to an age-related increase in cancellous bone anisotropy (Mosekilde 1989; Jayasinghe et al 1993). Once the horizontal trabeculae are eliminated, the vertical trabeculae carry the load alone and are liable to buckle under high vertical loading. Fracture occurs when any bone element is subjected to a load that it can not sustain. Load is necessary to stimulate growth, but excessive loading of bone which is not strong enough to sustain the load will only precipitate fracture.

The anisotropic architecture of the growth plate is retained even after it is mineralised, and is seen in all age animals. The abrupt change in the trabecular architecture proximally from beyond this site (about 3 cm to 4.5 cm from the distal condyle) in both the dorso-palmar and the medio-lateral planes is indicative of the associated strain in the midshaft due to the force exerted during lateral bending. Somewhat obliquely oriented vertical platelike trabeculae in both the dorso-palmar and the medio-lateral planes, change the trabecular arrangement into a true honeycomb. Such a morphological change toward the middle third is consistent with several previous studies (Turner et al 1975; Biewener et al 1983a; Rubin et al 1989) which demonstrated that the metacarpus is loaded in axial compression and medio-lateral bending. At the midshaft, the McIII is likely to undergo maximum degree of lateral bending. Consequently, the strain of the lateral bending is associated with

the strain of the axial compression. As soon as there is a change in loading condition, the strict dorso-palmar orientation of the trabeculae is obliterated. The horizontal medio-lateral components are exposed to suprathreshold strain which is translated in the change in architecture in medio-lateral trabeculae in the region about 4 cm proximal to the distal condyle, where the bone again reacts by apposition, with tension and compression assuming morphogenetic function.

This change in architecture of trabeculae in both the dorso-palmar and the medio-lateral planes following a change in loading environment is consistent with the conclusion of Carter and his co-workers (Fyhrie and Carter 1986; Carter et al 1989) that the cancellous bone structure can be described only in terms of joint loading from different directions. This also supports the hypothesis (Turner 1992) that the architecture of cancellous bone adapts itself to maintain a uniform and isotropic distribution of peak strain within the bone, so that the textural anisotropy exactly cancels the anisotropy of the peak principal stresses imposed upon cancellous bone. Compression and tension have similar morphogenetic effects on bone adaptation. Here, the trabeculae, also in the coronal plane are equally plate like structures which align obliquely and vertically, providing a suitable architecture as adaptation to strain directions. This explains the fate of the fracture; why it is curved after a certain axial extension.

While considering the high incidence of fracture in the distal condyle of the cannon bone, one should consider some relevant characteristics of this fetlock joint. It has a relatively small surface area in comparison to body size and the size of other limb joints; it has the greatest range of motion among all limb joints, and hence, has to withstand the greatest forces of movement of any of the joints; and flat racing horses convey all of their weight through this one joint during one phase of the gait. In response to repetitive loading during racing or training, the subchondral bone progressively thickens beneath sites of major weight bearing. Normally, subchondral bone in the palmar articular surface of the distal condyle of the cannon bone is more dense. There is a gross

increase in the sclerosis of sub-chondral bone including that in the dorsal articular surface, following repetitive trauma during racing or training. This is an exercise induced response of the subchondral cancellous bone to repetitive cyclic compression. The subchondral bone is stiffened. Hence, its shock absorbing capacity diminishes leading to an imbalance in weight transmission. Furthermore, articular cartilage over the non-compliant sclerotic bone may undergo gradual degeneration, thus aggravating the pathology. The cartilage fails to evenly distribute weight during locomotion to the underlying subchondral bone. Subsequent development of ischaemic necrosis of the sclerotic bone may also develop into traumatic osteochondrosis. Once fracture is initiated for any reason: either due to failure following excessive load bearing during strenuous exercise, or enhanced by any other existing pathology, the very morphology of the trabecular and the subchondral bone components favour the typical condylar fracture in this region. However, the presence of pathological evidence on the condylar surface of the fracture cases seen in this study demonstrate that some pre-existing pathology may enhance the failure of the distal condyle, although the very bone morphology (form and structure) of the equine metacarpal distal condyle itself provides an inherent weakness for the failure leading to fracture due to strenuous exercise in racing or training.

CHAPTER 4

THREE-DIMENSIONAL STUDIES IN THE ANISOTROPY OF ARTICULAR CARTILAGE.

4.1 INTRODUCTION

As in any synovial joint, the articular cartilage in distal condyles of the equine metacarpals bears a significant importance in the fetlock joint function. In synovial joints, it covers the extremities of bones on articulating surfaces, and thereby aids in the spreading of loads across the joint. This means that the surface itself is load bearing. In addition, it provides a fluid filled wear resistant surface, and plays a role in both lubrication and wear (Armstrong and Mow 1980). Water is the major constituent of cartilage; up to 60% - 80% of the tissue. A large portion of the interstitial fluid is free to move under a load or pressure gradient (Mow and Meyers 1983). This facilitates the load bearing. The load is not even throughout the articular head surface during movement of a joint at a given time; this is possibly translated into the different thickness of articular cartilage at different sites, observed (Oikawa et al 1989) over the distal metacarpal condyles in Thoroughbred horses.

The main constituents of articular cartilage are collagen and proteoglycan. Type II collagen constitutes about 90-95% of the total collagen content (Mayne and Mark 1983). Previously, Nimni and Deshmuk (1973) suggested that degenerative processes of cartilage may lead to metabolic changes in the chondrocytes, which include change from type II to type I collagen synthesis. However, Eyre et al (1980) contradicted this observation. Trace amount of other collagenous species including Type III, V, VI, IX, X and XI has also been reported to be present (Rhodes and Miller 1978, Morrison et al 1996).

Cells (chondrocytes) are sparingly distributed in cartilage, and exist without direct cell-cell contact (Kuettner and Pauli 1983). In human articular cartilage, the collagen fibrils vary throughout the matrix. Fibril diameter increases from within the superficial to deeper layers (McCall 1969; Muir et al 1970), and from the

chondrocyte outward. Around the chondrocytes is a pericellular halo of fine fibrils 4-10 nm in diameter, which appears to be specially rich in proteoglycans. Further from the cells are located capsular fibrils of larger diameter, and between this zones mature collagen fibrils of diameter 30-200 nm are present (Mayne and Mark 1983).

The pattern of distribution of collagen fibrils in articular cartilage has long been a subject of controversy. Benninghoff's (1925) model of collagen fibril organisation has attracted wide support (human: McCall 1969; Mow et al 1974; Minns and Stevens 1977; Human, dog, pig, rat, rabbit, guinea pig: Zambrano et al 1982; canine: Dunham et al 1988; human, dog and rabbit: Clark 1990a; human: Ome'lianenko 1989, 1991). This model describes collagen fibres in the articular cartilage as organised into three regions: the superficial, the middle, and the deep zone. The fibrils are roughly tangential to the articular surface and are densely packed in the superficial zone. The middle zone contains fibrils which are the arched continuation of the radial fibres of the deeper zone. The radial fibrils are of larger diameter and are found to travel into calcified cartilage underneath (human: Bullough and Goodfellow 1968; Redler 1974; Redler et al 1975; Lane and Weiss 1975; Minns and Stevens 1977; Jones and Boyde 1982). However, controversy exists as regard to the radial pattern of fibrils in the deep zone of the uncalcified cartilage (human: Weiss et al 1968; Clarke 1971b) where presence of randomly oriented fibres has been suggested. MacConaill (1951) suggested a more oblique orientation of fibres rather than the radial system. However, Broom and Myers (1980) suggested a 3D environment of vertically aligned fibres surrounding the cell bodies in the radial fibre zone. An additional, dense separate layer of small fibrils covering the tangential surface fibres has been demonstrated by many (human: Weiss et al 1968; human, dog, pig, rabbit and rat: Zambrano et al 1982; canine: Dunham et al 1988; Clark 1990a), which can be associated with the lamina splendens, initially described as a thin acellular layer of hyaline composition devoid of collagen fibrils, by MacConaill (1951), although some other researchers deny its presence (Aspden and Hukins 1979).

The thickness of the different zones varies in different

locations in the articular cartilage. The radial zone consisting of straight vertical fibres is dominant in the centre where the tangential and transitional zones contribute only about 5% of the total cartilage depth (human, dog and rabbit: Clark 1991). Different zones in the equine distal metacarpal condylar articular cartilage have also been demonstrated by Oikawa and co-workers (1989). However, their investigation was limited to the study of the change in articular cartilage thickness with increasing age; where they found no change to occur after 2 years of age. Also in humans, little change has been documented in the pattern of intact articular cartilage with increasing age in elderly individuals (Muir et al 1970).

Several other studies with polarised light and other techniques have attempted to identify the fibre orientation in different zones of the articular cartilage. Minns and Stevens (human: 1977) found fibrils running parallel to the surface in the superficial zone, but in random orientation. Bullough and Goodfellow (1968) and Meachim et al (1974) associated the direction of the long axes of the oval slits (split lines) which are produced on the articular surface when pierced with a round awl with the orientations of the collagen fibres in the superficial layers. Later, Clark (human, dog and rabbit: 1990a) could trace the radial fibres arching through the transitional zone, and extending into the surface to become flat and overlapped in a common direction. However, Kamalanathan and Broom's (1993) ultrastructural studies (bovine) revealed little evidence that the split-line direction correlated strongly with any preferred alignment of fibrils.

The basal zone of articular cartilage is calcified. The thickness of this lamina at approximately 0.1 mm is remarkably constant in different joints and species (Meachim and Stockwell 1973). Strong alignment of fibre bundles in the CC has been reported (Broom and Poole 1982). Calcified cartilage is separated from uncalcified cartilage by an irregular border known as the tidemark. It may be exposed as a mineral surface following the removal of the unmineralized matrix. The junction between uncalcified and calcified cartilage is comparatively weaker than the boundary between two

calcified tissues such as cartilage and bone (human: Kumar et al 1991). There is no continuity of fibres across the cartilage-bone interface (Human: Clark and Huber 1990). The extent of mineralisation of these two tissues is different (Boyde et al 1992). The subchondral bone is a well-defined cortical shell, and supports the joint cartilage (rabbit: Lemperg 1971). The thin bone plate is connected on its deep surface with the lattice-work of fine trabeculae of the epiphyseal region (human femoral condyle: Chai et al 1991). Brookes (1971) showed fine arterial terminals, possibly end arteries passing at random toward the subchondral bone plate. Subchondral vascular loops infrequently penetrate the calcified zone of the cartilage, but they are usually separated from the cartilage by a few osteonic lamellae or fine trabeculae of bone (Brookes 1971; Clark 1990b). Invasion by capillary loops of calcified cartilage, and in some occasions the tide mark has also been observed by electron microscopy (Redler et al 1975).

Scanning electron microscopy has long been used effectively for investigating fibre organisation, and to look for any special order of collagen in articular cartilage (Bullough and Goodfellow 1968; Redler 1974; Minns and Stevens 1977; Clark 1990a). Minns and Stevens (1977) studied collagen by dissolving away the non-collagenous matrix. Several studies (Human, sheep, rat: Boyde 1980; Jones and Boyde 1982; Chick: Shapiro and Boyde 1987) showed the 3D nature of the mineralising front in anorganic samples. Fresh cartilage is immersed in either cold 5-10% sodium hypochlorite or in warm (50°C) 5% sodium peroxide to remove all unmineralised organic matrix and cells (Boyde 1972; Boyde 1980; Boyde et al 1982, Jones and Boyde 1982; Boyde 1984). All mineralised parts that are linked to one another remain as skeleton.

Many of the above mentioned studies and techniques have focused on the ultrastructure of articular cartilage in humans and other animals. The three dimensional architecture of the equine metacarpal articular cartilage has not previously been reported. The aim of this investigation was to study the articular cartilage in distal condyles of the equine McIII particularly looking for any anisotropy in its three dimensional architecture which might match the

anisotropy seen in subchondral and immediate cancellous bone in equine distal third metacarpals (Chap. 3).

4.2 MATERIALS AND METHODS:

Table 4.1
Principal modes of preparation and study of samples.

1. Third metacarpal distal condylar articular cartilage sections (microtome or hand-cut)
2. Demineralisation of articular cartilage blocks in EDTA, microtome sections in different planes: transverse, sagittal and coronal.
3. Mounting in DPX.
4. 4mm square beams of McIII distal condyles cut with water cooled diamond saw, cleaned, dehydrated and embedded in Polymethyl methacrylate.
5. Polarised light microscopy.
6. Autofluorescence mode Confocal scanning light microscope (CSLM).
7. Enzymatic cleaning using Terg-azyme, 7.5 gms in 1 litre, 5-10 days, change of solution every day, 50°C.
8. Subchondral (sub-articular cartilage) bone blocks, cleaned.
9. 2% Hydrogen peroxide, 24 hrs.
10. NaOCL treatment
11. Gold sputter coating
12. Conventional SE SEM and BSE
13. CSLM of PMMA embedded beams and blocks.

Bone blocks of considerable size containing the notch adjacent to the sagittal ridge from more five animals were obtained, cleaned, embedded and coated following the procedure adopted to prepare the metacarpal beams (as described in chapter 3) for backscattered electron imaging (BSE) in order to observe any anisotropic structure in the mineralised cartilage. The same samples were examined in confocal scanning light microscope (CSLM) before coating.

Further samples from McIII distal condyles (1d, 6wkF, 2yF, 4yF and 24yF) were obtained and cleaned by treating in Terg-azyme as

described above. The bone samples were defatted in alcohol and methanol/chloroform before treating with 2% Hydrogen peroxide at 37°C for 24 hours (Boyde 1984, Jayasinghe et al 1993). This resulted in superficially anorganic samples by removing the superficial unmineralised matrix, while the mineralised collagen is retained in bone. The samples were air dried, coated with gold by sputtering, and examined in the SEM operated at 10 kV for both secondary electron imaging (SE) and backscattered electron imaging (Boyde 1972; Boyde and Jones 1983; Boyde et al 1986; Jayasinghe et al 1993; Boyde and Jones 1996).

Other blocks from the same animals were left untreated. Some anorganic samples (deproteinised) were prepared by treating the bone samples with a sodium hypochlorite solution at room temperature: 50% diluted solution of available bleach (Jones and Boyde 1982; Boyde et al 1982; Boyde and Jones 1983; Boyde 1984). The samples were treated alternately with ethanol to remove fat contained deep within the tissue. NaOCl treatment continued until the samples were visibly clean and white. Although time consuming, the result was satisfactory. The purpose was to digest away the collagen from the subchondral bone leaving the mineral component intact to allow study of the crystal orientation on the exposed surface of the calcified cartilage. After NaOCl extraction, the samples were thoroughly rinsed with distilled water to wash away the residual sodium chloride. The samples were air dried, and coated with gold by sputtering in a sputter coater for SEM for both secondary electron and backscattered electron imaging.

In addition, smaller rectangular blocks of articular cartilage were obtained by sawing in a water cooled diamond saw while frozen. Initially, a few thin sections cut vertically in dorso-palmar, medio-lateral planes, and transverse plane were obtained (hand cut sections) from one animal. Afterwards, all articular cartilage blocks were demineralised in EDTA (Warshwasky and Moore 1967). The cartilage blocks were kept immersed in 4.13% EDTA solution (pH 7.0-7.4) at 4°C (41.3gm EDTA and 4.4gm sodium hydroxide in 1000 ml distilled water) for two weeks. After demineralisation, the samples were embedded in wax before taking plane parallel sections at 25µm or

50μm in the same orthogonal planes. For each plane, two series of sections were obtained from each articular sample by rotating the block at right angle (90°) on the microtome knife. This was done to rule out artifacts in fibre arrangement due to the direction of pressure of the microtome knife. The sections were mounted in DPX for polarised light microscopy.

4.3 RESULTS

PLM studies showed four zones in the articular cartilage of the equine McIII, including the calcified cartilage zone. The features appeared different in the sections cut in different planes.

The longitudinal sagittal (dorso-palmar) sections, when seen with their vertical axes parallel to the "NS" (north-south) direction, appeared bright in CPL with varying intensities of brightness in different zones. The superficial and the intermediate zones were least bright (fig 4.1a,d); a distinct transition characterises the difference in the brightness between the intermediate and the radial fibre zones.

The radial fibre zone is the deepest zone of the unmineralised cartilage. The fibres extend further distally in the intermediate zone, where they arch in one direction (fig. 4.1a,d) on the AP axis to become continuous as the tangential fibres, parallel to the surface in the superficial zone (Fig. 4.1a-d). The chondrocyte lacunae were separated from one another, and were found distributed parallel to antero-posterior fibres (Fig. 4.1b,c). The arched fibres in the intermediate zone showed uniform appearance. In LPL, if the superficial fibres appeared dark; the rest was apparently bright. The superficial fibres appeared bright on rotation of the section (Fig. 4.1b-c). The arched fibres underwent extinction at different degrees of rotation (Fig. 4.1b-c).

The coronal sections (medio-lateral) examined with their vertical axes parallel to the "NS", exhibited a "non-directional texture" in the superficial and the intermediate zones (fig.4.2b). In CPL, the superficial and the intermediate zones were apparently

Figure 4.1

50 µm thick decalcified longitudinal sections in the antero-posterior (sagittal) plane of the articular cartilage from the distal condyle of McIII of a 4 year old animal.

a) CPL micrograph showing different zones of the AC.
Top = uncalcified superficial/intermediate zone
Centre = uncalcified radial fibre zone
bottom = calcified cartilage zone
bottom edge = bone.

b, c & d) show superficial, intermediate and uncalcified radial fibre zones only.

The fibres in the intermediate zone undergo extinction at different rotations of the specimen. Bright radial fibre zone is seen below the dark intermediate zone.

Comparison of **(b)** @ 45° stage rotation and **(c)** @ 65° rotation shows that brightness of radial fibre zone is orientation dependent (in bottom left hand corner of field).

b & c = LPL, **d** = CPL image of the same field as image **c**.

FW: a = 1.2mm, b = 550µm c) 550µm, d) 550µm

Figure 4.1

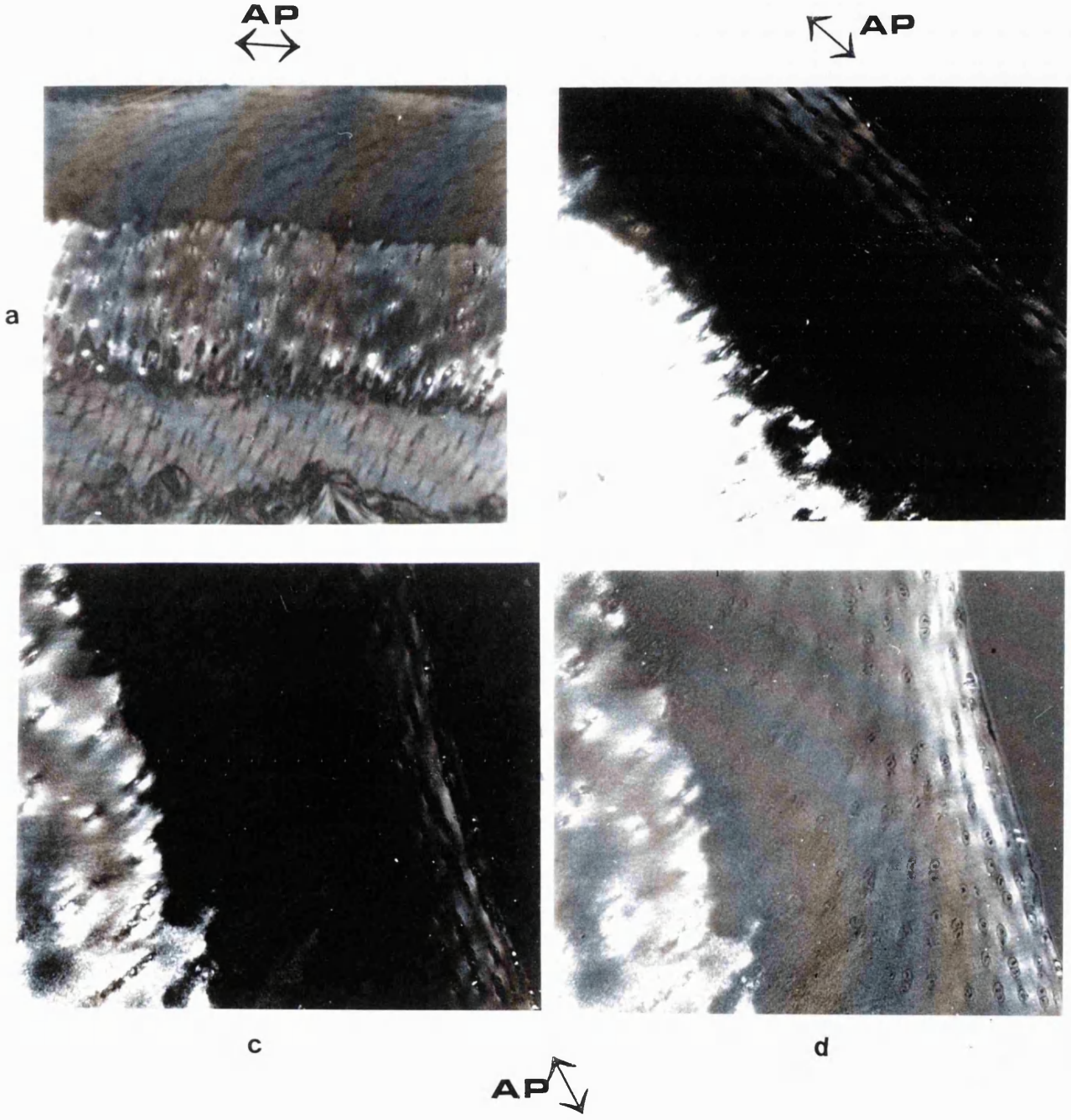

Figure 4.2

50 µm thick decalcified longitudinal sections in the medio-lateral (coronal) plane of the articular cartilage from the distal condyle of McIII of a 4 year old animal.

a) top edge = intermediate fibre zone
top centre = radial fibre zone
below centre = calcified cartilage zone
bottom edge = bone

b) top = superficial zone
top half = intermediate fibre zone
bottom half = radial fibre zone

c) top = superficial fibre zone
bottom = radial fibre zone.

The radial fibre zone is brighter than the rest, and is separated from the CC zone below by the irregular tide mark margin. The CC zone exhibits horizontal shadowing pattern which is parallel to the tide mark plane, and at right angle to the fibre direction.

The Superficial and the intermediate zones appear dark in LPL (c) when the section is viewed with its longitudinal axis parallel to either polar.

FW: a) 1.55 mm, b) 500 µm, c) 475µm.

Figure 4.2

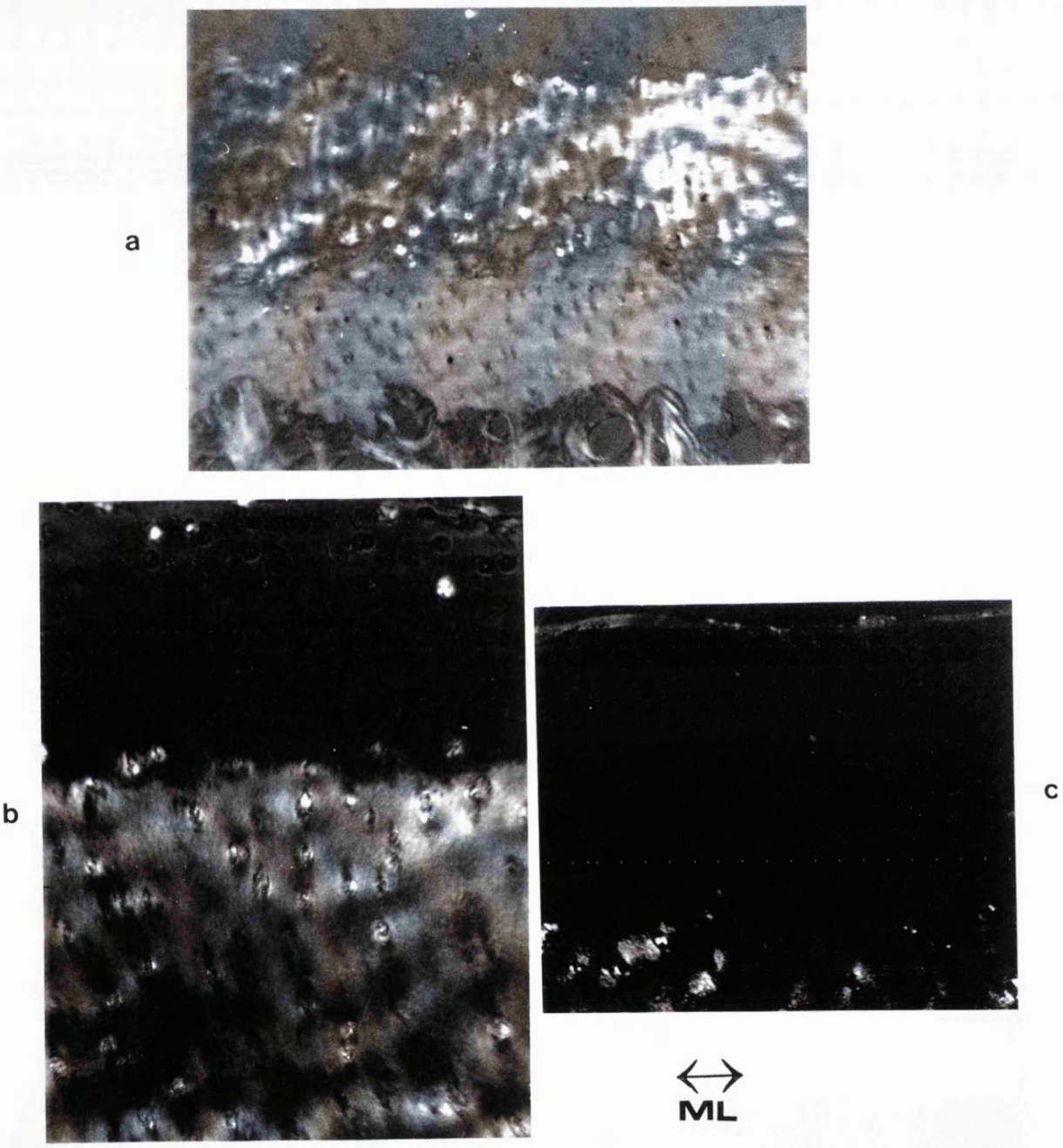

Figure 4.3

PLM images of 50µm thick decalcified longitudinal section in the antero-posterior (sagittal) plane of the articular cartilage from the distal condyle of McIII of a 4 year old animal.

a) CPL,

top = radial fibre zone

centre = calcified cartilage zone

bottom = bone

b) radial fibre zone at centre, LPL

c) radial fibre zone, LPL

a) The calcified cartilage zone shows a horizontal shadowing pattern at right angle to the fibre direction.

b) LPL image of the same section showing bright radial fibres, inclined either anteriorly or posteriorly.

c) LPL image of the same field as picture b with 20° rotation of the section. Radial fibres undergo complete extinction.

FW: a = 1200 µm, b = 450 µm, c = 450 µm

Figure 4.3

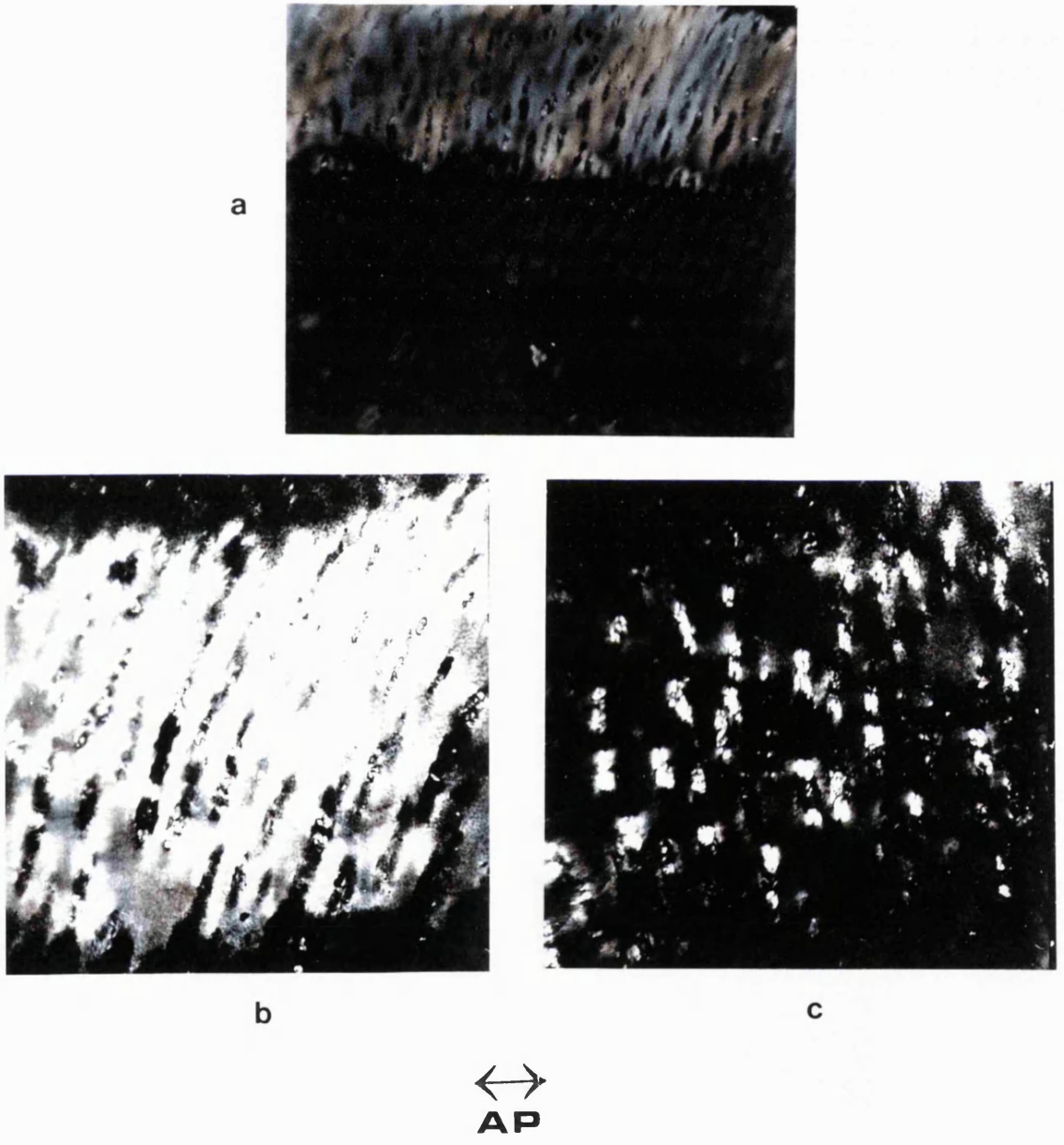

Figure 4.4

LPL images of 50µm thick decalcified longitudinal section in the medio-lateral plane of the articular cartilage from the distal condyle of McIII of a 4 year old animal showing

a) radial fibre zone, ML, LPL.

b) same field, different stage rotation.

a) straight bright radial fibres in LPL with 45° rotation of the section. FW = 525 µm.

b) showing extinction in the radial fibre zone with the section lying with its longitudinal axis parallel to either polar. FW: 500µm.

Figure 4.4

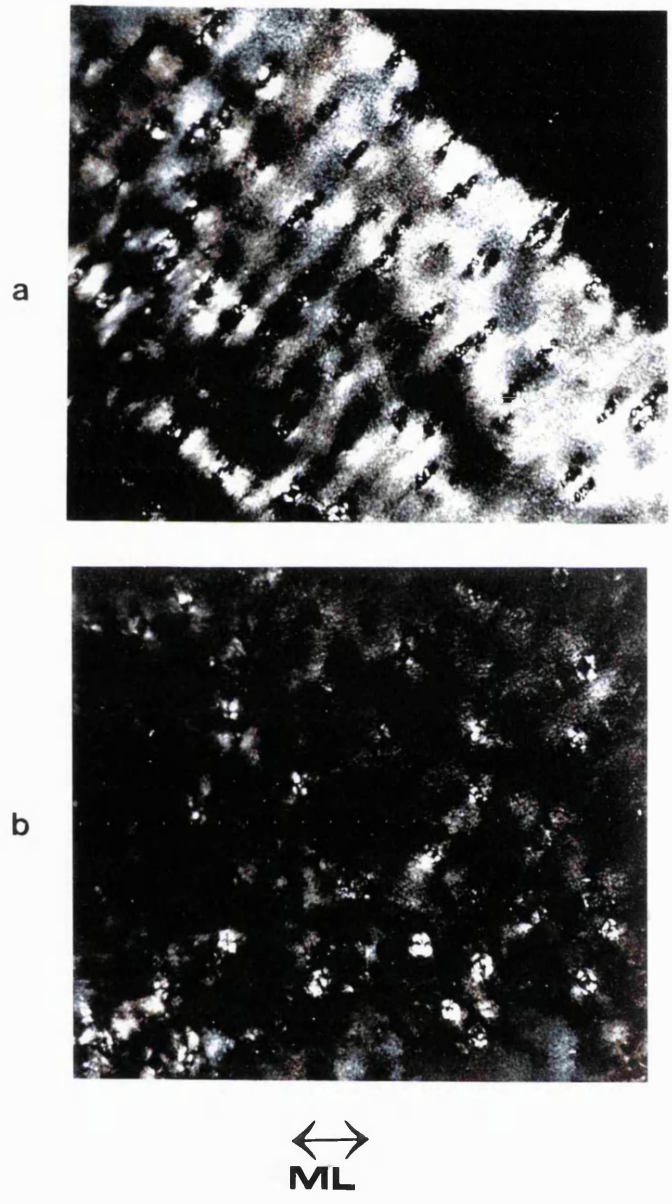

darker in the medio-lateral plane than in the antero-posterior plane (Fig. 4.2b). In both the zones, the chondrocyte distribution was random, and the lacunae appeared round (fig. 4.2b). In LPL, the superficial and the intermediate zones had underwent complete extinction when examined with the longitudinal axis of the section lying parallel to either polar (Fig. 4.2c). The arching of the fibres, and their continuation as tangential fibres in the superficial zone was not distinguishable in this plane. As stated, the chondrocyte lacunae were round and random in the intermediate zone (figures 4.2b), whilst in the sagittal plane, they were oblique, with their long axes directed in one direction, being parallel to the arched fibres (Fig 4.1a,d).

The radial fibre zone was the thickest of all the zones in the articular cartilage. The fibres were bright in both the sagittal and the coronal planes in CPL (fig. 4.3b; 4.4a). In the sagittal plane, the fibre bundles were inclined on the antero-posterior axis when examined with the vertical axis of the section lying parallel to the "NS" (Fig 4.3a-b). In LPL, maximal extinction of these fibres in the sagittal sections occured with 20° of rotation, indicating their orientation at 20° to the vertical axis (Fig. 4.3c). These fibres appeared maximally bright with further rotation of the specimen by ±45°.

The chondrocyte lacunae were elongated in shape, lying parallel to the radial fibres in the sagittal plane on the antero-posterior surface (fig. 4.3a-b); in the coronal plane on the medio-lateral surface, they appear somewhat elliptical (fig. 4.4a).

The radial fibre bundles on the medio-lateral surface of the longitudinal (vertical coronal) section undergo extinction in LPL, when the section is viewed with its longitudinal axes lie parallel to the planes of either of the polars (Fig. 4.4b); the fibres were maximally bright at 45° of rotation (Fig. 4.4a), and appear straight. This indicates that the radial fibres in the medio-lateral sections are vertical. The fibres in the intermediate zone appeared to be vertical and continuous with the radial fibre zone.

The calcified cartilage zone in the antero-posterior section shows horizontal shadowing pattern at right angle to the fibre

Figure 4.5

CPL images of thin hand-cut longitudinal sections in both

a) antero-posterior

b) medio-lateral

viewed in polarised light in water. The cells are not organised into columns (chondrons) in this one day animal.

Figure 4.5

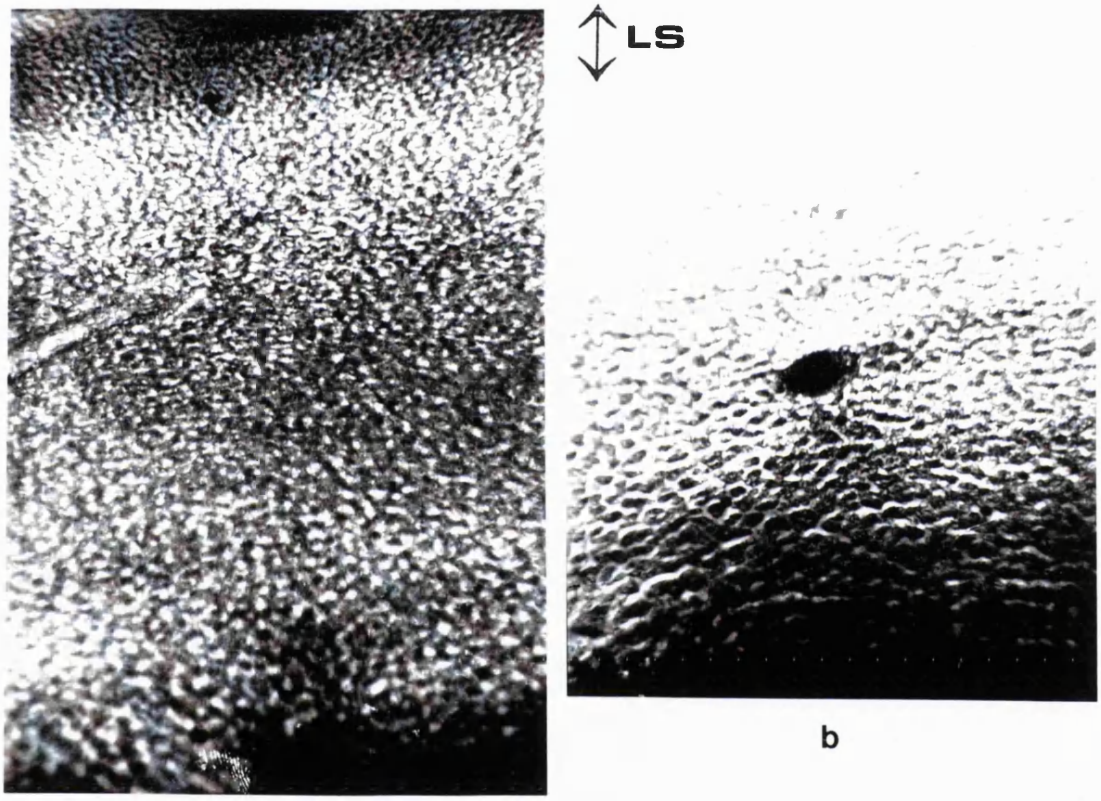

Figure 4.6

CPL images of thin hand-cut longitudinal sections of 6 week McIII in
a) antero-posterior
b) medio-lateral
viewed in polarised light in water showing vertical columns of chondrocyte lacunae near the bone cartilage interface.

Figure 4.6

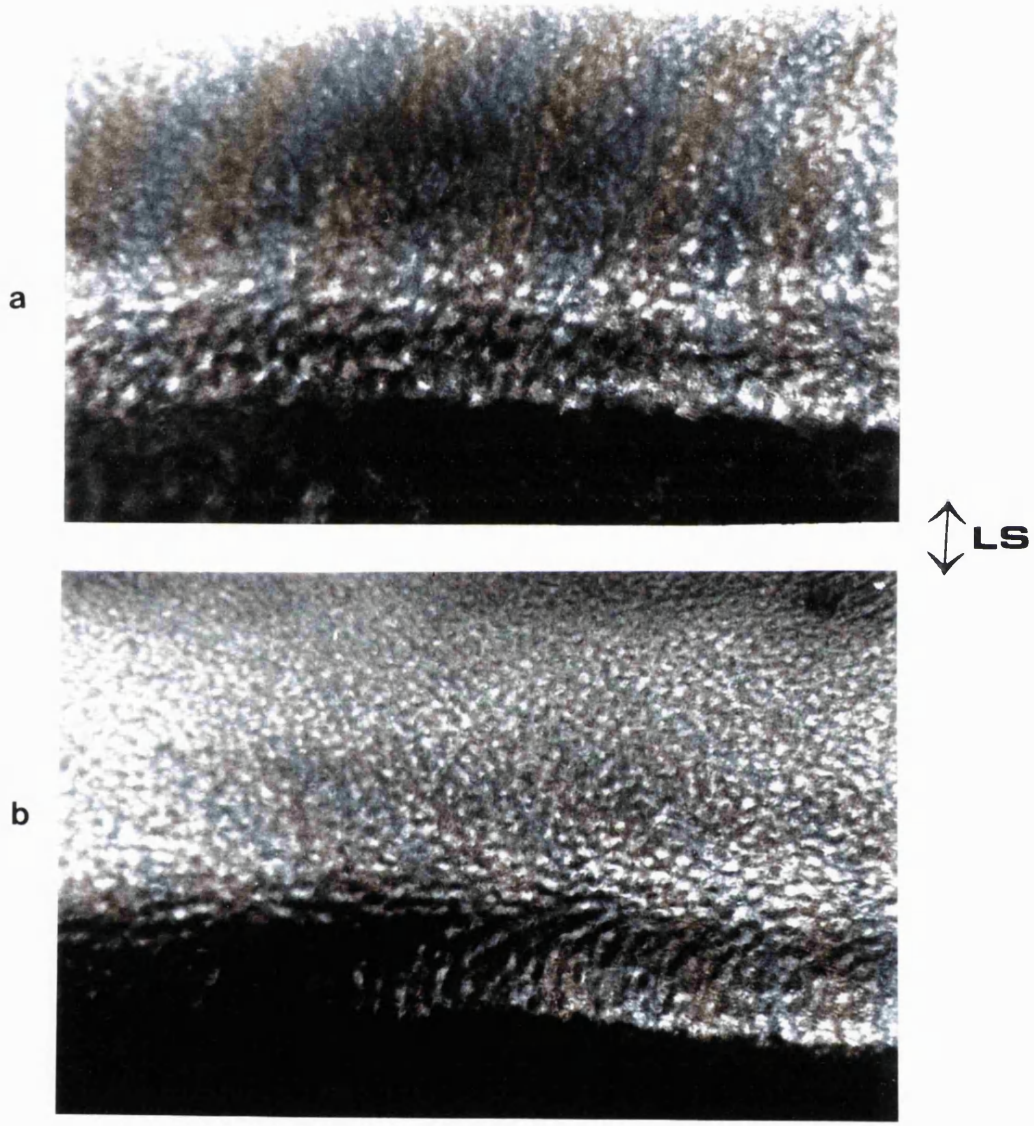

direction (fig. 4.3a). Similar pattern is seen in the CC zone in the medio-lateral surface (fig. 4.2a) plane.

At the extreme surface margin, a thin bright lamina was observed in which extinction occurred with the surface parallel with either polar.

The thin hand-cut longitudinal sections of articular cartilage from the distal condyle of the McIII of the two neonates (1 day and 6 week) examined in polarised light in water showed a different distribution of chondrocyte lacunae. The chondrocyte lacunae looked random in the whole of the cartilage section (vertical) of the 1 day old animal in the both planes (fig. 4.5a-b), whilst that of the six week old animal section showed a vertical distribution of chondrocyte lacunae near the cartilage bone interface in both the AP and ML planes (fig. 4.6a-b).

Mineralising front preparations revealed several features on the nude subchondral bone surface. Hydrogen peroxide treated preparations exhibited signs of the organisation of the collagenous matrix where fine fibrils were seen parallel to antero-posterior axis within chondrocyte lacuna walls (fig. 4.7b-d). Partial digestion of the collagen matrix resulted in dorso-palmar splits on the surface (fig. 4.8a-c). Chondrocyte lacunae with more mineralised pericellular margins were visible (fig. 4.7a)

Hypochlorite treated (anorganic) samples have the unmineralised matrix washed away from the tide mark zone (mineralising cartilage), giving a good chance of seeing the orientation of the (antero-posterior) slits (fig. 4.9c). The principal axis of the cartilage collagen has been seen as parallel vertical columns along the fractured wall (fig. 4.10a).

Some superficially anorganic samples exhibited antero-posterior fracture lines on the mineralising front surface (fig 4.10b-e). These fracture lines appeared during the drying process. Artificially fractured surface allow observation of the organisational features of the structures involved (Boyde 1972). These fracture lines were characteristically in the dorso-palmar direction in all samples suggesting their extension along existing antero-posterior splits in the underlying structures. Moreover,

Figure 4.7

SE images of the articular cartilage, distal McIII of a 2 year old and a 4 year old animals.

a, b & c) = 2y same field

d) 4y

The samples were partially digested in terg-azyme and Hydrogen peroxide. Predominant antero-posteriorly oriented parallel fibres are seen within the chondrocyte lacunae.

SE (10KV). Au sputter-coated.

Figure 4.7

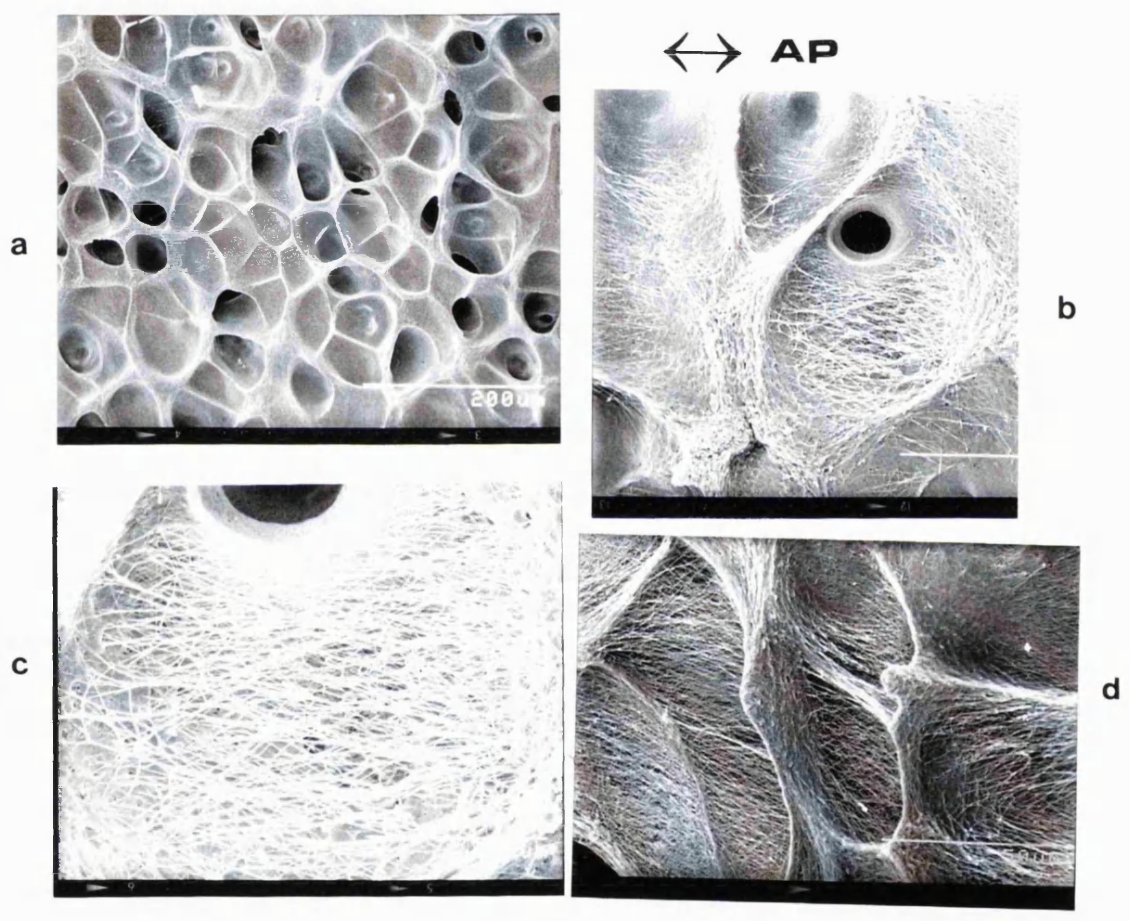

Figure 4.8

SE images of hydrogen peroxide treated subchondral bone surface of 24 year McIII showing antero-posterior fibres in partly digested matrix. Note the mineral deposition along the long axes of the fibres.
SE (10kV). Au sputter-coated.

Figure 4.8

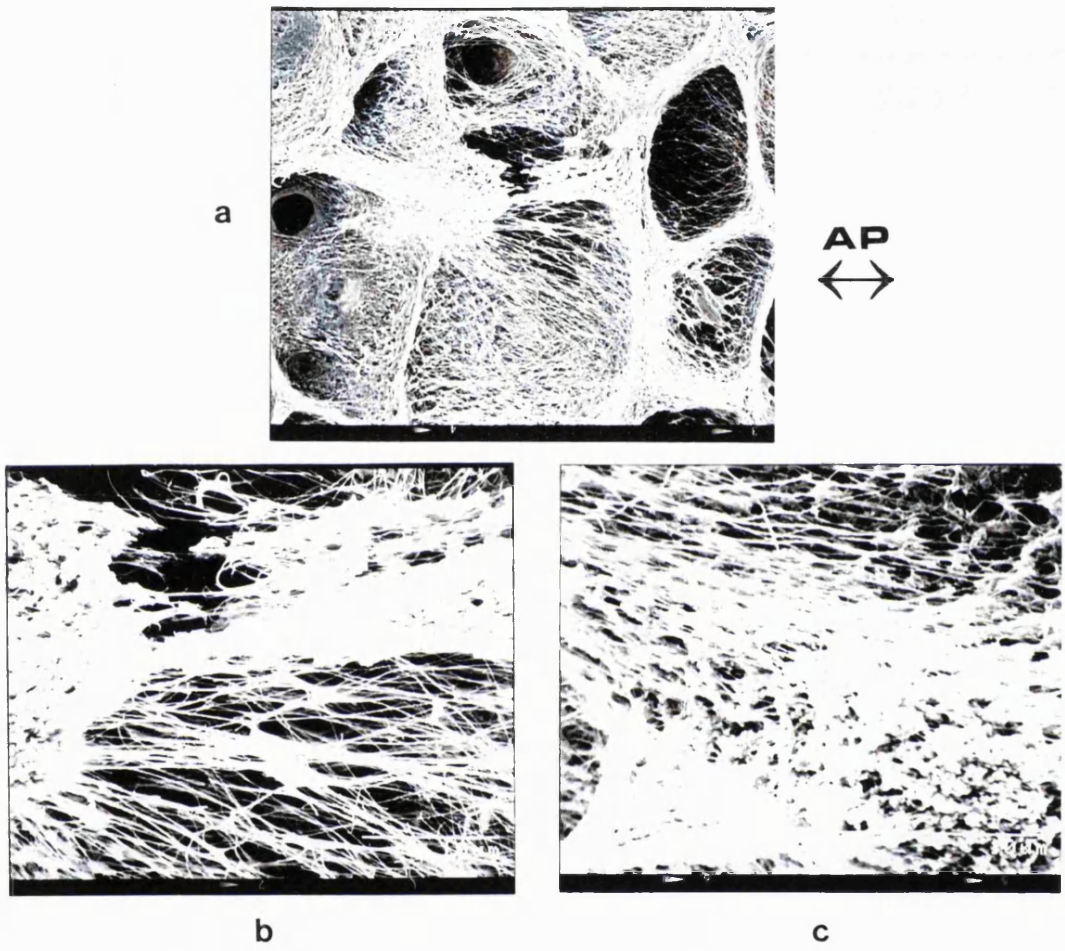

Figure 4.9

a) SE image of ML surface of a block from the McIII distal condylar region showing AP splits in the calcified cartilage.
SE (1.5 kV). Au sputter-coated.

b & c) Anorganic preparation of the subchondral bone mineralising front surface of two animals (2yF & 24yF) showing pericellular mineralisation. The 24y animal bone sample shows an antero-posterior split line.
SE (10 kV). Au sputter-coated.

Figure 4.9

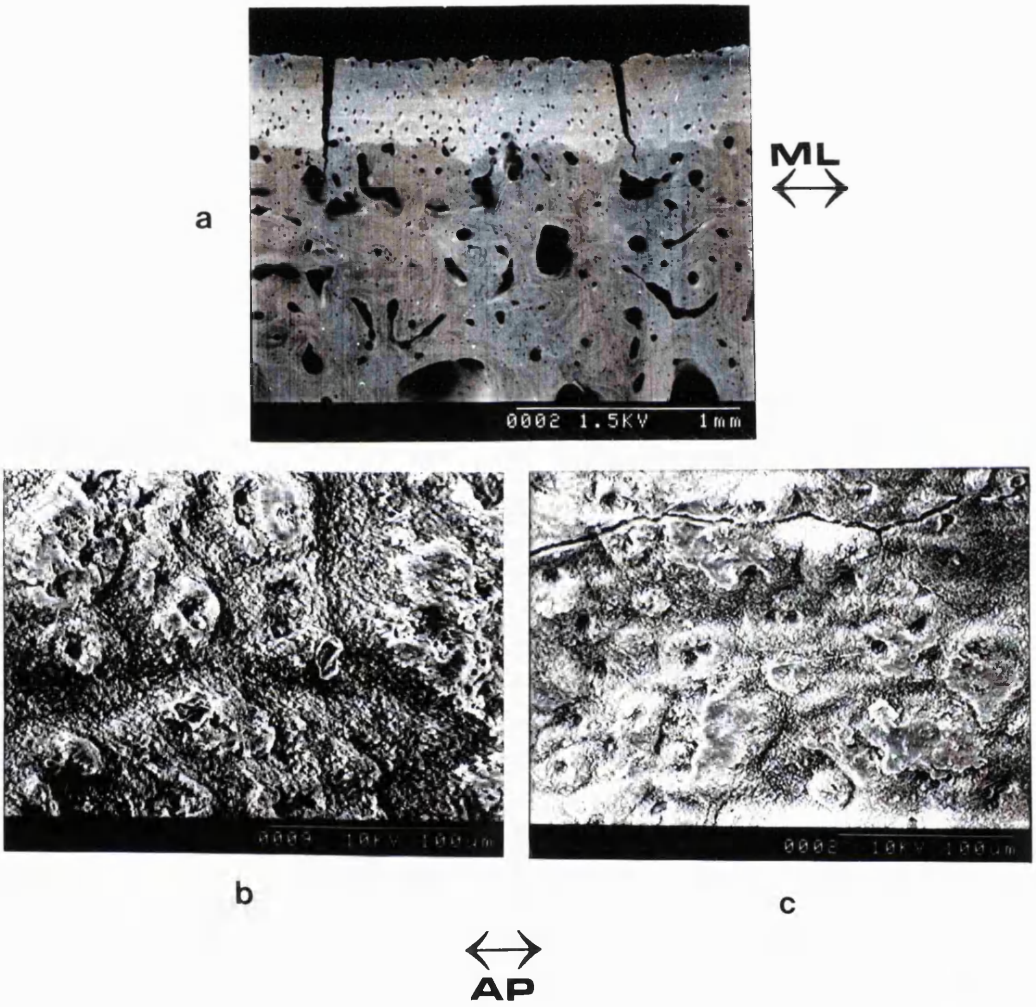

Figure 4.10

a) Hypochlorite treated subchondral bone surface (24yF) showing an AP split line. The vertical markings seen in the fractured wall show the principal axis of the cartilage collagen. SE (10 kV). Au-sputter coated.

b & c) Hydrogen peroxide treated subchondral bone surface (4yF) showing antero-posterior split lines. Vertical collagen fibres are seen in the fractured wall. SE (10 kV). Au-sputter coated.

d & e) Hydrogen peroxide treated subchondral bone surface of the same animal showing an antero-posterior split line. The collagen on both the walls has the same orientation.
SE (10 kV). Au-sputter coated.

Figure 4.10

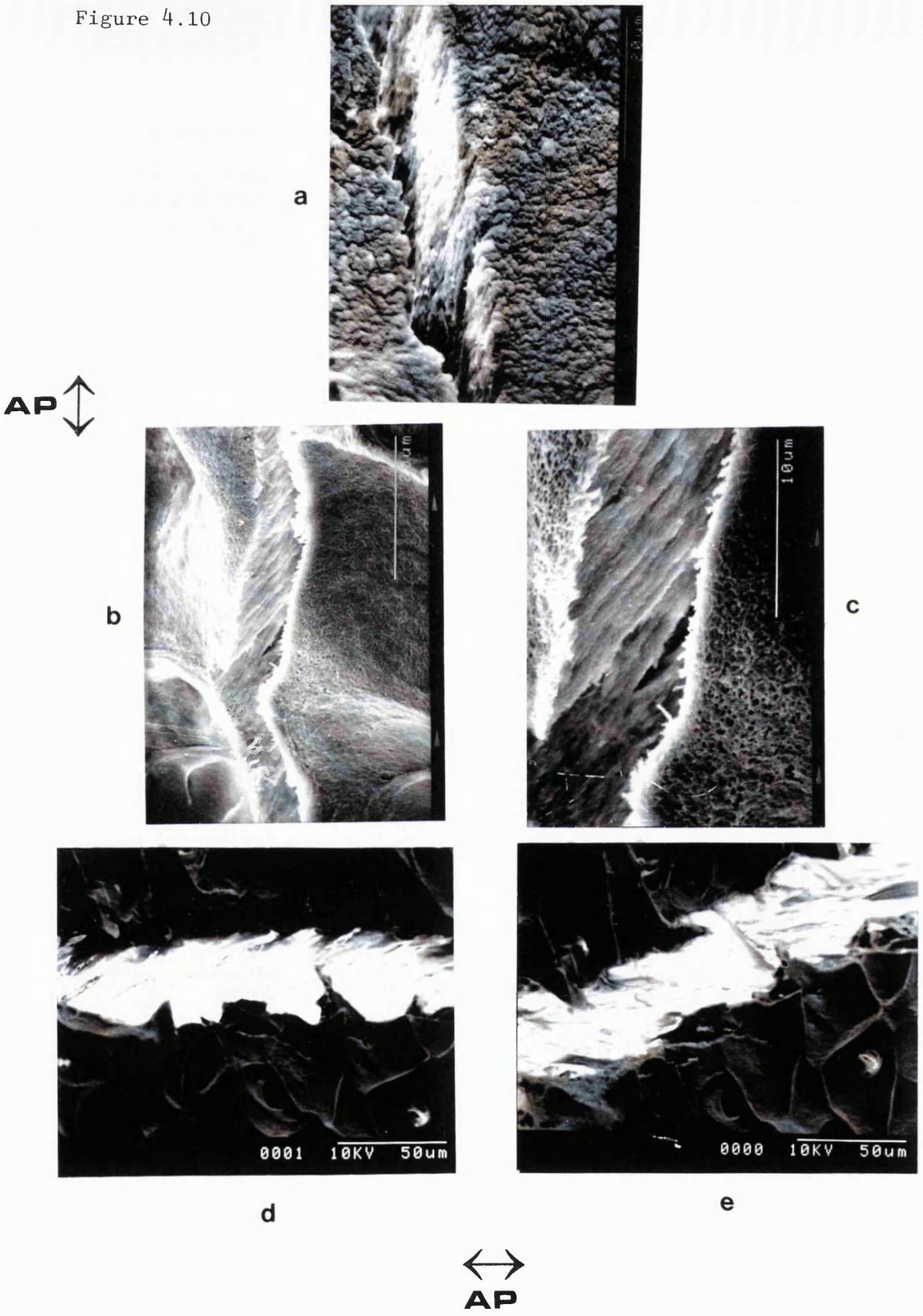

Figure 4.11

BSE images of PMMA embedded sub-articular cartilage bone blocks from distal condyles

a) 7 year old

b & c) 6 year old

showing vertical fibres, and splits in the calcified cartilage on the medio-lateral surface.

10kV. Carbon coated.

Figure 4.11

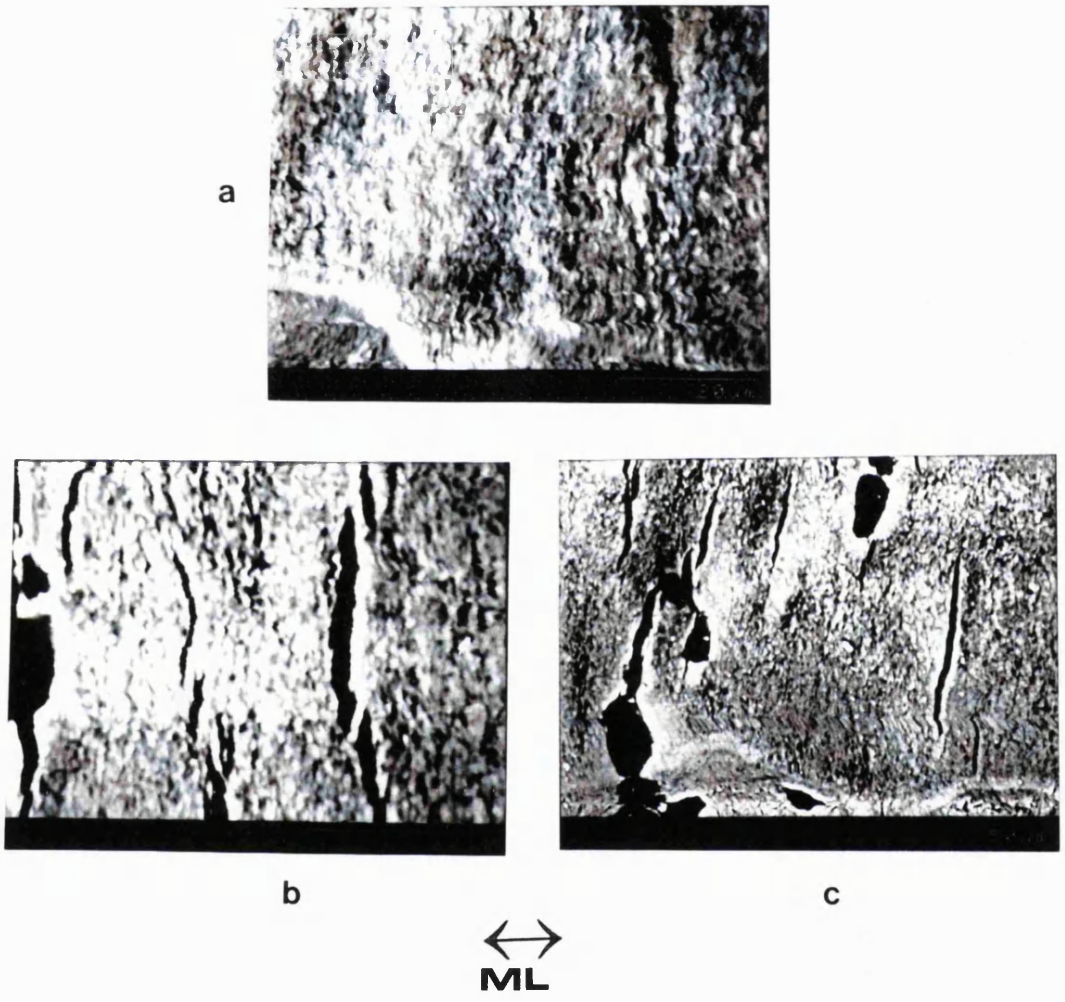

secondary electron imaging clearly displayed parallel collagen fibres in the fracture plane (fig. 4.10b-d).

Backscattered electron imaging of anorganic samples revealed the circumference of the vascular canals on the mineralising front surface to be more highly mineralised than the interterritorial matrix, a finding consistent with previous studies in human, rat and chick articular cartilage (Jones and Boyde 1982; Shapiro and Boyde 1987).

The articular ends of embedded beams and blocks in the coronal plane exhibited vertical splits in the calcified cartilage zone in both backscattered electron and confocal scanning light microscopic images (fig.4.11, and Chap. 3).

4.4 DISCUSSION

This study was carried out to ascertain if there is any structural anisotropy in the articular cartilage, and to examine its association with fractures, commonly seen in distal condyles of the cannon bone of Thoroughbreds.

Scanning electron microscopic study of anorganic samples provided a complete overview of the subchondral bone mineralising front. The primary intention was to see if there were antero-posterior splits on the surface; these were indeed found in this study.

The characteristic collagen fibre distribution (antero-posteriorly and parallel) within terg-azyme and hydrogen peroxide etched chondrocyte lacunae bases initially contributes to the developing anisotropy in calcified cartilage structure as revealed by secondary electron imaging during this study. Redler and co-workers (1975) also found bands of flattened fibrils parallel to the wavy surface of the calcified cartilage while examining the tidemark zone in humans, in addition to vertical fibrils extending from the non-calcified to calcified zones. Deposition of mineral crystals along the cellular circumference (pericellular mineralisation), where the crystals are oriented parallel to the collagen fibres along long axes, observed in this study, also contributes to the development of

an anisotropic architecture in this area. Mineral crystal deposition between cell columns, between cells, and along the long axes of collagen fibres has already been demonstrated (Jones and Boyde 1982, Boyde and Jones 1983). As mineralisation of the lamellar bone is initiated, the mineral deposition starts from within the collagen, subsequently spreading to adjacent matrix (Boyde 1972, 1974; Katz et al 1989; Glimcher 1989); long axis of crystals lie parallel to the fibres (Ascenzi et al 1965, 1978; Lees and Prostak 1988). Several prior studies demonstrate that the vertical fibres of the radial zone of uncalcified cartilage are continuous into the calcified cartilage (Bullough and Goodfellow 1968; Redler et al 1975; Jones and Boyde 1982; Boyde and Jones 1983; Clark 1990a). Columns of oriented collagen fibres in calcified cartilage as well as columns of cells occupying lacunae alongside the collagen fibres were described by Trueta and Little (1960).

Antero-posterior fracture lines in anorganic bone samples studied in SEM, showed collagen fibrils oriented vertically, parallel to the fracture wall in both anorganic and superficially anorganic preparations: contrasting views of both sides of such clefts would provide the answer to the question whether these splits develop along a plane at which there is a change of orientation, in the AP direction, of the principal axis of the bulk collagen fibres. The present study showed no such change of orientation of collagen fibres in both the sides of the splits.

Once the presence of anisotropy in calcified cartilage has been established, it is logical that it should be present in the non-mineralised cartilage as well. The pattern of collagen fibre distribution was determined by polarised light microscopy of sections of articular cartilage cut in different planes. The distribution of collagen fibre into three zones in the unmineralised cartilage as revealed by LPL and CPL in this study is consistent with several previous studies conducted in human and other animals (McCall 1969; Minns and Stevens 1977; Zambrano et al 1982; Clark 1990a, 1991). Further to this, several different features have also been documented during the present study.

The present study showed that the fibres in radial zone of the

articular cartilage are not strictly vertical. The bands of fibres are inclined on the dorso-palmar axis in one direction in one field of view. The radial fibres were found to constitute the greatest part of the thickness of the articular cartilage, and their continuity as arched fibres to tangential fibres on the surface is in agreement with Clark (1990a, 1991) who found similar results in man, dog and rabbit. In the present study, the collagen fibres in the superficial zone lying parallel to the surface were seen to be distributed antero-posteriorly in the vertical sagittal sections. Failure to see these fibres in the coronal sections confirms their characteristic antero-posterior orientation. The characteristic arching of the radial fibres in the intermediate zone which continue as superficial fibres seen in the present study, was not visible in the coronal plane, which suggests that radial fibres in the equine metacarpal distal condylar articular cartilage arch mainly antero-posteriorly. The obliquity of the radial fibres in the AP axis is consistent with the arching. This could be associated with the fact that the equine cannon bone is loaded in axial compression. Hence, the radial fibres buckle in a way that the resulting superficial fibres follow the direction of the load. It can be concluded that the vertical fibres of the radial zone of articular cartilage in a joint under unidirectional load arch only in the line of joint rotation. It is apparent that in a multidirectional loading condition, the vertical fibres in the radial zone will arch in multiple directions. This explains why some researchers (human: Clarke 1971a, Minns and Stevens 1977; Kamalanathan and Broom 1993) failed to find a predominant and uniform orientation of collagen fibres in the superficial zones of the articular cartilage in a joint of multidirectional loading. For the same reason some others (human: McCall 1969; Clarke 1971b; Redler 1974; Omelianenko 1989, 1991) failed to find a predominant orientation of fibres in the intermediate zone of uncalcified articular cartilage. Broom (1984a) also described a structural discontinuity in a plane below the articular surface. He argues that this plane provides a site for a change in overall orientation.

Cartilage collagen fibres lie parallel to the long axes of the

chondrocyte lacunae. Thus the shape, orientation and distribution of the lacunae, and their different appearance in different planes in several zones of the articular cartilage, also indicate the orientation of collagen fibres in the articular cartilage. The lacunae are elongated and parallel with one another in the AP axis in the superficial zone in sagittal sections. On the contrary, in the coronal plane, they appear round and random. The lacunae in the intermediate zone appear round and random in the coronal plane, whilst they appear elongated, oblique and oriented in the sagittal plane. In the radial zone, the lacunae are vertical and parallel with fibres in both the sagittal and coronal planes, although in the coronal plane the lacunae appear less elongated. The radial fibres continue into the calcified cartilage zone where they became mineralised. Although, the presence of lacunae in the mineralised cartilage, parallel to its vertical axis, is likely to favour the cleavage of the bone in both the planes, the antero-posteriorly inclined fibre bundles in the radial zone will give some natural resistance to the failure of the bone in the medio-lateral plane. The thin layer on the surface seen in this study is consistent with the presence of a surface layer with surface parallel fibres as observed in several previous studies on cartilage in other species (McConaill 1951; Zambrano et al 1982; Clark 1990a).

The less CPL bright superficial zones found during the present study, could possibly be associated with the difference in glycosaminoglycan content and their orientation in superficial and deeper zones. Glycosaminoglycan content is reduced in the superficial zone, increasing considerably with depth, and GAGs are highly oriented in the deeper zones (Muir et al 1970; Dunham et al 1988).

The random chondrocyte distribution throughout the depth of the articular cartilage in distal condyles of the neonate metacarpus found in this study is in agreement with Oikawa and co-workers (1989). However, they found no apparent pattern of arrangement of chondrocytes until after the age of six months. The present study revealed that the vertical distribution of chondrocytes in the radial zone begins as early as six weeks of age, but it takes a few months

to achieve a distinct orientation throughout the whole zone. Oikawa and co-workers suggested that after the age of six months, cells gain a characteristic orientation: parallel to the articular surface in the superficial zone, and perpendicularly to the surface in the mid to deep zone. The developing vertical distribution of chondrocytes near the cartilage bone interface in the six week old animal found in this study provides further evidence that gradual load bearing with increasing age brings a change in cellular orientation. The articular cartilage components undergo a process of adaptation to function while the bone starts carrying load with axial compression.

Unilateral direction of fibres on antero-posterior axis provide natural cleavage sites in their organisation which may extend further through radial fibres. In radial fibre zone, fracture always occurs vertically, never transverse (Broom 1984b, Silyn-Roberts and Broom 1990). More work will need to be done to chracterise the nature of underlying AP anisotropy in the calcified cartilage zone. It is shown here that there is a difference in the angulation of cartilage collagen between AP and ML sections, and in the splaying of collagen where it extends from the deep radial to the more superficial oblique layers. However, it can not be stated that a clear structurally based answer has been obtained.

Chondrocytes have very limited ability to regenerate their matrix. Once the articular cartilage is damaged, either due to mechanical or degenerative process, fibroblast like cells which arrive from the synovia and periosteal tissue (Green 1977) repair it. In equine carpal bones, mechanically induced lesions were seen to be healed with a combination of fibrous tissue and fibrocartilage (French et al 1989). When the fibrous matrix is unable to function efficiently, weight transmission leads to further destruction of the weight bearing area of the joint (Mayne and Mark 1983).

In any event, if a bone is loaded excessively, the change in articular cartilage indicates the pattern of possible extension of fracture through existing cleavage lines in the cartilage. Surface depressions seen on articular cartilage were due to the collapse of the surface layer into the underlying lacunae (human: Clarke 1971a). Excessive load caused roughness of the surface with occasional clefts

in articular cartilage (bovine: Saxena et al 1991). In the event of acute transarticular load (canine: Thompson et al 1991), clefts on the surface of the articular cartilage were also demonstrated. In the same study, fracture was seen to occur initially in the zone of calcified cartilage. This could be associated with the more mineralised calcified cartilage zone, since increased mineralisation leads to increased brittleness. The mechanical breach in the calcified cartilage gradually leads to subchondral changes which eventually give rise to osteoarthritic like degeneration within six months (Canine: Thompson et al 1991). Another site of failure in shear is the tidemark zone, as demonstrated in humans (Kumar et al 1991). Although, the continuity of vertical fibres from the deepest layer of the uncalcified articular cartilage into the calcified cartilage provides a tethering mechanism in the tidemark zone, once there is failure, it is clear that the gradual progress will follow the natural preferred cleavage plane within the involved structure. The extension will follow through the anisotropic structures of the subchondral bone (chap. 3).

The presence of denser subchondral bone tissue with loss of trabecular pattern, which appeared as compact bone in some animals (chap. 3) may be associated with degenerative lesions of articular cartilage (human: Chai et al 1991). Such sclerosis may be due to stress in the bone above the minimum threshold level for a longer period of time. The development of a degenerative articular lesion if any, may be a sequel to ongoing sclerosis. An alternative view is that the sclerosis is the consequence of the degenerative articular lesions. In the human osteoarthritic femoral head, Chai and co-workers (1991) found no evidence of microfracture in the sclerotic subchondral bone. However, the horses which exhibited the feature of compact sclerotic bone tissue in the present study had no fractures, even if these animals could be considered at risk, if the altered anatomy of the subchondral bone tissue will fail harmoniously to propagate the stress proximally, leading to an imbalance in weight transmission.

CHAPTER 5

SUMMARY, CONCLUSION AND FUTURE DIRECTION

The concept of the bone's adaptation to the bio-mechanical function is generally accepted. The present studies into the morphology of the equine radius cortical (chap. 2) bone, the McIII cancellous bone (chap. 3) and the articular cartilage (chap.4) determined some ineresting characteristic features.

The orientation of the collagen lamellae in the secondary osteons of the cortical bone has been a subject of controversy for a long time. The present study determined their orientation. The osteons contain alternating dark and bright lamellae. The dark lamellae which are extinguished in the plane of the section in the polarised light are determined to be composed of nearly longitudinal collagen fibres, whilst those appearing bright are composed of more oblique fibres, being at about 35° to the vertical axis of the osteons. This conclusion has been made following extensive studies of the sections of different planes in the polarised light (including the Universal stage microscope) and Scanning electron microscope. Resorbed slices, mechanically etched by the chick osteoclasts have been used in the SEM. Since the osteoblasts lay the collagen fibres, and determine their orientations, the orientation patterns unveiled during these studies appear more logical as regard to the possible changes in the position of the osteoblasts are required. The alternating nearly longitudinal and the more oblique lamellae are better suited to withstand the strain characteristic to the cranial, tension cortex and the caudal, compression cortex of the equine radii. The present study also determined the relative proportion of the longitudinal and the oblique lamellae in the field of the section. It is consistent with the previously reported findings that the caudal cortex is more remodelled than the cranial cortex, and that the cranial cortex contains secondary osteons with more predominantly longitudinal collagen fibres, whilst those in the caudal, compression cortex contains 2° osteons with more oblique collagen. That the oblique collagen is characteristic to the site

of compression is again confirmed in both the radii (chapter 2) and the metacarpal sections (chapter 3). However, the present study showed that the remodelling process is not dependent on age, rather it depends on the animal, and thus probably reflects previous life history differences.

The results have also been associated with the observations made during the study of the samples in autofluorescence confocal microscopy. The difference in the mineralisation density observed in the cranial and the caudal cortices is again associated with the functional activities and with the age of the animals. The bone which is less remodelled is more mineralised, whilst more remodelled bone is less. This finding is consistent to the previous knowledge that the cranial cortex is more mineralised than the caudal cortex.

In general, primary bone is more mineralised than the secondary bone. However, the secondary bone has been seen to become more mineralised than primary, where further remodelling is discontinued. This is consistent with the previous findings that in the elderly individuals, the intensity of the remodelling process (turnover) reduces, leading to excessive mineralisation density, and that the bone mineralisation density increases with age.

The continued remodelling process, as well as the absence of the remodelling, may both, at the extreme, reduce the bone quality (chap. 2 and 3). Excessive brittleness and/or porosity reduces the material strength; the bones become more prone to fracture.

Like the cortical bone, the trabecular architecture also changes to adapt to function. The present studies show a characteristic trabecular architecture to develop in the equine distal third metacarpal bone (chap. 3) after birth. The anisotropic trabecular architecture seen in the adult animals is not present in the neonates. The bone in the ex-epiphyseal region shows anisotropic architecture, where the trabeculae are predominantly antero-posterior vertical plates with elongated spaces between them. The medio-lateral cross bridges connect the trabeculae in the medio-lateral plane. The finding suggests the cause of a commonly occurring fracture in the equine forelimb ie the condylar fracture of the third metacarpal bone, since it is found that the architecture itself

favours the typical fracture in the region. The anisotropic architecture in the region has also been associated with the strains that the bone undergoes while taking load. It is seen that the characteristic trabecular architecture in the distal metacarpus are the result of compression, since the equine McIII is primarily loaded in rotatory axial compression.

The present study also demonstrated remodelling events which generate cement lines in the trabeculae as revealed by Confocal microscopy and BSE imaging (chap 3). These interfaces would obviously weaken the bone strength. Similar interfaces are generated in cortical bone following remodelling events (chap 2).

A wide range of variation exist between the bones of horses of different ages. Apparent bone trabecular density varies greatly between individuals; the variability is not age dependent as it is seen also in the radii (chap. 2). It is apparent that the functional activity of the animal is a major factor in determining the trabecular and the cortical bone mass. Extensive resorption and formation phases have been observed in the younger individuals. On the contrary, the older ones show a lower degree of renewal. Again, this is consistent with the finding that the older animal bone is more mineralised (chap. 2).

The orientation pattern of the collagen in different zones of the articular cartilage over the distal condyle of the equine third metacarpal bone has been determined. The radial fibres incline on the antero-posterior axis, and arch antero-posteriorly. This is associated with the fact that the metacarpal bone is axially loaded in compression. The findings are consistent with the previous reports that the radial fibres are continuous into the calcified cartilage zone (chap. 2 and chap. 3). The anisotropic structure seen in the calcified cartilage zone keeps pace with the development of the anisotropy seen in the trabecular architecture of the distal third of the third metacarpal bone. The reason that the bone initially fractures in the tide mark zone in the calcified cartilage is that the calcified cartilage is more mineralised and it contains anisotropic structure within it, albeit as yet improperly characterised.

The features seen in the present study indicate that the collagen orientation may change with the distribution pattern of strains in a given bone. The shaft of the human proximal femur could be an ideal site to examine, since the direction of strain is grossly changed in the shaft of the implanted femur in fracture cases where prostheses are used.

To study the anisotropic architecture in further details, similar hinged joints in other species should also be examined. In vitro fracture propagation study in both the cortical and the cancellous bones would provide important clues as to the preference of the fracture initiation and propagation.

It is apparent that the articular cartilage needs further study. Whole antero-posterior and medio-lateral sections of the articular cartilage of the third metacarpal distal condyle would provide further information, and would allow study of differences in the different regions of the cartilage.

REFERENCES

Ali NN, Jones SJ, Boyde A (1984a) Monocyte-enriched cells on calcified tissues. Anat Embryol 170:169-175

Ali NN, Boyde A, Jones SJ (1984b) Motility and resorption: Osteoclastic activity in vitro. Anat Embryol 170:51-56

Ali NN, Melhuish PB, Boyde A, Bennett A, Jones SJ (1990) Parathyroid Hormone, but not Prostaglandin E2, changes the shape of osteoblasts maintained on bone in vitro. J Bone Min Res 5(2):115-119

Armstrong CG, Mow VC (1980) Friction, Lubrication and Wear of synovial joints. In: Owen R, Goodfellow J, Bullough P (eds) Scientific foundations of orthopaedics and traumatology. pp 223-232

Ascenzi A, Bonucci E (1964) The ultimate tensile strength of single osteons. Acta Anatomy 44:160-183

Ascenzi A, Bonucci E, Bocciarelli DS (1965) An electron microscope study of osteon calcification. J Ultrastruct Res 12:287-303

Ascenzi A, Bonucci E (1967) The tensile properties of single osteons. Anat Record 158:375-386

Ascenzi A, Bonucci E (1968) The compressive properties of single osteon. Anat Record 161:377-392

Ascenzi A, Bonucci E (1976) Relationship between ultrastructural and pin test in osteons. Clin Orthop Rel Res 121:275-294

Ascenzi A, Bonucci E, Ripamonti A, Roveri N (1978) X-ray defraction and electron microscope study of osteons during calcification. Calcif Tiss Res 25:133-143

Ascenzi A (1988) The micromechanics versus the macromechanics of

cortical bone - a comprehensive presentation. J Biomed Eng 110: 357-363

Ascenzi A, Boyde A, Carando S, Portigliatti Barbos M (1990) The biomechanical basis of bone structure and remodelling. Ital J Miner Elec Metabolism. Vol 4(2):65-74

Aspden RM, Hukins DWL (1979) The lamina splendens of articular cartilage is an artefact of phase contrast microscopy. Proceedings of the Royal Society of London. B206:109-113

Athanasou NA, Quinn J, Bulstrode CJ (1992) Resorption of bone by inflammatory cells derived from the joint capsule of hip arthroplasties. J Bone Joint Surg Br 74(1):57-62

Athanasou NA, Quinn JM (1992a) Human tumour-associated macrophages are capable of bone resorption. Br J Cancer 65(4): 523-6

Athanasou NA, Quinn JM (1992b) Bone resorption by macrophage polykaryons of a pilar tumor of scalp. Cancer 70(2): 469-75

Benninghoff A (1925) Form und Bau der Gelenkknorpel in ihren Beziehungen zur Funktion. II. Zeitschrift fur Zellforschung and mikroskopische Anatomie 2:783-862

Biewener AA, Thomason J, Goodship AE, Lanyon LE (1983a) Bone stress in the horse forelimb during locomotion at different gaits: a comparison of two experimental methods. J Biomech 16(8):565-576

Biewener AA, Thomason J, Lanyon LE (1983b) Mechanism of locomotion and jumping in the forelimb of the horse(Equus): in vivo stress developed in the radius and metacarpus. J Zool (Lond) 201:67-82

Biewener AA, Dial KP (1992) In vivo strain in the pegeon humerus during flight. Am Zool 32:155A

Boyde A, Hobdell MH (1969) Scanning Electron Microscopy of Lamellar Bone. Z Zellforsch 93:213-231

Boyde A (1972) Scanning Electron microscope studies of bone. In: Bourne GH (ed) The Biochemistry and Physiology of Bone, Vol 1, 2nd edn. Academic press, New York. pp 258-310

Boyde A (1980) Electron microscopy of the mineralising front. Metab bone Dis Rel Res 2S:69-78

Boyde A (1980b) Evidence against osteocytic osteolysis. Metab Bone Dis Rel Res 2S:239-255

Boyde A, Jones SJ, Ashford J (1982) Scanning electron microscope observations and the question of possible osteocytic bone mini-(re-) modelling. In: Silbermann M, Slavkin HC (eds) Current advances in skeletogenesis. Int Cong Ser 589. Excerpta Medica, pp 305-314

Boyde A, Jones SJ (1983) Backscattered electron imaging of skeletal tissues. Metab Bone Dis Rel Res 5:145-150

Boyde A, Petran M, Hadravsky M (1983) Tandem scanning reflected light microscopy of internal features in whole bone and tooth samples. J Microsc 132:1-7

Boyde A (1984) Methodology of calcified tissue specimen preparation for scanning electron microscopy. In: Dickson GR (ed) Methods of Calcified Tissue Preparation. Elsevier, Amsterdam. pp 251-307

Boyde A, Bianco P, Portigliatti Barbos M, Ascenzi A (1984a) Collagen orientation in compact bone. A new method for the determination of the proportion of collagen parallel to the plane of compact bone sections. Metab Bone Dis Rel Res 5:299-308

Boyde A, Ali NN, Jones SJ (1984b) Resorption of dentine by isolated osteoclasts in vitro. Br Dent J 156:216-220

Boyde A, Maconnachie E, Reid SA, Delling G, Mundy GR (1986) Scanning electron microscopy in bone pathology: review of methods, potential and applications. Scanning Electron Microsc 1986/IV:1537-1554

Boyde A, Jayasinghe JAP, Jequier B (1989) Three-dimensional integram images of trabecular bone. Bone:10-12

Boyde A, Riggs CM (1990) The quantitative study of collagen in compact bone slices. Bone 11:35-39

Boyde A, Radcliffe R, Watson TF, Jayasinghe JAP (1990b) Continuous motion parallex in the display and analysis of trabecular bone structure. Bone 11:228

Boyde A, Howell PGT, Bromage TG, Elliot JC, Riggs CM, Bell LS, Kneissel M, Reid SA, Jayasinghe JAP, Jones SJ (1992) Applications of mineral quantitation of bone by histogram analysis of backscattered electron images. In: Slavkin H, Price P (eds) Chemistry and biology of mineralized tissues. Elsevier. pp 47-60

Boyde A, Elliot JC, Jones SJ (1993) Stereology and histogram analysis of backscattered electron images: Age changes in bone. Bone 14:205-210

Boyde A, Jones SJ, Aerssens J, Dequeker J (1995b) Mineral density quantitation of the human cortical iliac crest by Backscattered electron image analysis: Variations with age, sex, and degree of osteoarthritis. Bone 16:619-627

Brighton CT (1978) Structure and function of the growth plate. Clin Orthop 136:22-32

Brookes M (1971) The blood supply of bone. Butterworth, London.

Broom ND, Myers DD (1980) Fibrous waveforms or crimp in surface and subsurface layers of hyaline cartilage maintained in its wet

functional condition. Connect Tissue Res 7:165-175

Broom ND, Poole CA (1982) A functional-morphological study of the tidemark region of articular cartilage maintained in a non-viable physiological condition. J Anat 135:65-82

Broom ND (1984a) Further insights into the structural principles governing the function of articular cartilage. J Anat 139:275-294

Broom ND (1984b) The altered biomechanical state of human femoral head osteoarthritic articular cartilage. Arthritis Rheum 27:1028-39

Buckley MJ, Banes AJ, Levin LG, Sumpio BE, Sato M, Jordan R, Gilbert J, Link GW, Tran Son Tay R (1988) Osteoblasts increase their rate of division and align in response to cyclic, mechanical tension in vitro. Bone and Mineral 4:225-236

Bullough P, Goodfellow J (1968) The significance of the fine structure of the articular cartilage. J Bone Jt Surg Br 50B(4):852-857

Burr DB, Martin RB, Schaffler MB, Radin EL (1985) Bone remodelling in response to in vivo fatigue microdamage. J Biomech 18:189-200

Burr DB, Schaffler M, Yang K, Wu D, Lukoschek M, Kandzari D, Sivaneri N, Blaha J, Radin E (1989) The effects of altered strain environment on bone tissue kinetics. Bone 10:215-221

Burr DB, Stafford T (1990) Validity of the bulk-staining technique to separate artifactual from in vivo bone microdamage. Clin Orthop Rel Res 260:305-308

Burstein AH, Zika JC, Heiple KG, Klein L (1975) Contribution of collagen and mineral to the elastic-plastic properties of bone. J Bone Joint Surg 57A:956-961

Carando S, Portigliatti-Barbos M, Ascenzi A, Boyde A (1989) Orientation of collagen in human tibial and fibular shaft and possible correlation with mechanical properties. Bone 10:139-142

Carando S, Portigliatti-Barbos M, Ascenzi A, Riggs CM, Boyde A (1991) Macroscopic shape of, and lamellar distribution within, the upper limb shafts, allowing inferences about mechanical properties. Bone 12:265-269.

Carter DR, Hayes WC (1977) Compact bone fatigue damage-1. Residual strength and stiffness. J Biomech 10:325-337

Carter DR, Hayes WC (1977b) Compact bone fatigue damage: a microscopic examination. Clin Orthop Rel Res 127:265-274

Carter DR (1987) Mechanical loading history and skeletal biology. J Biomech 20:1095-1109

Carter DR; Orr TE; Fyhrie DP (1989) Relationships between loading history and femoral cancellous bone architecture. J Biomech 22(3):231-244

Chang-JS; Quinn-JM; Demaziere-A; Bulstrode-CJ; Francis-MJ; Duthie-RB; Athanasou-NA (1992) Bone resorption by cells isolated from rheumatoid synovium. Ann-Rheum-Dis. 51(11):1223-9

Cheng MZ, Zaman G, Lanyon LE (1994) Estrogen enhances the stimulation of bone collagen synthesis by loading and exogenous prostacyclin, but not prostaglandin E2, in organ cultures of rat ulnae. J Bone Miner Res 9(6):805-16

Civitelli R (1995) Cell- Cell communcation in bone. Calcif Tissue Int 56(Suppl 1):S29-S31

Chai BF, Tang XM, Li H (1991) Scanning electron microscopic study of subchondral bone tissues in osteoarthritic femoral head. Chin Med J

Engl. 104:503-9

Chambers TJ (1981) Phagocytic recognition of bone by macrophages. J Pathol 135:1-7

Chambers TJ (1985) The pathobiology of the osteoclast. J Clin Pathol 38:241-252

Clarke IC (1971a) Surface characteristics of human articular cartilage- a scanning electron microscope study. J Anat 108:23-30

Clarke IC (1971b) Articular cartilag: a review and scanning electropn microscopy study. J Bone and Jt surgery 53B:732-750

Clark JM (1990a) The organisation of collagen fibrils in the superficial zones of articular cartilage. J Anat 171:117-30

Clark JM (1990b) The structure of vascular channels in the subchondral plate. J Anat 171:105-15

Clark JM, Huber JD (1990) The structure of the human subchondral plate. J Bone Joint Surg Br 72(5):866-73

Clark JM (1991) Variation of collagen fiber alignment in a joint surface: a scanning electron microscope study of the tibial plateau in dog, rabbit, and man. J Orthop Res 9(2):246-57

Cohen J, Harris WB (1958) Three dimensional anatomy of Haversian systems. J Bone Jt. Surgery 40A:419-434

Cooper RR, Milgram JW, Robinson RA (1966) Morphology of the osteon. An electron microscopic study. J Bone Joint Surg 48A:1239-1271

Currey JD (1964) Some effects of aging in Human haversian systems. J Anat (Lond) 98:69

Currey JD (1968) Adaptation of bones to stress. J theor Biol 2:91-106.

Currey JD (1969a) The mechanical consequences of variation in the mineral content of bone. J Biomech 2:1-11

Currey JD (1969b) The relationship between the stiffness and the mineral content of bone. J Biomech 2:477-480

Currey JD (1984) Can strains give adequate information for adaptive bone remodelling? Calcif Tissue Int 36:S118-S122

Dallas SL, Zaman G, Pead MJ, Lanyon LE (1993) Early strain-related changes in cultured embryonic chick tibiotarsi parallel those associated with adaptive modeling in vivo. J Bone Miner Res 8(3):251-259

Dunham J, Shackleton DR, Billingham MEJ, Bitensky L, Chayan J, Muir IH (1988) A reappraisal of the structure of normal canine articular cartilage. J Anat 157:89-99

Dietrich JW, Goodson JM, Raisz LG (1975) Stimulation of bone resorption by various prostaglandins in organ culture. Prostaglandins 10:231-240

Dodds RA, Ali N, Pead MJ, Lanyon LE (1993) Early loading-related changes in the activity of glucose 6-phosphate dehydrogenase and alkaline phosphatase in osteocytes and periosteal osteoblasts in rat fibulae in vivo. J Bone Miner Res 8(3):261-7

Doty SB (1981) Morphological evidence of Gap junctions between bone cells. Calcif Tissue Int 33:509-512

Ebner von V (1875) Über den feineren Bau der Knochensubstanz. S b Akad Wiss Wien math-nat Ki 72:49-138

Eggli PS, Herrmann W, Hunziker EB, Schenk RK (1985) Matrix compartments in the growth plate of the proximal tibia of rats. Anat Rec 211:246-257

El-Haj AJ, Minter SL, Rawlinson SC, Suswillo R, Lanyon LE (1990) Cellular responses to mechanical loading in vitro. J Bone Miner Res. 5(9):923-32

Eriksen EF (1986) Normal and pathological remodeling of human trabecular bone: three-dimensional reconstruction of the remodeling sequence in normals and in metabolic bone disease. Endocr Rev 7:379-408

Eriksen EF, Axelrod DW, Melsen F (1994) Bone Macroanatomy and Microanatomy. In: Eriksen EF, Axelrod DW, Melsen F (eds) Bone Histomorphometry. Raven Press. pp 3-12

Evans FG, Vincentelli R (1969) Relations of collagen fibre orientation to some mechanical properties of human cortical bone. J Biomech 2:63-71

Evans FG, Vincentelli R (1974) Relations of the compressive properties of human cortical bone to histological structure and calcification. J Biomech 7:1-10

Evans FG (1974) The mechanical properties of human cortical bone. Acad Naz Lincei. Quad 208:3-28

Eyre DR, McDevitt CA, Billingham MEJ, Muir H (1980) Biosynthesis of collagen and other matrix proteins by articular cartilage in experimental osteoarthrosis. Biochem J 188:823-837

Fiala P, Hert J (1993) Principal types of functional architecture of cancellous bone in man. Func and Dev Morph 3(2):91-99

Frank RM, Frank P, Klein M, Fontaine R (1955) L'os compact humain

normal au microscope electronique. Arch Anat Micr Morph Exp 44:191-206

Frasca P, Harper RA, Katz JL (1977) Collagen fibre orientation in human secondary osteons. Acta Anat 98:1-13

French DA, Barber SM, Leach DH, Doige CE (1989) The effect of exercise on the healing of articular cartilage defects in the equine carpus. Vet Surg 18(4):312-21

Frost HM (1958) Preparation of thin undecalcified bone sections by rapid manual method. Stain Technol. 33:273-277

Frost HM (1959) Staining of fresh, undecalcified, thin bone sections. Stain Technol. 34:135-146

Frost HM (1960a) Micropetrosis. J Bone Joint Surg 42A:144-150

Frost HM (1960b) Presence of microscopic cracks in vivo in bone. Henry Ford Hosp Med Bull 8:27-35

Frost HM (1963) Bone remodelling dynamics. Charles C Thomas, Springfield, Illinois

Frost HM (1969) Tetracycline-based histological analysis of bone remodeling. Calcif Tissue Res 3:211-237

Frost HM (1973) Bone modelling and skeletal modelling errors. CC Thomas. Springfield, IL.

Frost HM (1985) In vivo osteocyte death. J bone Joint Surg 42-A:138-143

Frost HM (1985) The pathomechanics of osteoporosis. Clin Orthop 200:198-225

Frost HM (1986) Intermediary organisation of the skeleton. CRC Press, Boca Raton.

Frost HM (1988) Vital biomechanics: proposed general concepts for skeletal adaptations to mechanical usage. Calcif Tissue Int 42:145-156

Fyhrie DP, Carter DR (1986) A unifying principle relating stress to trabecular morphology. J Orthop Res 4:304-317

Gebhardt W (1905) Über functionelle wichtige Anordnungsweisen der feineren und gröberen Bauelemente des Wirbeltierknochens.II Spezieller Teil.I. Der Bau der Havers'schen Lamellensysteme und seine funktionelle Bedeutung. Arch Entwicklungsmech Org 20:187-322

Gardsell P, Johnell O, Nilsson BE (1989) Predicting fractures in women by using forearm bone densitometry. Calcif Tissue Int 44:235-242

Glimcher MJ (1989) Mechanism of calcification: role of collagen fibrils and collagen phosphoprotein complexes in vitro and in vivo. Anat Rec 224:139-153

Goldstein SA, Goulet R, McCubbrey D. (1993) Measurement and significance of three-dimensional architecture to the mechanical integrity of trabecular bone. Calcif Tissue Int 53(Suppl 1):S127-S133.

Green WT (1977) Articular cartilage repair. Clin Orthop Rel Res. 124:237-250

Gross TS, McLeod KJ, Rubin CT (1990) The skeletal consequences of extreme physical activity: The comparative strain milieu generated by treadmill and field conditions. Transactions of the Orthopaedic Research Society p.108

Grynpas MD (1993) Age and disease related changes in the mineral of bone. Calcif Tissue Int 53:(Suppl.1)57-64

Hagino H, Raab D, Kimmel D, Akhter M, Recker R (1993) The effects of ovariactomy on bone response to in vivo external loading. J Bone Miner Res 8:347-357

Hasegawa S, Sato S, Saito S, Suzuki Y, Brunette D (1985) Mechanical stretchinfg increases the number of cultured bone cells synthesising DNA and alters their pattern of protein synthesis. Calcif Tissue Int 37:431-436

Hasegawa K, Turner CH, Burr DB (1994) Contribution of collagen and mineral to the elastic anisotropy of bone. Calcif Tissue Int 55:381-386

Hayes WC, Snyder B (1981) Toward a quantitative formulation of Wolff's Law in trabecular bone. In: Cowin SC (ed) Mechanical Properties of Bone. pp. 43-68. ASME, New York.

Heaney RP (1993) Is there a role for Bone quality in fragility fractures. Calcif Tissue Int 53(Suppl 1):S3-S6

Heersche JNM (1978) Mechanism of osteoclastic bone resorption: A new hypothesis. Calcif Tissue Res. 26:81-84

Hert J, Liskova M, Landrgot B (1969) Influence of long term continuous bending on the bone. Folia Morph 17:389-399

Hert J, Liskova M, Landa JL (1971a) Reaction of bone to mechanical stimuli: Part 1. Continuous and intermittent loading of tibia in rabbit. Folia Morphol 19:290-317

Hert J, Skelenska A, Liskova M (1971b) Reaction of bone to mechanical stimuli: Part 5. Effect of intermittent stress on the rabbit tibia after resection of the peripheral nerves. Folia Morphol 19:378-387

Hert J (1992) A new explanation of the cancellous bone architecture. Func and Dev Morph 2(1):17-24

Hert J (1994) A new attempt at the interpretation of the functional architecture of the cancellous bone. J Biomech 27(2):239-242

Hunziker EB (1994) Mechanism of longitudinal bone growth and its regulation by growth plate chondrocytes. Micros Res Tech 28:505-519

Jacobson PC, Beaver W, Grubb SA, Taft TN, Talmage RV (1984) Bone density in Women: college athelets and older athletic women. J Orthop Res 2:328-332

Jaworski ZF, Lok E (1972) The rate of osteoclastic bone erosion in haversian remodeling sites of adult dogs rib. Calcif Tissue Res. 10:103-112

Jaworski ZFG (1992) Haversian system and Haversian bone. In: Hall BK (ed) Bone metabolism and mineralisation. Bone Vol 4. CRC Press. pp. 21-45

Jayasinghe JAP, Jones SJ, Boyde A (1993) Scanning electron microscopy of human vertebral trabecular bone surfaces. Virchows Arch (A) 422:25-34

Jayasinghe JAP, Jones SJ, Boyde A (1994) Three dimensional photographic study of cancellous bone in human fourth lumbar vertebral bodies. Anat Embryol 189:259-274

Johnson LC (1964) Morphological analysis: The kinetics of disease and general biology of bone. In: Bone Biodynamics (ed) Frost HM, Little brown, Boston

Johnson LC (1966) The kinetics of skeletel remodelling. In: Structural organisation of the skeleton. (eds) Mitch RA, Robinson RM, National Foundation of the March of Dimes, New York. pp 66-142

Jones HH, Priest JD, Hayes WC (1977h) Humeral hypertrophy in response to exercise. J Bone Jt Surg 59A:204-208

Jones SJ (1973) Morphological and experimental observations on bony tissues using the scanning electron microscope. PhD thesis, University of London

Jones SJ (1974) Secretory territories and rate of matrix production of osteoblasts. Calc Tiss Res. 14:309-315

Jones SJ, Boyde A, Pawley JB (1975) Osteoblasts and collagen orientation. Cell Tissue Res. 159:73-80

Jones SJ, Boyde A (1976a) Morphological Changes of Osteoblasts on vitro. Cell Tissue Res. 166:101-107

Jones SJ, Boyde A (1976b) Is there a relationship between osteoblasts and collagen orientation in bone. Israel J Med Sci 12(2):99-107

Jones SJ, Boyde A (1976c) Experimental study of changes in osteoblsastic shape induced by calcitonon and parathyroid extract in an organ culture system. Cell Tissue Res. 169:449-465

Jones SJ, Boyde A (1977a) The migration of osteoblasts. Cell Tiss Res 184:179-193

Jones SJ, Boyde A (1977b) Some morphological observations on osteoclasts. Cell Tiss Res 185:387-397

Jones SJ, Ness AR (1977) A study of the arrangement of osteoblasts of rat calvarium cultured in medium with or without added parathyroid extract. J Cell Sci. 25:247-263

Jones SJ, Boyde A (1979) Colonization of various natural substrates by osteoblasts in vitro. Scan Elec Micros 1979/II:529-538

Jones SJ, Boyde A, Shapiro IM (1981) The response of osteoblasts to parathyroid hormone (PTH-134) in vitro. Metab Bone Dis Rel Res 2:335-338

Jones SJ, Boyde A (1982) The junction between uncalcified and calcified cartilage. In: Silbermann M, Slavkin HC (eds) Current Advances in Skeletogenesis. Int Cong Series 589. Excerpta Medica, pp.362-367

Jones SJ, Boyde A, Ali NN (1984) The resorption of biological and non-biological substrates by cultured avian and mammalian osteoclasts. Anat Embryol 170:247-256

Jones SJ, Boyde A, Ali NN, Maconnachie E (1985) A review of bone cell and substratum interactions. Scanning 7:5-24

Jones SJ, Gray C, Sakamaki H, Arora M, Boyde A, Gourdie R, Green C (1993) The incidence and size of gap junctions between the bone cells in rat calvaria. Anat Embryol 187:343-352

Jones SJ, Boyde A (1994) Questions of quality and quantity - A morphological view of Bone Biology. Acta Anat Nippon 69:229-243

Kamalanathan S, Broom ND (1993) The biomechanical ambiguity of the articular surface. J Anat 183(3):567-578

Katz JL, Yoon HS, Lipson S, Maharidge S, Meunier A, Christel P (1984) The effects of remodelling on the elastic properties of bone. Calcif Tissue Int 36:S31-S36

Katz EP, Watchel E, Yamauchi M, Mechanic GL (1989) The structure of mineralised collagen fibrils. Con Tiss Res 21:149-158

Kember NF (1983) Cell kinetics of cartilage. In: Hall BK (ed) Cartilage. Structure, Function, and Biochemistry. Academic Press, New York. pp 149-179

Klein DC, Raisz LG (1970) Prostaglandins: Stimulation of bone resorption in tissue culture. Endocrinology 86:1436-1440

Kölliker A (1889) Handbuch der Gewebelehere des Menschen. 6th ed. W Englemann, Leipzig.

Krook L, Maylin G (1988) Fractures in Thoroughbred race horses. Cornell Vet 78(S-II):7-47

Krukowski M, Kahn AJ (1980) Normal osteoclast number and function in rat pups lacking paathyroid hormone. Experientia 26:871-872

Kuettner KE, Pauli BU (1983) Vascularity of cartilage. In: Hall BK (ed) Cartilage Vol. 1 Structure, Function, and Biochemistry. pp. 281-312.

Kumar P, Oka M, Nakamura T, Yamamuro T, Delecrin J (1991) Mechanical strength of osteochondral junction. Nippon Seikeigeka Gakkai Zasshi 65(11): 1070-77

Landis WJ (1995) The strength of acalcified tissue depends in part on the molecular structure and organisation of its constituent mineral crystals in their organic matrix. Bone 16:533-544

Lane JM, Weiss c (1975) Review of articular cartilage collagen research. Arthritis and Rheumatism 18:553-562

Lanyon LE (1974) Experimental support for the trajectorial theory of bone structure. J Bone Jt Surg 56B:160-166

Lanyon LE, Hampson WGJ, Goodship AE, Shah JS (1975) Bone deformation recorded in vivo from strain gauges attached to the human tibial shaft. Acta Orthop Scand 46:256-268

Lanyon LE, Baggot DG (1976) Mechanical function as an influence of the structure and form of bone. J Bone and Joint Surgery. 58(B):436-

443.

Lanyon LE, Maggi PT, Baggot DG (1979) The relationnship of the functional stress and strain to the process of bone remodelling: An experimental study on the sheep radius. J Biomech 12:593-600

Lanyon LE, Bourn S (1979) The influence of mechanical function on the development and remodeling of the tibia. J Bone Joint Surg 61A:263-272

Lanyon LE, Goodship AE, Pye CJ, MacFie JH (1982) Mechanically adaptive bone remodelling. J Biomech 15:141-154

Lanyon LE, Rubin CT (1984) Static vs. dynamic loads as an influence on bone remodelling. J Biomech 17:897-905

Lanyon LE (1987) Functional strain in bone tissue as an objective, and controlling stimulus for adaptive bone remodelling. J Biomech 20:1083-93

Lanyon LE. (1992a) The success and failure of the adaptive response to functional load- bearing in averting bone fracture. Bone 13:S17-S21

Lanyon LE (1992b) Control of bone architecture by functional load bearing. J Bone Miner Res 7:s369-s375

Lanyon LE (1993) Osteocytes, strain detection, Bone modelling and remodelling. Calcif Tissue Int. 53:(Suppl.1):102-107

Lacroix P (1951) The organisation of bone, McGraw-Hill, New York.

Lees S, Prostak K (1988) The locus of mineral crystallites in bone. Con Tiss Res 18:41-54

Lemperg R (1971) The subchondral bone plate of the femoral head in

adult rabbits. I. Spontaneous remodelling studied by microradiography and tetracycline labelling. Virchows Arch A: Pathol Anat Histol 352:1-13

Liskova M (1961) Growth changes in the architecture of cancellous bone in the femur of man (in Czech). Plzen. lek. sbor 15:123-128 cited by Hert J 1992.

Liskova M, Hert J (1971) Reaction of bone to mechanical stimuli: Part 1. Periosteal and endosteal reaction of the tibial diaphysis in rabbits to intermittent loading. Folia Morphol 19:301-317

MacConaill M A (1951) The movement of bones and joints. iv. The mechanical structure of articulating cartilage. J Bone and Joint Surgery 33B:251-257

McCall J G (1969) Ultrastructure of human articular cartilage. J Anat 104:586

Marotti G, Muglia MA (1988) A scanning electron microscope study of human bony lamellae. Proposal for a new model of collagen lamellar organisation. Arch Ital Anat Embriol 93:163-175

Marotti G (1990) The original contribution of the scanning electron microscope to the knowledge of bone structure. In: Bonucci E, Motta PM (eds) Ultrastructure of skeletal tissues. Kluwer Academic Publisher, Boston. pp 19-39

Marotti G (1993) A new theory of bone lamellation. Calcif Tissue Int 53(Suppl 1):S47-S56

Martin RB, Picket JC, Zinaich S (1980) Studies of skeletal remodelling in aging man. Clin Orthop Rel Res 149:268-282

Martin RB, Burr DB. (1982) A hypothetical mechanism for the stimulation of osteonal remodelling by fatigue damage. J Biomech

15:137-139

Martin RB, Burr DB (1989) The structure, function, and adaptation of compact bone. Raven Press, New York

Martin RB, Ishida J (1989) The relative effects of collagen fibre orientation, porosity, density, and mineralisation on bone strength. J Biomech 22:419-426

Mayne R, Mark K von der (1983) Collagens of cartilage. In: Hall BK (ed) Cartilage Vol 1. Structure, Function and Biochemistry. Academic press. pp. 181-214

McElhaney JH, Fogle JH, Melvin JW, Haynes RR, Roberts VL, Alem NM (1970) Mechanical properties of cranial bone. J Biomech 3:495-511

Meachim G, Stockwell RA (1973) The matrix. In: Freeman MAR (ed) Adult articular cartilage. pp. 1-50. Pitman, London.

Meachim G, Denham D, Emery IH, Wilkinson PH (1974) Collagen alignments and artificial splits at the surface of human articular cartilage. J Anatomy 118:101-118

Meagher DM (1976) Lateral condylar fractures of the metacarpus and metatarsus in Horses. Proc. 22nd Ann Conv, Am Assoc Equine Pract. pp 147-154

Melton LJ, Chao EYS, Lana J (1988) Biomechanical aspects of fractures. In:Riggs BL, Melton LJ (eds) Osteoporosis: etiology, diagnosis and management. Raven, New York. pp 111-131

Meyer GH (1867) Die architektur der spongiosa. Arch Anat Physiol wiss Med. 34:615-628

Meyer K (1960) Nature and function of mucopolysaccharides of connective tissue. In: Machmanshon D (ed) Molecular biology. Acad

Press, London, New York. pp 69-76

Minns RJ, Stevens FS (1977) The collagen fibril organization in human articular cartilage. J Anat 123(2):437-57

Mori S, Burr DB (1991) Increased intracortical remodelling following fatigue microdamage. Transactions, Combined meeting of the Othopaedic Research Societies of the USA, Japan, and Canada, Banff, Canada. Oct. pp 21-23

Morrison EH, Ferguson MWJ, Bayliss MT, Archer CW (1996) The development of articular cartilage: I. The spatial and temporal patterns of collagen types. J Anat 189: 9-22

Mosekilde L (1989) Sex differences in age-related loss of vertebral trabecular bone mass and structure-biomechanical consequences. Bone 10:425-432

Mosekilde L (1990) Consequences of the remodelling process for vertebral trabecular bone structure: a scanning electron microscopy study (uncoupling of unloaded structures). Bone Miner 10:13-35

Mow VC, Lai WM, Redler I (1974) Some surface characteristics of articular cartilage. 1. A scanninmg electron microscopy study and a theoretical model for the dynamic interaction of synovial fluid and articular cartilage. J Biomech 7: 449-456

Mow VC, Meyers ER (1983) Biomechanics of cartilage and its response to biomechanical stimuli. In: Hall BK (ed) Cartilage Vol 1 Structure, Function, and Biochemistry. pp 313-341

Muir H, Bullough P, Maroudas A (1970) The distribution of collagen in human articular cartilage with some of its physiological implications. J Bone Jt Surgery 52B:554-563

Mundy GR, Altman AJ, Gondek M et al (1977) Direct resorption of bone

by human monocytes. Science 196:1109-1111

Mundy GR, Varani J, Orr W, Gondek MD, Ward PA (1978) Resorbing bone is chemotactic for monocytes. Nature 275:132-135

Mundy GR, Roodman GD (1987) Osteoclast ontogeny and function. In: Peck WA (ed) Bone and mineral research / 5: 209-279

Nolan RD, Patridge NC, Godfrey HM, Martin TJ (1983) cyclooxygenase products of arachidonic metabolism by mouse bone in organ culture. Calcif Tissue Int 35:294-297

Norwood GL (1978) The bucked shin complex in thoroughbreds. Proc Am Assoc equine pract 24:319-336

Nunamaker DM (1986) The bucked shin complex. Proc Am Assoc equine pract 32:457-460

Nunamaker DM, Butterweck DM (1989) Bone modelling and remodelling in Thoroughbred racehorse: relationships of exercise to bone morphometry. Trans Orthopaed Res Soc 35:99

Nunamaker DM, Butterweck DM, Provost MT (1989) Some geometric properties of the third metacarpal bone: a comparison between the Thoroughbred and standardbred racehorse. J biomech 22(2):129-134

O'Brien TR (1977) Disease of the Thoroughbred fetlock joint- a comparison of radiographic signs with gross pathologic lesions. Proc. 23rd Ann Conv. Am Asoc Equine Pract. pp 367-380

O'Connor JA, Lanyon LE, McFie H (1982) The influence of strain rate on adaptive bone remodelling. J Biomech 15:767-781

Oikawa M, Yoshihara T, Kaneko M (1989) Age-related changes in articular cartilage thickness of the third metacarpal bone in the thoroughbred. Jpn J Vet Sci 51(4):839-842

Ome'lianenko NP (1989) Orientational analysis of the ultrastructural architecture of the fibrous base of human articular cartilage. Arkh Anat Gistol Embriol 97(7):39-47

Omelianenko NP (1991) A quantitative analysis of the ultrastructural organisation of extracellular components in human articular cartilage. Clin Orthop and Rel Res 266:34-41

Osborne D, Effmann E, Broda K, Harrelson J (1980) The development of the upper end of the femur, with special reference to its internal architecture. Radiology 137:71-76

Pannarale L, Braidotti P, d'alba L, Gaudio E (1994) Scanning electron microscopy of collagen fibre orientation in the bone lamellar system in Non-decalcified human samples. Acta Anat 151:36-42

Parfitt AM (1976) The actions of parathyroid hormone on bone: Relation to bone remodelling and turnover, calcium homeostasis, and metabolic bone disease. 1. Mechanisms of calcium transfer between blood and bone and their cellular basis: Morphological and kinetic approaches to bone turnover. Metabolism 25(7):809-844

Parfitt AM (1983a) The physiologic and clinical significance of bone histomorphometric data. In: Recker RR (ed) Bone histomorphometry: techniques and interpretation. Boca Raton, FL. CRC Press. pp 143-223

Pasquini C, Reddy VK, Ratzlaff MH (1978) Atlas of equine anatomy. Albion, Washington.

Recker RR (ed) Bone histomorphometry: Techniques and interpretation. Boca Raton, FL. CRC Press. pp 53-87

Parfitt AM (1984) Age-related structural changes in trabecular and cortical bone: cellular mechanisms and biomechanical consequences. Calcif Tissue Int 36:S123-S128

Parfitt AM (1987) Trabecular bone architecture in the pathogenesis and prevention of fracture. Am J Med 82(Suppl 1B): 68-72

Parfitt AM, Kleerekoper M, Villanueva AR (1987) Increased bone age: mechanisms and consequences. In: Christiansen C, Johansen JS, Riis BJ (eds) Osteoporosis 1987. Osteopress ApS, Copenhagen. pp 301-308

Pauwels F (1980) Biomechanics of the Locomotor Apparatus. Springer, Berlin.

Pead MJ, Suswillo R, Skerry TM, Vedi S,Lanyon LE (1988a) Increased ^{3}H-uridine levels in osteocytes following a single short load of dynamic bone loading in vivo. Calcif Tissue Int 43:92-96

Pead MJ, Skerry TM, Lanyon LE (1988b) Direct transformation from quiscence to bone formation in the adult periosteum following a single brief period of bone loading. J Bone Miner Res 3(6):647-656

Pead MJ, Lanyon LE (1989) Indomethacin modulation of load-related stimulation of new bone formation in vivo. Calcif Tissue Int 45(1):34-40

Piotrowski G, Sullivan M, Colahan PT (1983) Geometric properties of equine metacarpi. J Biomech 16(2):129-139

Pocock NA, Eisman JA, Yeates MG, Sambrook PN, Eberl S (1986) Physical fitness is a major determinant of femoral neck and lumbar spine bone mineral density. J Clin Invest 78:618-621

Pool RR, Meagher DM (1990) Pathologic findings and pathogenesis of racetrack injuries. Equine Practice 6(1):1-29

Portigliatti-Barbos M, Bianco P, Ascenzi A (1983) Distribution of osteonic and interstitial components in the human femoral shaft with reference to structure, calcification and mechanical properties. Acta Anat 115:178-186

Portigliatti Barbos M, Bianco P, Ascenzi A, Boyde A (1984) Collagen orientation in compact bone: ii. Distribution of lamellae in the whole of the human femoral shaft with reference to its mechanical properties. Metab Bone Dis Rel Res. 5:309-315

Portigliatti- Barbos M, Carando S, Ascenzi A, Boyde A (1987) On the structural symmetry of human femurs. Bone 8:165-169

Quinn JM, Athanasou NA (1992) Tumour infiltrating macrophages are capable of bone resorption. J Cell Sci. 101(Pt 3):681-6

Quinn JM, Matsumura Y, Tarin D, McGee JO, Athanasou NA (1994) Cellular and hormonal mechanisms associated with malignant bone resorption. Lab-Invest. 71(4):465-71

Ranvier J (1989) Traite technique d'histologie, 2nd ed. Savy, Paris.

Rawlinson SC, Mohan S, Baylink DJ, Lanyon LE (1993) Exogenous prostacyclin, but not prostaglandin E2, produces similar responses in both G6PD activity and RNA production as mechanical loading, and increases IGF-II release, in adult cancellous bone in culture. Calcif Tissue Int 53(5):324-329

Redler I (1974) A scanning electron microscopic study of human normal and osteoarthritic articular cartilage. Clin Orthop and Rel Res 103:262-268

Redler I, Mow VC, Zimmy ML, Mansell J (1975) The ultrastructure and biomechanical significance of the tide mark of the articular cartilage. Clin Orthop Rel Res. 112:357-362

Reid SA (1986) A study of lamellar organisation in juvenile and adult human bone. Anat Embryol 174:329-338

Reid SA, Boyde A (1987) Changes in the mineral density distribution in Human bone with age: image analysis using backscattered electrons

in the SEM. J Bone Miner Res 2:13-22

Richardson DW (1984) Medial condylar fractures of the third metatarsal bone in Horses. J Am Vet Med Assoc. 185(7):761-765

Rick MC, O'Brien TR, Pool RR, Meagher D (1983) Condylar fractures of the third metacarpal bone and third metatarsal bone in 75 horses: Radiographic features, treatments, and outcome. J Am Vet Med Assoc 183(3):287-296

Rico H, Gonzalez-Riola J, Revilla M, Villa LF, Gomez-Castresana F, Escribano J (1994) Cortical versus Trabecular bone mass: influence of activity on both bone components. Calcif Tissue Int 54:470-472

Riggs CM (1990) The relationship between mechanical function and microstructural properties of cortical bone in the race horse. PhD thesis, University of London.

Riggs CM, Lanyon LE, Boyde A (1993a) Functional associations between collagen fibre orientation and locomotor strain direction in cortical bone of the equine radius. Anat Embryol 187:231-238

Riggs CM, Vaughan LC, Evans GP, Lanyon LE, Boyde A (1993b) Mechanical implications of collagen fibre orientation in cortical bone of the equine radius. Anat Embryol 187:239-248

Rodan GA, Martin TJ (1981) The role of osteoblasts in hormonal control of bone resorption - a hypothesis. Calcif Tissue Int. 33:349-351

Rhodes RK, Miller EJ (1978) Physicochemical characterisation and molecular organisation of the collagen A and B chains. Biochemistry 17:3442-3448

Rooney JR (1969) Biomechanics of lameness in horse. Williams and Wilkins, Baltimore.

Rooney JR (1974) Distal condylar fractures of the cannon bone in the horse. Mod Vet Pract 55(2):113-114.
Rooney JR (1975a) Osteochondrosis in the horse. Mod Vet Prac 56(1):41-43

Rooney JR (1975b) Osteochondrosis in the horse. Mod Vet Prac 56(2):113-116

Rouiller C, Huber L, Kellenberger E, Rutishauser E (1952) La structure lamellaire de l'osteone. Acta Anat 14:9-22

Rouiller C (1956) Collagen fibres in connective tissue. In: Bourne GH (ed) The Biochemistry and Physiology of Bone, Academic press, New York. pp 104-147

Rubin CT, Lanyon LE (1982) Limb mechanics as a function of speed and gait: a study of functional strains in the radius and tibia of horse and dog. J Exp Bio 101:187-211

Rubin CT, Lanyon LE (1984) Regulation of bone formation by applied dynamic loads. J Bone Joint Surg(Am) 66:397-402

Rubin CT, Lanyon LE (1985) Regulation of bone mass by mechanical loading: The effect of peak strain magnitude. Calcif Tissue Int 37:411-417

Rubin CT, Lanyon LE (1987) Osteoregulatory nature of mechanical stimuli: unction as a determinant for adaptive remodelling in bone. J Orthop Res 5:300-310

Rubin CT, Vasu R, Tashman J, Seeherman H, McLeod KJ (1989) The non-uniform distribution of shear strains in functionally loaded bone: implications for a complex mechanical milieu. Trans Orthopaed Res Soc Vol. 35, p. 313

Ruth EB (1947) Bone studies. I. Fibrillar structure of adult human

bone. Am J Anat 80:35-53

Saxena RK, Sahay KB, Guha SK (1991) Morphological changes in the bovine articular cartilage subjected to moderate and high loadings. Acta Anat Basel 142(2):152-7

Schaffler MB, Burr DB. (1984) Primate cortical bone microstructure: relationship to locomotion. Am J Phys Anthropol 65:191-197

Schaffler MB, Radin EL, Burr DB (1989) Mechanicaland morphological effects of strain rate on fatigue of compact bone. Bone 10:207-214

Schaffler MB, Radin EL, Burr DB (1990) Long-term fatigue behavior of compact bone at low strain magnitude and rate. Bone 11:321-326

Schiller PC, Metha PP, Roos BA, Howard GA (1992) Connexin 43 as a potential mediator of PTH regulation of cell-cell communication in rat osteoblasts. J Bone Min Res 7(Suppl 1):S207

Schnitzer CM, Pettifor JM, Mesquita JM, Bird MDT, Schnaid E, Smyth AE (1990) Histomorphometry of illiac crest bone in 346 normal black and white south african adults. Bone Miner 10:183-199

Shapiro IM, Jones SJ, Hogg NM, Slusarenko M, Boyde A (1979) Use of the SEM for the study of the surface receptors of osteoclasts in situ. Scan Elec Micros II:539-545

Shapiro IM, Boyde A (1987) Mineralisation of normal and rachitic chick growth cartilage: vascular canals, cartilage calcification and osteogenesis. Scan Micros 1(2):599-606

Silyn-Roberts H, Broom ND (1990) Fracture behaviour of cartilage on bone in response to repeated impact loading. Connect Tissue Res 24:143-156

Skerry TM, Bitensky L, Chyen J, Lanyon LE (1988) Loading-related

reorientation of bone proteoglycan in vivo. Strain memory in bone tissue? J Orthop Res 6:547-551

Skerry TM, Bitensky L, Chayen J, Lanyon LE (1989) Early strain related changes in enzyme activity in osteocytes following bone loading in vivo. J Bone Miner Res 4(5):783-8

Steinberg ME, Truetta J (1981) Effects of activity on bone growth and development in the rat. Clin Orthop 156:52-60

Stover MS, Pool RR, Martin RB, Morgan JP (1992) Histological features of the dorsal cortex of the third metacarpal bone mid-diaphysis during postnatal growth in thoroughbred horses. J anat 181:455-469

Tappen NC (1977) Three dimensional studies of resorption spaces and developing osteons. Am J Anatomy 149:301-332

Taylor ML, Boyde A, Jones SJ (1989) The effect of fluoride on the pattern of adherence of osteoclasts cultured on and resorbing dentine: a 3-D assessment of vinculin-labelled cells using confocal optical microscopy. Anat. Embryol 180:427-435

Thomason JJ (1985) The relationship of structure to mechanical function in the third metacarpal bone of the horse, Equus caballus. Can J Zool 63:1420-1428

Thompson RC Jr, Oegema TR Jr, Lewis JL, Wallace L (1991) Osteoarthrotic changes after acute transarticular load. An animal model. J Bone Joint Surg Am. 73(7):990-1001

Truetta J, Little K (1960) The vascular contribution of osteogenesis. II. Studies with the electron microscope. J Bone & Joint Surgery 42B:367-376

Turner CH (1992) On Wolff's Law of trabecular architecture. J Biomech 25(1):1-9

Turner AS, Mills EJ, Gabel AA (1975) In vivo measurement of bone strain in the horse. Am J Vet Res 36:1573-1579

Urist MR, Macdonald NS, Moss MJ, Skoog WA (1963) Rarefying disease of the skeleton: observation dealing with agedand dead bone in patientswith osteoporosis. In: Mechanism of hard tissue destruction. Publication No. 75 of the American association for the Advancement of Science, Washington DC. pp 385-446

Vesely P, Boyde A, Jones SJ (1992) Behaviour of osteoclasts in vitro: contact behaviour of osteoclasts with osteoblast-like cells and networking of osteoclasts for 3D orientation. J Anat 181:277-291

Vincentelli R, Evans FG (1971) Relations among mechanical properties, collagen fibres and calcification in adult human cortical bone. J Biomech 4:193-201

Vincentelli R, Grigorov M (1985) The effect of haversian remodelling on the tensile properties of human cortical bone. J Biomech 18:201-207

Warner A (1988) The gap junction. J Cell Sci 89:1-7

Warshawsky H, Moore G (1967) J Histochem Cytochem 15:542-549

Weinmann JP, Sicher H (1955) Bone and Bones. In: Fundamentals of bone Biology. C.V.Mosby, St. Louis. pp 18-46

Weiss C, Rosenberg L, Helfet AJ (1968) An ultrastructural study of normal young adult human articular cartilage. J Bone & Jt Surgery 50A:663-674

Woo SLY, Kuei SC, Amiel D, Rutherfor DL, Doty D, Jemmott GF (1981) The effect of prolonged physical training on the properties of long bone: a study of Wolf's Law. J Bone Jt Surg 63A:780-786

Wong SYP, Kariks J, Evans RA, Dunstan CR, Hills E (1985) The effect of age on bone composition and viability in the femoral head. J Bone joint Surg 67A:274-283

Wolff J (1870) Über die innere Architektur der Knochen Und ihre bedeutung für die Frage vom Knochenwachstum. Arch. Pathol. Anat. Physiol. Klin Med. Virchows. Arch. 50:389-453

Wolff J (1892) The Law of bone remodelling (Das Gesetz der transformation der Knochen, Hirschwald). Translated by Maquet P & Furlong R (1986), Springer, Berlin.

Xia S, Ferrier J (1992) Propagation of a calcium pulse between osteoblastic cells. Biochem Biophys Res Commun 186:1212-1219

Zambrano NZ, Montes GS, Shigihara KM, Sanchez EM; Junqueira LCU (1982) Collagen arrangement in cartilages. Acta Anat 113:26-38

Zaman G, Dallas SL, Lanyon LE (1992) Cultured embryonic bone shafts show osteogenic responses to mechanical loading. Calcif Tissue Int 51(2):132-6

Ziegler O (1906) Studien uber die feinere Struktur des Rohrenknochens und dessen Polarisation. Dtsch Z Chir 85:248-263

Appendix 1

The use of Polarised light microscopy in determining collagen fibre orientation in bone.

Polarised light

Visible light is electromagnetic radiation with a wavelength between 400 - 700 nm. The orientation of this wave is perpendicular to the wavefront. Natural or unpolarised light has no preferential orientation. When only one vibration direction is allowed to pass, the resulting light is said to be linearly or plane polarised as its vibration direction is restricted to a single plane. Polarising filters are used to constrain the light passing through it to a single plane of vibration. These filters are commonly made from films of long-chain polymers stretched to bring the chains into a polarised configuration so that light vibrating along the directions of the chains is strongly absorbed, whilst light with its vibration component perpendicular to the chains is transmitted. If a second polarising filter is placed on top of the first, with its 'vibration' direction perpendicular to the first, no light can pass through and the polars are said to be crossed.

Isotropic Materials

The refractive index of a material is defined as the ratio of the velocity of light in air to the velocity of light in that medium. In an optically isotropic material, the velocity of light is constant, and is independent of the direction in which the light passes through it. Such a material absorbs or transmits polarised light equally in any direction. Thus optically isotropic media have only one refractive index and do not restrict the vibration direction of light passing through them so that they appear dark when placed between crossed polars whatever their orientation.

Anisotropic materials, birefringence or double refraction

Optically anisotropic materials exhibit birefringence: they transmit light with different velocities depending on the orientation

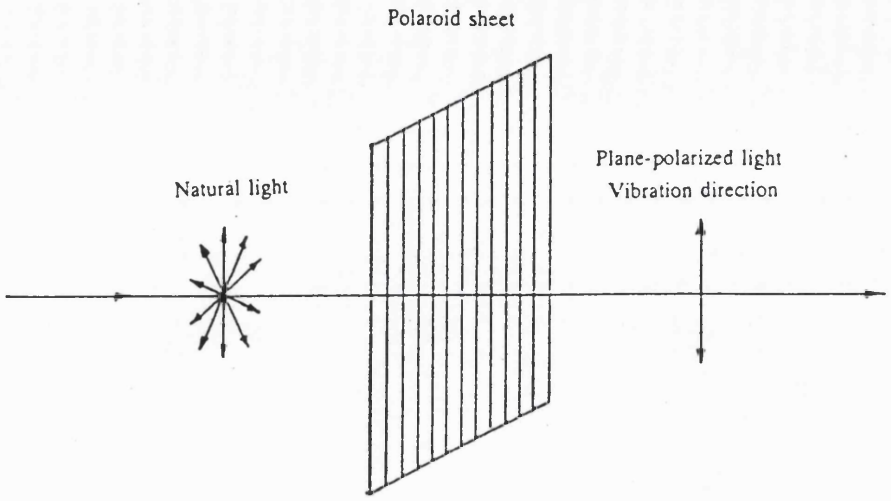

Figure A1.1 When a light beam with its vibration directions in all orientations pass through a polarising filter, it is converted to a plane polarised light. Its vibration directions are in a single plane. (From Robinson and Bradbury 1992, Qualitative polarized light microscopy, Oxford Science Publications).

of the material, i.e. there are different refractive indices depending upon direction. For the materials with which we are concerned in this thesis, there are two extreme values of the refractive index. Such materials are called doubly refractive or birefringent. Except for light propagating along the isotropic or optic axis, the velocity of a ray which is polarised in one direction is different from that of another polarised in a contrasting direction. One ray suffers a relative 'retardation' with respect to the other, and there is an 'optical path difference' between the two components of the light when they emerge from the other side of the sample.

Polarised light microscopy is used to examine optically anisotropic objects. The presence of anisotropy in an object indicates polarity and order. Such objects appear bright on a dark field in certain orientations between crossed polars. Thus polarised light distinguishes singly refracting (isotropic) from doubly

refracting (anisotropic) media. The ordinary polarised light microscope gives some information, although not complete, about the orientations of the constituent structures in a complex anisotropic object.

The appearance of a bright part in an image of an object under crossed polars may be due to one or more of the following,

i) "Intrinsic birefringence" due to the spatial arrangement of atomic groups and molecules in crystalline structures (excluding cubic crystals). Hexagonal crystals including the apatite like crystals in bone have uniaxial birefringence.

ii) "Form birefringence" originates when objects which are small in at least one dimension with respect to the wavelength of light are regularly oriented within a medium of different refractive index. These objects may or may not be intrinsically birefringent. The intensity of "form birefringence" varies with the difference between the two refractive indices.

iii) "Birefringence of flow" is obtained when structures are preferentially oriented in a moving stream of liquid;

iv) "Strain birefringence" occurs when there is a preferential orientation of structures or realignment of chemical bonds induced by mechanical stress.

The birefringence has a sign. If the larger velocity is found for light vibrating parallel with the long axis of the elongated elements, the birefringence is said to be positive: if the reverse, negative.

If "intrinsic" and "form" birefringence are of the same sign, their effects are additive: if of opposite sign, they oppose each other. The net birefringence will have the sign of the more intense of the two.

Thickness as a variable

The thicker the sample, the more the optical path difference, for a given orientation. Two objects having the same thickness may show differing retardation: the object in which the difference between the two refractive indices is greater appears brighter than

the object with a smaller difference.

Optic axis

All anisotropic structures have at least one direction, known as an optic axis, along which the velocity is the same for light polarised in all vibration directions. They appear isotropic 'dark' when viewed along its optic axis. Although the optic axis commonly coincides with the length of a fibre, it does not always coincide with the physical dimensions of an object. The orientation of optic axes can be radial, tangential or helical. In these cases, there is no single direction in which the fibres appear isotropic. The optic axis specifies a direction, rather than an axis of rotation. Biological tissues are in general uniaxial, possessing a single optic axis which may be only determined by careful sectioning in a number of planes.

Difference between isotropic and anisotropic materials

Doubly refracting media differ from isotropic substances in that they i) show a range of refractive indices, the difference between the highest and lowest values determining the birefringence; ii) generally restrict the vibration directions of light passing through them; iii) can be conceived to act as beam splitters. Each light wave entering the medium is divided into two components which travel at different speeds in different directions; iv) have one (or two, but not in the case of bone) direction(s) in which the beam, if it enters, is not split. This is called the 'optic axis'. For monochromatic light entering along an optic axis there is only one speed of travel having one refractive index. The vibration direction of such light is not affected: in this direction, this anisotropic object appears isotropic.

Description of a conventional polarising microscope

Linearly polarised light microscope

When a birefringent specimen is placed between crossed polars, it resolves the incident plane polarised light into two components polarised in mutually perpendicular directions. If rotated between

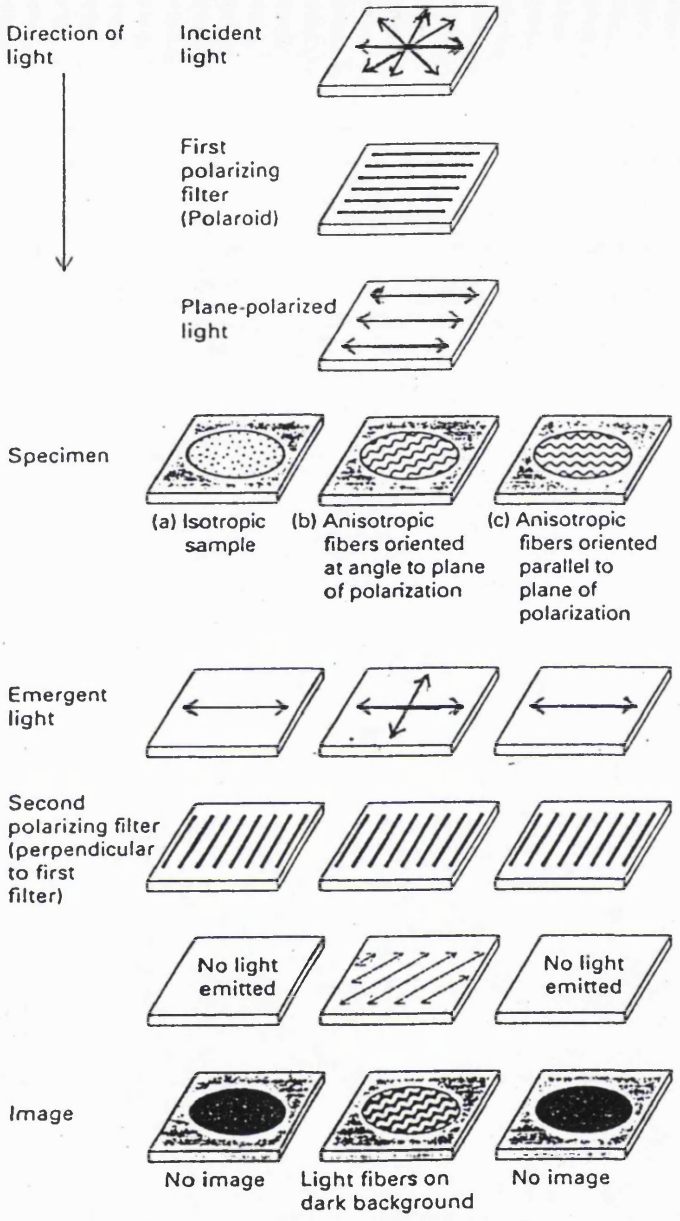

Figure A1.2 Principles of polarisation microscopy. (From Darnell et al 1990, Molecular Cell Biology, Scientific American Books, Inc.)

crossed polars, the birefringence varies in intensity. An object with its structure axis perpendicular to the optic axis disappears completely every 90° during a full rotation with a change in

brightness as it rotates. The specimen appears maximally bright when its optic axis is oriented at 45° to the azimuths transmitted by the polarisers. At every 90° of rotation there is a position of zero intensity. This extinction position occurs when the permitted vibration directions of light in the specimen are parallel with the polariser or the analyser. During rotation with respect to crossed polarisers, four positions of extinction and four of maximum brightness are shown by birefringent specimens. It must be remembered that a birefringent specimen viewed along its optic axis always appears isotropic (dark). Tilted fibres appear brighter in proportion to the angle between the fibre and the optic axis of the microscope. From the presence or absence of extinction positions under crossed polars, and the maximum brightness reached in the 45° positions, one can characterise the orientations of a fabric with respect to the plane of section of an anisotropic object.

Circularly polarised light microscope:

Using plane polarised light, bright parts of an image undergo extinction every 90° of rotation. This is a disadvantage in studying a whole section. The extinction positions can be eliminated by inserting crossed quarter wave plates, one before and one after the specimen. A quarter-wave plate is a uniform piece of birefringent material (mica, quartz, or extruded plastic) of a thickness such that mutually perpendicularly polarised components of a chosen wavelength experience a phase shift of 90°, so that a circularly polarised light beam is formed. The action of the quarter-wave plate can be explained by considering that two beams plane-polarised in mutually perpendicular directions travelling through the plate form circularly polarised beams of opposite handedness. Beyond the quarter-wave plate, the two interfere to form a plane-polarised beam vibrating in an azimuth that is rotated (relative to light incident on the specimen from the polariser) through an angle equal to one-half the phase difference between the beams. The recombination of the light waves as they are re-united along the same optical path is known as interference.

The common polarised light microscope has

i) a polariser before the specimen;

ii) an analyser after the specimen, which can be removed from the light path by sliding or tilting;

iii) a rotating stage to facilitate orientation studies;

iv) a system of centring the stage rotation to the optical axis of the microscope for each objective, and for centring each objective to

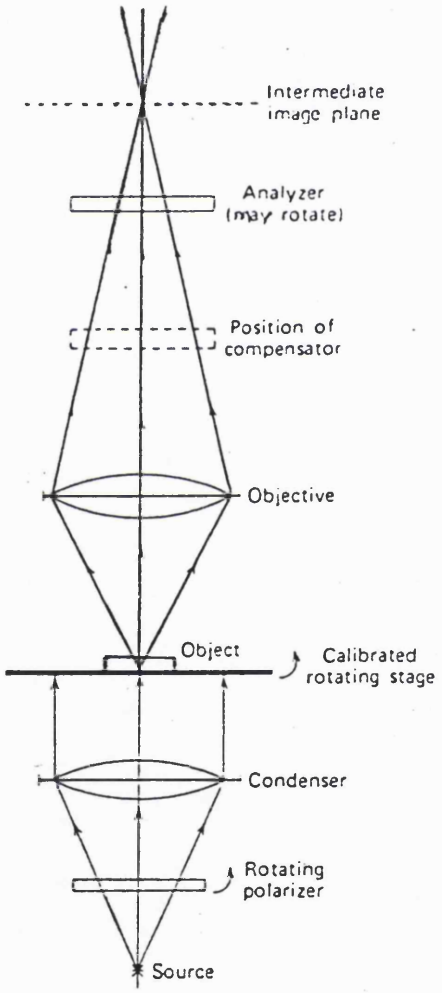

Figure A1.3 Basic design of a polarising microscope. (From Slayter and Slayter 1970, Optical Methods in Biology, Cambridge University Press).

the common optical axis of the instrument;
v) an accessory slot for a retardation plate between analyser and polariser.

The Universal stage:

The Universal stage has several axes of rotation. The section may be centred, rotated, and tilted between the condenser and objective lenses of the microscope. Thus the optical axis of the sample being examined may be aligned to be either parallel or perpendicular to the optical axis of the microscope.

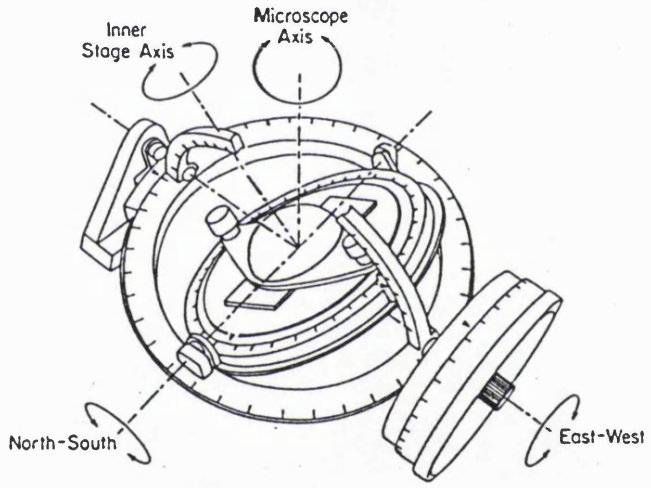

Figure A1.4 The Leitz Universal stage. The calibrated curved arcs are for measuring the angle of tilt, and the glass hemispheres positioned above and below (not in the picture) the tissue section prevent addition of reflections from oblique glass surfaces during tilting of the specimen. (From Finlay et al 1989, J Microscopy 155(2):213-226).

The section is placed between the two glass hemispheres which are secured with the Universal stage. The hemispheres minimise optical image distortion, reflection and refraction related to the tilting of the stage. Calibrated measuring arcs and inner stage are

used for obtaining tilt and rotation angles. The "azimuth" angle is the angle in the plane of tissue section measured by the rotation of the circular inner stage. The elevation angle is the inclination out of the plane of the stage measured on the right or left arc.

The dominant birefringence component of bone is due to its collagen content. The arrangement of collagen fibres and mineral composition is highly ordered. The crystals are aligned in nearly the same direction as the collagen fibres. The total birefringence is the sum of the positive uniaxial form birefringence of the collagen, and the negative uniaxial intrinsic birefringence of hydroxyapatite crystals.

The limitations encountered in conventional polarising microscopy in determining bone collagen fibre orientation in three dimensions can be removed by the use of the Universal stage. Such stages have been used primarily in the study of the crystal structures in strongly birefringent geological materials. The use of the Universal stage has been reported in the study of orientation of arterial and muscle components in heart and brain (Smith et al 1981; Canham et al 1986, 1991; Finlay et al 1989). Until now, no attempt had been made to explore the use of this method in the determination of collagen fibre orientation in bone.

Birefringent regions viewed between crossed polars appear both bright and dark in sequence with rotation and tilting of the Universal stage. Extinction, for an area of fibres, is the angular position with least light intensity, and indicates that the optic axis in that area is parallel to that of the polariser or the analyser. If collagen fibres are aligned perpendicular to the neutral tilt position of the microscope stage, so that there is extinction in all rotation positions, signs of birefringence may be looked for by tilting the inner stage. Compact bone slices are examined for extinction whilst rotating the object at different degrees of tilt.

Tilting a section to high angles may lead to overlapping of adjacent Haversian systems, thus masking the extinction. It is possible to reduce the chance of the overlapping of collagen layers by i) using thinner sections; or ii) using sections of the cortex

cut in different planes to facilitate the determination of the optic axes of the fibres more precisely, and iii) tilting thin oblique sections to reduce the extent of overlapping.

There is obviously a problem with using a tilting stage in that the apparent section thickness increases with tilt, which will increase the optical path difference and the brightness. By cutting sections obliquely, one can reduce the need to examine sections at very high tilts in determining the extinction positions.

References cited in Appendix 1

Canham PB, Finlay HM, Whittaker P, Starkey J (1986) The tunica muscularis of human brain arteries: three dimensional measurements of alignment of the smooth muscle mechanical axis, by polarized light and the Universal stage. Neurol Res 8:66-74

Canham PB, Finlay HM, Dixon JG, Ferguson SE (1991) Layered collagen fabric of cerebral aneurysms quantitatively assessed by the Universal stage and polarized light microscopy. Anat Rec 231:579-592

Darnell JE, Lodish H, Baltimore D (1990) Molecular Cell Biology, 2nd ed. Scientific American Books, Inc. p.845

Finlay HM, Whittaker P, Hicks JG, Taylor CPS, Park YW, Canham PB (1989) Spatial orientation of arterial sections determined from aligned vascular smooth muscle. J Micros 155(2):213-226

Robinson PC, Bradbury S (1992) Qualitative polarized light microscopy, Oxford Science Publications. p.6

Slayter EM, Slayter HS (1992) Light and Electron Microscopy, Cambridge University Press. p.169

Smith JFH, Canham Pb, Starkey J (1981) Orientation of collagen in the tunica adventitia of the human cerebral artery measured with polarized light and the Universal stage. J Ultrastruct Res 77:133-145

APPENDIX 2 Publications arising from this thesis

Abstracts published:

1. Haroon MY, Riggs CM, Boyde A (1994) A structural predisposition to Spontaneous fracture in racehorse bone. J Anat 185:230.

2. Haroon Y, Hall SJB, Gray C, Jones SJ and Boyde A (1994) Autofluorescence Confocal Microscopy of Bone. Scanning 16(4):253.